

UNIVERSITA' DEGLI STUDI DI VERONA

DEPARTMENT OF BIOTECHNOLOGY

SCHOOL OF NATURAL SCIENCES AND ENGINEERING

PhD IN NANOSCIENCE AND ADVANCED TECHNOLOGIES

CYCLE XXXII

**NEW Ln(III) COMPLEXES AS POTENTIAL OPTICAL PROBES FOR  
BIOLOGICAL APPLICATIONS**

S.S.D. CHIM/03

Coordinator: Prof. Franco Tagliaro

Tutor: Prof. Fabio Piccinelli

PhD Candidate: Chiara De Rosa

Quest'opera è stata rilasciata con licenza Creative Commons Attribuzione – non commerciale Non opere derivate 3.0 Italia. Per leggere una copia della licenza visita il sito web:

<http://creativecommons.org/licenses/by-nc-nd/3.0/it/>



**Attribuzione** Devi riconoscere una menzione di paternità adeguata, fornire un link alla licenza e indicare se sono state effettuate delle modifiche. Puoi fare ciò in qualsiasi maniera ragionevole possibile, ma non con modalità tali da suggerire che il licenziante avalli te o il tuo utilizzo del materiale.



**NonCommerciale** Non puoi usare il materiale per scopi commerciali.



**Non opere derivate** —Se remixi, trasformi il materiale o ti basi su di esso, non puoi distribuire il materiale così modificato.

**NEW Ln(III) COMPLEXES AS POTENTIAL OPTICAL PROBES FOR BIOLOGICAL APPLICATIONS**

Chiara De Rosa

PhD Thesis

Verona, 10 December 2019

ISBN

## Sommario

*Le singolari proprietà delle transizioni f-f nei complessi trivalenti di Lantanidi sono la principale ragione delle crescenti applicazioni nel campo del biosensing, dove la lunga durata di emissione, le bande di emissione nitide e facilmente riconoscibili, l'elevata differenza energetica tra le radiazioni assorbite ed emesse oltre ai brevi tempi di vita della fluorescenza consentono l'enorme vantaggio di isolare il loro caratteristico segnale di emissione dall' indesiderata fluorescenza di fondo dei campioni biologici.*

*Inoltre, i complessi luminescenti di Eu(III) e Tb(III) sono i candidati più impiegati a causa della bassa sensibilità del loro stato eccitato agli effetti di spegnimento vibrazionale causati da oscillatori OH, NH o CH, spesso presenti nelle soluzioni per il campo dell'imaging.*

*Alla luce di ciò, i complessi di Eu(III) e Tb(III) sono stati ampiamente sfruttati come sensori per specie metaboliche, nel rispetto delle condizioni fisiologiche, consentendo il rilevamento di rilevanti biomarcatori clinici nella diagnostica biomedica e nell'imaging.*

*Per questi scopi, un'elevata resa quantica di luminescenza e d'intensità di risposta sono indispensabili. L'elevata intensità del segnale è possibile grazie alla presenza di opportuni ligandi aromatici tramite l'effetto dell'antenna, ed è solitamente correlata alla concentrazione dell'analita bersaglio.*

*In questo progetto di dottorato, una nuova libreria di complessi idrosolubili a base di Eu(III) e Tb(III) costituiti da un nucleo comune chirale di 1,2-diamminocicloesano (DACH) è stata sintetizzata con successo, completamente caratterizzata (anche in soluzione) e impiegata per la rilevazione di importanti bioanaliti quali: bicarbonato, L-lattato, albumina e citrato principalmente attraverso luminescenza totale (TL) e luminescenza a polarizzazione circolare (CPL). Questi analiti sono i principali costituenti del liquido extracellulare, come il siero umano.*

## **Abstract**

*The unique properties of f-f transitions in trivalent lanthanide complexes are the understandable reason of increasing applications in biosensing field, where their long emission lifetimes, the sharp and easily recognizable emission bands in addition to the large shift between the absorbed and emitted radiation besides a short-lived background fluorescence permit the great advantage to isolate their emission signal from the undesired background fluorescence of the biological samples.*

*Furthermore, luminescent complexes of Eu(III) and Tb(III) are the most employed candidates due to the low sensitivity of their excited state to vibrational quenching effects caused by OH, NH, or CH oscillators, frequently present in solution and imaging environments.*

*For these reasons, Eu(III) and Tb(III) complexes have been extensively exploited as sensors of species in physiological conditions, by allowing the detection of relevant clinical biomarkers in biomedical diagnostics and imaging.*

*For these purposes, a high luminescence emission quantum yield and overall luminosity (or brightness) are strongly required and the intensity of the luminescent response, that it is enhanced with heteroaromatic ligands via antenna effect, is usually correlated to the concentration of target analyte.*

*In this PhD project, a library of new water soluble Eu(III) and Tb(III) complexes based on the chiral fragment 1,2-diaminocyclohexane (DACH) has been successfully synthesized, completely characterized (also in solution) and employed for analytical detection of important bio-analytes such as: bicarbonate, L-lactate, serum albumin, and citrate through mainly total luminescence (TL) and circularly polarized luminescence (CPL). These analytes are the main constituents of extracellular fluid, such as human serum.*

## Table of contents

Sommario.....	3
Abstract.....	4
Abbreviations.....	8
List of ligands.....	9
List of Ln-complexes.....	10
<b>CHAPTER 1- Lanthanide luminescence (TL and CPL) .....</b>	<b>13</b>
1.1 Introduction .....	13
1.2 The total luminescence (TL).....	19
1.3 Circularly Polarized Luminescence (CPL) .....	24
1.4 Experimental results- Effect of the counterion on Circularly Polarized Luminescence (CPL) of Eu(III) and Sm(III) complexes.....	29
1.4.1 UV-visible Absorption and Electronic Circular Dichroism (ECD).....	30
1.4.2 Total Luminescence (TL), CPL and luminescence decay kinetics.....	33
1.4.2.1 Eu-complexes.....	33
1.4.2.2 Sm-complexes.....	40
1.4.3 Effect of the counterion on Circularly Polarized Luminescence (CPL) of Eu(III) and Sm(III) complexes: procedures, techniques and characterization.....	45
1.5 References .....	49
<b>CHAPTER 2-Lanthanide complexes: applications for sensing in biomedicine.....</b>	<b>53</b>
2.1 Introduction .....	53
2.2 Toolkit of the lanthanides luminescent bioprobes .....	54
2.2.1 Water solubility.....	54
2.2.2 Stability and Selectivity.....	56
2.3 Classification and applications of lanthanide probes in bioimaging.....	56
2.3.1 $\beta$ -Diketonate Probes .....	57
2.3.2 Encapsulated probes.....	59
2.3.3 Aliphatic Polyaminocarboxylate and Carboxylate Probes .....	60
2.3.4 Helicates.....	71
2.4 References .....	73
<b>CHAPTER 3- Experimental results: New Ln(III) complexes as luminescence bioprobes.</b>	<b>79</b>
3.1 Complexes of rare earth ions embedded in Poly(lactic-co-glycolic acid)(PLGA) nanoparticles: Characterization and spectroscopic study.....	79
3.1.1 Introduction.....	79
3.2 Water insoluble Eu(III) complexes: encapsulation in PLGA for bioimaging purposes.....	79
3.2.1 PLGA luminescent nanoparticles: physical characterization .....	82
3.2.2 Thermal stability of the luminescent PLGA NP'S .....	92
3.3 Water soluble Ln(III) complexes: toward biosensing applications .....	95
3.3.1 Design and Synthesis.....	95

3.3.2 New Eu(III)-based complex with a C <sub>1</sub> symmetric chiral ligand.....	100
3.3.2.1 Synthesis.....	100
3.3.2.2 Optical spectroscopy.....	102
3.3.3 Complexes of rare earth ions embedded in Poly(lactic-co-glycolic acid)(PLGA) nanoparticles: procedures, techniques and characterization.....	105
3.3.4 New Eu(III)-based complex with a C <sub>1</sub> symmetric chiral ligand: procedures, techniques and characterization.....	110
3.4 References.....	113
<b>CHAPTER 4- Interaction of new Ln(III) complexes with relevant bioanalytes .....</b>	<b>116</b>
4.1 Introduction .....	116
4.2 Complexes structure: synthesis and characterization .....	119
4.2.1. Synthesis .....	119
4.2.2. Characterization: Stability constant.....	122
4.2.2.1 Potentiometric titrations.....	125
4.2.2.2 Spectrophotometric titrations.....	130
4.2.2.3 Characterization: UV-visible absorption and luminescence.....	136
4.2.3. Data elaboration and computational models .....	143
4.3 Sensing of HCO <sub>3</sub> <sup>-</sup> : the screening in cuvette with Ln-complexes based on Pyridine and Quinoline rings.....	149
4.3.1. Introduction .....	149
4.3.2. Ln(III)-complexes-HCO <sub>3</sub> <sup>-</sup> adducts: luminescence and affinity constants.....	150
4.3.3. Conclusions: general remarks on Bicarbonate ion .....	155
4.4 Sensing of Serum albumin (BSA): the screening in cuvette with Ln-complexes based on Pyridine and Isoquinoline rings (1R, 2R) .....	156
4.4.1. Introduction .....	156
4.4.2. Luminescence: evolution of the emission spectra during the titration.....	157
4.4.2.1 Luminescence: excitation spectra and <sup>5</sup> D <sub>0</sub> lifetimes measurements.....	159
4.4.2.2 Luminescence: fluorescence of the protein.....	162
4.4.3. Conclusions .....	168
4.5 Experimental part: procedures, techniques and characterization .....	169
4.5.1. Materials .....	169
4.5.2. Synthesis .....	170
4.5.3. Elemental analysis.....	181
4.5.4. Potentiometric titrations .....	181
4.5.5 Spectrophotometric titrations .....	182
4.5.6 Luminescence and decay kinetics .....	183
4.5.7. Luminescence sensing of HCO <sub>3</sub> <sup>-</sup> .....	186
4.5.8. Molecular Docking (MD) .....	186
4.6 References.....	187
<b>CHAPTER 5-High Throughput Screening (HTS) for detection of bioanalytes by means of Eu(III)-complexes based on Isoquinoline.....</b>	<b>192</b>
5.1 Introduction .....	192

5.2 Sensing of the main components of ECF.....	193
5.2.1. The oxophilic anions .....	193
5.2.2 The Bicarbonate ions: luminescence and binding constants.....	194
5.2.3 The promising Citrate ion: luminescence and binding constants.....	197
5.2.3.1 Introduction.....	197
5.2.3.2 Ln(III)complexes-Citrate adducts: effects of the interferences.....	198
5.2.3.3 Minor interferences: luminescence studies.....	206
5.2.3.4 Citrate: the detection in extracellular fluid.....	207
5.2.4. Sensor membrane for Citrate in biosamples.....	215
5.2.4.1 Principle of method.....	215
5.2.4.2 Fabrication of sensor membrane.....	216
5.2.4.3 Results and discussions.....	218
5.2.4.4 Conclusions.....	223
5.3 Experimental part: procedures, techniques and characterization.....	224
5.3.1. Materials.....	224
5.3.2. Luminescence and decay kinetics measurements.....	224
5.3.3. Sensing experiments.....	225
5.4 References.....	227
Final Conclusions.....	229
Acknowledgements.....	233

## **Abbreviations**

TL: Total luminescence

Ln: Generic lanthanide

ECD: Electronic Circular Dichroism

glum: luminescence dissymmetry factor

DACH: 1,2-diaminocyclohexane

TTA: 2-Thenoyltrifluoroacetyl-acetate

OTf: Triflate ion (-OSO<sub>2</sub>CF<sub>3</sub>)

PET: Positron Emission Tomography

NIR: near Infrared

NPs: nanoparticles

CPNs: conjugated polymer nanoparticles

PeT: Photo Induced Electron Transfer

PLGA: Poly(lactic-co-glycolic acid)

DLS: dynamic light scattering

ZP: zeta potential

AFM: atomic force microscopy

PBS: phosphate buffered saline

MOPS: 4-Morpholinepropanesulfonic acid buffer

Emf: Electromotive force

DFT: Density Functional Theory

EDG: electron donating group

DIBALH: Diisobutylaluminium hydride

DCM: dichloromethane

ACN: acetonitrile

EtOH: ethanol



AcOEt: ethyl acetate

Cy: cyclohexane

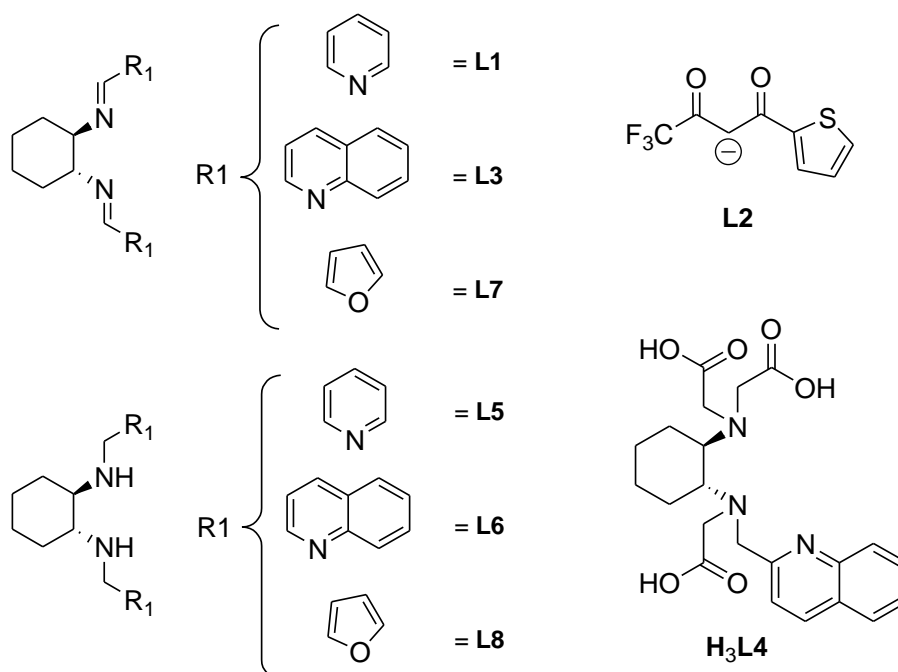
MeOH: methanol

Rf: retention factor

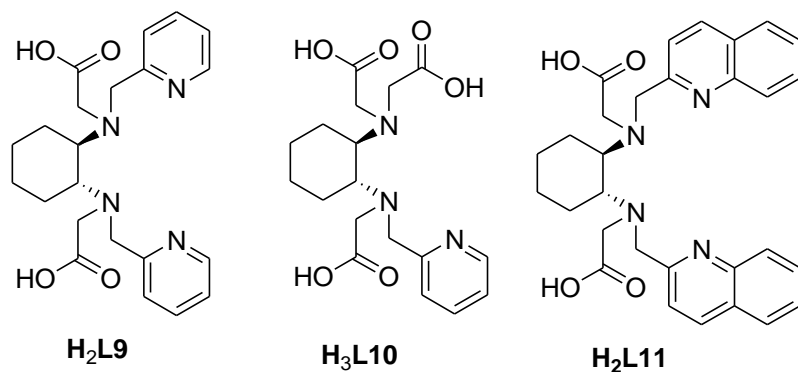
ECF: extracellular fluid

## List of Ligands

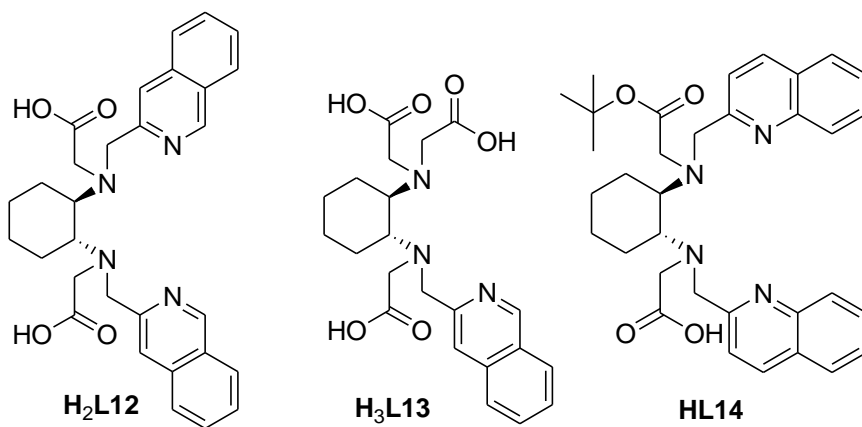
Chapter 1, 3, 4:



Chapter 4:

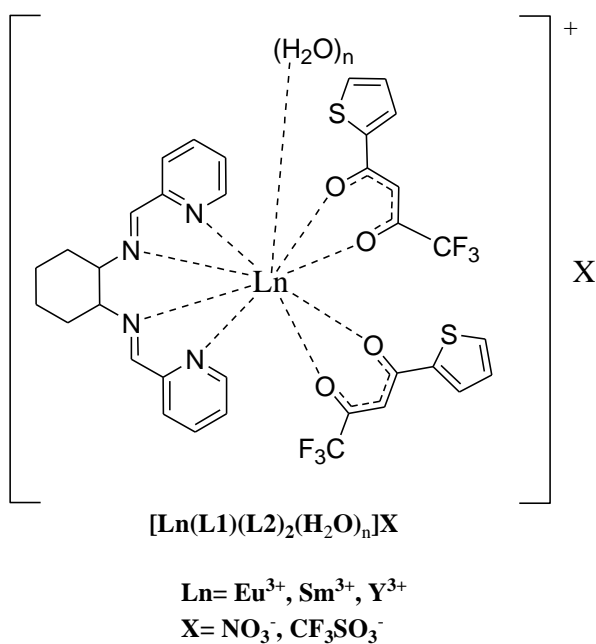


Chapter 4:

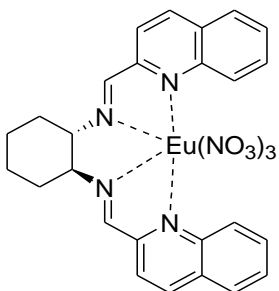


**List of Ln-complexes**

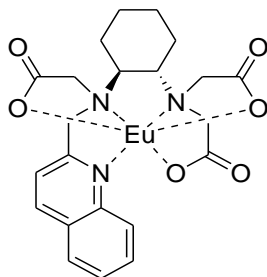
Chapter 1:



Chapter 3, 4:

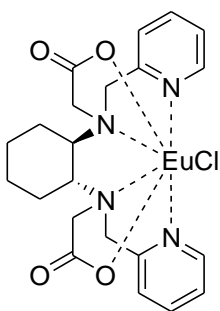


**Eu(L3)(NO<sub>3</sub>)<sub>3</sub>**

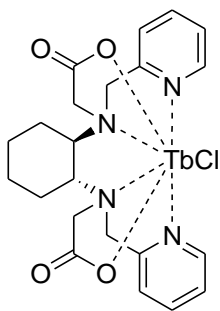


**Eu(L4)**

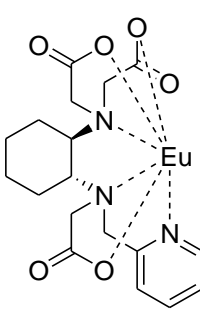
Chapter 4:



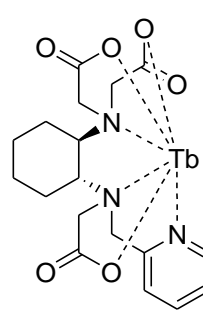
**Eu(L9)Cl**



**Tb(L9)Cl**

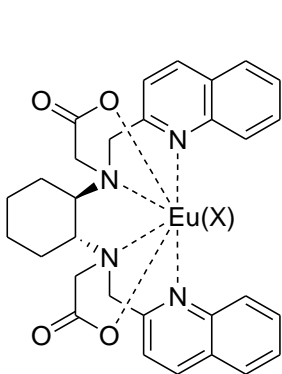


**Eu(L10)**

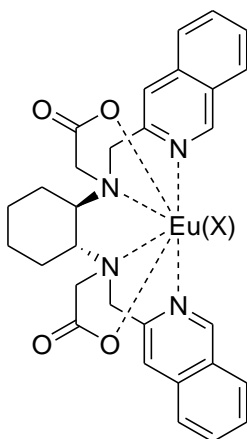


**Tb(L10)**

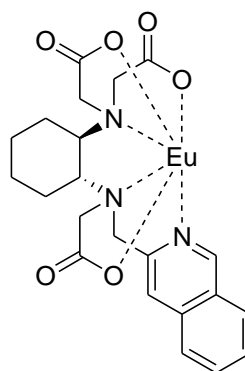
Chapter 3, 4:



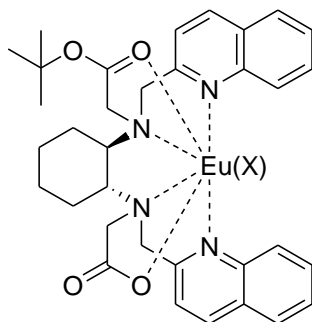
**Eu(L11)X**  
**X=Cl<sup>-</sup>, <sup>-</sup>OSO<sub>2</sub>CF<sub>3</sub>**



**Eu(L12)X**  
**X=Cl<sup>-</sup>, <sup>-</sup>OSO<sub>2</sub>CF<sub>3</sub>**



**Eu(L13)**



**Eu(L14)X**  
**X=Cl<sup>-</sup>**

# CHAPTER 1- Lanthanide luminescence (TL and CPL)

## 1.1. Introduction

The lanthanide ions range from lanthanum (Z:57) to lutetium (Z:71) with an electronic configuration consisting of a xenon core and 4f valence electrons, [Xe]4f<sup>n</sup>. The states originated from different electronic configuration can be represent by the term  $^{2S+1}L_J$  in which S and L are respectively the total electron spin and orbital angular momentum, and J denote the total angular momentum. The mixing of the electrons into the levels by considering the contribution of all quantum numbers are reported in the Russell Saunders Coupling scheme, where the ground state is deduced by Hund's rules.<sup>1</sup> The typical energy diagram<sup>2</sup> obtained for each trivalent lanthanides is reported in the Dieke diagram (Figure 1).

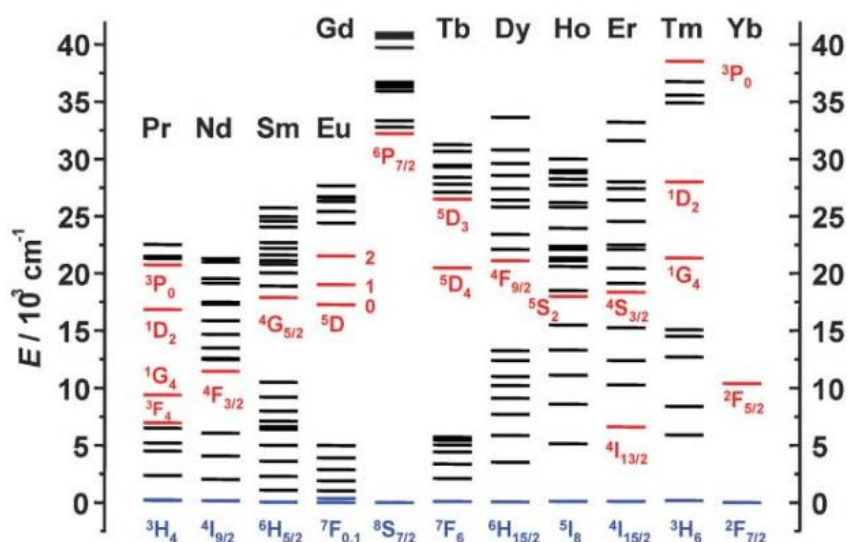


Figure 1 Partial energy diagrams for the lanthanide aquo ions. The main luminescent levels are drawn in red, and the fundamental level is evidenced in blue.

The unique properties of the lanthanide ions are essentially due to their peculiar electronic structure, where the 4f orbitals are shielded from the surroundings thanks to the filled 5s<sup>2</sup> and 5p<sup>6</sup> orbitals. The poor shielding of nuclear charge offered by 4f orbitals it is the cause of an effect known as “the lanthanide contraction”, in which the 6s electrons are drawn towards the nucleus, thus resulting in a smaller atomic radius with progressive increase of the atomic number (Figure 2).

These feature makes more similar the radius of  $\text{Ho}^{3+}$  and  $\text{Er}^{3+}$  to that one of  $\text{Y}^{3+}$ , by allowing the comparison between the chemical coordination chemistry of Yttrium and the rare earths.<sup>3</sup>

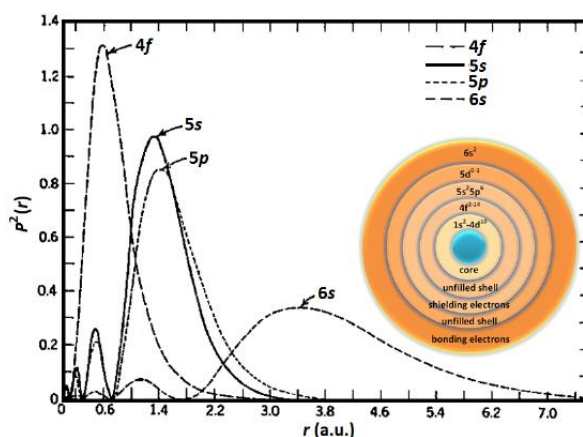


Figure 2: Square of the radial wavefunctions for the 4f, 5s, 5p and 6s energy levels from Hartree-Fock.<sup>4</sup>

The lanthanide ions are conveniently represented by sharp and easily recognizable spectra, due to their intrinsic nature of the core orbitals 4f. As the consequence of the shielding by the core orbitals, the selection rules forbidding f-f transitions are weakly relaxed by the surroundings environment, by keeping their atomic nature. The monochromatic purity of lanthanide emission<sup>2</sup> (Figure 3) in complexes or as free ions could be efficiently exploited in technological applications.

The more stable oxidation state is +3, although +2 and +4 valences are also possible in particular conditions.

Ln	Excited state <sup>a</sup>	$\tau_{\text{rad}}/\text{ms}^b$	End state <sup>c</sup>	Lumin. type <sup>d</sup>	$\lambda/\text{nm}^e$	Emission color	
Pr	$^1\text{G}_4$	n.a.	$^3\text{H}_J$	4-6	P	1300	NIR
	$^1\text{D}_2$	n.a.	$^3\text{F}_J$	2-4	P	890, 1060	NIR
Nd	$^3\text{P}_0$	n.a.	$^3\text{H}_J$	4-6	F	525-680	Orange
	$^4\text{F}_{3/2}$	0.42	$^4\text{I}_J$	9/2-15/2	F	1060	NIR
Sm	$^4\text{G}_{5/2}$	6.26	$^6\text{H}_J$	5/2-15/2	P	590	Orange
Eu	$^5\text{D}_0$	9.67	$^7\text{F}_J$	0-6	P	620	Red
Gd	$^6\text{P}_{7/2}$	10.9	$^8\text{S}_{7/2}$		P	312	UV
Tb	$^5\text{D}_4$	9.02	$^7\text{F}_J$	6-0	P	550	Green
Dy	$^4\text{F}_{9/2}$	1.85	$^6\text{H}_J$	15/2-5/2	P	570	Yellow-orange
Ho	$^5\text{F}_5$	n.a.	$^5\text{I}_J$	8-4	F	970, 1450	NIR
	$^5\text{S}_2$	0.37	$^5\text{I}_J$	8-4	F	540	Green
Er	$^4\text{S}_{3/2}$	0.66	$^4\text{I}_J$	15/2-9/2	F		
Tm	$^4\text{I}_{13/2}$	n.a.	$^4\text{I}_{15/2}$		F	1530	NIR
	$^1\text{G}_4$	n.a.	$^3\text{H}_J$	6-4	P		
Yb	$^2\text{F}_{5/2}$	1.2 <sup>f</sup>	$^2\text{F}_{7/2}$		F	980	NIR

Figure 3. Main luminescent transition of trivalent lanthanide aquo ions.<sup>5</sup>

a) Main excited states; b) radiative lifetimes; c) Range of J-values; d) F: fluorescence, P: phosphorescence; e) Wavelengths of the most intense transitions.

The strong attraction toward the nucleus not allows the involvement of the orbitals

4f in the coordination chemistry of the  $\text{Ln}^{3+}$ , thus the available orbitals in the coordination with the ligands are the empty 6s, 6p and 5d.

The weak influence of the ligands coordination on the f-f transitions is attributed on the lost in degeneracy of the J-levels due to the well-known crystal field effect. This leads to a further splitting of the  $(2J+1)$ -fold degenerate free ion states into the so-called Stark levels (or crystal-field levels). The strength of the crystal field determines the magnitude of the splitting, its symmetry the number of Stark levels that arise. The most common geometry is in low symmetry, in this case the free ion levels split into  $(2J+1)$  Stark levels, for J integer. If the J values are half-integer, the Kramers degeneracy is still retained, but the maximum number of Stark levels is  $(J+1/2)$ . Despite the mentioned effect, the influence of the crystal field is relatively weak and the splittings are just in the order of  $10^2 \text{ cm}^{-1}$  (Figure 4).

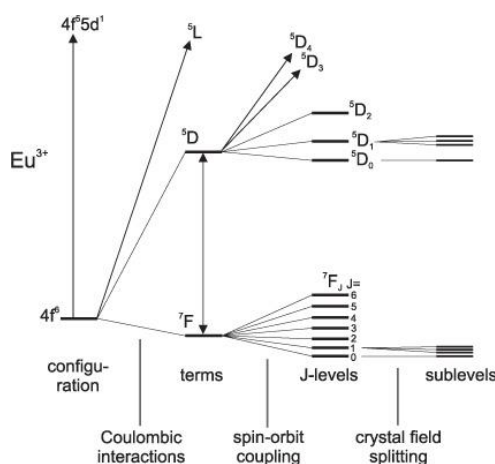


Figure 4. Diagram representing the interactions leading to the splitting of the electronic energy levels of  $\text{Eu}^{3+}$  ion. <sup>6</sup>

The absorption of the light by the lanthanide ions involves essentially electric dipole transitions (ED) with odd parity and magnetic dipole (MD) transitions. All  $4f^n$  states of the free lanthanide ions have the same parity, consequently the f-f transitions through electric dipole are forbidden for the Laporte's rules, and only MD dipole transitions are allowed (in principle also electric quadrupole) (Table 1).

Transition <sup>a</sup>	Dipole character <sup>b</sup>	Wavelength range (nm)	Relative intensity <sup>c</sup>	Remarks
<sup>5</sup> D <sub>0</sub> → <sup>7</sup> F <sub>0</sub>	ED	570–585	vw to s	Only observed in C <sub>2v</sub> , C <sub>3v</sub> and C <sub>s</sub> symmetry
<sup>5</sup> D <sub>0</sub> → <sup>7</sup> F <sub>1</sub>	MD	585–600	s	Intensity largely independent of environment
<sup>5</sup> D <sub>0</sub> → <sup>7</sup> F <sub>2</sub>	ED	610–630	s to vs	Hypersensitive transition; intensity very strongly dependent on environment
<sup>5</sup> D <sub>0</sub> → <sup>7</sup> F <sub>3</sub>	ED	640–660	vw to w	Forbidden transition
<sup>5</sup> D <sub>0</sub> → <sup>7</sup> F <sub>4</sub>	ED	680–710	m to s	Intensity dependent on environment, but no hypersensitivity
<sup>5</sup> D <sub>0</sub> → <sup>7</sup> F <sub>5</sub>	ED	740–770	vw	Forbidden transition
<sup>5</sup> D <sub>0</sub> → <sup>7</sup> F <sub>6</sub>	ED	810–840	vw to m	Rarely measured and observed

<sup>a</sup> Only transitions starting from the <sup>5</sup>D<sub>0</sub> level are shown.

<sup>b</sup> ED = induced magnetic dipole transition, MD = magnetic dipole transition.

<sup>c</sup> vw = very weak, w = weak, m = medium, s = strong, vs = very strong.

Table 1. Overview of the transitions observed in luminescence spectra of europium(III) compounds. <sup>7</sup>

In the crystal lattice, if a rare-earth occupies a site with inversion symmetry, the transitions between the 4f<sup>n</sup> levels are strictly forbidden as electric-dipole transition (parity selection rule). The only possible transitions are the magnetic-dipole transitions which obey the selection rule  $\Delta J=0, \pm 1$  (from J=0 to J=0 is forbidden).

On the other hand, if there is no inversion symmetry in the crystal lattice, the electric-dipole transitions are not so strictly forbidden. The uneven components of the crystal field are present exclusively when the lanthanide ion occupies a lattice without inversion symmetry. Under these conditions, those components mix a small amount of opposite-parity wavefunctions (like 5d) into the 4f wavefunctions, by allowing, even if in low entity, the intraconfigurational 4f<sup>n</sup> transitions. It can be said that the forbidden 4f-4f transition *steal* the intensity from the allowed 4f-5d transition. <sup>8</sup>

The <sup>5</sup>D<sub>0</sub>-<sup>7</sup>F<sub>2</sub> and <sup>5</sup>D<sub>0</sub>-<sup>7</sup>F<sub>4</sub> transitions, in europium (III) ion, particularly sensitive to the loss of inversion symmetry, are called forced hypersensitive electric dipole transitions. As already mentioned, the weak effect of the ligands coordination causes the crystal field effect. With this in mind, the trivalent Europium ion is one of the most used lanthanide for many reasons. Firstly, since the ground state (<sup>7</sup>F<sub>0</sub>) and the major emitting excited state (<sup>5</sup>D<sub>0</sub>) are non-degenerate, they are not splitted by the crystal-field effect 2J+1, and consequently the interpretation of the experimental absorption and luminescence spectra are facilitated. In fact, the main advantages of the Europium trivalent ion is the pure and single transition from the not-splitted emitting excited level <sup>5</sup>D<sub>0</sub> (J=0) to the acceptor levels <sup>7</sup>F<sub>(0-6)</sub> resulting in more defined and recognizable transitions, useful for obtaining structural information.



In this context, the  ${}^5D_0 \rightarrow {}^7F_0$  transition is useful for the determination of the presence of non-equivalent sites in a host crystal or for determination of the number of different europium(III) species in solution, because maximum one peak is expected for a single site or species, due to the non-degeneracy of the  ${}^7F_0$  and  ${}^5D_0$  levels.

The intensity of the hypersensitive transition  ${}^5D_0 \rightarrow {}^7F_2$  or the ratio  $R$  of the intensities of the  ${}^5D_0 \rightarrow {}^7F_2$  and  ${}^5D_0 \rightarrow {}^7F_1$  transitions, [ $R = I({}^5D_0 \rightarrow {}^7F_2)/I({}^5D_0 \rightarrow {}^7F_1)$ ] is often used as a measure for the asymmetry degree of the  $\text{Eu}^{3+}$  site. A dominant hypersensitive transition, connected to a low symmetry around the  $\text{Eu(III)}$  ion.<sup>7</sup>

In view of the poor probability of the forbidden  $f-f$  transitions, low molar absorption coefficients (not above  $10 \text{ M}^{-1} \text{ cm}^{-1}$ ) were unfortunately observed. A direct excitation of the lanthanide ions could be possible by employing excitation source with intense energy, condition not always viable, especially for application in the biological field. The low efficiency of the  $f-f$  transitions could be overcome with an indirect excitation source, upon excitation of an organic chromophore (sensitizer or antenna) followed by the transfer of the excitation energy to the lanthanide ion. The whole process is known as “*antenna effect*” and its schematic representation is given in the Figure 5.

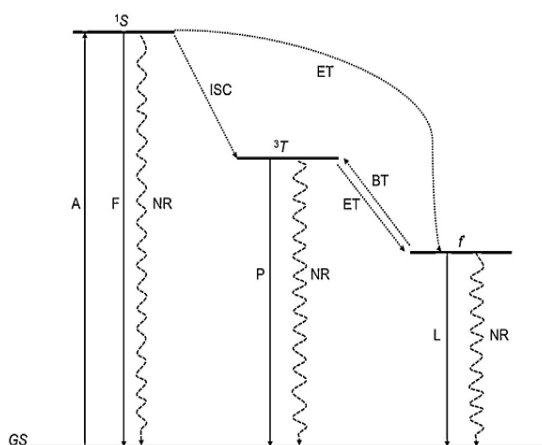


Figure 5. Schematic diagram of the antenna effect. A – absorption, F – fluorescence, P – phosphorescence, L – luminescence, ISC – intersystem crossing, ET – energy transfer, BT – back energy transfer, NR – non-radiative deactivation,  ${}^1S$  – first excited singlet state,  ${}^3T$  – lowest excited triplet state, GS – ground state,  $f$  – excited level of the metal.

In 1942 Weissman discovered that intense metal-centered luminescence was detected for Europium(III) complexes bearing salicylaldehyde, benzoylacetone,

dibenzoylmethane and meta-nitrobenzoylacetone upon excitation within the intrinsic absorption region of the organic ligands.<sup>9</sup>

Upon UV excitation of the ligand, the energy it is transferred to the excited state <sup>1</sup>S state. This first condition implies high values of molar absorption coefficient of the ligand ( $\epsilon$ ). In literature, Parker and co-workers reported a  $\text{Eu}^{3+}$ -complex possessing a  $\epsilon$  value of  $15000\text{-}30000 \text{ M}^{-1} \text{ cm}^{-1}$  at 337 nm.<sup>10</sup>

Afterwards, the excited organic molecule could undergo through different pathways: a) fast internal conversion to the lower vibrational levels of the <sup>1</sup>S state, for example upon interactions with solvents molecules; b) radiative deactivation to the ground state (F, fluorescence,  $S_1 \rightarrow S_0$ ), or c) via non-radiative intersystem crossing from the singlet state  $S_1$  to the triplet state  $T_1$ . This level can be deactivated radiatively to the ground state  $S_0$  by the spin-forbidden transition  $T_1 \rightarrow S_0$  (phosphorescence). The latter condition is particularly favored in  $\text{Gd}^{3+}$  ion. It is worth pointing out that the f–f transitions of  $\text{Gd}^{3+}$  are located at high energies due to the extreme stability of its half-filled f-shell ( $f^7$ ), being the lowest-energy f–f transition around 310 nm. For this reason, in Gd(III)-based complexes no antenna effect from a common organic chromophore is usually detected. Accordingly, Gd(III) complexes are frequently characterized by emissive intraligand (IL) states at lower energies. Lanthanide ions produce a heavy-atom effect to ligands by inducing increased spin–orbit coupling. Gd (III) in particular, due to its heavy-atom effect and paramagnetism (the so called paramagnetic metal effect), can induce a strong singlet/triplet mixing in the ligands.<sup>11</sup>

As a consequence, the fluorescence of the ligand is quenched since intersystem crossing becomes faster, with the final effect to enhance the Phosphorescence (P) process ( $^3T \rightarrow S_0$ ). Furthermore, the radiative lifetime of the triplet decreases and the phosphorescence quantum yield grows.<sup>12-15</sup>

Moreover, intra-ligand phosphorescence of several Gd(III) complexes appear also at room temperature<sup>16-19</sup> revealing the importance for technological applications. As last step of the antenna effect, the triplet state can transfer its excitation energy to the excited level of the lanthanide ions, completing the ligand to metal energy transfer (LMET).

## 1.2. *The total luminescence (TL)*

In coordination compounds, the overall efficiency of the lanthanide luminescence is strictly related to the capability of the designed complex to absorb the photons and transfer the excitation energy to the lanthanide ion. This is quantitatively well expressed in the equation (1a and 1c).

$$\Phi_{ext} = B = \varepsilon_{ant} * \Phi_{tot} \quad (eq. 1a)$$

$$\Phi_{tot} = \Phi_{Ln} * \eta_{ISC} * \eta_{ET} \quad (eq. 1b)$$

$$\Phi_{ext} = B = \varepsilon_{ant} * \Phi_{Ln} * \eta_{ISC} * \eta_{ET} \quad (eq. 1c)$$

The external quantum yield or overall luminosity [ $\Phi_{ext}$  or *Brightness* (B, eq. 1a and 1c), i.e. number of emitted photons / number of incident photons], is due to the product of the molar absorption coefficient  $\varepsilon$  and the total quantum yield,  $\Phi_{tot}$  (equation 1a) that in turn is equal to the intrinsic lanthanide quantum yield  $\Phi_{Ln}$ , multiplied by the efficiency of the intersystem crossing,  $\eta_{ISC}$  and by the efficiency of the energy transfer processes,  $\eta_{ET}$  (eq. 1b).

The energy transfer process could takes places through two main mechanisms, which involve directly the excited states of the ligands and the excited 4f levels of the lanthanide ion.<sup>7</sup>

One mechanism is called exchange energy transfer mechanism and requires the superimposition between the donor and the acceptor orbitals. The overlap between the emission spectrum of the donor (ligand) and the absorption spectrum of the acceptor ( $\text{Ln}^{\text{III}}$  ion) (spectral overlap) is also required, as in the case of dipole-dipole interaction, which is the second quite common process on the basis of energy transfer. The efficiency of the exchange process is ruled by the ratio  $1/e^r$ , where r it is the distance lanthanide-antenna. For this reason, the mechanism is active in a very short range of lanthanide-antenna distances.

ET process is due mainly to a dipole-dipole or dipole-multipole interactions, when involves a singlet excited state of the ligand ( $S_1$ ).

On the contrary, when the  $T_1$  excited state is involved, the exchange interaction dominates the ET process. This is due to the electronic spin selection rules.<sup>19</sup>

The probability of the ET process via dipole-dipole interactions (Förster mechanism) is related to additional features such as: i) probability of d-d transitions of the donor and the acceptor and the refractive index of the medium. As the distance dependence is described by  $1/r^6$ , where  $r$  = distance lanthanide-antenna, this interaction is efficient in a longer range of lanthanide-antenna distances.<sup>21</sup>

According to the aforementioned spectral overlap, in order to have an efficient energy transfer from the triplet state to the lanthanide, the triplet state should be located at least  $1500\text{ cm}^{-1}$ , but preferably  $2000$  to  $3500\text{ cm}^{-1}$  above the emitting level of the lanthanide ion.<sup>7</sup>

In particular, the undesired thermal repopulation at room temperature of the  $T_1$  can be avoided with an energy gap between  $T_1$  and the acceptor level of the lanthanide ion  $\geq 1850\text{ cm}^{-1}$ .<sup>22</sup>

In the case of too low energy difference between the triplet level and the excited lanthanide level, an undesirable back transfer (BT) can occur by drastically decreasing the energy transfer efficiency. On the other hand, if the energy of the triplet level is below the lowest emitting level of the lanthanide ion, the energy transfer will not take place at all. With this in mind, the lanthanide luminescence in coordination compounds is therefore highly sensitive to the energy position of the triplet level of the ligand.

In the case of the most used lanthanide ions, the acceptor excited state is  $20400\text{ cm}^{-1}$  for the  $^5D_4$  of the Tb(III) ion and  $17200\text{ cm}^{-1}$  for the  $^5D_0$  of the Eu(III) ion. For the aforementioned reasons, the energy for the triplet should be around  $22250\text{ cm}^{-1}$  for the optimal energy transfer to the  $^5D_4$  of the Tb(III) ion while at  $\approx 19000\text{ cm}^{-1}$  for the optimal energy transfer to  $^5D_0$  of the Eu(III) ion.

One of the causes of the not-radiative transitions of the lanthanides is attributed to the presence in the environment of some vibrational modes characterized by high energy. These modes are capable to de-activate the excited states of lanthanide ions by means of the *multiphonon relaxation (MRP) process*.

The efficiency of the MRP process is dependent on the energy gap between the emitting level and the one just below of the lanthanide ion. MPR is important if the energy gap is bridged by less than four vibrational quanta (Figure 6).

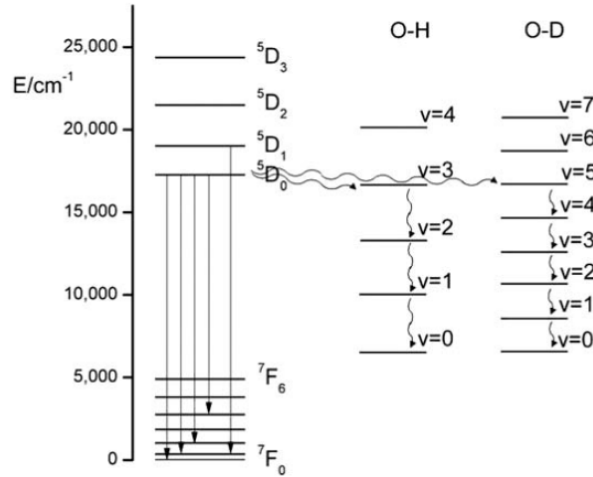


Figure 6. Radiative transitions of Eu(III) and non-radiative quenching through O-H and O-D bonds

The  ${}^5D_0$  emitting state of europium is at  $12000\text{ cm}^{-1}$  above the highest  ${}^7F_J$  level. This energy gap is covered by three O-H vibrational quanta (vibrational energy  $3600\text{ cm}^{-1}$ ). On the other hand, for the intrinsic nature of the bond O-D, the vibrational energy is lower, and in the case of the deuterium oxide the MPR is less efficient since five vibration quanta of O-D vibration ( $2200\text{ cm}^{-1}$ ) are necessary to fill the energy gap of europium. For this reason, water molecules are particularly effective in the non-radiative quenching of lanthanide excited states.

The number of water molecules bound to the metal ( $q$ , hydration number) can be determined using *Horrock's equation* (Equation 2-3).<sup>23,24</sup>

$$q = A * (\Delta K_{obs} - B) \quad (eq.2)$$

$$\Delta K_{obs} = K_{H_2O} - K_{D_2O} = \frac{1}{\tau_{H_2O}} - \frac{1}{\tau_{D_2O}} \quad (eq.3)$$

where A and B are empirical constants, K is the reciprocal of  $1/\tau$ ,  $\tau$  is the observed lifetime in water and in deuterium oxide.

Usually, in biological applications, the metal ion is surrounded by several biomolecules and for this reason, in addition to O-H vibrations of water, other vibrations, such as N-H (3300 cm<sup>-1</sup>) and C-H (2900 cm<sup>-1</sup>), could significantly contribute to vibrational quenching of Ln(III)-centered emission.<sup>24</sup>

The coordination numbers of lanthanide ions are usually above 6, and the most common are 7, 8 and 9<sup>25</sup> but they could reach also 12.<sup>26</sup>

In aqueous solution, the coordination number is usually 9 for the early lanthanides (La-Sm) and 8 for the later ones (Dy-Lu), with intermediate lanthanides (Eu, Gd and Tb) showing either of both or mixtures in equilibrium. A recent study<sup>27</sup> shows that n = 9 for all [Ln(H<sub>2</sub>O)<sub>n</sub>]<sup>3+</sup> in aqueous solution, apart from Ln = Lu (n = 8).

As previously mentioned, one of the peculiar properties of the lanthanides are the longer lifetimes respect to that one of the traditional fluorophore. The intensity of an emission transition is usually described in terms of the spontaneous emission probability (or Einstein's coefficient of spontaneous emission A). These values can be calculated for both MD and ED transitions trough the Judd-Ofelt theory.<sup>28</sup>

The radiative lifetime of the emitting level (J') is characteristic of each lanthanide ion and it is represented by the following equation (4), where the sum  $\Sigma$  is overall lower-lying levels.

$$\tau_{J'}^r = \frac{1}{\sum_{J'} A} \quad (eq.4)$$

Unfortunately, the observed lifetimes are perturbed by several additional pathways of de-excitation of the emitting level J', such as MPR and ET processes.

$\tau_{obs}$  can be written as depicted in equation (5):

$$\tau_{obs} = \frac{1}{\sum_{J'} A + W_{MPR} + \sum W_{ET}} \quad (eq.5)$$

where W is the rate of the involved process. The relative importance of radiative and not-radiative transitions is usually expresses by the *radiative quantum efficiency*  $\eta$ , also called *intrinsic quantum yield*  $\Phi_{Ln}$  (eq.6), i.e. number of emitted photons / number of absorbed photons by the lanthanide ion.

$$\frac{\tau_{obs}}{\tau_r} = \eta = \Phi_{Ln} \text{ (eq. 6)}$$

In an ideal case where the contribution of  $W_{MPR}$  and  $W_{ET}$  are equal to zero, the  $\tau_{obs}$  is equal to the  $\tau_r$  and the radiative quantum efficiency should be equal to 100%.

According to the equation 1b is possible to correlate the  $\Phi_{tot}$  with the  $\Phi_{Ln}$  for calculating the so-called sensitization efficiency ( $\eta_{sens}$ ) (eq. 7).

$$\eta_{sens} = \eta_{ISC} * \eta_{ET} = \frac{\Phi_{tot}}{\Phi_{Ln}} \text{ (eq. 7)}$$

In an ideal case, the efficiency terms of the intersystem crossing,  $\eta_{ISC}$  and by the energy transfer processes,  $\eta_{ET}$  are equal to 1 (usually they are  $<1$ ) and the total quantum yield  $\Phi_{tot}$  should be equal to the intrinsic quantum yield  $\Phi_{Ln}$ .

One of the most common methods for determining *the total quantum yield* in solution involves the use of standards. In the literature, the common employed standards are quinine bisulfate, fluorescein, and Rhodamine 6G.<sup>29</sup>

In order to get a reliable value of quantum yield it is necessary that the emission spectra are corrected. In the modern instrument this operation occurs automatically; this correction takes into account that the output of the xenon lamp is not uniform throughout the entire wavelength range and gratings change their efficiency.

The equation for calculating the total quantum yield is reported in the following equation (8).

$$\Phi_{tot(u)} = \frac{A_s * F_u * n_u^2}{A_u * F_s * n_0^2} * \Phi_s \text{ (eq. 8)}$$

The term  $u$  is referred to the unknown sample, and the  $s$  term to the standard.  $A$  is the absorbance at the excitation wavelength,  $F$  is the integrated emission area across the band, and  $n$  is the index of refraction of the solvent. In particular  $n_u$  is that one of the unknown sample and  $n_0$  is attributed to the standards solvent, both at the sodium D line and the temperature of the emission measurement. It is necessary to underline that for this measure, the values of the absorbance of

sample and standard must be similar and small (e.g. below 0.10). Furthermore, it should be more appropriate if the unknown sample and standard are in the same solvent. If this is not possible, a correction for the difference in refractive indices of the solvents must be done.<sup>30</sup>

Suitable standards for comparative determination of luminescence quantum yields in solution are reported in Table 2.

<u>Region</u>	<u>Compound</u>	<u>Solvent</u>	$\Phi_f$
270-300 nm	Benzene	Cyclohexane	0.05±0.02
300-380 nm	Tryptophan*	H <sub>2</sub> O (pH 7.2)	0.14±0.02
300-400 nm	Naphthalene	Cyclohexane	0.23±0.02
315-480 nm	2-Aminopyridine	0.1 N H <sub>2</sub> SO <sub>4</sub>	0.60±0.05
360-480 nm	Anthracene	Ethanol	0.27±0.03
400-500 nm	9,10-Diphenyl-anthracene	Cyclohexane	0.90±0.02
400-600 nm	Quinine Bisulfate	1 N H <sub>2</sub> SO <sub>4</sub>	0.546
600-650 nm	Rhodamine 101	Ethanol	1.0±0.02
600-650 nm	Cresyl Violet	Methanol	0.54±0.03

Table 2. Fluorescence quantum yield references ( $\Phi_f$ ) in various emission range at 25° C.<sup>29</sup>

Alternatively, the fluorescence quantum yield can be measured directly by employing optical devices such as the integrating sphere (also called *Ulbricht sphere*). An integrating sphere is a spherical cavity with highly-reflective (diffusive) surfaces that allows spatial integration of incoming light flux.

These materials show diffused reflectance distributed nearly according the Lambert law and the total value of reflectance is between 92 and 99 % for wavelengths from UV-B to near IR; it means that during each reflection a negligible percentage of light flux is lost.<sup>31</sup>

### 1.3. *Circularly Polarized Luminescence (CPL)*

The circularly polarized luminescence spectroscopy was exploiting since 30 years ago. CPL is a chiroptical technique which is attracting a great interest due to its wide range of applications in technological and biomedical fields,<sup>32-36</sup> essentially



by combining the sensitivity of the luminescence compounds with high brightness and the specificity of chiroptical response.

The possibility to observe the influence of the metal-ion surroundings on the CPL and CD (Circularly Dichroism) spectra represent an additional mean to study the complexity of the interaction between the ‘chiral biological world’ and the lanthanide luminescent compounds as probes.

The sophisticated and expensive instrumentations do not allow a routine use, for these reasons, the use of the CPL and CD spectra it is mainly performed by specialized research group. Furthermore, besides to the above mentioned reasons, some drawbacks like the presence of optical artefacts from various source, and electronic problems associated to weak difference signals make more challenging their use as common techniques.

In order to understand the circularly polarized luminescence phenomenon, it is fundamental to discuss the basics of the light polarization.

The unpolarized light is an electromagnetic wave constituted by an electric (E) and magnetic H field perpendicular each other and also perpendicular to the axis of propagation. Both fields are oscillating along different random direction.<sup>37</sup>

In the linearly polarized light, the electric field can be described as a vector which oscillates along one direction, perpendicular to the axis of propagation<sup>38</sup> (Figure 7).

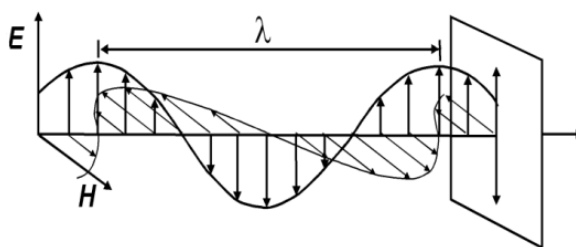


Figure 7. Schematic representation of a linearly polarized light.

In a linearly polarized light the electric field is described by a vector that, according to the parallelogram rule, can be represented by the sum of other two vectors describing the electric fields of two circularly polarized radiations, one left and the other right-handed (Figure 8a).

When the light interacts with a chiral material, as well as our Ln-complexes based on the chiral 1,2-cyclohexanediamine, one of the two circularly polarized components (left or right-handed) is preferentially absorbed and thus the vector describing the electric field of that component undergoes change of the length. The resulting vectorial sum gives rise to a vector which is circularly polarized (Figure 8b). This is the principle of the *circular dichroism*. The same principle applied to the emission of light allows us to understand the *circularly polarized luminescence*.

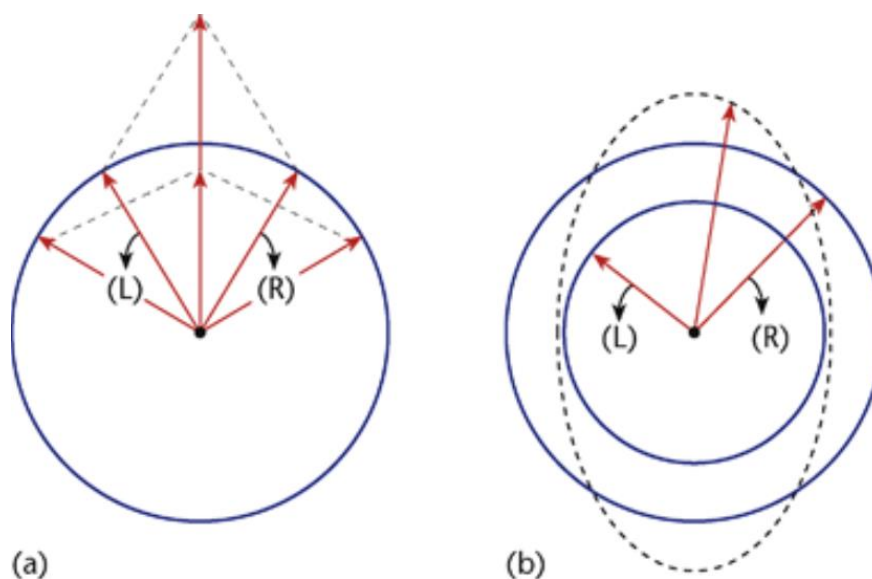


Figure 8. a) Linearly polarized light. The electric vector is composed by the sum of two vectors left and right-handed with the same length. b) Circularly polarized light. The electric vector is composed by the sum of two vectors left and right-handed with different length.

When CPL light is emitted, one component of the CP light is preferentially emitted, giving rise to a different emission intensity of the two components (eq. 9) where  $I_L$  and  $I_R$  are respectively the left and right circularly polarized light.

$$\Delta I \equiv I_L - I_R \text{ (eq. 9)}$$

The measurement of absolute emission intensity  $I$  require long time and procedures, for this reason the CPL spectra are expresses as depicted in equation (10):

$$g_{lum} = \frac{\Delta I}{\frac{1}{2}(I_L + I_R)} = \frac{I_L - I_R}{\frac{1}{2}(I_L + I_R)} \text{ (eq. 10)}$$

where  $g_{lum}$  is dimensionless and it is known as *luminescence dissymmetry factor*. It is connected to the degree of the polarization of the incoming light.

In the presence of chiral ligands,  $g_{lum}$  is different from zero; for the best of our knowledge the values for Europium (III) and Terbium (III) complexes are commonly included around 0.1 and 0.5, while for the traditional organic fluorophores the values are limited between 0.01 and 0.1.<sup>39,40</sup>

In such cases, even though the ground-state distribution of a mixture of chiral molecules is racemic, it is possible to get the CPL signal if the excited state can be enriched in one of the enantiomers. This experiment was reported in the work of C.L Maupin and J.P Riehl.<sup>41</sup>

Since the commercial instrumentation is poorly available, all the CPL measurements presented in my PhD thesis have been recorded with a homemade spectrofluoropolarimeter<sup>42,43</sup> available at Pisa University, in the research group of the Prof. Di Bari.

The basic configuration of device designed to get CPL is reported in Figure 9.

A laser system or UV lamp coupled with an excitation monochromator or a combination of filters is employed as the excitation source. As already mentioned, some optical artefacts could interfere during the measurements, commonly the presence of linear polarization in the emission. With this in mind, the signal emission is collected at an angle of 90.0° from the direction of the excitation beam, in order to avoid the detection light from the excitation source.

The luminescence from the chiral sample is first directed through a photoelastic polarization modulator (PEM), afterwards in a linear polarizer composed by focusing lenses or filters to prevent birefringence. The role of linear polarizer is to ensure that the detected light entering the monochromator is always polarized in the same direction, by preventing artefacts associated with the emission detection that it is polarization sensitive.

The PEM is made of an isotropic, clear optical material that generates an oscillating birefringence at a fixed frequency. This creates a periodic phase shift at a frequency, that it is capable to convert either right or left circularly polarized emitted light to linearly polarized light oriented at 45° to the PEM crystal axis. In this way, both PEM and linear polarizer permit the pass of alternately left then right circularly polarized light.

Afterwards, the emission light is detected by a photomultiplier tube and the originating signal is sent into an amplifier-discriminator.

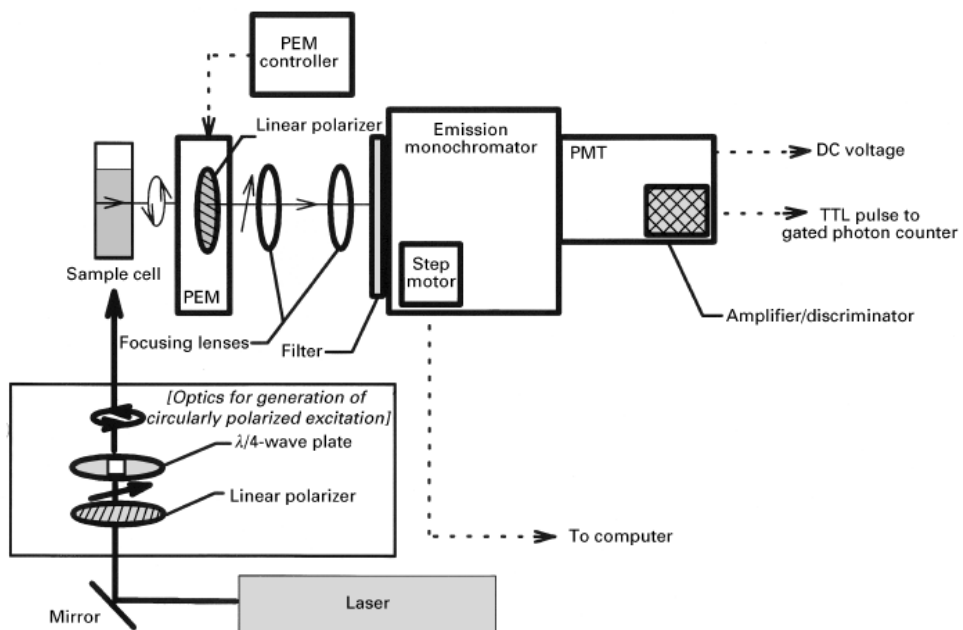


Figure 9. Schematic diagram of an instrument designed to measure circularly polarized luminescence

#### 1.4. ***EXPERIMENTAL RESULTS- Effect of the counterion on Circularly Polarized Luminescence (CPL) of Eu(III) and Sm(III) complexes***

In this contribution, both enantiopure nitrate  $[\text{LnL1}(\text{L2})_2(\text{H}_2\text{O})]\cdot\text{NO}_3$  and triflate  $[\text{LnL1}(\text{L2})_2(\text{H}_2\text{O})]\cdot\text{CF}_3\text{SO}_3$  Eu(III) complexes; with **L1** = N,N'-bis(2-pyridylmethylidene)-1,2-(*R,R+S,S*)-cyclohexanediamine,<sup>44,45</sup> **L2** = 2-thenoyltrifluoroacetyl-acetonate (commercially available) and one chiral tetradentate Schiff base NNNN ligand (Figure 10) have been synthesized and characterized, by using also chiroptical technique such as Electronic Circular Dichroism (ECD) and CPL (Figure 17).

With the aim to enlarge the repertory of Samarium complexes exhibiting CPL, a similar study has been performed on analogous Sm(III) complexes (Figure 13).

The encapsulation of the water insoluble and chiral  $[\text{Eu}(\text{L1})(\text{L2})_2(\text{H}_2\text{O})]\cdot\text{CF}_3\text{SO}_3$  complex in PLGA nanoparticles entails a potential advantage, that is the use of CPL spectroscopy<sup>46</sup> as a tool to investigate such biocompatible material.

Since the chiral cyclohexanediamine has been employed in both enantiomeric forms, it has been possible to exploit the nanoparticles PLGA-Ln(III)-complexes based on L2 (= 2-thenoyltrifluoroacetyl-acetonate) even for CPL measurements. Even if the encapsulated complex has not shown CPL activity, further CPL studies on the single molecule revealed a good CPL activity and an unexpected role of the counterion (triflate or nitrate) and of the solvent (dichloromethane, acetonitrile and methanol).<sup>47</sup>

In all cases, both ligands are capable to sensitize the luminescence of both metal ions upon absorption of light around 280 and 350 nm. Despite their similar Total Luminescence (TL) and ECD spectra, the CPL activity of the complexes is strongly influenced by a synergistic effect of the solvent and the counterion.

For this contribution, a recent paper reported by Wada et al.<sup>48</sup> has inspired our work. In this context they proved that the chiral geometric environment around Eu(III) and also its CPL signature can undergo a substantial change depending on the addition of further achiral molecules [acetone or triphenylphosphine oxide (tppo)] which coordinate the metal ion. It means that a simultaneous contribution

of chiral and achiral ligands can be taken into account when chiroptical activity such as CPL is concerned. In principle, this is quite unexpected, since usually only chiral molecules are capable to determine the chiroptical properties of a compound.

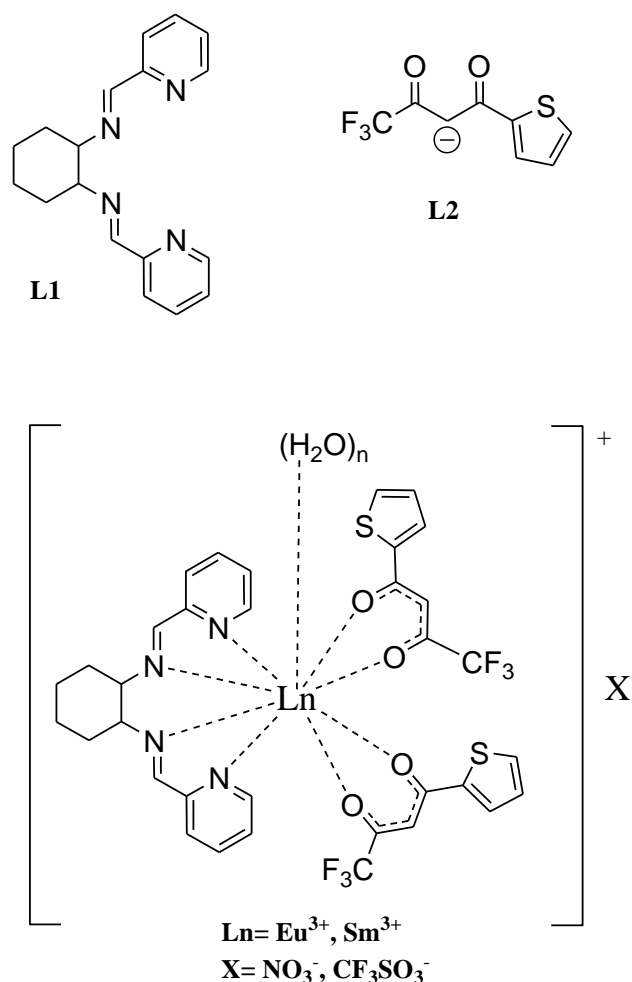


Figure 10. Molecular structure of the ligands and Ln-complexes under investigation in the present contribution. Ln = Sm and Eu; X = NO<sub>3</sub> and CF<sub>3</sub>SO<sub>3</sub>; n = 0 or 1. Both enantiomers of the ligand have been employed.

#### 1.4.1. UV-visible Absorption and Electronic Circular Dichroism (ECD)

Since the UV-visible electronic absorption spectra and ECD spectra of the triflate complexes [EuL1(L2)<sub>2</sub>(H<sub>2</sub>O)]CF<sub>3</sub>SO<sub>3</sub> and [SmL1(L2)<sub>2</sub>(H<sub>2</sub>O)]CF<sub>3</sub>SO<sub>3</sub> in

acetonitrile are perfectly superimposable, the effect of the employed metal ion (Sm or Eu) on this chiroptical property is completely negligible (Figure 11).

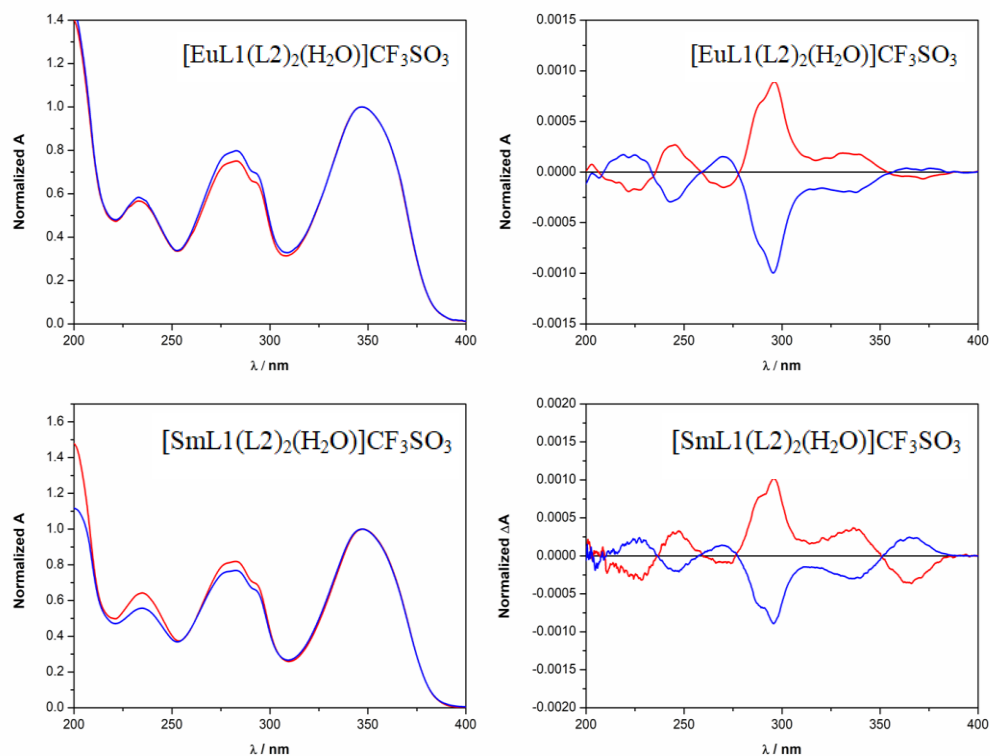


Figure 11. UV-visible absorption (left) and ECD (right) spectra of  $[\text{EuL1}(\text{L2})_2(\text{H}_2\text{O})]\cdot\text{CF}_3\text{SO}_3$  (top) and  $[\text{SmL1}(\text{L2})_2(\text{H}_2\text{O})]\cdot\text{CF}_3\text{SO}_3$  (bottom) in acetonitrile. The spectra of the *R,R* enantiomers are reported in blue while the spectra of the *S,S* enantiomers are reported in red. Both UV-Vis and ECD spectra are normalized on the maximum absorbance value of the band centered at 350 nm.

The absorption band around 350 nm can be attributed to the diketonate-centered singlet-singlet  $\pi\text{-}\pi^*$  enolic transition<sup>49</sup> whereas the absorption band peaking around 280 nm is due to the electronic transitions involving both the pyridine ring and the conjugated C=N group (i.e.  $\pi\text{-}\pi^*$ ,  $n\text{-}\pi^*$  transitions) of the ligand L1.<sup>46</sup> The sign of the ECD bands reflects the stereochemistry of the chiral ligand L1, which is also capable to favour a preferred sense of twist of the diketonates, as demonstrated by a dichroic signal around 350 nm, where only the absorption of tta takes place.

Some slight differences either in the absorption and ECD spectra are detected upon changing the solvent from acetonitrile to methanol and by using nitrate instead of triflate as counteranion (Figure 12-14).

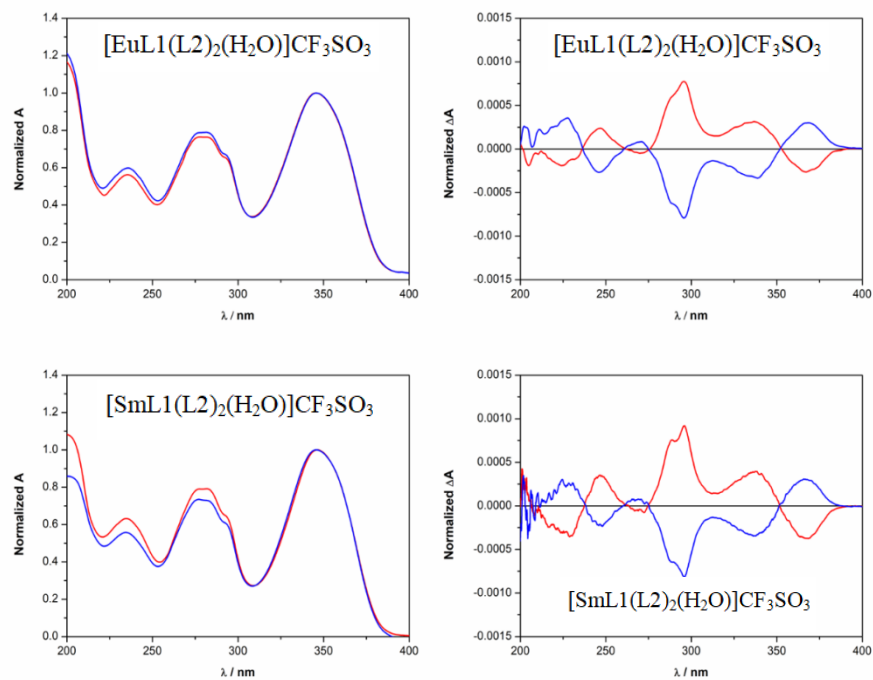


Figure 12. UV-visible Absorption (left) and ECD (right) spectra of  $[\text{EuL1}(\text{L2})_2(\text{H}_2\text{O})]\cdot\text{CF}_3\text{SO}_3$  (top) and  $[\text{SmL1}(\text{L2})_2(\text{H}_2\text{O})]\cdot\text{CF}_3\text{SO}_3$  in methanol.

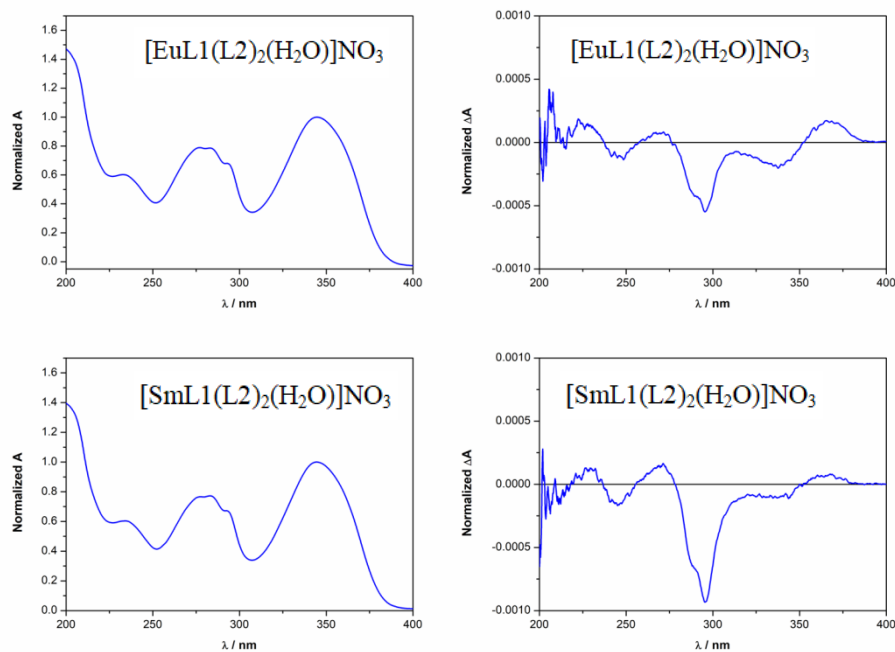


Figure 13. UV-visible Absorption (left) and ECD (right) spectra of  $[\text{EuL1}(\text{L2})_2(\text{H}_2\text{O})]\cdot\text{NO}_3$  (top) and  $[\text{SmL1}(\text{L2})_2(\text{H}_2\text{O})]\cdot\text{NO}_3$  (down) in acetonitrile (the complexes with *R,R* stereochemistry are chosen as representative).



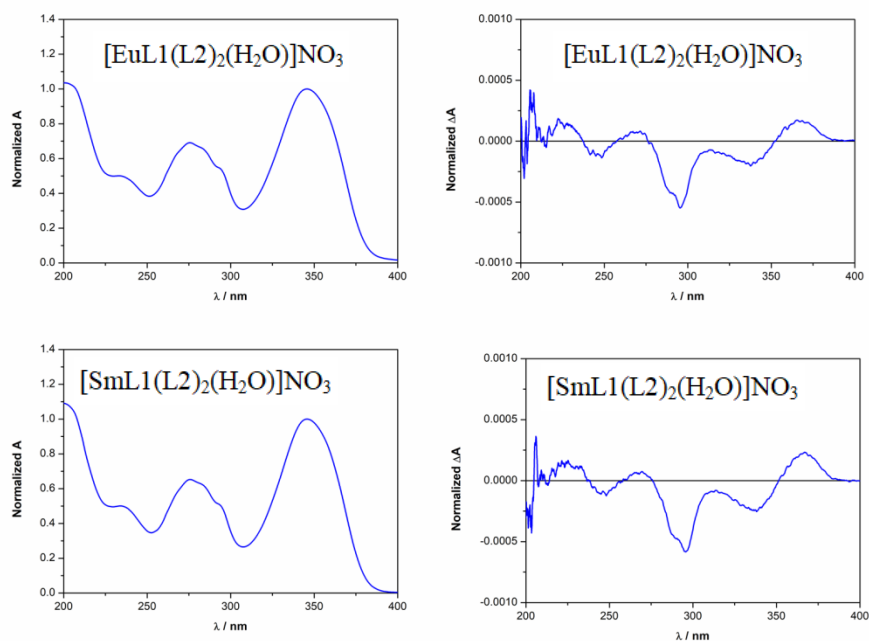


Figure 14. UV-visible Absorption (left) and ECD (right) spectra of  $[\text{EuL1}(\text{L2})_2(\text{H}_2\text{O})]\cdot\text{NO}_3$  (top) and  $[\text{SmL1}(\text{L2})_2(\text{H}_2\text{O})]\cdot\text{NO}_3$  (down) in methanol (the complexes with *R,R* stereochemistry are chosen as representative).

Most probably, the small differences are due to some minor structural rearrangements for the different lanthanide ion, solvent and counterion.

## 1.4.2. Total Luminescence (TL), CPL and luminescence decay kinetics

### 1.4.2.1. Eu complexes

The TL spectra of the  $[\text{EuL1}(\text{L2})_2(\text{H}_2\text{O})]\cdot\text{CF}_3\text{SO}_3$  and  $[\text{EuL1}(\text{L2})_2(\text{H}_2\text{O})]\cdot\text{NO}_3$  are compatible with an emitting Eu(III) ion surrounded by a crystal field whose geometry deviates significantly from the inversion symmetry, as the  ${}^5\text{D}_0 \rightarrow {}^7\text{F}_2$  transition dominates the spectra (Figure 15 and 17).

As already discussed, the typical red luminescence of Eu(III) is sensitized by either *Pyridine L1* ( $\approx 280$  nm) and *L2 ligand* ( $\approx 350$  nm).

Upon changing of solvent and counterion, whereas minor differences were detected for the TL spectra, considerable effects are recorded for the CPL spectra. Whilst the CPL signatures of the two enantiomers of the triflate complexes are the exact specular images in all the employed solvents, the intrinsic shape of the CPL spectra is strongly dependent on the solvent (Figure 15).

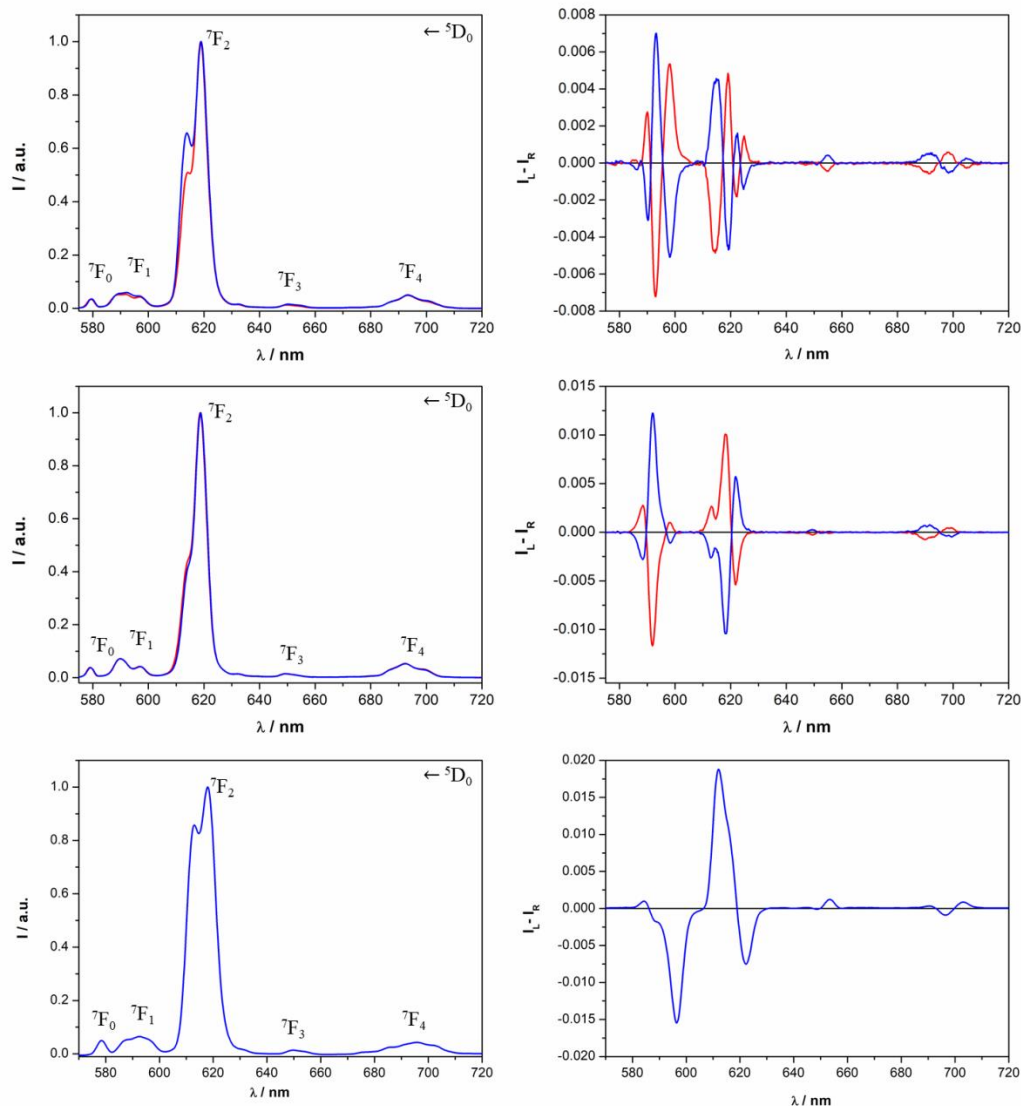


Figure 15. TL (left) and CPL (right) spectra of  $[\text{EuL1}(\text{L2})_2(\text{H}_2\text{O})]\cdot\text{CF}_3\text{SO}_3$  complex dissolved in acetonitrile (top), methanol (middle) and dichloromethane (bottom) ( $\lambda_{\text{exc}}=365$  nm). The spectra of the *R,R* enantiomer are reported in blue while the spectra of the *S,S* enantiomer are reported in red. Both the TL and CPL intensities are normalized on the maximum of the  ${}^5\text{D}_0 \rightarrow {}^7\text{F}_2$  transition.

Moreover, it is worth noting that  $[\text{EuL1}(\text{L2})_2(\text{H}_2\text{O})]\cdot\text{CF}_3\text{SO}_3$  complex possessing the same ligand stereochemistry shows CPL spectra which are nearly inverted when the complex is dissolved in methanol and dichloromethane (Figure 15 and 16).

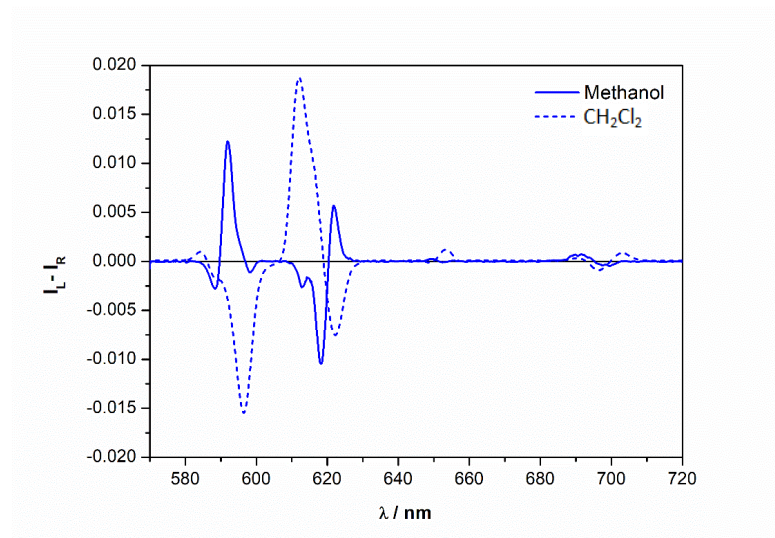


Figure 16. Comparison between the normalized CPL spectra of  $(R,R)$ - $[\text{EuL1}(\text{L2})_2(\text{H}_2\text{O})]\cdot\text{CF}_3\text{SO}_3$  in methanol (blue line) and in dichloromethane (dashed blue line).

In addition, for the  ${}^5\text{D}_0 \rightarrow {}^7\text{F}_2$  transition, we observed three bands in methanol and four bands, two positive and two negative, in acetonitrile (in the TL spectra only two bands are visible in both cases).

As far as the nitrate complex  $[\text{EuL1}(\text{L2})_2(\text{H}_2\text{O})]\cdot\text{NO}_3$  in which the ligand L1 possesses  $R,R$  stereochemistry is concerned, we observed the same behaviour described for the triflate complex in methanol and dichloromethane (Figure 17). In contrast to the CPL spectrum of  $[\text{EuL1}(\text{L2})_2(\text{H}_2\text{O})]\cdot\text{CF}_3\text{SO}_3$  in acetonitrile, the one of  $[\text{EuL1}(\text{L2})_2(\text{H}_2\text{O})]\cdot\text{NO}_3$  in this same solvent is more similar to the spectrum recorded in dichloromethane (Figure 17).

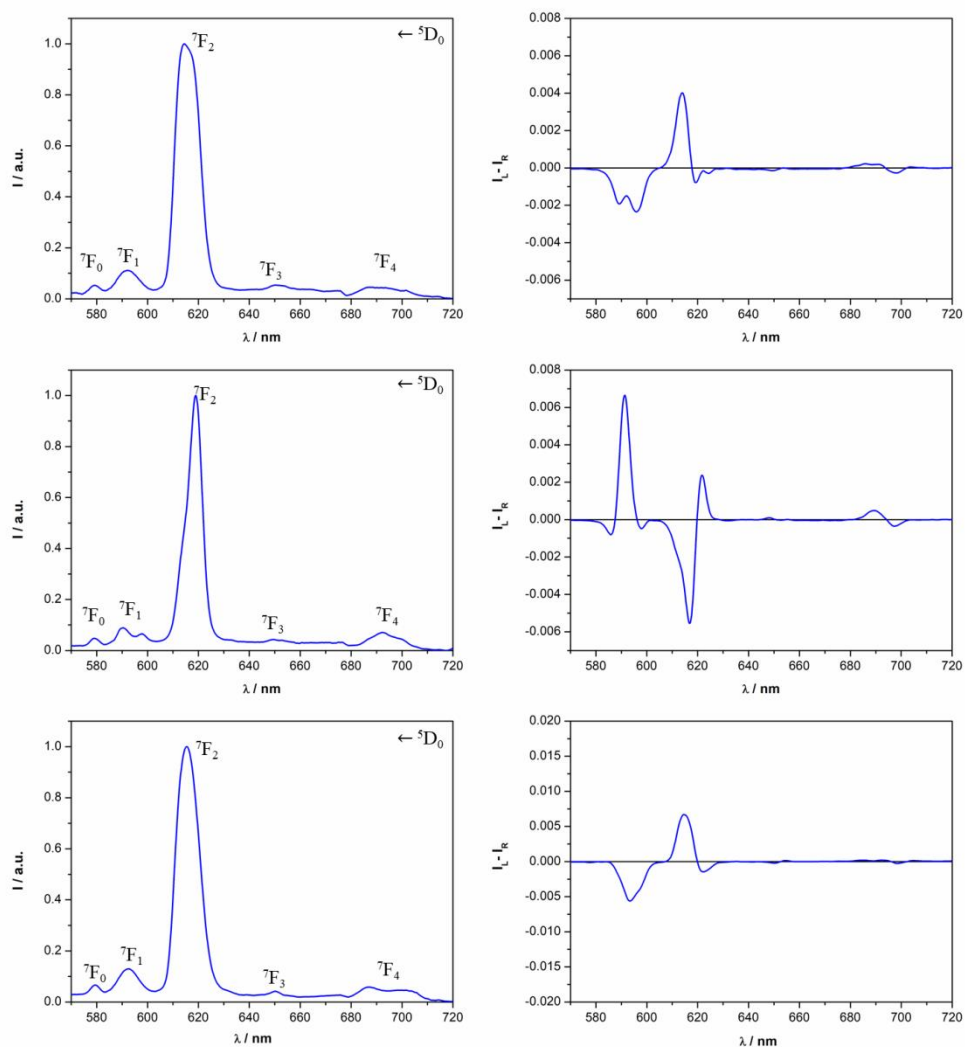


Figure 17. TL (left) and CPL (right) spectra of  $[\text{EuLi}(\text{L}2)_2(\text{H}_2\text{O})]\cdot\text{NO}_3$  complex dissolved in acetonitrile (top), methanol (middle) and dichloromethane (bottom) ( $\lambda_{\text{exc}}=365$  nm). Both the TL and CPL intensities are normalized on the maximum of the  ${}^5\text{D}_0 \rightarrow {}^7\text{F}_2$  transition. The ligand L has R,R stereochemistry.

In conclusion, it is clear that both the nature of the solvent and counterion play a crucial role for determining the CPL activity of the complex. It is worth noting that in the case of the enantiopure triflate and nitrate Eu complexes, the CPL spectra in acetonitrile is superimposable to weighed linear combinations of two CPL spectra of the same complex recorded in methanol and dichloromethane (Figure 18).

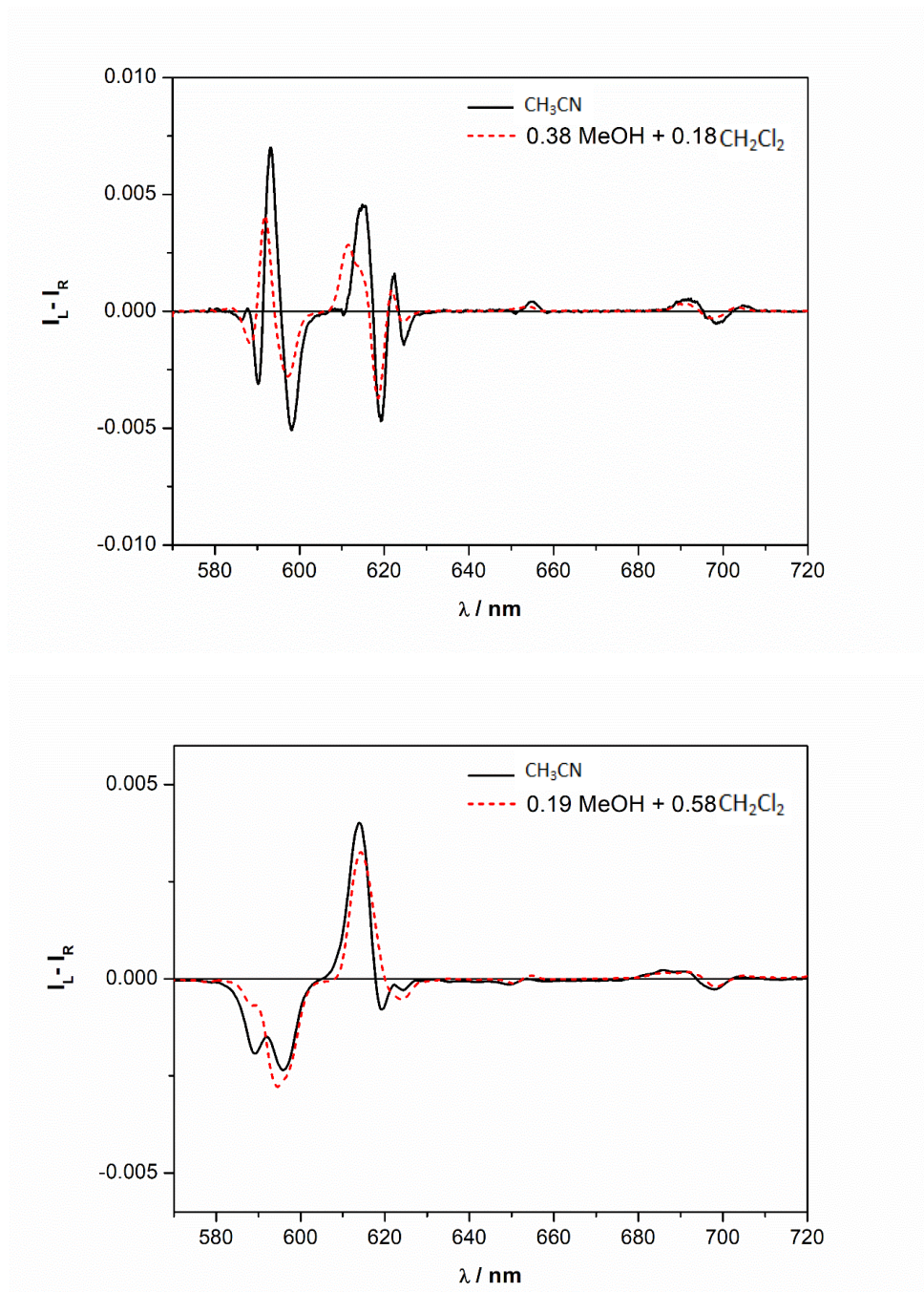


Figure 18. Top: CPL spectra of  $(R,R)\text{-[EuL1(L2)}_2(\text{H}_2\text{O})]\cdot\text{CF}_3\text{SO}_3$  when dissolved in acetonitrile (black line) and as a linear combination of the CPL signature in methanol and dichloromethane (red dashed line). Bottom: CPL spectra of  $(R,R)\text{-[EuL1(L2)}_2(\text{H}_2\text{O})]\cdot\text{NO}_3$  when dissolved in acetonitrile (black line) and as a linear combination of the CPL signature in methanol and dichloromethane (red dashed line).

In order to explain the *intrinsic CPL spectra footprint* of the two complexes in different solvents, it was supposed that *in apolar solvents* such as dichloromethane, both *triflate and nitrate anions are directly bound to the metal cation*, whereas *in the polar and protic methanol they are completely dissociated*.

In this way, the presence or absence of the anion in the first coordination sphere of Eu(III) is capable to determine two different CPL signature (Figure 15 and Figure 17).

In the case of acetonitrile as solvent, the overall CPL spectra are the results of the coexistence of both dissociated and undissociated species, but their relative amounts depend on the counteranion. In fact, in the case of triflate there is a prevailing presence of the dissociated species whilst in the case of nitrate the situation is the opposite (a qualitative comparison it is possible by the different intensities in Figure 18). These findings are reasonable explained with the different coordination ability of the corresponding anion.

Since the nitrate anion has an high affinity for the lanthanide ions if compared to coordinating solvents ( $\text{NO}_3^- > \text{DMSO}$  (dimethylsulfoxide)  $> \text{DMF}$  (N,N-dimethylformamide)  $> \text{H}_2\text{O} > \text{CH}_3\text{CN}$  (acetonitrile)),<sup>50</sup> the nitrates behave as non-electrolytes in anhydrous  $\text{CH}_3\text{CN}$ , also at low concentration (0.2 mM)<sup>51</sup> and relatively high amounts of a strong donating ligand like DMSO (concentration ratio  $[\text{DMSO}]/[\text{Ln}^{3+}] = 9$ ) are needed in order to replace the nitrate ion from the inner coordination sphere.<sup>50</sup> The triflates are considered good electrolytes in  $\text{CH}_3\text{CN}$ , and they are completely dissociated at concentration lower than 0.05 mM in anhydrous  $\text{CH}_3\text{CN}$ .<sup>52</sup>

As far as the degree of polarization of the emitted light and the decay kinetics of the  $^5\text{D}_0$  Eu(III) excited state are concerned, the highest values of the luminescence dissymmetry factor  $g_{\text{lum}}$  for all the Eu(III) complexes are reported in Table 3, together with the observed excited state lifetimes.

Complex	$g_{\text{lum}}$			observed lifetime (ms)		
	solvent			solvent		
	DCM	methanol	$\text{CH}_3\text{CN}$	DCM	$\text{CH}_3\text{OH}/\text{CD}_3\text{OD}$	$\text{CH}_3\text{CN}$
( <i>R,R</i> )- [EuL1(L2) <sub>2</sub> (H <sub>2</sub> O)]·CF <sub>3</sub> SO <sub>3</sub>	-0.23	+0.17	+0.11	0.54(1)	0.57(1)/ 0.75(1)	0.44(1)
( <i>R,R</i> )- [EuL1(L2) <sub>2</sub> (H <sub>2</sub> O)]·NO <sub>3</sub>	-0.05	+0.07	-0.02	0.53(1)	0.42(1)/ 0.52(1)	0.53(1)

Table 3. Values of the emission dissymmetry factor  $g_{\text{lum}}$  and  $^5\text{D}_0$  Eu(III) excited state lifetimes of the Eu(III) complexes under investigation dissolved in different solvents. The  $g_{\text{lum}}$  values are referred to the most intense component of the  $^5\text{D}_0 \rightarrow ^7\text{F}_1$  transition.

The highest  $|\text{glum}|$  is recorded for  $[\text{EuL1}(\text{L2})_2(\text{H}_2\text{O})]\cdot\text{CF}_3\text{SO}_3$  in dichloromethane. Interestingly, the magnitude and the signs of the  $\text{glum}$  factors retrace at a glance the chemical behaviour of both the triflate and nitrate complexes in the three different solvents. In fact, the  $R,R$  enantiomers of the complexes present the highest negative  $\text{glum}$  values in  $\text{CH}_2\text{Cl}_2$  and the highest positive  $\text{glum}$  values in methanol, whilst in acetonitrile the  $\text{glum}$  factors reach an intermediate value. In particular, in the case of the triflate complex in acetonitrile,  $\text{glum}$  is positive and closer to the one recorded in methanol, as expected given the low coordinating ability of the anion. On the other hand, the  $\text{glum}$  for the nitrate complex in  $\text{CH}_3\text{CN}$  is negative and closer to the one recorded in  $\text{CH}_2\text{Cl}_2$ , thus indicating that the anion is essentially coordinated to the lanthanide ion.

All the decay curves are well fitted by a single exponential function, (for nitrate complexes, Figure 19; for triflate complexes, see ref. [46]) and the lifetimes in methanol and  $\text{CH}_2\text{Cl}_2$ , which represent the two extreme cases, are rather similar in the case of triflate complexes. As discussed in this reference<sup>46</sup> the presence of one water molecule in the inner coordination sphere of the metal ion when the triflate complex is dissolved in  $\text{CH}_3\text{CN}$ , is responsible of the multiphonon relaxation phenomenon, which reduces the value of the observed lifetime.

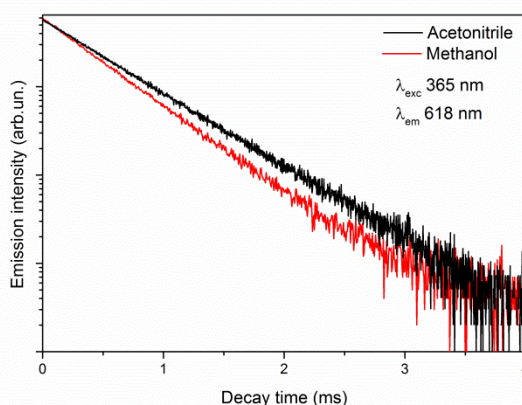


Figure 19. Room temperature decay curves of the  $^5D_0$   $\text{Eu}(\text{III})$  emission excited around 365 nm in methanol and acetonitrile solutions for  $[\text{EuL1}(\text{L2})_2(\text{H}_2\text{O})]\cdot\text{NO}_3$ . The decay curves of the complex in dichloromethane are not shown, as it is superimposable to the one recorded in acetonitrile.

In the case of nitrate complexes, it is worth noting the similarity of the observed lifetimes in  $\text{CH}_2\text{Cl}_2$  and  $\text{CH}_3\text{CN}$  (0.53 ms, Table 3). This finding is in agreement

with the conclusions drawn by CPL spectroscopy: in fact, due to the high affinity toward the metal center, the chelation of nitrate contributes to hinder the access to Eu(III) ion by solvent molecules and consequently the solvent molecules ( $\text{CH}_2\text{Cl}_2$  or  $\text{CH}_3\text{CN}$ ) does not show any influence on the lifetime value.

Furthermore, the addition of one drop of  $\text{D}_2\text{O}$  in the  $\text{CH}_3\text{CN}$  solution of the nitrate complex should increase the value of the Eu(III) lifetime if water molecules are bound to the metal ion, since as a consequence of  $\text{D}_2\text{O}/\text{H}_2\text{O}$  exchange, high energy vibrations (OH) capable to reduce the value of the Eu(III) observed lifetime by multiphonon relaxation process, are removed from the inner coordination sphere. Since upon  $\text{D}_2\text{O}$  addition the lifetime values does not change significantly [0.50(1) vs 0.53(1) ms], the presence of bound water can be ruled out.

When the  $[\text{EuL1}(\text{L2})_2(\text{H}_2\text{O})]\cdot\text{NO}_3$  complex is dissolved in deuterated methanol ( $\text{CD}_3\text{OD}$ ), an increase of the Eu(III) lifetime value was detected. From the equation reported in the literature<sup>53</sup> the number of bound methanol molecules ( $m$ ) can be obtained by  $m = 2.1 * \left( \frac{1}{\tau_{\text{obsCH}_3\text{OH}}} - \frac{1}{\tau_{\text{obsCD}_3\text{OD}}} \right)$ .

The calculated value of  $m = 1.0(5)$  is compatible with the presence of one methanol molecule in the inner coordination sphere of the metal center. The same conclusion can be drawn for the triflate complex.<sup>46</sup>

Moreover, the quite similar luminescence decay times, recorded for triflate and nitrate complexes dissolved in different solvents, is indicative of a similar intrinsic quantum yield (in the 50-70% range), already determined for  $[\text{EuL1}(\text{L2})_2(\text{H}_2\text{O})]\cdot\text{CF}_3\text{SO}_3$ .<sup>46</sup>

#### 1.4.2.2. *Sm complexes*

From the inspection of the TL and CPL spectra (Figure 20 and Figure 21), we can conclude that all Sm(III)-based complexes efficiently emit polarized light, in particular around 600 nm (corresponding to  $^4\text{G}_{5/2} \rightarrow ^6\text{H}_{7/2}$  transition). Other than the luminescence of Eu(III) the tta ligand ( $\lambda_{\text{exc}}=365$  nm) is capable to effectively transfer its excitation energy to Sm(III).



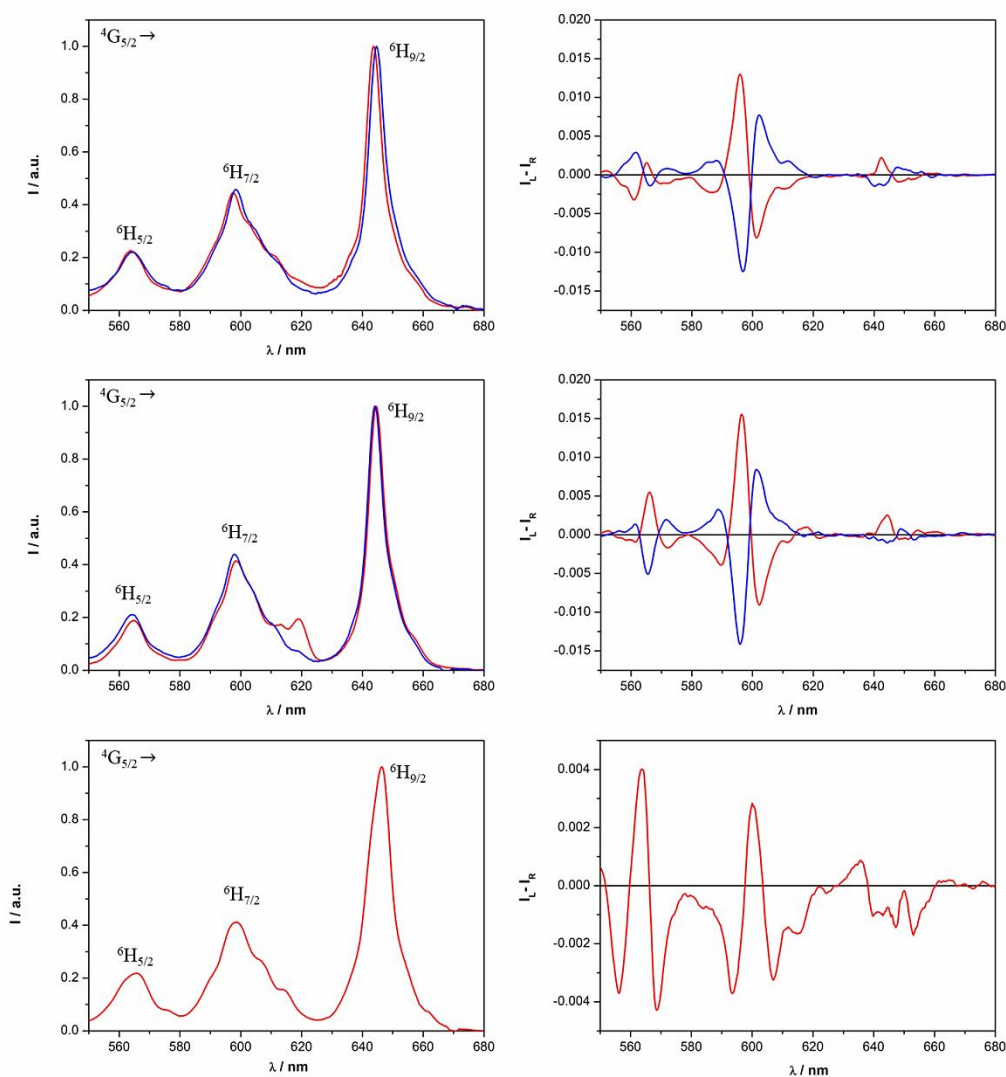


Figure 20. TL (left) and CPL (right) spectra of  $[\text{SmL1}(\text{L2})_2(\text{H}_2\text{O})]\cdot\text{CF}_3\text{SO}_3$  complex dissolved in acetonitrile (top), methanol (middle) and dichloromethane (bottom) ( $\lambda_{\text{exc}}=365$  nm). The spectra of the *R,R* enantiomer are reported in blue while the spectra of the *S,S* enantiomer are reported in red. Both the TL and CPL intensities are normalized on the maximum of the  ${}^4\text{G}_{5/2}\rightarrow{}^6\text{H}_{9/2}$  transition.

In contrast to the analogous Eu(III) complexes, independently of the solvent the sequences of the signals in the CPL spectra of triflate Sm(III) complexes are quite similar. However, in acetonitrile and methanol the intensities of the CPL bands associated to the  ${}^4\text{G}_{5/2}\rightarrow{}^6\text{H}_{7/2}$  ( $\sim 600$  nm) transition are higher than the ones recorded in dichloromethane. In the case of the CPL spectra of nitrate Sm(III) complexes (Figure 21), the main differences can be seen in the region centered around 560 nm ( ${}^4\text{G}_{5/2}\rightarrow{}^6\text{H}_{5/2}$ ): in  $\text{CH}_3\text{CN}$  and  $\text{CH}_2\text{Cl}_2$  only one CPL band is present, whilst in methanol there are three CPL bands.

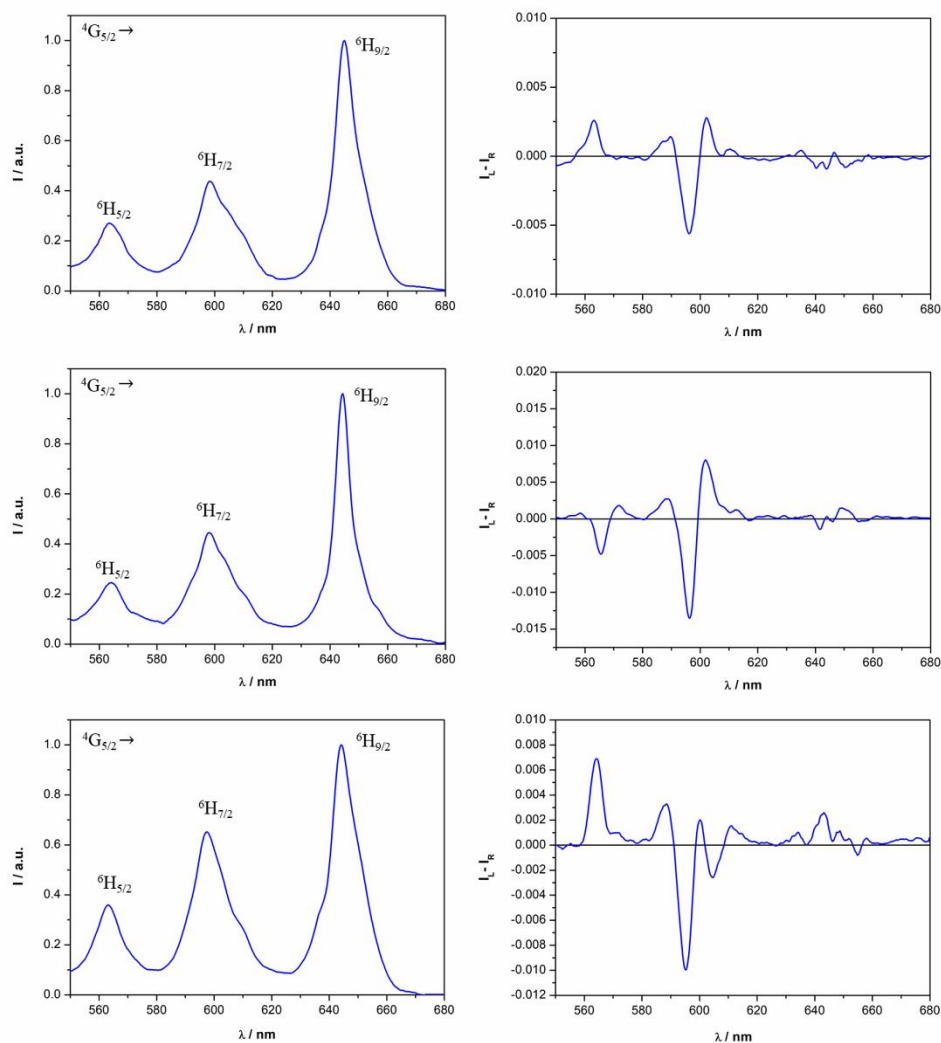


Figure 21. TL (right) and CPL (left) spectra of  $[\text{SmL1}(\text{L2})_2(\text{H}_2\text{O})_2]\cdot\text{NO}_3$  complex dissolved in acetonitrile (top), methanol (middle) and dichloromethane (bottom). The complexes with *R,R* stereochemistry are chosen as representative.

These aspects can be related once again to the role of the counterion. Triflate and nitrate should be significantly coordinated to Sm(III) in DCM whilst they should be preferentially dissociated in methanol. In acetonitrile however, triflate ion is preferentially dissociated while nitrate ion is still preferentially coordinated to the metal center. The values of luminescence dissymmetry factor  $g_{\text{lum}}$  and the observed excited state lifetimes are reported in the Table 4 (see also Figure 22).

Complex	$g_{lum}$			observed lifetime ( $\mu s$ )		
	solvent			solvent		
	CH <sub>2</sub> Cl <sub>2</sub>	MeOH	CH <sub>3</sub> CN	CH <sub>2</sub> Cl <sub>2</sub>	CH <sub>3</sub> OH/ CD <sub>3</sub> OD	CH <sub>3</sub> CN
( <i>S,S</i> )- [SmL1(L2) <sub>2</sub> (H <sub>2</sub> O)]· CF <sub>3</sub> SO <sub>3</sub>	+0.007	+0.035	+0.03	28.1(1)	17.9(1)/ 37.8(1)	25.2(1)
( <i>R,R</i> )- [SmL1(L2) <sub>2</sub> (H <sub>2</sub> O)]· NO <sub>3</sub>	-0.016	-0.034	-0.015	28.3(1)	18.6(1)/ 32.6(1)	25.6(1)

Table 4. Values of the emission dissymmetry factor  $g_{lum}$  and  $^4G_{5/2}$  Sm(III) excited state lifetimes of the Sm(III) complexes under investigation dissolved in different solvents. The  $g_{lum}$  values are referred to the positive band of the  $^4G_{5/2} \rightarrow ^6H_{7/2}$  transition in the case of (*S,S*)-[SmL1(L2)<sub>2</sub>(H<sub>2</sub>O)]·CF<sub>3</sub>SO<sub>3</sub> and to the negative band in the case of (*R,R*)-[SmL1(L2)<sub>2</sub>(H<sub>2</sub>O)]·NO<sub>3</sub>

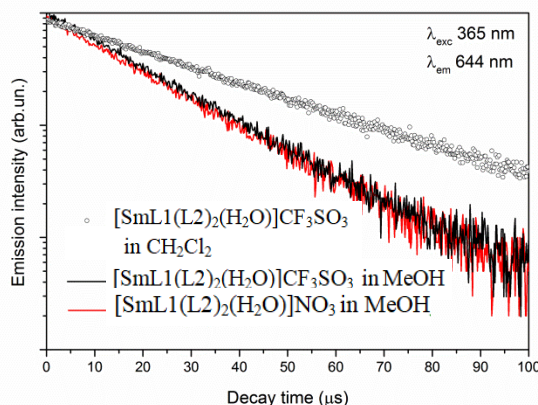


Figure 22. Room temperature decay curves of the  $^4G_{5/2}$  Sm(III) emission excited around 365 nm in dichloromethane (CH<sub>2</sub>Cl<sub>2</sub>) and methanol (MeOH) solutions for [SmL1(L2)<sub>2</sub>(H<sub>2</sub>O)]·NO<sub>3</sub> and [SmL1(L2)<sub>2</sub>(H<sub>2</sub>O)]·CF<sub>3</sub>SO<sub>3</sub>.

The highest absolute value of  $g_{lum}$  is obtained for the complexes when they are dissolved in methanol. Conversely to the Eu(III) complexes, in the case of Sm(III), being the sequence of the signals of the  $^4G_{5/2} \rightarrow ^6H_{7/2}$  transition essentially the same, the signs of the  $g_{lum}$  for the same enantiomer do not change in the three investigated solvents. As expected, the values of the  $|g_{lum}|$  factors recorded in CH<sub>3</sub>CN lie close to the ones recorded in methanol in the case of the triflate complex, and close to the one recorded in CH<sub>2</sub>Cl<sub>2</sub> for the nitrate complex.

Also the decay curves of the Sm(III) luminescence are well fitted by a single exponential function. As the values of the observed lifetimes fall in the  $\mu\text{s}$  range in all the solvents, we can conclude that the Sm(III) emission efficiency is not so low even in non-deuterated solvents. In this context, it is useful to remind that a good Sm(III) cryptate emitter shows a lifetime around 90  $\mu\text{s}$  in deuterated methanol.<sup>54</sup> Clearly, L1 and L2 ligands can protect effectively the metal ion from the intrusion of solvent molecules capable to activate the multiphonon relaxation mechanism. Unlike the analog triflate Eu(III) complexes, where one water molecule was detected in the inner coordination sphere, when the complex was dissolved in  $\text{CH}_3\text{CN}$ , in the case of triflate (and nitrate) Sm(III) complexes no water molecule should be present in the close proximity of the cation, since the lifetime observed in this solvent are relatively high (at least higher than in the case of methanol solution). This conclusion is supported by the  $\text{D}_2\text{O}/\text{H}_2\text{O}$  exchange experiments in  $\text{CH}_3\text{CN}$ , described above for Eu(III) complexes. Both for  $[\text{SmL1}(\text{L1})_2(\text{H}_2\text{O})]\cdot\text{CF}_3\text{SO}_3$  and  $[\text{SmL1}(\text{L2})_2(\text{H}_2\text{O})]\cdot\text{NO}_3$  the value of the Sm(III) lifetime does not change significantly upon addition of one drop of  $\text{D}_2\text{O}$  to the  $\text{CH}_3\text{CN}$  solution of the complexes [28.8(1) ms and 27.5(1) ms, respectively]. Nitrate and triflate complexes when dissolved in the same solvent showed a very similar luminescence lifetime. The lower lifetime values recorded in methanol are compatible with the presence of high energy vibrations (OH) close to the metal center, capable to activate a multiphonon relaxation process. Accordingly, when the triflate and nitrate complexes are dissolved in  $\text{CD}_3\text{OD}$ , the value of the Sm(III) lifetime increases (Table 4) in line with a  $\text{CD}_3\text{OD}\rightarrow\text{CH}_3\text{OH}$  substitution in the inner coordination sphere.

Concluding, it has been widely discussed the unexpected role of the counterion (triflate or nitrate) and the solvent (dichloromethane, acetonitrile and methanol) on the CPL activity of Eu(III) and Sm(III) complexes containing tta and a tetra-aza pyridine-based chiral ligand as antennae.

In particular, in the Eu(III) complexes, the CPL spectra of the species possessing the *same ligand stereochemistry* are nearly inverted if dichloromethane or Methanol are employed. This effect is attributed to the presence (in dichloromethane) or absence (in methanol) of the anion in the first coordination

sphere of Eu(III). An intermediate situation is observed in acetonitrile, even though nitrate is preferentially coordinated to the metal ion whilst the triflate is preferentially dissociated. To the best of our knowledge, this is the first case where achiral entities (counteranion and solvent) play such a strong effect on the CPL activity of chiral Ln(III) complexes, despite both their total luminescence and ECD spectra are nearly unaffected.

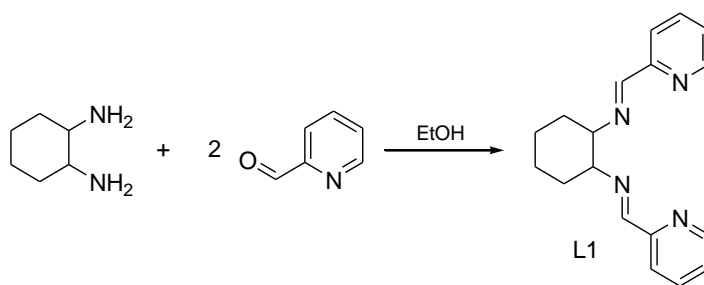
### ***1.4.3. Effect of the counterion on Circularly Polarized Luminescence (CPL) of Eu(III) and Sm(III) complexes: procedures, techniques and characterization***

#### ***1.4.3.1. Materials***

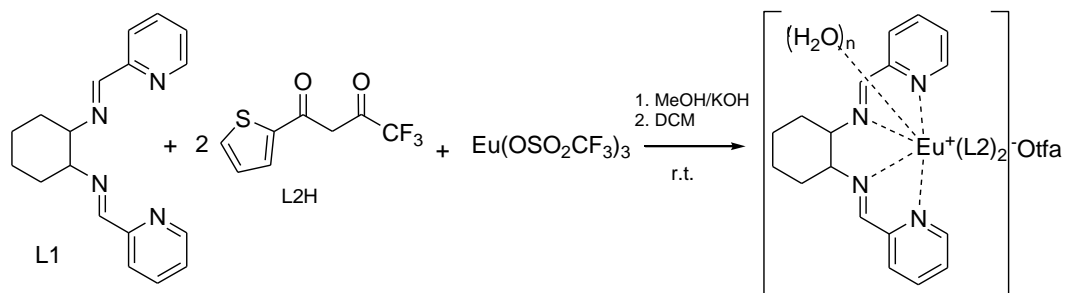
Eu(CF<sub>3</sub>SO<sub>3</sub>)<sub>3</sub>, Sm(CF<sub>3</sub>SO<sub>3</sub>)<sub>3</sub>, Eu(NO<sub>3</sub>)<sub>3</sub>·6H<sub>2</sub>O and Sm(NO<sub>3</sub>)<sub>3</sub>·6H<sub>2</sub>O (Merck, 98%) were stored under vacuum for several days at 80°C and then transferred in a glove box.

#### ***1.4.3.2. Synthesis***

*N,N'*-bis(2-pyridylmethylidene)- 1,2-(*R,R+S,S*)-cyclohexanediamine (**L1**) were synthesized by following the procedures reported in literature from our research group<sup>44,45</sup> (Scheme 1), as well as the complex [Eu**L1**(**L2**)<sub>2</sub>(H<sub>2</sub>O)]·CF<sub>3</sub>SO<sub>3</sub> that was synthesized as reported in the previous literature<sup>46</sup> (Scheme 2).



*Scheme 1. Synthesis of imine L1*

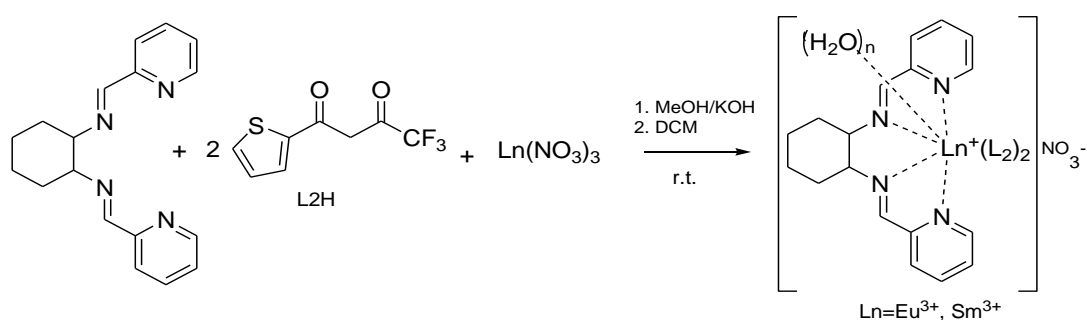


Scheme 2. Synthesis of complex  $[EuL1(L2)_2(H_2O)_n] \cdot CF_3SO_3$

***N,N'*-(cyclohexane-1,2-diyl)bis(1-(pyridin-2-yl)methanimine) (L1).** In a flask containing an ethanol solution (2mL) with 1,2-diamminocyclohexane (1.3 gr, 0.01167 mol), a ethanolic solution (2 mL) of pyridine-2-carbaldehyde (2.5 gr, 0.023 mol) has been slowly added at 0°C. After the adding, the ice-bath has been removed to establish the room temperature for 12h. The white product precipitating has been filtered and washed three times with cold ethanol (5 mL). To increase the yield the ethanol solution can be concentrated to obtain other precipitate. White solid. Yield 75%.  $^1H$  NMR (600 MHz,  $CDCl_3$ )  $\delta$  (ppm): 8.53 (d,  $J = 4.5$  Hz, 2H), 8.30 (s, 2H), 7.87 (d,  $J = 7.9$  Hz, 2H), 7.63 (t,  $J = 7.3$  Hz, 2H), 7.20 (dd,  $J = 6.7, 5.4$  Hz, 2H), 3.58 – 3.47 (m, 2H), 1.91 – 1.73 (m, 6H), 1.57 – 1.42 (m, 2H).  $^{13}C$  (50 MHz,  $CDCl_3$ )  $\delta$  (ppm): 161, 154, 149, 136, 124, 121, 73, 32, 24. **LC-MS:**  $m/z$  293[M+1]. IR (KBr pellet):  $\nu = 1645$  (N=C imine stretch), 1585 (pydine stretch), 1566 (pydine stretch), 1467 (pydine stretch), 1434 (pydine stretch), 1434 (pydine stretch), 791 (pydine stretch), 769 (pydine stretch), 993 (pyridine bend), 619 (pyridine bend).

**[Eu(L1)(L2)<sub>2</sub>(H<sub>2</sub>O)]·CF<sub>3</sub>SO<sub>3</sub>.** 78 mg (0.342 mmol) of Htta (2-Thenoyltrifluoroacetyl-acetone) has been completely dissolved in methanol (2mL) solution containing 19 mg (0.342 mmol) of KOH. The clear solution has been slowly added to methanol solution (2ml) containing 50 mg (0.171 mmol) of *N,N'*-(cyclohexane-1,2-diyl)bis(1-(pyridin-2-yl)methanimine) L1 and 102 mg (0.171 mmol) of Eu(OTfa)<sub>3</sub>. The final solution has been stirred for 1 hour a room temperature. After this time, the solvent has been removed under reduced pressure and the desiderated product extracted through 6 mL of DCM. Yield: 50%. IR (KBr pellet):  $\nu = 1645$  (C=N imine stretch), 1537 (carbonyl group stretch), 1029 (pyridine bend), 638 (pyridine bend).

**[EuL1(L2)<sub>2</sub>(H<sub>2</sub>O)]·NO<sub>3</sub>** was synthesized as depicted in Scheme 3, by performing the following procedure: at room temperature, 76 mg (0.342 mmol) of Htta (2-Thenoyltrifluoroacetyl-acetone, Merck) have been dissolved in a methanol (1.5 mL) solution containing 19 mg (0.342 mmol) of KOH. The clear solution was slowly added to a methanol solution (2mL) of the enantiopure *R,R* ligand L1 [50 mg (0.171 mmol)] and Eu(NO<sub>3</sub>)<sub>3</sub>·6H<sub>2</sub>O [76.4 mg (0.171 mmol)]. The final mixture was stirred for 30 minutes at room temperature and then the solvent was removed under reduced pressure. The desired product was obtained in a good yield as yellowish powder upon extraction in dichloromethane (6 mL) followed by solvent removal under reduced pressure. [EuL1(L2)<sub>2</sub>(H<sub>2</sub>O)]·NO<sub>3</sub>: Yield 92%. Elemental Anal. Calc. for C<sub>34</sub>H<sub>28</sub>EuF<sub>6</sub>N<sub>5</sub>O<sub>7</sub>S<sub>2</sub> (MW 948.7): C, 43.04; H, 2.97; N, 7.38; O, 11.81. Found: C, 42.87 ; H, 2.90; N, 7.26; O, 11.87. In acetonitrile: ε (279 nm): 27290 M<sup>-1</sup>cm<sup>-1</sup> (pyridine ring absorption); ε (347 nm): 35570 M<sup>-1</sup>cm<sup>-1</sup> (tta absorption).



Scheme 3. Synthesis of complexes [LnL1(L2)<sub>2</sub>(H<sub>2</sub>O)<sub>n</sub>]·NO<sub>3</sub>, with Ln=Eu<sup>3+</sup>, Sm<sup>3+</sup>.

**[SmL1(L2)<sub>2</sub>(H<sub>2</sub>O)]·CF<sub>3</sub>SO<sub>3</sub>** was synthesized as depicted in Scheme 3, by performing the following procedure: at room temperature, 53.3 mg (0.240 mmol) of Htta (2-Thenoyltrifluoroacetyl-acetone) have been dissolved in a methanol (1.5 mL) solution containing 13.5 mg (0.240 mmol) of KOH. The clear solution was slowly added to a methanol solution (1.5 mL) of the ligand L1 [35 mg (0.120mmol)] and Sm(CF<sub>3</sub>SO<sub>3</sub>)<sub>3</sub> [71.6 mg (0.120 mmol)]. The final mixture was stirred for 1 hour at room temperature and then the solvent was removed under reduced pressure. The desired product has been obtained in a good yield as

yellowish powder upon extraction in dichloromethane (5 mL) followed by the removal of the solvent under reduced pressure. The synthesis was performed by using both the enantiomers of the ligand L1.  $[\text{SmL1}(\text{L2})_2(\text{H}_2\text{O})]\cdot\text{CF}_3\text{SO}_3$ : Yield 84%. Elemental Anal. Calc. for  $\text{C}_{35}\text{H}_{30}\text{F}_9\text{N}_4\text{O}_8\text{S}_3\text{Sm}$  (isomer *R,R*; MW 1052.2): C, 39.95; H, 2.87; N, 5.32; O, 12.16. Found: C, 39.80 ; H, 2.98; N, 5.25; O, 12.09. In acetonitrile:  $\epsilon$  (280 nm):  $26560 \text{ M}^{-1}\text{cm}^{-1}$  (pyridine ring absorption);  $\epsilon$  (347 nm):  $34877 \text{ M}^{-1}\text{cm}^{-1}$  (tta absorption).

$[\text{SmL1}(\text{L2})_2(\text{H}_2\text{O})]\cdot\text{NO}_3$  was synthesized as depicted in Scheme 3, by performing the following procedure: at room temperature, 53.3 mg (0.240 mmol) of Htta (2-Thenoyltrifluoroacetyl-acetone) have been dissolved in a methanol (1.5 mL) solution containing 13.5 mg (0.240 mmol) of KOH. The clear solution was slowly added to a methanol solution (1.5 mL) of ligand L1 [35 mg (0.120 mmol)] and  $\text{Sm}(\text{NO}_3)_3\cdot 6\text{H}_2\text{O}$  [53.3 mg (0.120 mmol)]. The final mixture was stirred for 1 h at room temperature and then the solvent was removed under reduced pressure. The desired product has been obtained in a good yield as yellowish powder upon extraction in dichloromethane (5 mL) followed by the removal of the solvent under reduced pressure.  $[\text{SmL1}(\text{L2})_2(\text{H}_2\text{O})]\cdot\text{NO}_3$ : Yield 95%. Elemental Anal. Calc. for  $\text{C}_{34}\text{H}_{28}\text{F}_6\text{N}_5\text{O}_7\text{S}_2\text{Sm}$  (isomer *R,R*; MW 947.1): C, 43.12; H, 2.98; N, 7.39; O, 11.83. Found: C, 42.94 ; H, 2.90; N, 7.33; O, 11.69. In acetonitrile,  $\epsilon$  (279 nm):  $26750 \text{ M}^{-1}\text{cm}^{-1}$  (pyridine ring absorption);  $\epsilon$  (347 nm):  $34870 \text{ M}^{-1}\text{cm}^{-1}$  (tta absorption).

#### 1.4.3.3. Luminescence and decay kinetics

Room temperature luminescence was measured with a Fluorolog 3 (Horiba-Jobin Yvon) spectrofluorometer, equipped with a Xe lamp, a double excitation monochromator, a single emission monochromator (mod. HR320), and a photomultiplier in photon counting mode for the detection of the emitted signal. All the spectra were corrected for the spectral distortions of the setup.

In decay kinetics measurements, a Xenon microsecond flashlamp was used and the signal was recorded by means of multichannel scaling method. True decay times were obtained using the convolution of the instrumental response function



with an exponential function and the least-square-sum-based fitting program (SpectraSolve software package).

The spectra were recorded on CH<sub>3</sub>CN (0.4 mM) and methanol (0.4 mM) solutions, as for the CPL spectra (see below).

#### 1.4.3.4. *Circularly Polarized Luminescence (CPL)*

CPL spectra were recorded with the home-made spectrofluoropolarimeter described previously.<sup>55</sup> The spectra were recorded on CH<sub>3</sub>CN (0.4 mM) and methanol (0.4 mM) solutions in a 1 cm-cell. The samples were excited at 365 nm, with a 90° geometry between the detector and the light source.

#### 1.4.3.5. *Electronic Circular Dichroism (ECD)*

ECD spectra were recorded with a Jasco J710 spectropolarimeter on CH<sub>3</sub>CN 2 mM and CH<sub>3</sub>OH 2 mM solutions in a 0.02 cm-cell.

## 1.5. *References*

1. [X. Chen, Y. Liu, D. Tu, Lanthanide-Doped Luminescent Nanomaterials; Nanomedicine and Nanotoxicology; Springer Berlin Heidelberg: Berlin, Heidelberg, **2014**].
2. [J. G., Bünzli, C., Piguet *Chem. Soc. Rev.*, **2005**, 34, 1048–1077].
3. [P. Falconnet, *J. Alloys and Compounds*, **1993**, 192, 114–117].
4. [A.J. Freeman, R.E. Watson. *Phys. Rev.* **1962**, 127, 2058–2075].
5. [W. T. Carnall, Handbook on the Physics and Chemistry of Rare Earths, ed. K. A. Gschneidner, Jr., L. Eyring, Vol. 3, Ch. 24, North Holland Publ. Co., Amsterdam, **1979**].
6. [J.Vuojola, T. Soukka, *Meth. Appl. in Fluo.* , **2014**, Vol 2, Nr 1].
7. [K. Binnemans, *Coord. Chem. Rev.*, **2015**, 295, 1–45].
8. [G. Blasse, B. C. Grabmaier Lum. Mat. Springer-Verlag, Berlin, **1994**].
9. [S.I. Weissman, *J. Chem. Phys.* **1942**, 10, 214–217].
10. [J. W. Walton, A. Bourdolle, S. J. Butler, M. Soulie, M. Delbianco, B. K. McMahon, R. Pal, H. Puschmann, J. M. Zwier, L. Lamarque, O. Maury, C. Andraud, D. Parker, *Chem. Commun.*, **2013**, 49, 1600–1602].

11. [S. Tobita, M. Arakawa, I. Tanaka, *J. Phys. Chem.* **1985**, 89, 5649].
12. [W.F. Sager, N. Filipescu, F.A. Serafin, *J. Phys. Chem.* **1965**, 69, 1092].
13. [G.A. Crosby, R.J. Watts, S.J. Westlake, *J. Chem. Phys.* **1971**, 55, 4663].
14. [R.E. Whan, G.A. Crosby, *J. Mol. Spectrosc.* **1962**, 8, 315].
15. [J.A. Kemlo, T.M. Shepherd, *J. Chem. Soc., Faraday Trans.* **1977**, 73, 1850].
16. [A. Strasser, A. Vogler, *Chem. Phys. Lett.* **2003**, 379, 287].
17. [A. Strasser, A. Vogler, *Inorg. Chim. Acta* **2004**, 357, 2345].
18. [M. Mihorianu, M. Leonzio, M. Monari, L. Ravotto, P. Ceroni, M. Bettinelli, F. Piccinelli, *Chem. Select* **2016**, 1 (9), 1996–2003].
19. [M. Mihorianu, M. Leonzio, M. Bettinelli, F. Piccinelli, *Inorg. Chim. Acta* **2015**, 438, 10–13].
20. [D.L. Dexter, *Chem. Phys* **1953**, 21(5), 836-850].
21. [A. Bettencourt-Dias, *Curr. Org. Chem.* **2007**, 11 (16), 1460–1480]; Forster, T. *Ann. Phys.* 1948, 437 (1-2), 55-75].
22. [M. Latva, H. Takalo, V.-M. Mukkala, C. Matachescu, J.C. Rodriguez-Ubis, J. Kankare *J. Lumin.* **1997**, 75, 149].
23. [R. M. Supkowski, W. D. W. Horrocks, *Inorg. Chim. Acta* **2002**, 340, 44–48].
24. [W. D. W. Horrocks, D. R. Sudnick, *J. Am. Chem. Soc.* **1979**, 101, 334–340].
25. [H.C. Aspinall, M.R. Tillotson, *Polyhedron*, **1994**, 13 3229; G. Kauffman, Coordination Chemistry of the Lanthanide Elements- One Hundred Years of Development and Understanding, **1967**].
26. [S. A. Cotton, J. M. Harrowfield, (2012). Encyclopedia of Inorganic and Bioinorganic Chemistry, R. A. Scott (Ed.)].
27. [P. D'Angelo, A. Zitolo, V. Migliorati, G. Chillemi, M. Duvail, P. Vitorge, S. Abadie, R. Spezia, *Inorg. Chem.* **2011**, 50, 4572–4579].
28. [J. G. Bünzli, *Coord. Chem. Rev.* **2015**, 293–294, 19–47].
29. [H. Ishida, J. G. Bünzli, A. Beeby *Pure Appl. Chem.* **2016**, 88(7), 701–711].
30. [D.F. Eaton *Pure Appl. Chem.*, **1988**, 60, 7, 1107-1114].
31. [Technical Guide: Integrating Sphere Theory and Applications (LabSphere Inc.), available from <http://www.labsphere.com>].
32. [C. M. G. dos Santos, A. J. Harte, S. J. Quinn, T. Gunnlaugsson, *Coord. Chem. Rev.* **2008**, 252, 2512–2527].
33. [M. H. V. Werts, *Sci. Prog.* **2005**, 88, 101–131].
34. [T. Wu, X. Z. You, P. Bouř, *Coord. Chem. Rev.* **2015**, 284, 1–18].

35. [T. aki Uchida, K. Nozaki, M. Iwamura, *Chem. - An Asian J.* **2016**, 11, 2415–2422].
36. [A. P. S. Samuel, J. L. Lunkley, G. Muller, K. N. Raymond, *Eur. J. Inorg. Chem.* **2010**, 3343–3347].
37. [H. A. Haus, J. R. Melcher, *Electromagnetic Fields and Energy* (Prentice-Hall, **1989**, ISBN 0-13-249020-X)].
38. [J. D. Jackson, *Classical Electrodynamics* **1998**, (3rd ed.) Wiley, ISBN 0-471-30932-X].
39. [F. Zinna, L. Di Bari, *Chirality* **2015**, 27 (1), 1–13].
40. [J. L. Lunkley, D. Shirotni, K. Yamanari, S. Kaizaki, G. Muller, *J. Am. Chem. Soc.* **2008**, 130 (42), 13814–13815].
41. [C.L Maupin, J.P. Riehl *Electr. Spectr. Appl.* **1999**].
42. [F. Zinna, T. Bruhn, C. A. Guido, J. Ahrens, M. Bröring, L. Di Bari, G. Pescitelli, *Chem. - A Eur. J.* **2016**, 22, 16089–16098].
43. [C.L Maupin, J.P. Riehl, *Electr. Spectr. Appl.* **1999**].
44. [F. Piccinelli, A. Speghini, M. Monari, M. Bettinelli, *Inorg. Chim. Acta* **2012**, 385, 65].
45. [F. Piccinelli, M. Bettinelli, A. Melchior, C. Grazioli, M. Tolazzi, *Dalton Trans.* **2015**, 44, 182].
46. [M. Leonzio, M. Bettinelli, L. Arrico, M. Monari, L. Di Bari, F. Piccinelli *Inorg. Chem.* **2018**, 57, 10257–10264].
47. [L. Arrico, C. De Rosa, L. Di Bari, F. Piccinelli, submitted for publication].
48. [S. Wada, Y. Kitagawa, T. Nakanishi, M. Gon, K. Tanaka, K. Fushimi, Y. Chujo, Y. Hasegawa, *Scientific Rep.* **2018**, 8:16395].
49. [E. S. Andreiadis, N. Gauthier, D. Imbert, R. Demadrille, J. Pécaut, M. Mazzanti, *Inorg. Chem.* **2013**, 52, 14382-14390].
50. [J.C.G. Bünzli, J.P. Metabanzoulou, P. Froidevaux, L.P. Jin, *Inorg. Chem.* **1990**, 29, 3875-3881].
51. [J.C.G. Bünzli, M.M. Vuckovic, *Inorg. Chim. Acta* **1983**, 73, 53].
52. [A.F.D. de Namor, S. Chahine, O. Jafou, K. Baron, *J. Coord. Chem.* **2003**, 56 1245].
53. [R. C. Holz, C. A. Chang, W. De. W. Horrocks, *Inorg. Chem.* **1991**, 30, 3270-3275].
54. [E. Kreidt, L. Arrico, F. Zinna, L. Di Bari, M. Seitz, *Chem. Eur. J.* **2018**, 24, 13556 –13564].

55. [A. Wagh, S. Y. Qian, B. Law *Bioconjugate Chem.* **2012**, 23, 981–992].

## CHAPTER 2-Lanthanide complexes: applications for sensing in biomedicine

### 2.1. *Introduction*

Since the optical imaging represent a fundamental component of several biomedical techniques, the need to satisfy the requirements of the modern bioanalysis and bioimaging is becoming of outstanding importance. The various advantages of using the lanthanide complexes as bioprobes, is the main explanation for justifying the continuous exploiting over the last 35 years.

One of the first uses goes up to the end of the 1970s, in which the aim of lanthanide luminescence was to replace radio-analyses. In these bioassays, some lanthanide macrocyclic complexes based on polyaminocarboxylates are conjugated to specific antibodies and the luminescence is detected after the biochemical reaction is completed, by involving a fluoro-immunoassays DELFIA (dissociation-enhanced lanthanide fluorescence immunoassay) or a FRET (Fluorescence resonance energy transfer)-based protocol.<sup>1</sup>

The convenience of lanthanide luminescent bioprobes for immunoassays, was a consequent extension to imaging purposes.<sup>2</sup>

As already discussed, since the intraconfigurational f-f transitions are forbidden, the lifetime of the excited state are long (ms range) by allowing the use of time gated detection which increases the sensitivity of the optical response.

The time-resolved measurements use a time delay  $t_d$  between an excitation pulse and the time at which the emission is detected. In this technique, the sample is illuminated with a pulsed light source, commonly a cheap flash lamp or LED.

The detector is turned on or off depending on the advancement of the experiment. At the initial pulse  $t=0$ , the detector is switched on after a delay time, then the luminescence of the probe is measured. The complete experiments last just 1-4 ms, for this reason the light measurements could be repeated several times for second, by enhancing the signal-to-noise ratio and therefore the sensitivity of the technique.

In this way, the  $t_d$  allows to discriminate the emission of lanthanide probe from the shorter-lived background signals, whose signal rapidly decays.<sup>3</sup>

Besides the large Stokes' shift (difference between excitation and emission wavelengths) and the narrow emission peaks, another fundamental advantage justifying the employment of lanthanide complexes as probes is their high stability. In fact, since they are not easily oxidized or photobleached, they can be stored at room temperature for years.

As widely described, the lanthanide luminescence involves the *antenna process*; since the sensitization by the ligands *via* the energy transfer mechanism to the metal center is considerably fast, the photodegradation of the ligand is substantially overcome.<sup>4</sup>

## 2.2. *Toolkit of the lanthanides luminescent bioprobes*

The specific targeting to vehicular the probes toward a selective compartment remains one of the major challenges to solve. The possibility to get more versatility in vivo or in vitro experiments could be influenced by the impact of the hydrophobicity and charge of the lanthanide metal complexes on the cell viability and cell association<sup>5</sup>, including their membrane permeability.<sup>6-10</sup>

Furthermore, the in vivo or in vitro localization of the optical probe affects the type of analytes that can be detected. A probe with an extracellular location is particularly suitable to detect analytes such as group I ions, polysaccharides, hormones, or other signaling molecules.<sup>5</sup>

In order to get a suitable lanthanide luminescent bioprobe, a list of crucial requirements rules the design of the metal complex, as listed below.

### 2.2.1. *Water solubility*

Since usually an organic antenna is composed by an extended system of heteroaromatic rings, the complete solubilization of the Ln-complex in aqueous system is not trivial.

The development of a water-soluble compound could be obtained by employing hydrophilic groups on the ligand backbone. With this in mind, some cationic groups (e.g., ammonium substituents), anionic groups (e.g., phosphonates or sulfonates), or hydrophilic groups can be conveniently exploited for this aim. The

insertion of hydrophilic groups based on polyethylene glycol (PEG) is of huge interest and has been already reported. For instance, the well-known texaphyrin lutetium or gadolinium complex (Figure 1) designed by Sessler and co-workers consisted in a porphyrin containing these solubilizing PEG-moieties, which was exploited in the development of active anticancer agents.<sup>11</sup>

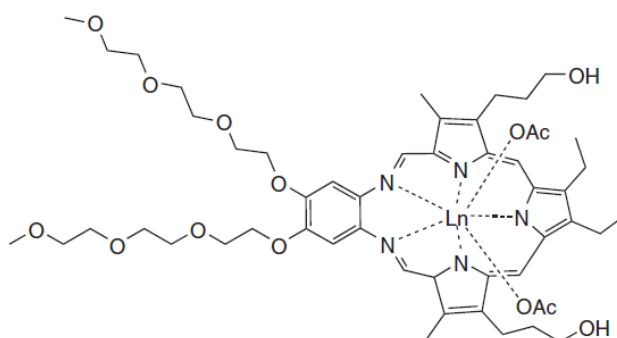


Figure 1. Ln = Gd: the gadolinium texaphyrin is an effective radiation sensitizer active toward tumor cells. Ln = Lu: the lutetium complex has potentiality for photodynamic therapy, active for breast cancer or brain tumor cells.

On the other hand, the solubility in water could be ensured by inserting also carboxylic groups, as demonstrated in my PhD project.

In this context, it is important to know the speciation curves of the functional groups sensitive the pH environment, in order to study the chemical equilibria of the ligands under investigation. With this in mind, it is possible to calculate the formation constants of the Ln(III)-complexes by following the absorbance changes with acid-base spectrophotometric titrations.

In addition, the possibility to introduce amine and carboxylic pendants represents a convenient way to easily form bioconjugates, by exploiting the chemistry of the coupling reactions. One of the most traditional coupling reactions is performed with water-soluble carbodiimide crosslinker such as 1-ethyl-3-[3-dimethylaminopropyl]carbodiimide hydrochloride (EDC), sometimes followed by a second activation process in the presence of N-hydroxysuccinimide (NHS) or sulfo-NHS, prior to coupling with an amine. Furthermore, the excess of activating agents can be easily removed by acidic aqueous treatments. These NHS additives commonly enhance the yields and decrease the amount of collateral byproducts.

### **2.2.2. *Stability and Selectivity***

Another fundamental feature it is the high stability in solution, more precisely a high thermodynamic stability and the kinetic inertness at physiological pH (around 7.4) is required.

Especially, in biomedical field, one of the most usual drawbacks is the *transmetallation process*, more precisely the possibility to have cation exchange with some endogenous cations present in the biological environment. This could be a serious issue in the case of  $Zn^{2+}$  and  $Ca^{2+}$  that are present in high concentration ( $10^{-3}$  M) in lysosomes.<sup>12</sup>

In addition, low complex stability could give rise to the release in solution of free toxic metal ion.

An efficient bioprobe should show tunable luminescence properties as a function of the presence in solution of a particular analyte showing a sort of selectivity in experiments on complex matrix. It should be also underlined that a precise excitation wavelength must be selected. Optical probes characterized by an excitation wavelength lower than 300 nm are useless, since the majority of the biomolecules strongly absorb UV light in that spectral range. Furthermore, the irradiation in the UV/blue spectral range is rather phototoxic.

### **2.3. *Classification and applications of lanthanide probes in bioimaging***

The luminescent molecular probes have attracted great interest owing to their high sensitivity with broad dynamic range in the detection of specific bio-analytes.

Commonly, the analytes are detected thanks to considerable changes in the luminescence intensity or wavelength. Nevertheless, in biological applications, where the analyte could be in low concentration or many other interfering biochromophores could response, the accuracy of the detection is drastically reduced by evidencing the necessity of another approach to overcome this drawback. As previously described at the beginning of this chapter, such purpose is reached by employing the *time-gated luminescence*, an efficient spectroscopic technique already cited at the beginning of this chapter.



In this section, the main classes of probes employed in bioimaging are reviewed.

### 2.3.1. $\beta$ -Diketonate Probes

The main representative  $\beta$ -diketonates used as ligands for  $\text{Ln}^{3+}$  ions are depicted in Figure 3.

The  $\beta$ -diketonate-based lanthanide complexes efficiently emit not only visible but also near-infrared luminescence.<sup>13, 14</sup>

The quantum yields efficiency of some ternary Eu(III) complexes reach values up to 85%.<sup>15</sup>

Most probably, the  $\beta$ -diketonates induce an appreciable mixing of ligand orbitals into 4f wave functions. Consequently, the Laporte's forbidden f-f transitions become more probable, and the observed lifetimes are shorter.<sup>16</sup>

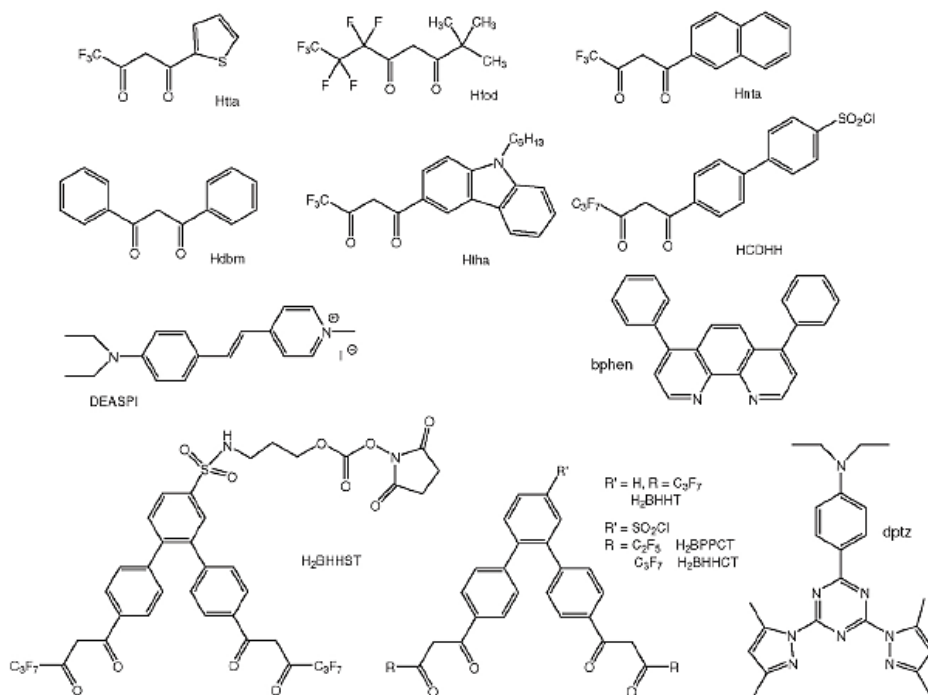


Figure 3.  $\beta$ -diketonates and ancillary ligands used in biosensing.

Several applications involve the employment of lanthanide  $\beta$ -diketonates complexes.<sup>17-19</sup>

In particular, they are broadly used in the field of micro-organism imaging. In the research of Yuan and co-workers, the initial chlorosulfonyl derivative (BHHCT) was conveniently coupled to an aminoacidic residue of the BSA (Bovine Serum Albumin) by obtaining the sulfonylaminopropyl-ester-N-succinimide Moiety (BHHST). The luminescent properties are improved by inserting the triazine derivative (dpbt), an excellent antenna for Eu(III). The obtained conjugate  $[\text{Eu}(\text{BHHCT})(\text{dpbt})]^+$  complex-protein displays a wide excitation range up to 387 nm, a relatively long lifetime around 460  $\mu\text{s}$ , and a quantum yield of 27% in  $\text{NaHCO}_3$  0.05 M, pH 8.5. The remaining primary amino acids of BSA are cross-linked to SA (Streptavidin) with glutaraldehyde to produce an active bioconjugate (Figure 4) capable to chelate various microorganisms such as the *Giardia lamblia*, also known as *Giardia intestinalis*, which is a flagellated parasitic microorganism, that colonizes and reproduces in the small intestine, causing *giardiasis*.<sup>20</sup>

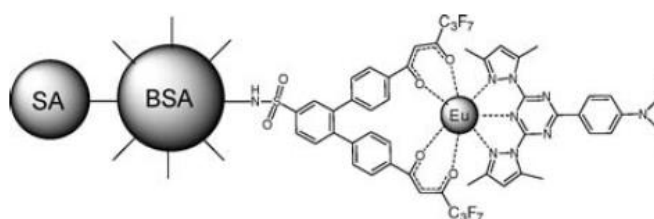


Figure 4. Active bio-conjugate for *Giardia lamblia* imaging.

The use of the BHHCT complexes has been also successfully employed in the agriculture field, in the investigation of the interaction between oligochitosan and tobacco cells.

This natural polysaccharide (poly  $\beta$ -N-acetyl-D-glucosamine) derived from chitin, has a wide spectrum of antibacterial activity, effective fungicides, inhibiting spore germination and mycelial growth, so it is an interesting alternatives to chemicals

for controlling post-harvest diseases and prolonging fruit and vegetable storage life.<sup>21</sup>

### 2.3.2. *Encapsulated probes*

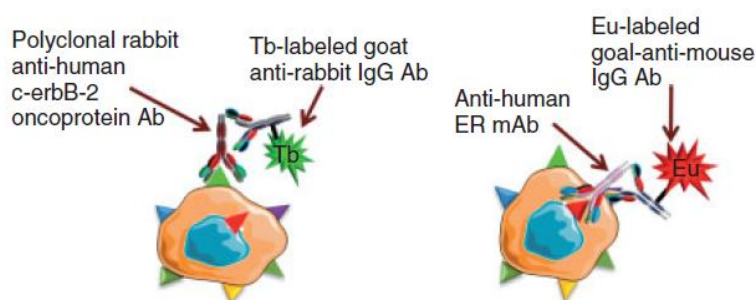
The lanthanide complexes could be encapsulated in different matrices. In the field of optical imaging, several visible<sup>22-25</sup> and NIR-emitting<sup>26-28</sup> organic dyes have been successfully encapsulated and employed in *in vivo* experiments.

In addition, multifunctional nanoparticles capable to carry both drugs and dyes have been designed for multimodal theranostic purposes.<sup>29-32</sup>

One of the most common biopolymer used for this purpose is the Poly(lactic-co-glycolic acid) PLGA, as reported by Naik and co-workers. In these -PLGA based-nanoparticles, is possible to control the release of drugs thanks to a local heating by microwave irradiation of a magnetic iron core contained inside the nanoparticles, that it is capable to increase the rate of a dye release.<sup>33</sup>

Another interesting application which exploits the encapsulation of the probe in nanoparticles is reported in the work of Moreira and co-workers (Figure 5). The nanoparticles are conjugated to an IgG monoclonal antibody for target-specific bioassays.

In particular, two receptors, the estrogen receptors (ERs) and Her2/neu (human epidermal growth factor receptor) are overexpressed in breast cancer cells and located on the nuclear membrane or on the cell membrane, respectively. The goal is to take advantage of red-emitting Eu-bioprobe and green-emitting Tb-bioprobe for detecting simultaneously both receptors.<sup>34</sup>



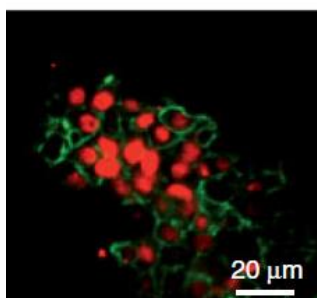


Figure 5. Her2/neu detected by green-emitting Tb-bioprobes and ER stained with red-emitting Eu-bioprobes

### 2.3.3. Aliphatic Polyaminocarboxylate and Carboxylate Probes

It is surely one of the most exploited classes of Ln-complexes for biosensing and imaging applications. The main representative compounds are certainly the lanthanides complexes bearing the ligand frameworks of DTPA (diethylenetriaminepentaacetic acid) and DOTA (1,4,7,10-Tetraazacyclododecane-1,4,7,10-tetraacetic acid), as the well-known  $[\text{Gd}(\text{DTPA})(\text{H}_2\text{O})]^{2-}$  was approved as contrast agent for magnetic resonance imaging in 1988, followed one year later by  $[\text{Gd}(\text{DOTA})(\text{H}_2\text{O})]^-$  (Figure 6).

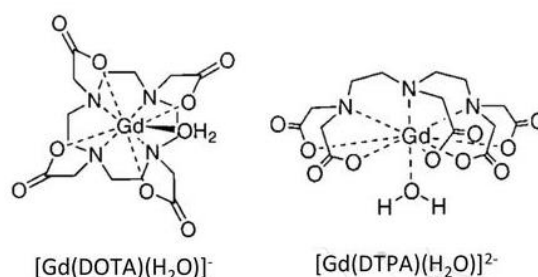


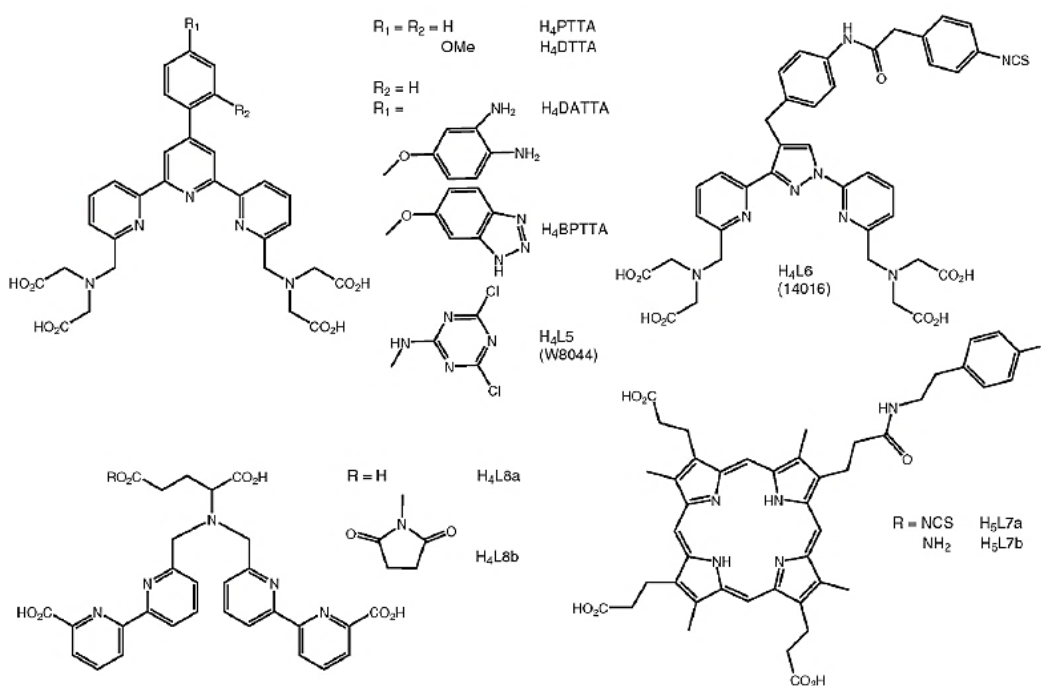
Figure 6. Gd(III) complexes based on DOTA and DTPA ligands for imaging.

The easy derivatization of the core opens the possibility to get a wide number of derivatives well studied for their thermodynamics and kinetics properties.<sup>35</sup>

As far as the bio-applications are concerned, many luminescent tags are designed with the aim of imaging various analytes and proteins within living cells.

An interesting approach was reported by Soini and co-workers for the identification of blood leukocytes, by using the luminescent properties of four different metal complexes.<sup>36</sup>

The final aim of this proposed assay is the identification of neutrophils, eosinophils and T-lymphocytes by time-resolved microscopy with the help of the metal chelates (Figure 7), while Syto 25™ is a green nucleus stain which works with all cells (Figure 7). Afterwards, the leucocyte mixtures are incubated in a one-step procedure in phosphate buffered saline (pH 7.4) buffer with a combination of luminophore-conjugated antibodies recognising neutrophil and lymphocyte-specific markers.



Label	$\lambda_{\text{max}}$ (exc), nm	Excitation $\lambda$ /nm (bandpass)	$\lambda_{\text{max}}$ (em), nm	Detection $\lambda$ /nm (bandpass)	Decay time ( $\mu\text{s}$ )
[Eu(L5)] <sup>-</sup>	292	340 (25)	613	615 (4)	1600
[Tb(L6)] <sup>-</sup>	335	340 (25)	545	545 (4)	1100
[Pd(L7a)] <sup>3-</sup>	390	545 (10)	667	673 (10)	700
[Pt(H <sub>3</sub> L7b)] <sup>3-</sup>	380	530 (10)	647	642 (10)	80
Syto 25™	521	470 (20)	556	525 (25)	<sup>a</sup>

<sup>a</sup> Prompt fluorescence

Figure 7. Luminescent bioprobes used for detection of leucocytes.

Another interesting application for this class concerns the influence of the pH environment on the emission intensity ratio and variation of the excited state lifetime.

With this in mind, the probes that can report changes to the pH environment of certain cellular compartments could be used in the monitoring of several pathological and physiological cellular processes. A similar purpose was reported in the work of McMahon and co-workers<sup>37</sup> in which the Europium probes were used for determination of pH change within the endoplasmic reticulum of living cells.

A family of Eu(III) complexes based on the 1,4,7,10-tetraazacyclododecane macrocyclic framework incorporating either an azathioxanthone or azaxanthone sensitizing moiety were mainly employed (Figure 8). As result of the pH fluctuations, the metil-sulphonamide pendant can bind reversibly to the lanthanide ion, by changing the metal coordination environment.

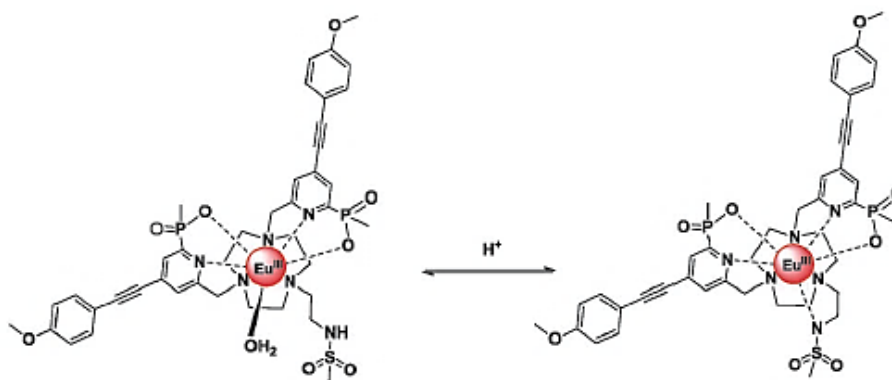


Figure 8. pH dependency of the sulphonamide moiety.<sup>37</sup>

The modification around the first coordination sphere has a big influence also on the hydration number ( $q$ ) of the lanthanide, by affecting the overall emission quantum yield. In Figure 9, the Eu(III) emission spectra as a function of pH (0.1 M NaCl, 298 K) is reported revealing a substantial and reversible changes in the fine splitting of the  $\Delta J = 1$  transition and also in the form of the  $\Delta J = 2$  and  $\Delta J = 4$  spectral bands. In addition, upon basification, two new bands at 625 nm and 688 nm were also observed.

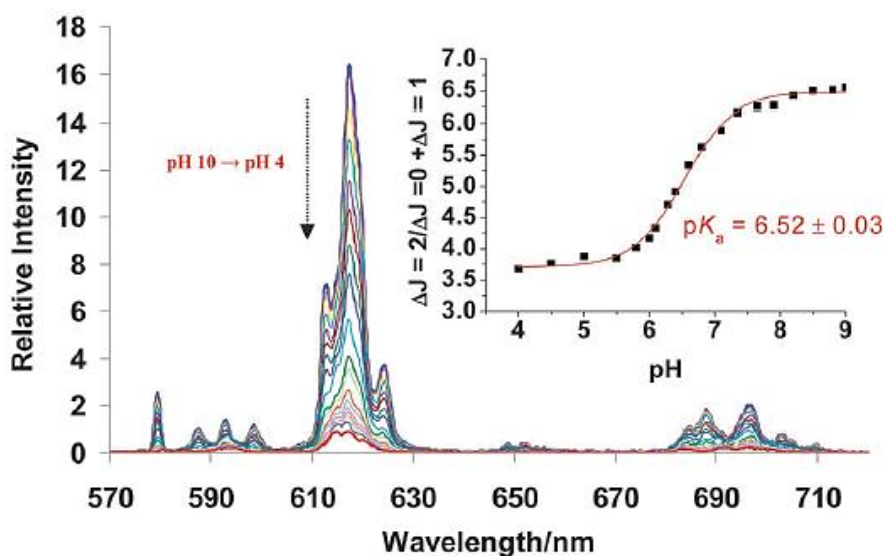


Figure 9. Variation of the Eu(III) emission of EuL complex depicted in fig.8, as a function of pH. <sup>37</sup>

In a previous work reported by Kim and co-workers it was demonstrated that the large proton permeability of the endoplasmic reticulum membrane allows a noticeable correlation between the pH within the cytoplasm and the endoplasmic reticulum. In this context, it is possible a preliminary study to predict the capability of the probe to respond to pH changes *in cellulo*. The experiment is performed by altering the pH of endoplasmic reticulum from 7.7 to 6.0 (by varying the pH of the growth medium and adding nigericin (0.2 mM) to allow  $K^+/H^+$  exchange), where the consequent response is detected by microscopy.<sup>38</sup>

A similar purpose to investigate the pH changes within the cellular compartment, it was also performed by D.G. Smith and co-workers by employing a family of Eu and Tb complexes based on azaxanthone sensitizer (Figure 10) to measure the equilibrium of bicarbonate concentrations directly human serum and in cellular mitochondria of bicarbonate in several different cell types with confocal microscopy.<sup>39</sup>

As far as the biomedical applications are concerned, a rapid method to detect bicarbonate levels in serum is crucial either in emergency medicine for evaluating metabolic acidosis and in chronic kidney disease patients.<sup>40-42</sup>

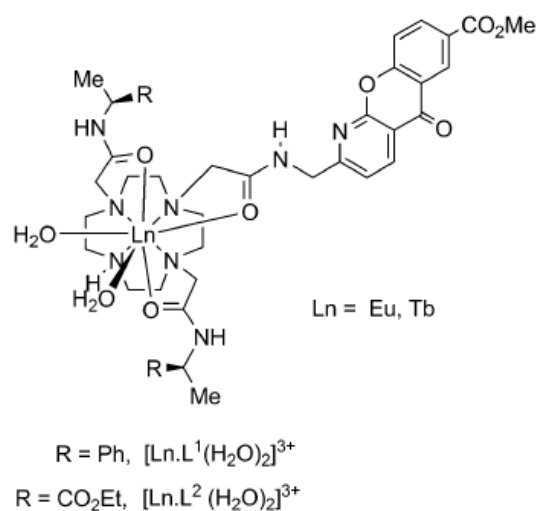


Figure 10. An example of the EuL complex structure to detect the bicarbonate ion in mitochondria upon displacement of water molecules.<sup>39</sup>

In order to consider the effect of the natural interferences composing the extracellular fluid, the intrinsic binding affinities for the bicarbonate anion were evaluated with the simultaneous presence of biocomponents such as: lactate, citrate, phosphate and serum albumin. The triphosphate, ATP, was also included in these studies, since it is present at 1 mM concentrations within mitochondria, and it is also capable of binding to the lanthanide complexes. The investigated anions were used at their typical extracellular concentrations, and HSA (Human Serum Albumin) was present at its normal extracellular concentration of 0.4 mM. Since, the normal concentration of bicarbonate in extracellular fluid is around 24-27 mM<sup>43</sup> they were added increasing amount of the analyte in a range within 10-35 mM, by obtaining a noticeable increase of the emission intensity and a slight shift in the  $\Delta J=2$  maximum from 614 to 616 nm, which it is essentially due the displacement of the water molecules from the metal center (Figure 11).



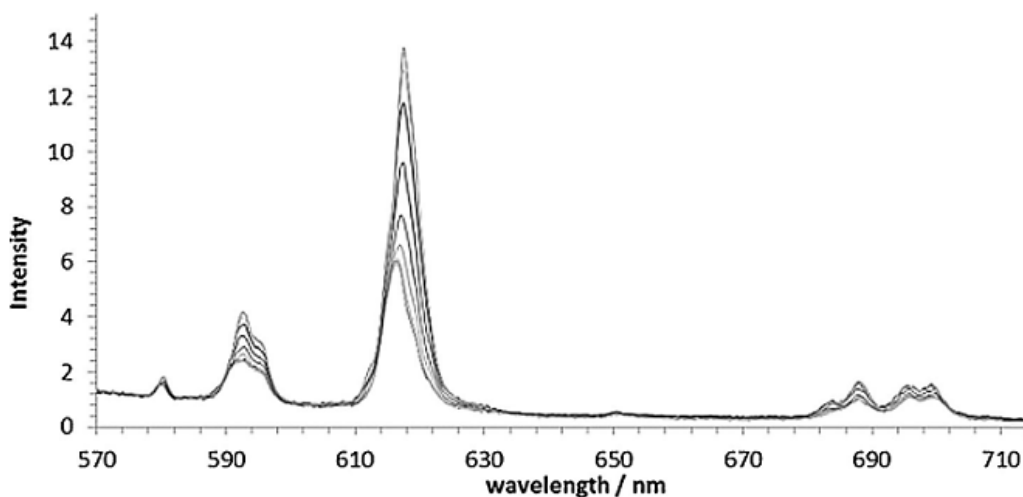


Figure 11. Variation of the Eu(III) emission spectrum for  $[Eu-L^2]^{3+}$ , in a background solution containing HSA (0.4 mM), citrate (0.13 mM), lactate (2.3 mM), phosphate (0.7 mM) and ATP (1 mM), following by addition of sodium bicarbonate up to 30 mM (pH 7.40, 50  $\mu$ M complex, 298 K, I=0.1 M NaCl,  $\lambda_{exc}$ =332 nm). From [39].

In addition to the polyaminocarboxylate probes sensitive to the pH changes of the environment, the literature reports many examples for controlling the lanthanide luminescence. Several applications concerned the modulation of the electron transfer to the metal center or the capture of the antenna by endogenous ions. This latter is described by Kotova<sup>44</sup> and co-workers who developed a luminescent lanthanide sensor based on 4,7-diphenyl-1,10-phenanthroline-disulfonate (BPS) as antenna (Figure 12), which was capable to modify the europium emission upon the coordination with Fe(II). In biology, the possibility to detect the presence of metals plays a crucial role, since several biomolecules composing the human proteome contains metal cations, as catalyst of some metabolic pathways, or as cofactors. Furthermore, a reliable qualitative and quantitative method to detect the biometals it is fundamental, since the metal imbalance in tissues and cells are correlated to a noticeable number of diseases.<sup>45-47</sup>

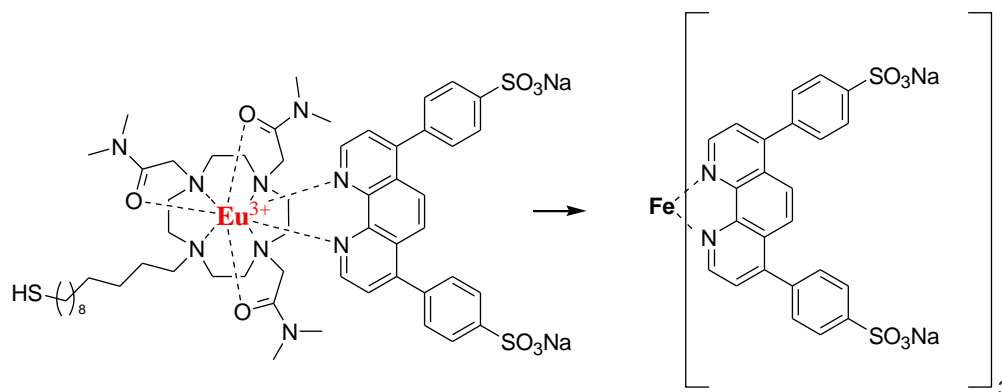


Figure 12. Structure of the Eu(BPS) complex used for detection of Fe(II). From [44].

The principle of the assay method is based on the removal of the antenna BPS due to the higher affinity for Fe(II) ion for the coordination with the metal center, by “switching off” the luminescence signal. The resulting displacement generates a consistent decrease of the hypersensitive  ${}^5D_0$ - ${}^7F_2$  transition (Figure 13), by allowing a detection limit of the BPS for the Fe(II) ions around 10 pM, which it is significantly above the traditional employed colorimetric methods.<sup>48-50</sup>

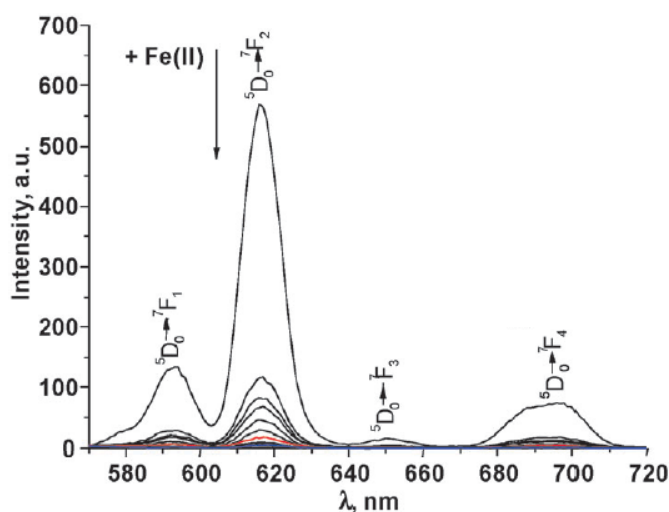


Figure 13. Variation of the Eu(III) emission of Eu-BPS complex depicted in fig.8, upon addition of Fe(II), (0-4 equiv.) in HEPES-buffered solution (pH 7.4).

On the other hand, the presence of metal ions could also promote the luminescence emission, as reported in the work of Weitz<sup>51</sup> and co-workers.

In biology, the alkali metal ions are essential for the regulation of membrane polarization and osmotic pressure. For this reason, the possibility to get activation

or a deactivation of the luminescence emission in relationship with the flux of the alkali ions is very important in neuroimaging applications.

The above mentioned purpose was reached by employing the Eu(III) emission of a probe based on a macrocyclic DOTA like supported by a crown ether to enhance the stability in biological means and phenanthridine ring as antenna conjugated to the crown ether at the 4 position (Figure 14).

The cation- $\pi$  interaction of the  $K^+$  ions towards the electron-rich  $\pi$  phenanthridine ring influences the excited energy levels of the antenna resulting in a enhance of the energy transfer process.

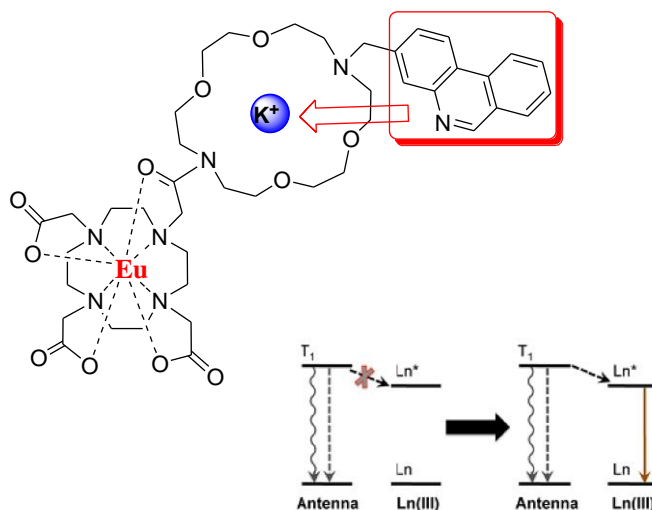


Figure 14. Turn-on response of the luminescence emission in the presence of  $K^+$  ion. [Ref. 51]

The double capability to enhance or interrupt the signal is essentially due to the fast kinetics of binding and dissociation of the adduct  $K^+$ -probe, in addition to the high sensitivity and selectivity. Since the affinity of the  $K^+$  ions is higher for the phenanthridine's nitrogen than the crown ether, the detection of the ion within the typical extracellular range 3.5–5.3 mM<sup>52</sup> under physiological condition was successfully performed by allowing the future application in imaging field.

Post-modifications of the antenna could opportunely modulate the transfer of the electrons on the lanthanide, by signaling the presence of specific analytes. Such purpose was exploited in the study of Lippert and co-workers for detecting the presence of reactive oxygen species (ROS) like the hydrogen peroxide ( $H_2O_2$ ).<sup>53</sup>

In biology, the ROS species cover a wide family of molecules essential for the human health.<sup>54-63</sup>

As far as the  $H_2O_2$  is concerned, it is involved in several physiological stimuli, in the regulation of cellular processes, like growth and proliferation<sup>64-66</sup> differentiation<sup>67, 68</sup> migration<sup>69, 70</sup> and phagocytosis<sup>71, 72</sup> in addition to aging<sup>73, 74</sup> and diseases involving cancer<sup>75-77</sup> diabetes<sup>78-80</sup> and neurodegenerative disorders.<sup>81-83</sup>

A 7-fold coordinating DOTA-like core is functionalized with a boronate ester which upon chemoselective interaction with hydrogen peroxide, it is conveniently converted to the electron-rich phenol group. The electron-withdrawing boronate group acts as a cage, by hampering the sensitization of the  $Tb^{3+}$  ion (Figure 15). The “turn-on” switch of the luminescence is due to the phenol ring that, upon deprotection of boronate unit, is now available to act as a suitable antenna for Tb luminescence.

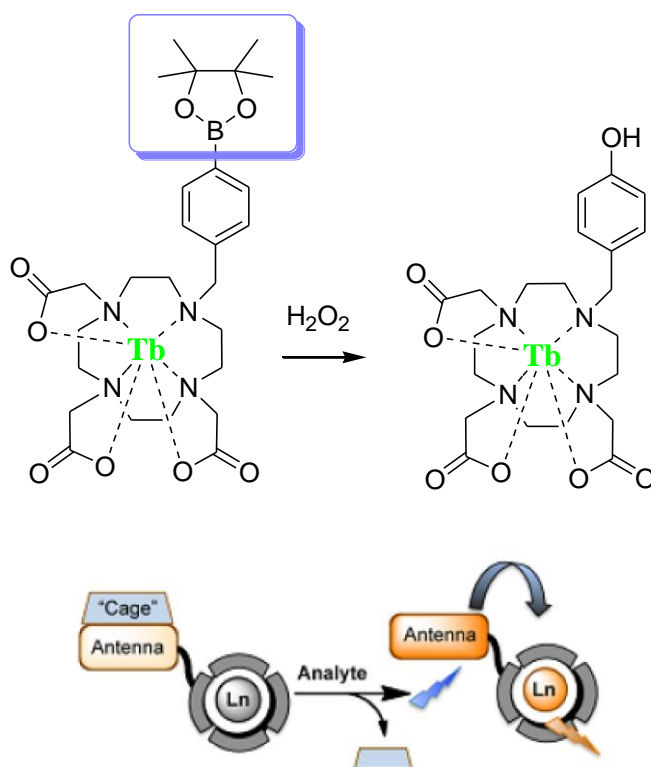


Figure 15. Turn-on response of the luminescence emission, upon oxidation of the antenna with  $H_2O_2$ . [Ref. 53]

The above-mentioned compound is also employed for the detection of hydrogen peroxide in living systems. In such applications, the main strategy is the time-gated luminescence detection of hydrogen peroxide, due to the obtained long-lived lanthanide emission ( $\Phi = 0.054$ ,  $t = 1.23$  ms) upon conversion of the initial complex in the oxidative product.<sup>53</sup>

The capability to modulate the electrons transfer to the lanthanide is a property not only employed in the above-mentioned work of *Lippert*, but it is widely exploited in many biology assays. The electron transfer from a “chemotype-masking” to the metal center is known as *Photo Induced Electron Transfer* (PeT), with the secondary effect to influence the antenna effect. If the photoexcitation of the antenna induces the electron transfer from the HOMO orbital of the cage (or *Pet switch*) to  $S_0$  level of the antenna, the Ln(III)-sensitization is lost. The presence of the hydrogen peroxide reported in the *Lippert*'s work oxidizes the antenna and then the *PeT switch* is not capable to transfer electrons to  $S_0$  anymore. Therefore, the Ln(III)-sensitization is restored (Figure 16).

With this in mind, the photoexcited molecule can act as a good oxidizing agent or a good reducing agent, according to the chemical structure and the nature of the analytes in the environment.

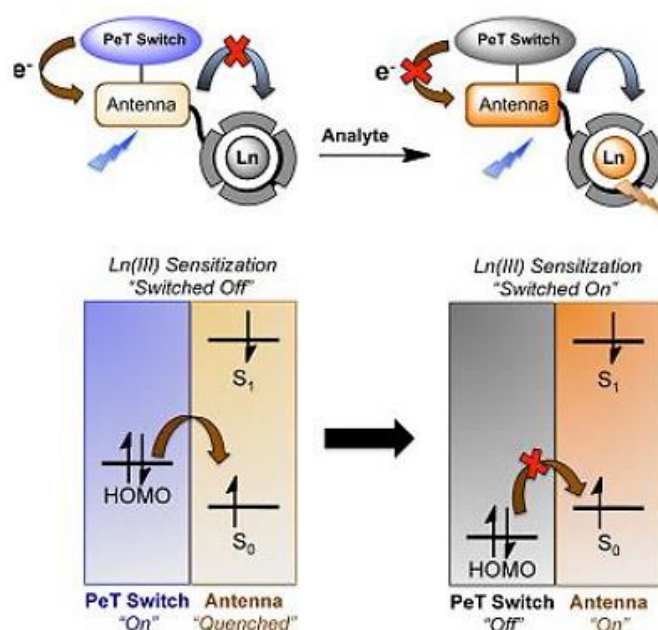


Figure 16. Schematic mechanism of the Photo Induced electrons transfer (PeT)

Chen<sup>84</sup> and co-workers developed a probe to detect the presence of Nitric oxide (NO), a reactive species containing one unpaired electron. In biology, it is important since it is involved in many processes.<sup>85-88</sup>

In humans, the nitric oxide is a signaling molecule in many physiological and pathological processes; moreover, it is an efficient vasodilator in the blood, with a half-life of a few seconds.<sup>89</sup>

NO is lipid-soluble and thus it is easily dispersed from the site where it is produced<sup>90</sup> for this reason a reliable and real-time method plays a crucial role. The strategy involved is to employ a probe bearing an electronrich o-diaminophenyl group. The interaction with the NO under aerobic conditions generates the corresponding benzotriazole derivative, and the photoinduced electron transfer (PeT) is interrupted, resulting in the turn-on of the probe (Figure 17).

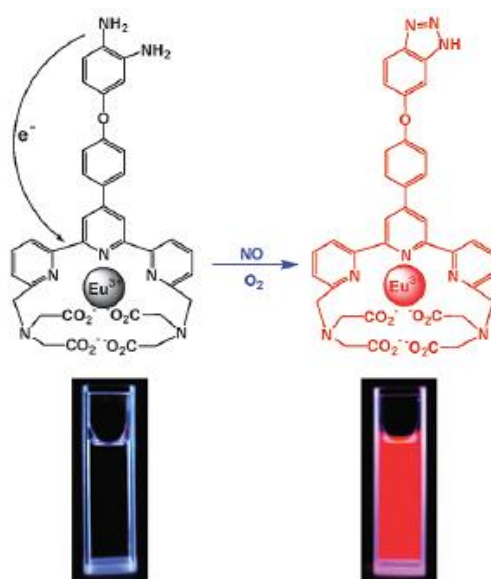


Figure 17. Structure of the Eu(III) complexes used to detect the NO through inhibition of PeT. [Ref. 90]

A selective probe to detect the presence of Cu(II) and Hg(II) ions in water is described in the work of McMahon and Gunnlaugsson.<sup>91</sup>

A sensitive method to reveal that ions, is of great importance for both environmental and biomedical purposes.<sup>92-106</sup>

In biomedicine, many Cu(II)-adducts play a crucial role in several enzymatic processes, whilst free Cu(II) can be fatal for various biological processes, such as *Wilson* and *Menkes* diseases.<sup>107, 108</sup>

As far as the Hg(II) ion is concerned, it is well known that it can accumulate in the blood–brain barrier resulting in severe neurological disorders.<sup>100-105</sup>

The above mentioned purposes employ a Tb(III) macrocycle DOTA like bearing as antenna an aniline moiety opportunely functionalized with a iminodiacetate unit suitable to bind the Cu(II) and Hg(II) in aqueous solution. The coordination results in a substantial decrease of the Tb(III) emission for both metal transitions (Figure 18).

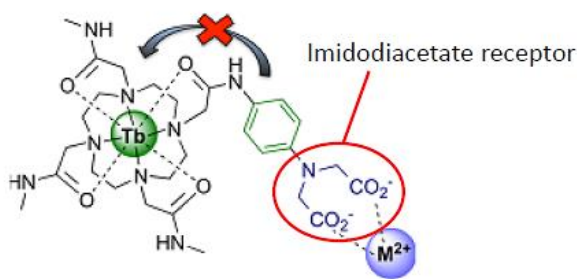


Figure 18. Structure of the Tb(III) complex to detect Cu(II) and Hg(II) ions. From [91]

#### 2.3.4. *Helicates*

As far as the helicates class is concerned, some representative compounds are constituted of a tridentate ligands, such as bis(benzimidazole)pyridines<sup>109</sup> or dipicolinates (DPA)<sup>110</sup>, which wrap around Ln(III) ions to yield saturated 9-coordinate complexes whose the ligand strands are hold together by weak intramolecular  $\pi$ - $\pi$  interactions. Lanthanide tris(dipicolinates) are quite stable in water at physiological pH, a fundamental feature for biosensing application, in particular, after suitable derivatisation, as multi-photonexcited stains.<sup>111</sup>

These molecules bearing two lanthanide ions have been successfully employed for protein structure investigation as reported in the work of Barthelmes and co-workers, where a library of water-soluble hexadentate dinuclear helicates with DPA core fitted with two benzimidazole chromophoric units has been obtained in good yields (Figure 19).<sup>112</sup>

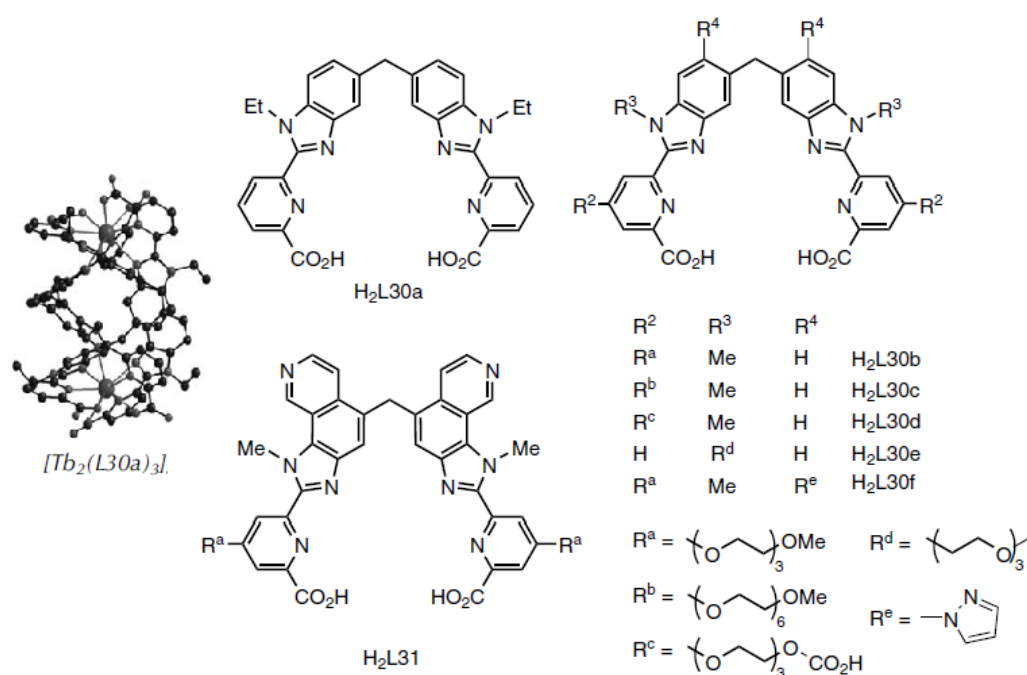


Figure 19. Hexadentate ligands for the self-assembly of lanthanide dinuclear helicates. [From 112]

The most important photophysical features for the  $[Eu_2(L)_3]$  helicates are summarized in Table 1. The most impressive features are surely the large molar absorption coefficients, around  $85.000 \text{ M}^{-1} \text{ cm}^{-1}$ , that they are far larger than those exhibited by most lanthanide bioprobes, long lifetimes, in addition to sizeable quantum yields in aqueous solution.

Ligand	% 2:3 <sup>a</sup>	$\text{Log } \epsilon^b$	(A-E) <sup>c</sup> , $\text{cm}^{-1}$	(E-E) <sup>c</sup> , $\text{cm}^{-1}$	$Q_{Eu}^L$ $\pm 10\%$	$\tau_{obs}^d$ , ms $\pm 2\%$	$\tau_{rad}^d$ , ms $\pm 12\%$	$Q_{Eu}^{Eu e}$ $\pm 12\%$	$\eta_{sens}^f$ $\pm 16\%$
$H_2L30a$	99.5	n.a.	156	28	0.24	2.4	6.9	0.37	0.67
$H_2L30b$	97.1	4.93	161	31	0.21	2.4	6.9	0.36	0.58
$H_2L30c$	92.9	n.a.	146	31	0.19	2.4	6.3	0.37	0.52
$H_4L30d$	n.a.	n.a.	180	n.a.	0.15	2.4	7.4	0.33	0.45
$H_2L30e$	89.2	n.a.	162	38	0.11	2.2	6.2	0.36	0.30
$H_2L30f$	92.5	4.97	168	26	0.15	2.5	6.4	0.40	0.38
$H_2L31$	94.6	4.90	177	34	0.09	2.3	6.7	0.35	0.26

<sup>a</sup> Percentage of the  $[Eu_2L_3]$  helicate for  $[L]_t = 4.5 \times 10^{-4} \text{ M}$

<sup>b</sup> Molar absorption coefficient of the helicate ( $\text{M}^{-1} \text{ cm}^{-1}$ )

<sup>c</sup> Splitting of the  $^5D_0 \rightarrow ^7F_1$  transition at 10K in water/glycerol 9/1, v/v (see text)

<sup>d</sup>  $Eu(^5D_0)$  radiative lifetime (see Equation 4.10)

<sup>e</sup> Intrinsic quantum yield (see Equation 4.10)

<sup>f</sup> Ligand sensitisation efficiency (see Equation 4.10)

Table 1. Photophysical properties of solutions of the helicates  $[Eu_2(L30i)_3]$  ( $i = a-f$ ) and  $[Eu_2(L31)_3]_6$  in aqueous solution (Tris-HCl 0.1 M) at pH 7.4 and 295 K. [Data from references: 16, 34, 113].

Since these probes are binuclear, the cytotoxicity is an important prerequisite to consider for the sensing and imaging of live biomaterials.



The collected data demonstrate that the cytotoxicity of all the tested helicates is negligible, with half inhibitory concentration  $IC_{50} > 500 \mu\text{M}$ . Some of these results were also confirmed by the lactase dehydrogenase (LDH) test, which allows an evaluation of damages caused to the cell membrane by determining the LDH leakage out of the cell. In the case of  $[\text{Eu}_2(\text{L30e})_3]$ , this leakage was found to be less than 4% for three tested cell lines.

## 2.4. *References*

1. [J.-C.G. Bünzli, *Chem. Rev.* **2010**, 110, 2729].
2. [J.-C.G. Bünzli, in: A. de Bettencourt-Dias (Ed.), *Luminescence in Lanthanide Coordination Compounds and Nanomaterials* Wiley-Blackwell, Oxford, **2014**, pp. 125.]
3. [J. Yuan, G. Wang, *TrAC - Trends Anal. Chem.* **2006**, 25, 490–500].
4. [J.-C.G. Bünzli, *J. Lum.* **2016**, 170, 866-878].
5. [K. L. Peterson, J. V. Dang, E. A. Weitz, C. Lewandowski, V. C. Pierre, *Inorg. Chem.* **2014**, 53 (12), 6013–6021].
6. [A. G. Weidmann, A. C. Komor, J. K. Barton, *Philos. Trans. R. Soc. A* **2013**, 371, 1995].
7. [C. A. Puckett, J. K. Barton, *J. Am. Chem. Soc.* **2007**, 129 (1), 46–47].
8. [A. S. Chauvin, F. Thomas, B. Song, C. D.B. Vandevyver, J. C. G. Bünzli, *Philos. Trans. R. Soc. A* **2013**, 371 (1995)].
9. [E. J. New, A. Congreve, D. Parker, *Chem. Sci.* **2010**, 1 (1), 111–118].
10. [B. S. Murray, E. J. New, R. Pal, D. Parker, *Org. Biomol. Chem.* **2008**, 6 (12), 2085–2094].
11. [J. L. Sessler and R. A. Miller, *Biochem.*, **2000**, 59, 733].
12. [J.-C. G. Bünzli, A.-S. Chauvin, C. D. B. Vandevyver, B. Song, S. Comby. *An. N. Y. Acad. Sci.*, **2008**, 1130, 97–105].
13. [M. P. Tsvirko, S. B. Meshkova, V. Y. Venchikov, Z. M. Topilova, D. V. Bol'shoi, *Opt. Spectrosc.* (Engl. Transl.), **2001**, 90, 669–673].
14. [K. A. Gschneidner, J.-C. G. Bünzli, V. K. Pecharsky, editors. Amsterdam, Elsevier Science B.V. **2007**, Vol. 37, Ch. 235, 217–470].
15. [J.-C. G. Bünzli, S. V. Eliseeva In Yam V. W.-W., editor. *Comprehensive Inorganic Chemistry II*. Ch. 8. 03, **2012**, Amsterdam, Elsevier B.V].

16. [J.-C. G. Bünzli, A.-S. Chauvin, H. K. Kim, E. Deiters, S. V. Eliseeva, *Coord. Chem. Rev.* **2010**, 254, 2623-2633].
17. [S. Nagl, M. I. J. Stich, M. Schaferling, O. S. Wolfbeis. *Anal. Bioanal. Chem.*, **2009**, 393, 1199–1207].
18. [W. J. Calvo, B. B. Lieber, N. Hopkins, A. K. Wakhloo, *Am. J. Neurorad.*, **2001**, 22, 691–697].
19. [J. L. Yuan, K. Matsumoto, *J. Pharm. Biomed. Anal.*, **1997**, 15, 1397–1403].
20. [J. L. Yuan, G. Wang, H. Kimura, K. Matsumoto, *Anal. Sci.*, **1998**, 14, 421-423].
21. [W. H. Guo, Z. Q. Ye, G. L. Wang, X. M. Zhao, J. L. Yuan, Y. G. Du. *Talanta*, **2009**, 78, 977–982].
22. [A. Reisch, A. Runser, Y. Arntz, Y. Mély, A. S. Klymchenko *Acs Nano*, **2015**, 9 (5), 5104–5116].
23. [J. Hu, J. Guo, Z. Xie, D. Shan, E. Gerhard, G. Qian, J. Yang *Acta Biomater.*, **2016**, 29, 307–319].
24. [C. Fornaguera, N. Feiner-Gracia, G. Calderó, M.J. García-Celmac, C. Solans *Colloids and Surfaces B: Biointer.* **2016**, 147, 201–209].
25. [T. Betancourt, K. Shah, L. Brannon-Peppas *J. Mater Sci: Mater Med* **2009**, 20, 387–395].
26. [P. P. Wyss, L. C. Herrera, N. S. Bouteghmes, M. Sarem, W. Reichardt, J. Leupold, J. Hennig, V. P. Shastri *ACS Omega* **2016**, 1, 182–192].
27. [L. J. Cruz, I. Que, M. Aswendt, Alan Chan, M. Hoehn, C. Löwik *Nano Res.* **2016**, 9(5), 1276–1289].
28. [R. Reul, N. Tsapis, H. Hillaireau, L. Sancey, S. Mura, M. Recher, J. Nicolas, J.-L. Coll, E. Fattal *Polym. Chem.*, **2012**, 3, 694-702].
29. [A. J. Mieszawska, Y. Kim, A. Gianella, I. van Rooy, B. Priem, M. P. Labarre, C. Ozcan, D. P. Cormode, A. Petrov, R. Langer, O. C. Farokhzad, Z. A. Fayad, W. J. M. Mulder *Bioconjugate Chem.* **2013**, 24, 1429–1434].
30. [P. Zhao, M. Zheng, C. Yue, Z. Luo, P. Gong, G. Gao, Z. Sheng, C. Zheng, L.Cai *Biomaterials* **2014**, 35, 6037-6046].
31. [B. Zheng, Y. Bai, H. Chen, H. Pan, W. Ji, X. Gong, X. Wu, H. Wang, J. Chang *Biomater. Sci.* **2018**, 6, 1379-1389].
32. [A. Topete, D. Melgar, M. Alatorre-Meda, P. Iglesias, B. Argibay, S. Vidawati, S. Barbosa, J. A. Costoya, P. Taboada, V. Mosquera *J. Mater. Chem. B*, **2014**, 2, 6967-6977].

33. [S. Naik, E. E. Carpenter *J. of Appl. Phis.* **2008**, 103, 07A313].
34. [V. Fernandez-Moreira, B. Song, V. Sivagnanam, A.-S. Chauvin, C. D. B. Vandevyver, M. A. M. Gijs, I. A. Hemmilä, H.-A. Lehr, and J.-C. G. Bünzli, *Analyst*, **2010**, 135, 42].
35. [A. Bianchi, L. Calabi, F. Corana, S. Fontana, P. Losi, A. Maiocchi, L. Paleari, B. Valtancoli, *Coord. Chem. Rev.*, **2000**, 204, 309–393].
36. [A. E. Soini A. Kuusisto, N. J. Meltola, E. Soini, L. Seveus. *Microsc. Res. Techn.*, **2003**, 62, 396–407].
37. [B. K. McMahon, R. Pal, D. Parker *Chem. Commun.*, **2013**, 49, 5363-5365].
38. [J. H. Kim, L. Johannes, B. Goud, C. Anthony, C. A. Lingwood, R. Daneman, S. Grinstein, *Proc. Natl. Acad. Sci. U. S. A.*, **1998**, 95, 2997].
39. [D. G. Smith, R. Pal, D. Parker, *Chem. - A Eur. J.* **2012**, 18, 11604–11613].
40. [C. A. Wagner, J. Kovacikova, P. A. Stehberger, C. Winter, C. Benabbas, N. Mohebbi, *Neph. Phys.* **2006**, 103, 1].
41. [J. D. Kopple, K. Kalantar-Zadeh, R. Mehrotra, *Kidney Int.* **2005**, 67, S21].
42. [M. J. Martin, E. FitzSullivan, A. Salim, T. V. Berne, S. Towfigh, *Arch. Surg.* **2005**, 140, 745].
43. [S. J. Butler, D. Parker, *Chem. Soc. Rev.*, **2013**, 42, 1652–1666].
44. [O. Kotova, S. Comby, T. Gunnlaugsson, *Chem. Commun.*, **2011**, 47, 6810-6812].
45. [R. McRae, P. Bagchi, S. Sumalekshmy, C. J. Fahrni, *Chem. Rev.*, **2009**, 109, 4780].
46. [C. Lodeiro, J. L. Capelo, J. C. Mejuto, E. Oliveira, H. M. Santos, B. Pedras, C. Nunez, *Chem. Soc. Rev.*, **2010**, 39, 2948].
47. [E. L. Que, D. W. Domaille and C. J. Chang, *Chem. Rev.*, 2008, 108, 1517; K. L. Haas, K. J. Franz, *Chem. Rev.*, **2009**, 109, 4921].
48. [S. Pehkonen, *Analyst*, **1995**, 120, 2655].
49. [E. P. Achterberg, T. W. Holland, A. R. Bowie, R. F. C. Mantoura, P. J. Worsfold, *Anal. Chim. Acta*, **2001**, 442, 1].
50. [U. Hase, K. Yoshimura, *Analyst*, **1992**, 117, 1501].
51. [E. A. Weitz, V. C. Pierre *Chem. Commun.*, **2011**, 47, 541–543].
52. [J. R. Lakowicz, *Principles of Fluorescence Spectroscopy*, Springer, New York, 2006].
53. [A. R. Lippert, T. Gschneidner, C. J. Chang, *Chem. Commun.*, **2010**, 46, 7510–7512].

54. [D. Harman, *Proc. Natl. Acad. Sci. U. S. A.*, **1981**, 78, 7124].
55. [R. A. Floyd, *Science*, **1991**, 254, 1597].
56. [B. D'Autreaux, M. B. Toledano, *Nat. Rev. Mol. Cell Biol.*, **2007**, 8, 813].
57. [C. C. Winterbourn, *Nat. Chem. Biol.*, **2008**, 4, 278].
58. [S. G. Rhee, *Science*, **2006**, 312, 1882].
59. [J. R. Stone, S. Yang, *Antioxid. Redox Signaling*, **2006**, 8, 243].
60. [E. A. Veal, A. M. Day, B. A. Morgan, *Mol. Cell*, **2007**, 26, 1].
61. [E. W. Miller and C. J. Chang, *Curr. Opin. Chem. Biol.*, **2007**, 11, 620].
62. [L. B. Poole, K. J. Nelson, *Curr. Opin. Cell Biol.*, **2008**, 12, 18].
63. [C. E. Paulsen, K. S. Carroll, *ACS Chem. Biol.*, **2010**, 5, 47].
64. [J. Foreman, V. Demidchik, J. H. Bothwell, P. Mylona, H. Miedema, M. A. Torres, P. Linstead, S. Costa, C. Brownlee, J. D. Jones, J. M. Davies and L. Dolan, *Nature*, **2003**, 422, 442].
65. [M. Geiszt and T. L. Leto, *J. Biol. Chem.*, **2004**, 279, 51715].
66. [G. Groeger, C. Quiney, T. G. Cotter, *Antioxid. Redox Signaling*, **2009**, 11, 2655].
67. [H. Sauer, G. Rahimi, J. Hescheler, M. Wartenberg, *FEBS Lett.*, **2000**, 476, 769].
68. [J. Li, M. Stouffs, L. Serrander, B. Banfi, E. Bettiol, Y. Charnay, K. Steger, K. H. Kraus, M. E. Jaconi, *Mol. Biol. Cell*, **2006**, 17, 3978].
69. [M. Ushio-Fukai, *Cardiovasc. Res.*, **2006**, 71, 226].
70. [P. Niethammer, C. Grabher, A. T. Look, T. J. Mitchison, *Nature*, **2009**, 459, 996].
71. [J. D. Lambeth, *Nat. Rev. Immunol.*, **2004**, 4, 181].
72. [K. Bedard, K.-H. Krause, *Physiol. Rev.*, **2007**, 87, 245].
73. [T. Finkel, N. J. Holbrook, *Nature*, **2000**, 40, 1250].
74. [M. Giorgio, M. Trinei, E. Migliaccio, P. G. Pelicci, *Nat. Rev. Mol. Cell Biol.*, **2007**, 8, 722].
75. [J. P. Fruehauf, F. L. Meyskens, Jr., *Clin. Cancer Res.*, **2007**, 13, 789].
76. [T. Finkel, M. Serrano, M. A. Blasco, *Nature*, **2007**, 448, 767].
77. [K. Ishikawa, K. Takenaga, M. Akimoto, N. Koshikawa, A. Yamaguchi, H. Imanishi, K. Nakada, Y. Honma, J. Hayashi, *Science*, **2008**, 320, 661].
78. [N. Houstis, E. D. Rosen, E. S. Lander, *Nature*, **2006**, 440, 944].
79. [R. Pop-Busui, A. Sima, M. Stevens, *Diabetes/Metab. Res. Rev.*, **2006**, 22, 257].
80. [D. Jay, H. Hitomi, K. K. Griendling, *Free Radical Biol. Med.*, **2006**, 40, 183].

81. [M. P. Mattson, *Nature*, **2004**, 430, 631]
82. [M. T. Lin, M. F. Beal, *Nature*, **2006**, 443, 787].
83. [S. DiMauro, E. A. Schon, *Annu. Rev. Neurosci.*, **2008**, 31, 91].
84. [Y. Chen, W. Guo, Z. Ye, G. Wang, J. Yuan, *Chem. Commun.*, **2011**, 47, 6266–6268].
85. [R. M. J. Palmer, A. G. Ferrige, S. Moncada, *Nature*, **1987**, 327, 524].
86. [S. H. Snyder, *Science*, **1992**, 257, 494].
87. [J. M. Zimmet, J. M. Hare, *Circulation*, **2006**, 114, 1531].
88. [S. Jasid, M. Simontacchi, C. G. Bartoli, S. Puntarulo, *Plant Physiol.*, **2006**, 142, 1246].
89. [Hou, Y.C; Janczuk, A; P.G. Wang, *Current Pharmaceutical Design*, **1999**, 5 (6), 417–41].
90. [M. W. Vaughn, L. Kuo, J. C. Liao, *Am. J. Physiol. Heart Circ. Physiol.*, **1998**, 274, H1705].
91. [B. K. McMahon, T. Gunnlaugsson, *Tetrahedron Lett.*, **2010**, 51, 5406–5410].
92. [M. Andrews, J. E. Jones, L. P. Harding, S. J. A. Pope, *Chem. Commun.* **2010**, 46].
93. [S. J. A. Pope, R. H. Laye, *Dalton Trans.* **2006**, 3108].
94. [K. Hanaoka, K. Kikuchi, H. Kojima, Y. Urano, T. Nagana, *Angew. Chem., Int. Ed.* **2003**, 42, 2996].
95. [K. Hanaoka, K. Kikuchi, H. Kojima, Y. Urano, T. Nagana, *J. Am. Chem. Soc.* **2004**, 126, 12470].
96. [P. D. Selid, H. Xu, E. M. Collins, M. Collins, J. X. Zhao, *Sensors*, **2009**, 9, 5446].
97. [A. Torrado, G. K. Walkup, B. Imperiali, *J. Am. Chem. Soc.* **1998**, 120, 609].
98. [M. Beltramello, M. Gatos, F. Mancin, P. Tecilla, U. Tonellato, *Tetrahedron Lett.* **2001**, 42, 9143].
99. [J. Yoon, N. E. Ohler, D. H. Vance, W. D. Aumiller, U. Tonellato, *Tetrahedron Lett.* **1997**, 38, 3845].
100. [B. C. Barja, P. F. Aramendia, *Photochem. Photobiol. Sci.* **2008**, 7, 1391].
101. [Y. Liu, M. Yu, Y. Chen, N. Zhang, *Bioorg. Med. Chem.* **2009**, 17, 3887].
102. [J. Y. Kwon, J. Hyun Soh, Y. Yoon, J. Yoon, *J. Supramol. Chem.* **2004**, 16, 621].
103. [M. Tian, H. Ihmels, *Chem. Commun.* **2009**, 3175].

104. [N. Wanichacheva, M. Siriprumpoonthum, A. Kamkaew, K. Grudpan, *Tetrahedron Lett.* **2009**, 50, 1783].
105. [Y. Hasegawa, R. Hieda, T. Nakagawa, T. Kawai, *Helv. Chim. Acta* **2009**, 92, 2238].
106. [B. Sarkar, *Chem. Rev.* **1999**, 99, 2535].
107. [M. C. Lindar, M. Hazegh-Azam, *Am. J. Clin. Nutr.* **1996**, 63, 8218].
108. [B. Sarker, *Handbook on Metals in Clinical and Analytical Chemistry*; Marcel Dekker: New York, **1994**].
109. [C. Piguet, A. F. Williams, G. Bernardinelli, J.-C. G. Bünzli. *Inorg. Chem.*, **1993**, 32, 4139–4149].
110. [A. -L. Gassner, C. Duhot, J.-C. G. Bünzli, A.-S. Chauvin. *Inorg. Chem.*, **2008**, 47, 7802–7812].
111. [A. Picot, A. D'Aléo, P. L. Baldeck, A. Grichine, A. Duperray, C. Andraud, O. Maury. *J. Am. Chem. Soc.*, **2008**, 130, 1532–1533].
112. [K. Barthelmes, A. M. Reynolds, E. Peisach, H. R. A. Jonker, N. J. De Nunzio, K. N. Allen, B. Imperiali, H. Schwalbe, *J. Am. Chem. Soc.*, **2011**, 133, 808–819].
113. [E. Deiters, B. Song, A.-S. Chauvin, C. Vandevyver, J.-C. G. Bünzli. *Chem. Eur. J.*, **2009**, 15, 885–900].

## **CHAPTER 3- EXPERIMENTAL RESULTS: New Ln(III) complexes as luminescence bioprobes**

### ***3.1. Complexes of rare earth ions embedded in Poly(lactic-co-glycolic acid) (PLGA) nanoparticles***

#### ***3.1.1. Introduction***

Optical probes based on lanthanide complexes are certainly one of the most important classes of molecules in the field of molecular medicine, because of their properties such as high sensitivity, and easy detection.

Furthermore, compared to organic dyes, they possess longer lifetimes, and lower sensitivity to photobleaching. These lanthanide bioprobes should be highly stable in water, small propensity to dissociation at low concentration and analyte-dependent luminescence properties (e.g., *biosensing* in vitro or in vivo applications).

If the probe cannot be directly used in aqueous solution, the encapsulation in different matrices (e.g., biocompatible nanoparticles) could be a good strategy to exploit also water insoluble Ln-complexes, as shown in the following study. The optical properties of these probes can be also used to visualize organs, cells, etc. such as in the field of bioimaging applications.

### ***3.2. Water insoluble Eu(III) complexes: encapsulation in PLGA for bioimaging purposes***

In this context, a lipophilic and water-insoluble luminescent Eu(III) complex has been encapsulated in the biocompatible Poly(lactic-co-glycolic acid (PLGA) polymer,<sup>1</sup> by using two compositions: Poly(lactic(50%)-co-glycolic acid(50%), PLGA 50:50 and Poly(lactic(75%)-co-glycolic acid(25%), PLGA 75:25. As clearly discussed, the efficiency of both encapsulation and Eu(III) luminescence are strongly dependent on the nature of the complex.

PLGA is one of the most successfully developed biodegradable and biocompatible polymers. Furthermore, they are FDA (Food and Drug Administration) and EMA

(European Medicine Agency) approved in drug delivery systems for parenteral administration and there are several well described formulations and methods of production adapted to various types of drugs i.e. hydrophilic or hydrophobic small molecules or macromolecules. PLGA is also capable to protect drug and dye from degradation<sup>2</sup> and to guarantee a sustained release and its surface properties can be modified to provide better interaction with biological materials and to target nanoparticles to specific organs or cells.<sup>3,4</sup>

Moreover, the PLGA nanoparticles (NP's) can be seen as very efficient "nanocarrier" both for drugs and contrast agents. In the field of optical imaging, several visible<sup>5-8</sup> and NIR-emitting<sup>9-11</sup> organic dyes have been successfully encapsulated and employed in *in vivo* experiments.

In order to obtain excellent brightness a strong dye loading without aggregation-caused quenching (ACQ) is required.<sup>12</sup> ACQ is a considerable problem and it is responsible for conflicting interpretations of data in the quantitative analysis of whole-body optical imaging.<sup>13</sup> In order to prevent false observations in whole-body fluorescence imaging of NP distribution, it is important to verify that fluorescence dyes do not quench in NPs and the fluorescence intensity increases linearly with the NP concentration. Only recently several strategies of dye design were proposed to overcome ACQ in polymer NPs. In particular, aggregation induced emission (AIE) and dye modification with bulky side groups and use of bulky hydrophobic counterions.<sup>14</sup> Most of the fluorophores are organic molecules that show significant overlap between the excitation and emission spectra [in particular, near-infrared (NIR) ones] and therefore exhibit high fluorescence backgrounds during *in vivo* imaging. To overcome this drawback, two dyes have been incorporated in the same PLGA nanoparticle and the energy transfer process from the donor to the acceptor dye is employed. The larger gap between the excitation and emission maxima (>100 nm) ensures a reduction of the background signal.<sup>15</sup> A similar process is exploited when conjugated polymer nanoparticles (CPNs) capped with PLGA transfer its excitation energy to a hydrophobic NIR dye, which is encapsulated within the nanoparticles.<sup>16</sup>



All the above mentioned drawbacks could be overcome by using the luminescent Ln(III) complexes as emitting species. Even though these compounds have been poorly employed to date,<sup>17</sup> we believe that they should have a bright role in this field. As already described in previous parts, the Eu(III) and Tb(III) complexes show several advantages: i) they can emit visible light with a large gap between the excitation and emission maxima, thanks to the well-known ligand to metal energy transfer (antenna effect); ii) they do not usually suffer from ACQ phenomenon and iii) by using a time-gated detection it is possible to isolate their emission (excited state lifetimes in the ms range) from autofluorescence (excited state lifetimes in the ns-ps range) in complex microenvironments such as cells, tissues or living animals. In addition, due to the close similarity between the ionic radii of Y(III) and Ln(III), also isostructural Y(III) complexes could be conveniently entrapped in PLGA nanoparticles. Radioactive Y(III) species embedded in biocompatible nanoparticles could be used in nuclear medicine as Positron Emission Tomography (PET) contrast agents.<sup>18</sup> Precisely, we mainly discuss the synthesis, the characterization and the spectroscopic study of PLGA nanoparticles containing an Eu(III)-based complex where two anionic tta (2-Thenoyltrifluoroacetyl-acetonate), one chiral tetradentate Schiff base NNNN ligands surround the Eu(III) ion (Figure 1).

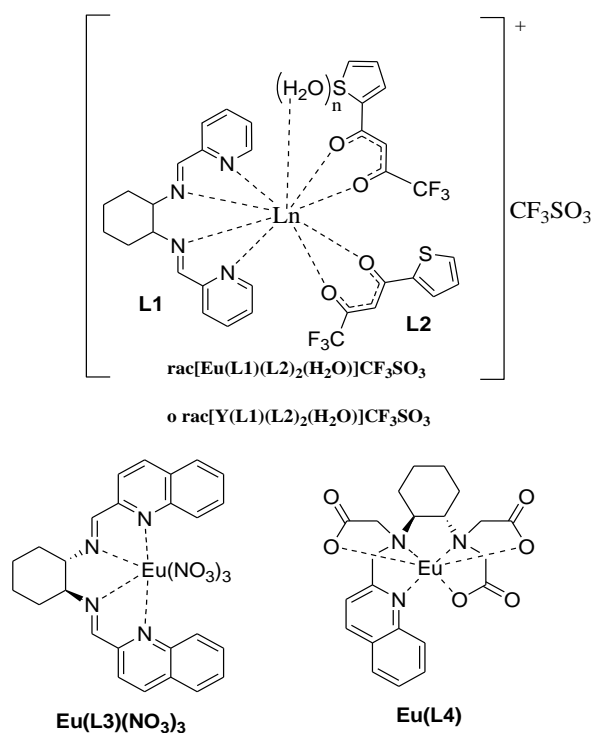


Figure 1. Complexes based on L1 (=N, N'-bis(2-pyridylmethylidene)-1,2-(R,R+S,S)-cyclohexanediamine) and L2 (=2-thenoyltrifluoroacetyl-acetonate, L3 (N, N'-bis(2-quinolylmethylidene)-1,2-(R,R+S,S)-cyclohexanediamine), L4 (N-quinolyl-N,N',N'-trans-1,2-cyclohexylenediaminetriacetic acid) under investigation.

Two different polymeric compositions [Poly(lactic(50%)-co-glycolic acid(50%)) and Poly(lactic(75%)-co-glycolic acid(25%))] were employed, and the Eu(III) luminescence in correlation with time and temperature was studied. A similar purpose involving the use of PLGA NP's as host material was also performed for the analogous Y(III) complex ( $[\text{Y}(\text{L1})(\text{L2})_2(\text{H}_2\text{O})]\cdot\text{CF}_3\text{SO}_3$ ).

### 3.2.1. PLGA luminescent nanoparticles: physical characterization

As already mentioned, two composition of PLGA nanoparticles containing different Ln(III) complexes (Ln = Y and Eu) were used: 1) (50:50) more hydrophilic and 2) (75:25) more hydrophobic. According to the protocol previously set up by our research groups for the synthesis of the ligand L1,<sup>19</sup> the new  $\text{rac}[\text{Y}(\text{L1})(\text{L2})_2(\text{H}_2\text{O})]\cdot\text{CF}_3\text{SO}_3$  complex has been obtained in a good chemical yield and high degree of purity.

Both complexes  $[\text{Eu}(\text{L1})(\text{L2})_2(\text{H}_2\text{O})]\cdot\text{CF}_3\text{SO}_3$  and  $[\text{Y}(\text{L1})(\text{L2})_2(\text{H}_2\text{O})]\cdot\text{CF}_3\text{SO}_3$   $\text{Eu}(\text{L3})(\text{NO}_3)_3$  and  $\text{Eu}(\text{L4})$  have been encapsulated in PLGA to get six different samples called:

- Sample 1 (S1):  $[\text{Eu}(\text{L1})(\text{L2})_2(\text{H}_2\text{O})]\cdot\text{CF}_3\text{SO}_3$  embedded in PLGA 50:50
- Sample 2 (S2):  $[\text{Eu}(\text{L1})(\text{L2})_2(\text{H}_2\text{O})]\cdot\text{CF}_3\text{SO}_3$  embedded in PLGA 75:25
- Sample 3 (S3):  $[\text{Y}(\text{L1})(\text{L2})_2(\text{H}_2\text{O})]\cdot\text{CF}_3\text{SO}_3$  embedded in PLGA 50:50
- Sample 4 (S4):  $[\text{Y}(\text{L1})(\text{L2})_2(\text{H}_2\text{O})]\cdot\text{CF}_3\text{SO}_3$  embedded in PLGA 75:25
- Sample 5 (S5):  $\text{Eu}(\text{L4})$  embedded in PLGA 50:50
- Sample 6 (S6) :  $\text{Eu}(\text{L3})(\text{NO}_3)_3$  embedded in PLGA 50:50

In Figure 2, the DLS diagram of  $[\text{Eu}(\text{L1})(\text{L2})_2(\text{H}_2\text{O})]\cdot\text{CF}_3\text{SO}_3$  embedded in PLGA 75:25 (sample S2) dispersed in Phosphate buffered saline (PBS) is depicted.

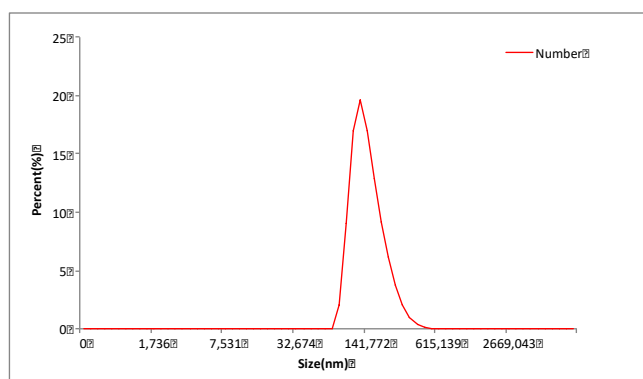


Figure 2. DLS diagram of  $[\text{Eu}(\text{L1})(\text{L2})_2(\text{H}_2\text{O})]\cdot\text{CF}_3\text{SO}_3$  embedded in PLGA 75:25 (sample S2) dispersed in PBS. The Z-size reported in table 1 is the average value calculated on three different samples.

A family of nanoparticles whose diameters are distributed around 193 nm with a standard deviation of 54 nm was efficiently obtained. The synthesis of the  $[\text{Ln}(\text{L1})(\text{L2})_2(\text{H}_2\text{O})]\cdot\text{CF}_3\text{SO}_3$  ( $\text{Ln} = \text{Y}$  and  $\text{Eu}$ ) embedded in PLGA gives rise to nanoparticles whose dimensions range between 130 and 250 nm when PLGA 50:50 is employed (Table 1); whereas the same nanoparticles obtained with PLGA 75:25 are slightly bigger (145-279 nm range).

Embedded complex	PLGA employed							
	50:50				75:25			
	Z-size (esd)	AFM size (esd)	Z-pot.	Tm	Z-size (esd)	AFM size (esd)	Z-pot.	Tm
None	180(48)	–	–10.7	29.1(3)	182(47)	–	–4.47	34.0(1)
[Eu(L1)(L2) <sub>2</sub> (H <sub>2</sub> O)]·CF <sub>3</sub> SO <sub>3</sub>	187(53)	179(26)	–5.58	33.5(1)	204(59)	195(40)	–4.51	38.0(1)
[Y(L1)(L2) <sub>2</sub> (H <sub>2</sub> O)]·CF <sub>3</sub> SO <sub>3</sub>	200(54)	188.8(1)	–5.37	33.1(1)	219(60)	194.5(1)	–4.27	37.1(1)

Table 1. Size (nm), Z-potential (mV) and melting temperature (T<sub>m</sub>; °C) of PLGA 50:50 and 75:25 nanoparticles: empty or embedding [Eu(L1)(L2)<sub>2</sub>(H<sub>2</sub>O)]·CF<sub>3</sub>SO<sub>3</sub> and [Y(L1)(L2)<sub>2</sub>(H<sub>2</sub>O)]·CF<sub>3</sub>SO<sub>3</sub> complexes.

The particle size estimated in PBS (with Dynamic Light Scattering-DLS technique) is in agreement with the one determined by Atomic Force Microscopy-AFM (Table 1) and Z-potential shows, as expected, negative values for all the synthesized nanoparticles. In fact, on the PLGA nanoparticles surfaces there should be residual carboxylic groups, which are deprotonated at the working pH<sup>20</sup>.

As far as the shape of the obtained nanoparticles is concerned, in Figure 3 the AFM analysis is depicted showing a regular spherical shape of the nanoparticles radii (range: 180-200 nm).

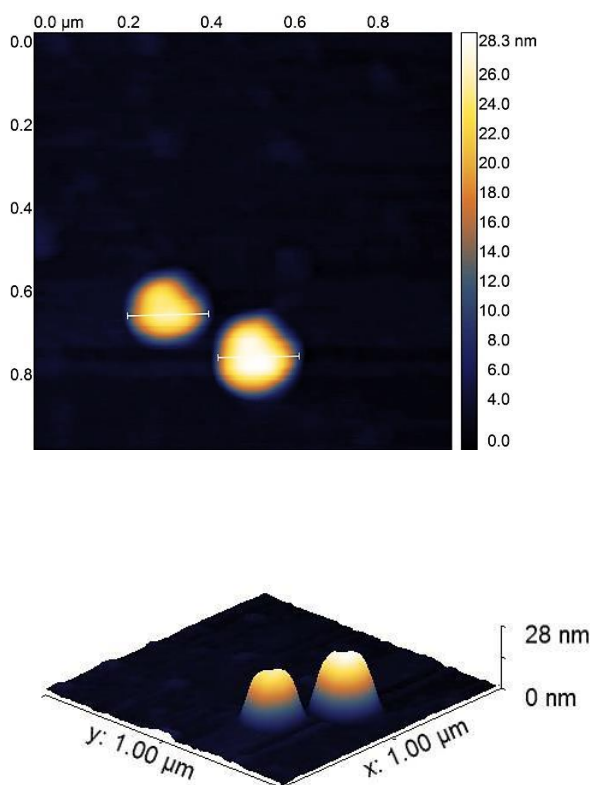
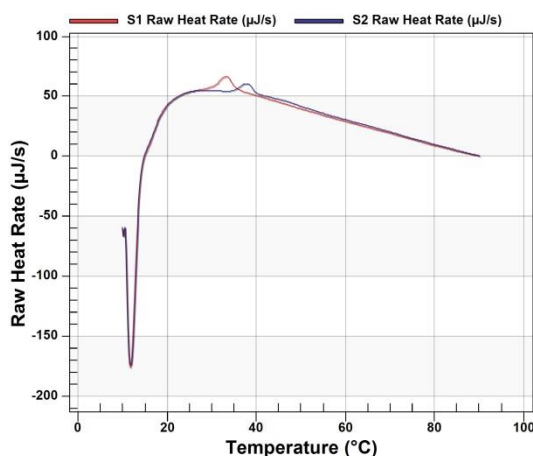


Figure 3. AFM images of [Y(L1)(L2)<sub>2</sub>(H<sub>2</sub>O)]·CF<sub>3</sub>SO<sub>3</sub> complex embedded in PLGA 75:25

In Table 1, the melting temperature ( $T_m$ ) of the PLGA polymer is also reported. This temperature is connected to the stability of the system as a function of the temperature and it is related to the breaking of weak interactions such as dipole-dipole, Van Der Waals and hydrogen bond interactions responsible of the assembly of the nanoparticles. It is worth noting that, the NP's (75:25, sample S2), containing a higher quantity of the poly-lactic component, are more thermally resistant than the 50:50 ones (sample S1), since they show a melting temperature around 37-38°C ( $T_m$  is around 33°C for the 50:50 system, Table 1 and Figure 4).

(a)



(b)

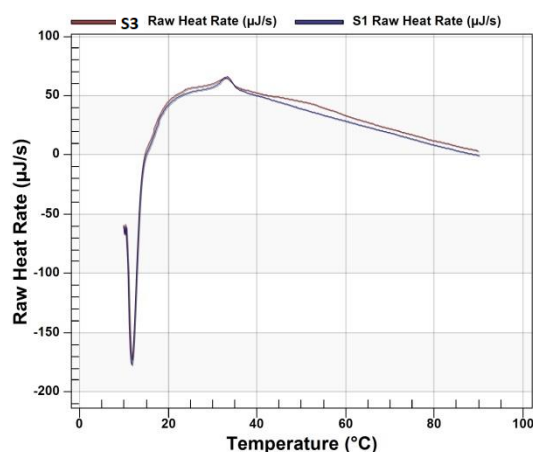


Figure 4. Superimposition of DSC diagram for (a) S1 ( $\text{Eu}(\text{LI}(\text{L2})_2(\text{H}_2\text{O}))\cdot\text{CF}_3\text{SO}_3$  complex embedded in PLGA 50:50, red line) and S2 ( $\text{Eu}(\text{LI}(\text{L2})_2(\text{H}_2\text{O}))\cdot\text{CF}_3\text{SO}_3$  complex embedded in PLGA 75:25, blue line), and (b) S3 ( $\text{Y}(\text{LI}(\text{L2})_2(\text{H}_2\text{O}))\cdot\text{CF}_3\text{SO}_3$  complex embedded in PLGA 50:50) and S1.

The thermal stability of these nanoparticles is a very important feature, as far as biomedical applications such as bioimaging are concerned. The empty PLGA

nanoparticles show a melting temperature of 34°C and 29°C, for the 75:25 and 50:50 compositions, respectively. In conclusion, the presence of the complexes inside the PLGA nanoparticles gives rise to an increased thermal stability of the assembly.

The UV-Visible electronic absorption spectra of Y(III) and Eu(III) complexes are very similar (Figure 5).

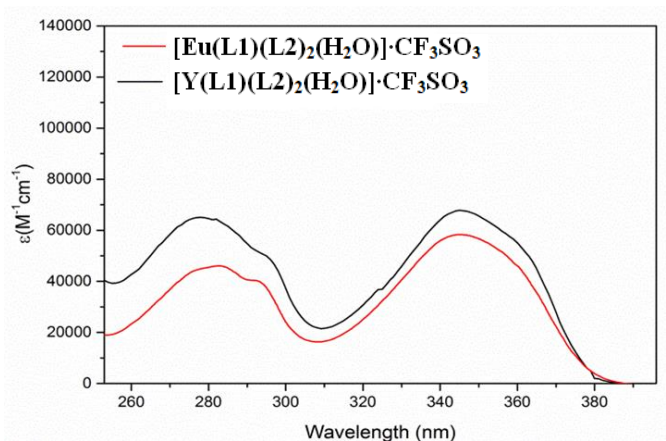
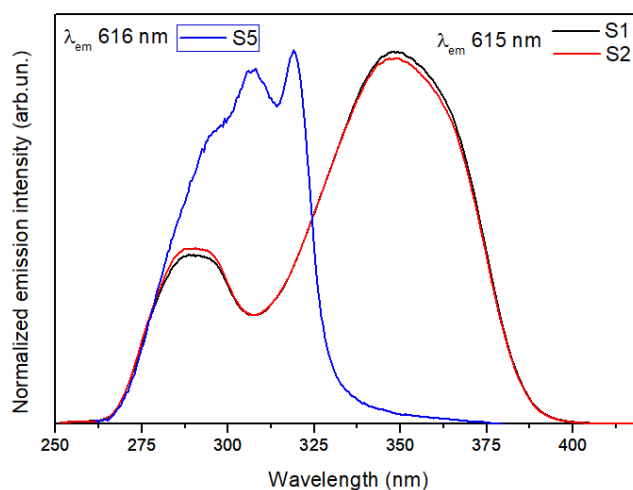


Figure 5. UV-Visible electronic absorption spectrum of  $[Eu(L1)(L2)_2(H_2O)]\cdot CF_3SO_3$  and  $[Y(L1)(L2)_2(H_2O)]\cdot CF_3SO_3$  dissolved in acetonitrile.

Besides to the (Eu or Y)tta-complexes, even the complexes  $Eu(L3)(NO_3)_3$  (S6) and  $Eu(L4)$  (S5) were investigated with the same purposes of encapsulation in PLGA polymer, although with very low efficiency (Figure 6b and 8).

The luminescence excitation and emission spectra of Eu(III)-based complexes embedded in PLGA nanoparticles suspended in a buffered phosphate aqueous solution are shown in Figure 6.

(a)



(b)

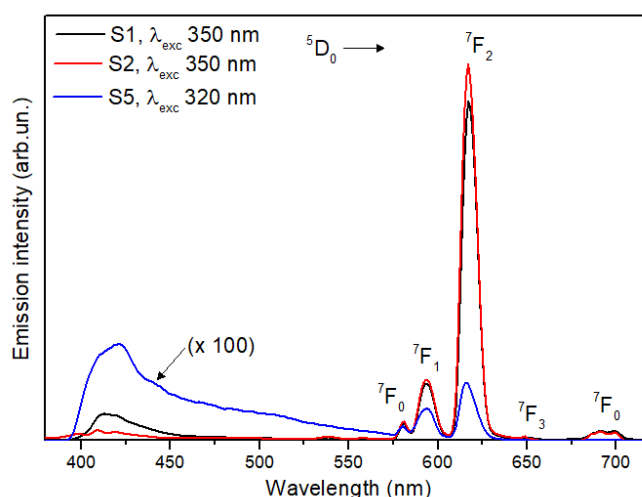


Figura 6. (a) Luminescence excitation spectra (normalized) and (b) Luminescence emission spectra of S1 ( $\text{Eu}(\text{L1})(\text{L2})_2(\text{H}_2\text{O})\cdot\text{CF}_3\text{SO}_3$  complex embedded in PLGA 50:50, S2 ( $\text{Eu}(\text{L1})(\text{L2})_2(\text{H}_2\text{O})\cdot\text{CF}_3\text{SO}_3$  complex embedded in PLGA 75:25, and S5  $\text{Eu}(\text{L4})$  complex embedded in PLGA 50:50, all suspended in phosphate buffer aqueous solution.

The excitation spectra recorded in aqueous solution for the nanoparticles containing  $[\text{Eu}(\text{L1})(\text{L2})_2(\text{H}_2\text{O})\cdot\text{CF}_3\text{SO}_3]$  complex synthesized with the different PLGA composition (50:50, sample S1 and 75:25, sample S2) are identical and superimposable with the excitation spectra of the complex alone.<sup>19</sup> The presence of two excitation bands centered at around 280 nm and 350 nm is a clear indication of a ligand to metal energy transfer from the ligands L1 and L2

respectively. It is interesting to note that the sensitization of the Eu(III) luminescence can be achieved upon excitation in a wide UV spectral range (250-400 nm). Potentially, this gives the opportunity to choose the more suitable excitation wavelength. In particular, the excitation peak around 350 (in the N-UV region) is particularly attractive for biomedical application since this wavelength is hardly absorbed by interfering biomolecules necessarily present in a real matrix. Otherwise, in the case of embedded Eu(L4) complex in PLGA 50:50 (sample S5) formulation, only a peak centered around 320 nm is detected (Figure 6b).

A close inspection of the luminescence emission spectra for Eu(L1)(L2)<sub>2</sub>(H<sub>2</sub>O)]·CF<sub>3</sub>SO<sub>3</sub> complex embedded in the two different PLGA formulations reveals that the two spectra are virtually identical, except for the intensity of <sup>5</sup>D<sub>0</sub>→<sup>7</sup>F<sub>2</sub> emission peak around 615 nm, which is slightly higher for the 75:25 PLGA assembly (Figure 6b). Consequently, the values of the asymmetry ratio, R<sup>21, 22</sup> in (1):

$$R = \frac{I(^5D_0 \rightarrow ^7F_2)}{I(^5D_0 \rightarrow ^7F_1)} \quad (1)$$

indicative of the degree of asymmetry of the coordination polyhedron around the Eu(III) ion, is slightly higher in the case of the 75:25 composition (R = 6.0 for 75:25 and 5.6 for 50:50). On the other hand, even though the <sup>5</sup>D<sub>0</sub>→<sup>7</sup>F<sub>2</sub> emission band dominates the spectrum also when the complex alone is dissolved in organic solvent such as acetonitrile and methanol, we calculate a considerable different value of the asymmetry ratio (R around 12, Figure 7), compatible with a higher asymmetry of the Eu(III) coordination sphere.



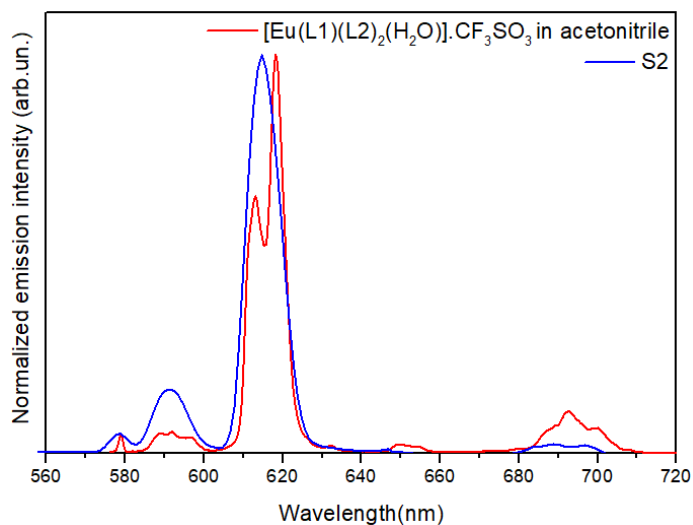


Figure 7. Luminescence emission spectra of S2 ( $[Eu(L1)(L2)_2(H_2O)] \cdot CF_3SO_3$  complex embedded in PLGA 75:25) suspended in phosphate buffer aqueous solution and  $[Eu(L1)(L2)_2(H_2O)] \cdot CF_3SO_3$  dissolved in acetonitrile;  $\lambda_{exc} = 350$  nm.

This discrepancy underlines the non-innocent role of the environment, once the complex is embedded in PLGA polymer. We also detect, for both compositions, the presence of a small broad peak above 400 nm, attributable to ligands fluorescence (Figure 6b). Also this finding is in agreement with the presence of a polymer-complex interaction, which affects the luminescence properties of the coordination compound. Since no ligand fluorescence has been observed for the complex alone in solution<sup>19</sup> and the fluorescence band is almost absent in the case 75:25 composition, we can suppose that the Eu(III) complex is less perturbed when embedded in PLGA containing a higher amount of poly-lactic acid.

As far as the complexes  $Eu(L3)(NO_3)_3$  and  $Eu(L4)$  4 are concerned, when  $Eu(L4)$  is embedded in the PLGA nanoparticles, upon excitation in the ligand absorption band, only a very low luminescence intensity is detected (Figure 6b) and the emission band around 420 nm, due to the quinoline fluorescence<sup>23</sup> dominates the spectrum. Moreover, whereas the characteristic absorption peaks of  $[Ln(L1)(L2)_2(H_2O)] \cdot CF_3SO_3$  ( $Ln = Eu, Y$ ) are clearly detectable in the electronic absorption spectra of the PLGA NP's (Figure 8), in the case of  $Eu(L4)$ , the absorption peak of the complex is covered by the PLGA absorption. This is a clear indication of ineffective incorporation of  $Eu(L4)$  in the polymer NP's.

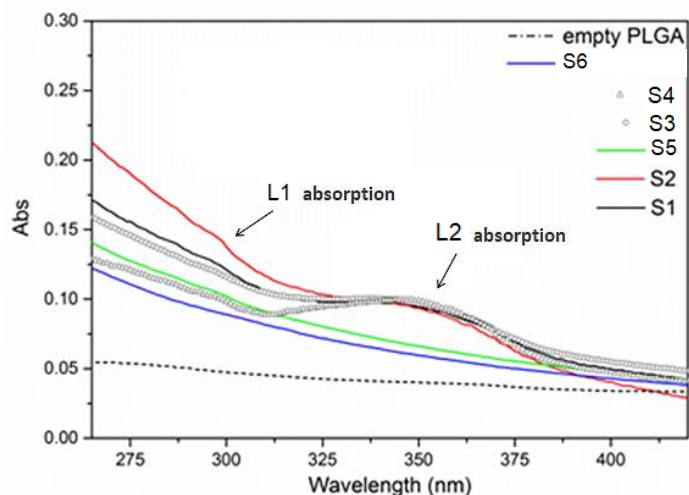


Figure 8. Electronic absorption spectra of S1 ( $\text{Eu}(\text{L1})(\text{L2})_2(\text{H}_2\text{O})\text{]} \cdot \text{CF}_3\text{SO}_3$  complex embedded in PLGA 50:50), S2 ( $\text{Eu}(\text{L1})(\text{L2})_2(\text{H}_2\text{O})\text{]} \cdot \text{CF}_3\text{SO}_3$  complex embedded in PLGA 75:25), S5  $\text{Eu}(\text{L4})$  complex embedded in PLGA 50:50, S3 ( $\text{Y}(\text{L1})(\text{L2})_2(\text{H}_2\text{O})\text{]} \cdot \text{CF}_3\text{SO}_3$  complex embedded in PLGA 50:50), S4 ( $\text{Y}(\text{L1})(\text{L2})_2(\text{H}_2\text{O})\text{]} \cdot \text{CF}_3\text{SO}_3$  complex embedded in PLGA 75:25), S6 ( $\text{Eu}(\text{L3})(\text{NO}_3)_3$  embedded in PLGA 50:50) and empty PLGA nanoparticles; all compounds are suspended in phosphate buffer aqueous solution.

Furthermore, as already mentioned, the  $\text{Eu}(\text{L4})$  molecules embedded in PLGA NP's (Figure 6b) undergoes structural changes of the metal complex, due to polymer-complex interaction, which affects the luminescence properties of the coordination compound, and thus the efficiency of ligand to metal energy transfer. In this context, it is worth remembering that when the complex is dissolved in water, the antenna effect properly works and the ligand fluorescence was not observed at all.<sup>24</sup> The same behaviour was recorded also for  $\text{Eu}(\text{L3})(\text{NO}_3)_3$ , since the high  $\text{Eu}(\text{III})$  emission intensity detected for  $\text{Eu}(\text{L3})(\text{NO}_3)_3$  complex in the solid state<sup>23</sup> is completely quenched when it is embedded in PLGA polymer and only the ligand fluorescence is recorded. The small quantity of embedded  $\text{Eu}(\text{L3})(\text{NO}_3)_3$  complex maybe undergoes a de-coordination of the metal ion giving rise to a "free"  $\text{Eu}(\text{III})$  ion bound to water molecules and/or carboxylic groups belonging to PLGA nanoparticles.

In the case of  $[\text{Y}(\text{L1})(\text{L2})_2(\text{H}_2\text{O})\text{]} \cdot \text{CF}_3\text{SO}_3$ , only the fluorescence of the L1 ligand is detected in the emission spectrum, upon excitation around 280 nm.<sup>25</sup> Because of the very inefficient  $\text{Eu}(\text{III})$  luminescence emission for  $\text{Eu}(\text{L4})$  and  $\text{Eu}(\text{L3})(\text{NO}_3)_3$ , these complexes are not further investigated.

The total quantum yield ( $\Phi_{\text{Tot}}$ ), that it is the number of photons emitted by the lanthanide ion/number of photons absorbed by the ligand was calculated for  $[\text{Eu}(\text{L1})(\text{L2})_2(\text{H}_2\text{O})]\cdot\text{CF}_3\text{SO}_3$  complex embedded in 50:50 and 75:25 PLGA NP's.

The total quantum yields ( $\Phi_{\text{Tot}}$ ) have been obtained by secondary methods described in literature<sup>26</sup> by measuring the visible emission spectrum of quinine bisulfate in 1N  $\text{H}_2\text{SO}_4$  solution, a fluorescence quantum yield reference sample ( $\Phi = 54.6\%$ ).  $\Phi_{\text{Tot}}$  for the complexes has been calculated by  $[(A_s \cdot F_u \cdot n^2) / (A_u \cdot F_s \cdot n_0^2)] \cdot \Phi_s$  equation; where: u subscript refers to unknown and s to the standard and other symbols have the following meanings:  $\Phi$  is quantum yield, A is absorbance at the excitation wavelength, F the integrated emission area across the band and n's are respectively index of refraction of the solvent containing the unknown (n) and the standard ( $n_0$ ) at the sodium D line and the temperature of the emission measurement (Figure 9).

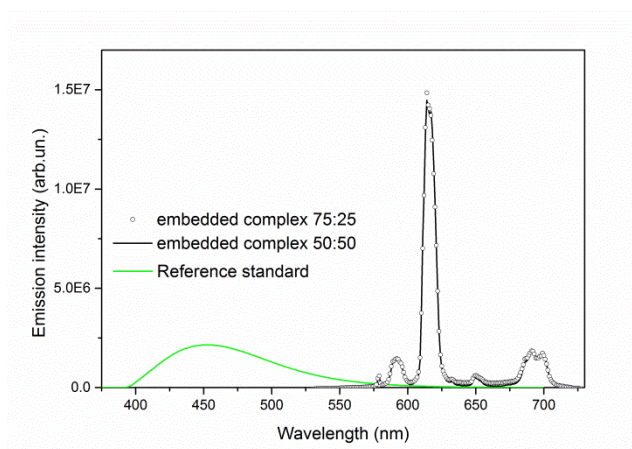


Figure 9. Overlap of the emission spectra of the reference standard and  $[\text{Eu}(\text{L1})(\text{L2})_2(\text{H}_2\text{O})]\cdot\text{CF}_3\text{SO}_3$  for the Quantum Yield measurement. Slits width was adjusted as 2/2 nm for excitation and 1.5/1.5 nm for emission.  $A_s = 0.06$ ;  $A_u = 0.14$  and  $0.13$  for the PLGA 50:50 and 75:25, respectively.  $\lambda_{\text{exc}} = 347$  nm and  $350$  nm, for the standard and the embedded complexes, respectively.

Both samples show a good  $\Phi_{\text{Tot}}$  value (20% for the former, 25% for the latter). In the field of bioimaging applications, these results are quite encouraging, since the quantum yield of many lanthanide and d-block compounds employed for cellular imaging is in the 4-10% range.<sup>27,28</sup> The slightly higher  $\Phi_{\text{Tot}}$  recorded for the complex embedded in the 75:25 PLGA composition is consistent with the lower

intensity of the emission band attributable to the ligand fluorescence than in the case of PLGA 50:50 (Figure 6b).

### 3.2.2. Thermal stability of the luminescent PLGA NP'S

In order to check the stability of these NP's over the time and temperature, the evolution of the luminescence emission spectra at 20°C and 37°C (Figure 10) of the most promising embedded Eu-based complexes ( $[\text{Eu}(\text{L1})(\text{L1})_2(\text{H}_2\text{O})]\cdot\text{CF}_3\text{SO}_3$ ) (both the 50:50 and 75:25 compositions) was monitored.

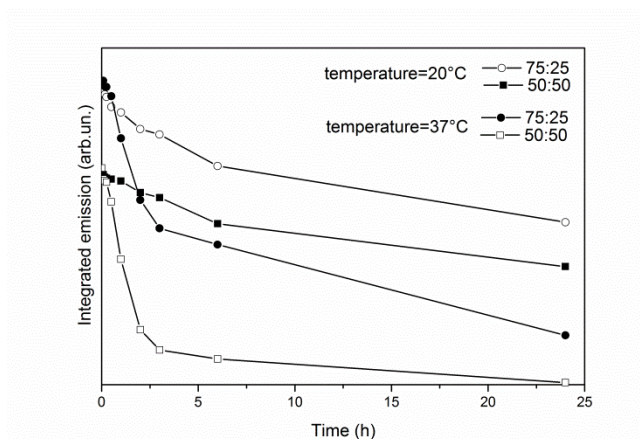


Figure 10. Evolution over the time of the Eu(III) integrated emission intensity for  $[\text{Eu}(\text{L1})(\text{L2})_2(\text{H}_2\text{O})]\cdot\text{CF}_3\text{SO}_3$  complex embedded in PLGA 50:50 and PLGA 75:25 at two different temperature (20 and 37 °C).

In the first hours (0-6 h), the Eu(III) integrated emission intensity decrease at both temperatures. This behaviour is justified with the breaking of the PLGA framework and the release of the complex in solution, which it is more significant at higher temperatures (37°C), in particular in the case of PLGA 50:50, whose melting temperature (33°C) is significantly lower than the one of PLGA 75:25(37°C). After 6h, the kinetic of the luminescence decrease is slower either for the different temperature and compositions. It is worth noting that, at 37°C, after 24 h, a significant Eu(III) emission signal from the 75:25 system is still detected, by evidencing that the more thermally stable 75:25 PLGA framework ensures better luminescent properties for a possible employment of this compound in *in vitro* optical imaging applications. Considering the 75:25 compositions, in order to justify a reasonable explanation for the progressive decrease of the Eu(III) luminescence over the time, both the excitation spectra (Figure 11) and the

luminescence decay curves of the  $^5D_0$  excited state of Eu(III) (Figure 12a) were recorded at 37°C and followed up to 24h.

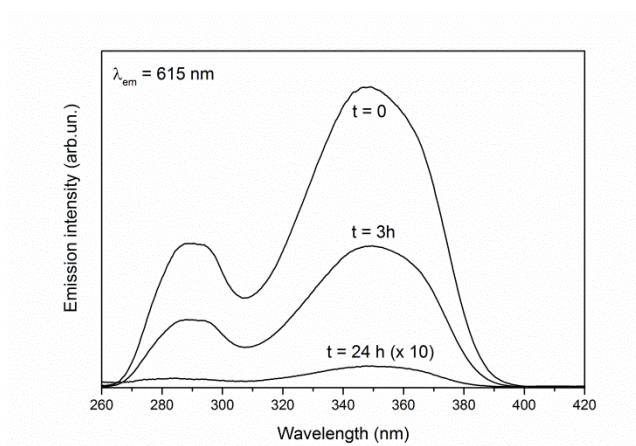
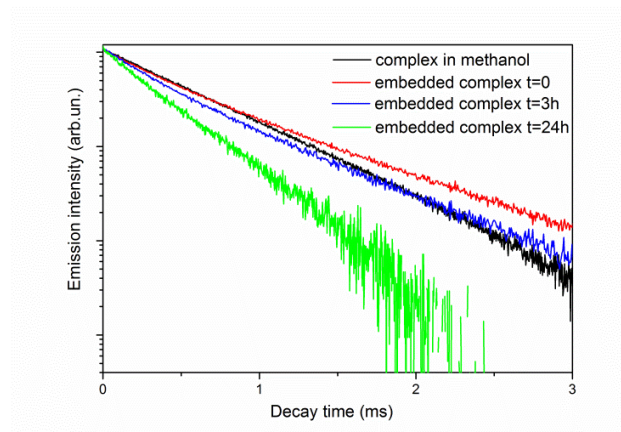


Figure 11. Evolution of the excitation spectra of Eu(III) over the time (0→24 h) for  $[Eu(L1)(L2)_2(H_2O)] \cdot CF_3SO_3$  complex embedded in PLGA 75:25 at 37°C, in phosphate buffer aqueous solution. The excitation spectra at  $t=0$  is superimposable to the one of the complex alone in the solid state or dissolved in an organic solvent.

(a)



(b)

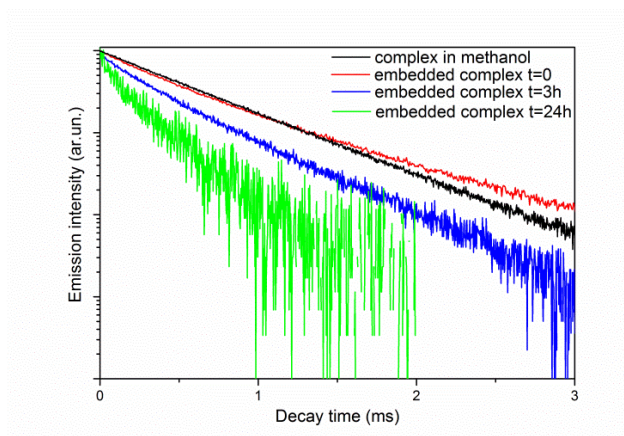


Figure 12. Evolution of the decay curves of the  $^5D_0$  excited state of Eu(III) over the time (0→24 h) for  $[\text{Eu}(\text{L1})(\text{L2})_2(\text{H}_2\text{O})]\cdot\text{CF}_3\text{SO}_3$  complex embedded in (a) PLGA 75:25 at 37°C, in phosphate buffer aqueous solution ( $\lambda_{\text{exc}} = 350 \text{ nm}$ ;  $\lambda_{\text{em}} = 615 \text{ nm}$ ); (b) PLGA 50:50 at 37°C, in phosphate buffer aqueous solution ( $\lambda_{\text{exc}} = 350 \text{ nm}$ ;  $\lambda_{\text{em}} = 615 \text{ nm}$ ). The decay curve of the complex in methanol is also reported as a reference [26].

Whereas the decay profile of the complex alone  $[\text{Eu}(\text{L1})(\text{L2})_2(\text{H}_2\text{O})]\cdot\text{CF}_3\text{SO}_3$  dissolved in organic solvents<sup>19</sup> is perfectly fitted by a single exponential function, the same was not possible for the decay profiles of its assembly with PLGA. In these cases, the best estimation of the excited state lifetime is given by the 1/e folding time, which decreases over the time at 37°C (0.55 ms, t=0; 0.48 ms, t= 3h and 0.37 ms, t=24h for the 75:25 formulation). The decay time for the Eu(III) complex embedded in PLGA 50:50 is similar at t=0 (0.52 ms) but it decreases quickly over the time (0.40 ms, t=3h and 0.30 ms, t=24h; Figure 12b). Probably, upon breaking of the PLGA assembly, more significant at higher temperatures and for PLGA 50:50, the water molecules from the solvent may have access to the metal center and they activate the well-known multiphonon relaxation process,<sup>29,30</sup> shortening the Eu(III) lifetime. In addition, the donating groups of PLGA polymer (i.e. OH and COOH) could chelate the metal ion and a de-coordination (even in part) of the L1 and L2 ligands should also occur. Both phenomena (de-coordination and multiphonon relaxation process) are compatible with the evolution of the excitation spectrum over the time shown in Figure 11. Moreover, a further proof of the partial de-coordination from the PLGA np's is the progressive turbidity of the solution due to the low solubility and stability in aqueous solution of either  $[\text{Eu}(\text{L1})(\text{L2})_2(\text{H}_2\text{O})]\cdot\text{CF}_3\text{SO}_3$  and its ligands.

Concluding, it has been evidenced that the nature of the embedded Eu(III) complex can affect the efficiency of complex encapsulation into biocompatible PLGA NP's. In particular, it is well known that the present PLGA formulations are suitable for embedding hydrophobic rather than hydrophilic complexes.<sup>31</sup> By means of luminescence spectroscopy, the non-innocent role of the PLGA polymer was demonstrated. In particular, as a consequence of the PLGA-complex interaction, Eu(III) undergoes de-coordination that compromises an efficient luminescence emission of Eu(III) in Eu(L3)(NO<sub>3</sub>)<sub>3</sub> and Eu(L4) complexes. On the contrary, [Eu(L1)(L2)<sub>2</sub>(H<sub>2</sub>O)]·CF<sub>3</sub>SO<sub>3</sub> is efficiently internalized and the Eu(III) luminescence emission quantum yield reaches good a value (total quantum yield;  $\Phi_{\text{Tot}} = 25\%$ ) for the composition PLGA 75:25. This composition guarantees also a higher value of T<sub>m</sub> (38 °C instead of 33°C, in the case of PLGA 50:50), which ensure a slower release of the complex at the temperature of 37°C.

Finally, by using the same ligands, PLGA is also capable to efficiently embed the analogous [Y(L1)(L2)<sub>2</sub>(H<sub>2</sub>O)]·CF<sub>3</sub>SO<sub>3</sub> complex where, if Y(III) is radioactive, could be employed in the field of nuclear imaging, as PET contrast agent. With this in mind, PLGA(75:25)-[Eu(L1)(L2)<sub>2</sub>(H<sub>2</sub>O)]·CF<sub>3</sub>SO<sub>3</sub> and PLGA(75:25) [Y(L1)(L2)<sub>2</sub>(H<sub>2</sub>O)]·CF<sub>3</sub>SO<sub>3</sub> systems can be respectively considered promising candidates for optical and nuclear imaging applications.

### 3.3. *Water soluble Ln(III) complexes: toward biosensing applications*

#### 3.3.1. *Design and Synthesis*

All the members of the new library of water soluble Eu(III) and Tb(III) complexes are constituted by a chiral 1,2-diaminocyclohexane (DACH) in the ligand moiety. This feature allows to generate CPL (Circularly Polarized Luminescence) from the lanthanide, which has found interesting applications in chirality sensing<sup>32,33</sup> and medical imaging techniques.<sup>34</sup>

In the past, our research group have designed and synthesized several ligands based on the chiral DACH (1,2-cyclohexanediamine) motif and pyridine or

furan<sup>35,36</sup> or quinoline<sup>23</sup> as heteroaromatic antennae, capable to efficiently sensitize the Eu(III) luminescence (Figure 13).

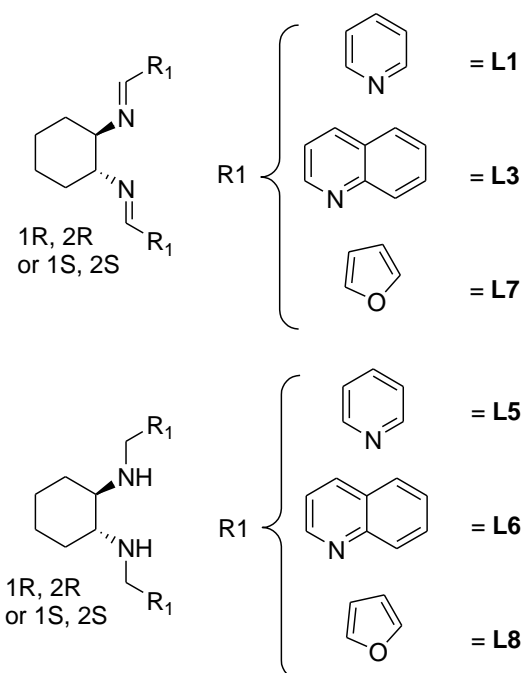


Figure 13. Ligands for sensitizing Eu(III) luminescence

As can be seen from the structure, whilst the molecule L1, L3, L7 and the corresponding Ln(III) complexes are perfectly soluble in organic solvents like acetonitrile or dichloromethane, they are not soluble in water; therefore, unless they are not embedded in biocompatible nanoparticles, the direct employment in biological fluid is not possible. For this reason, some more hydrophilic and water soluble Eu(III) and Tb(III) complexes bearing two (Eu(L9)Cl, Tb(L9)Cl, Figure 14)<sup>37</sup> or one (Eu(L10), Tb(L10) Figure 14) Pyridine ring as sensitizer have been obtained in good yield and purity.<sup>24</sup>



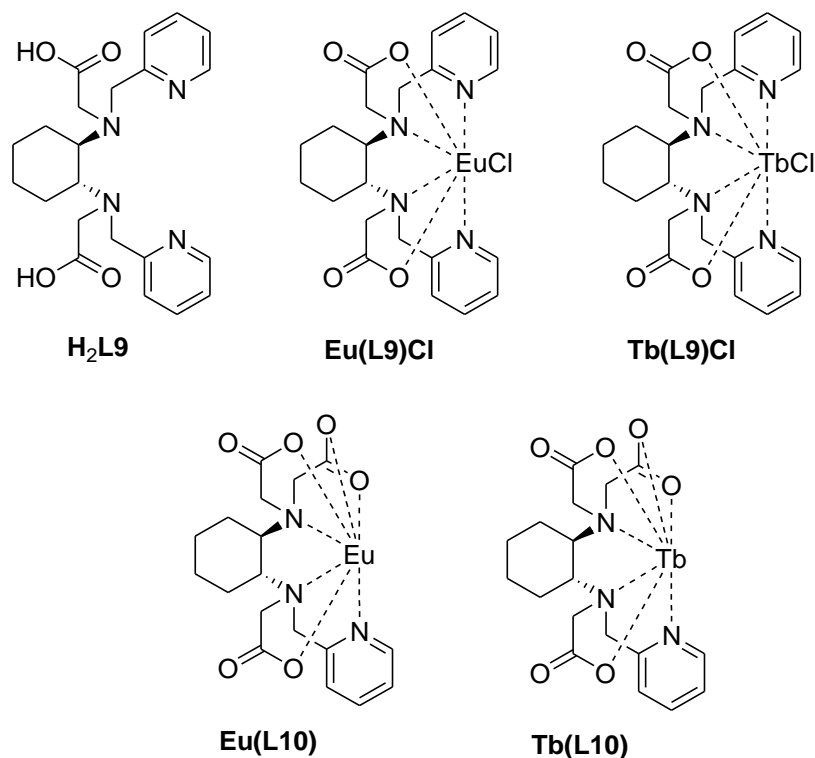


Figure 14. Eu and Tb complexes based on Pyridine rings, where H<sub>2</sub>L<sub>9</sub> = N,N'-bis(2-pyridylmethyl)-trans-1,2-diaminocyclohexane-N,N'-diacetic acid, L<sub>10</sub> = N-picolyl-N,N',N'-trans-1,2 cyclohexylenediaminetriacetate.

The above reported Ln-complexes are *i) soluble in water*, thanks to the presence of two carboxylate groups that also increase the *stability* of the complex in protic polar solvents. On the other hand, the typical excitation wavelengths around 265/270 nm strongly interfere with the absorption wavelengths of the biological background. This drawback has been successfully overcome during my PhD project, by extending the library with further ligands suitable to absorb in a different spectral range. In particular, the Eu(III)-complexes containing *quinoline* (3, 4-Figure 15) or *isoquinoline* (5, 6-Figure 15) whose excitation wavelengths (318 nm in the case of quinoline derivatives and 325/330 nm in the case of isoquinoline ones) are *quite far from the typical values of the common biochromophore absorptions*

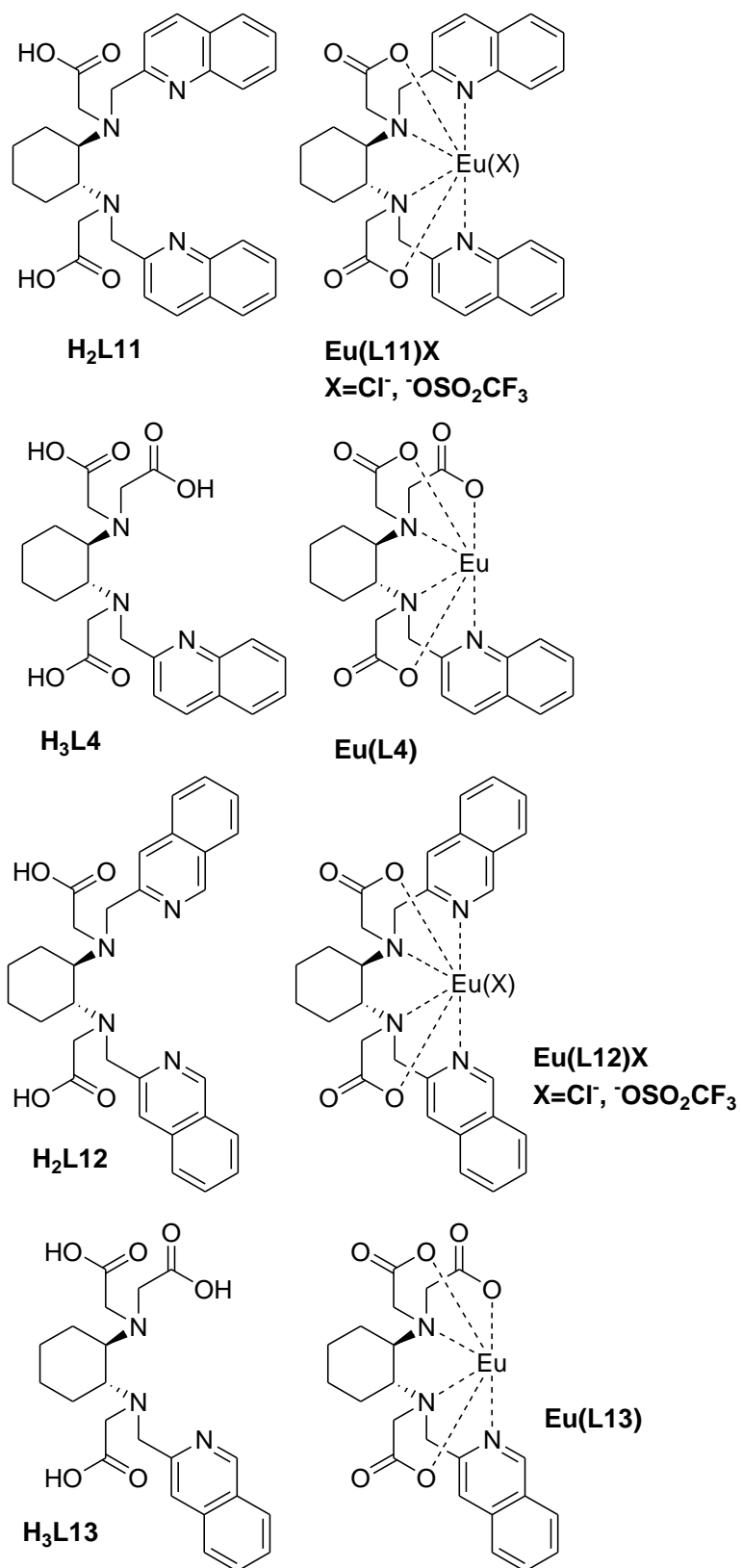


Figure 15. Eu(III) complexes based on Quinoline and Isoquinoline rings, where L11= *N,N'*-bis(2-quinolinmethyl)-*trans*-1,2-diaminocyclohexane *N,N'*-diacetate); L4= *N*-quinolyl-*N,N',N'*-*trans*-1,2-cyclohexylenediaminetriacetate); L12= *N,N'*-bis(2-isoquinolinmethyl)-*trans*-1,2-diaminocyclohexane *N,N'*-diacetate); L13= *N*-isoquinolyl-*N,N',N'*-*trans*-1,2-cyclohexylenediaminetriacetate).

While the pyridine ring is capable to sensitize both Eu(III) and Tb(III) luminescence,<sup>25</sup> the quinoline<sup>23</sup> and isoquinoline rings effectively sensitize only Eu(III) ion. Another crucial feature that must be considered during the design of the luminescent probes concerns the *choice of the metal center*.

In principle, all the lanthanide ions showing *f-f* emission can be employed in the design of a probe, but in practice only few are really used.

The main rare earths adopted for sensing purposes are usually Eu(III), Tb(III), Dy(III), Nd(III), Yb(III) and Sm(III), due to their emissions in the Visible-NIR range, where the detection of the signal can be obtained with high sensitivity and low scattering. Nevertheless, Eu(III) and Tb(III) are the most employed in virtue of their i) longer luminescent lifetime (millisecond range), ii) the less sensitive quenching by singlet oxygen and iii) the lower efficiency of the multiphonon relaxation process. Moreover, the non-degeneracy of the <sup>5</sup>D<sub>0</sub> emissive state of the Eu<sup>3+</sup> permits to have simple emission spectra which can be easily related to the local symmetry around the metal ion.

The narrow emission of lanthanides offers advantages for the quantification of the analytes by means of ratiometric analysis. For these purposes, a common ratiometric method is based on the employment of Eu(III) and Tb(III) ions by recording the intensity at two or more wavelengths, with the final results of extreme sensitivity and correction for interfering factors even at low level of absolute intensities. If the ratio of the recorded intensities changes upon the interaction with the targets of interest, it could be conveniently used as a self-referenced signal.<sup>38,39</sup>

As far as the *coordination number* is concerned, although the lanthanide organic chemistry commonly involves 7-9 as coordination number, it was conveniently adopted a not saturated core scaffold bearing a *6-fold coordination ability* for sensing purpose. In fact, in the vast majority of cases, the sensing process is due to the binding of the analyte to the metal center. For these reasons not all the metal coordination sites should be occupied by the ligand but by easily displaceable solvent molecules.

Moreover, since all the trivalent lanthanide ions present high charge densities and smaller ionic sizes, they are classified as Hard acids and, according to the "hard"

and “soft” (Lewis) acids and bases” (HSAB) theory they interact more strongly with hard bases than soft bases. Typically, hard bases are *nitrogen or negatively charged oxygen atoms*.

As clearly depicted in the above mentioned Ln(III)-complex structures, the donor atoms involved in the chelation with the metal center show a typical “soft” characteristic. They are *nitrogen or negatively charged oxygen atoms*.

The synthesis, characterization and biosensing applications of the luminescence probes depicted in Figure 14 and 15 will be widely discussed in Chapter 4.

### **3.3.2. New Eu(III)-based complex with a C1 symmetric chiral ligand.**

During the design of the protocol for the synthesis of L11, I came across an interesting discovery. In particular, the deprotection of the tert-butyl ester function can be performed selectively on only one group. The relative Eu(III) complex is soluble in an aqueous-alcoholic solution (water:MeOH=9:1).<sup>40</sup>

#### **3.3.2.1. Synthesis**

The synthesis of the new chiral ligand N,N'-bis[(2-quinolylmethyl)-cyclohexanediamine-N-tert-butylacetate N'-acetic acid **L14** and its Eu complex (**Eu(L14)Cl**) is presented (Figure 16).

The compound L6 has been prepared following literature procedure.<sup>41</sup> The synthesis of the other compounds is discussed in detail in the experimental section. As far as the synthesis of the compound **HL14** is concerned, it is worth noting the uncommon selective deprotection of only one tert-butyl group. This has been possible thanks to the employment of mild conditions, such as the use of a weak acidic molecule (formic acid). This selective deprotection is already known in the literature.<sup>42</sup> Although natural products containing tert-butyl groups are considered rare,<sup>43</sup> several different substance classes such as peptides, terpenes, carbinols, esters and even a ketone bearing a tert-butyl group have been widely described in the literature.<sup>44</sup>

Moreover, the occurrence of tert-butyl groups in natural products may induce specific geometries that are essential for further biotransformation, or (in the case of toxins) render biotransformation impossible to the predator; in the latter case, the tert-butyl structure could be viewed as a protecting group.

As far as the coordination chemistry toward trivalent lanthanides is concerned, the presence of EDG groups (Electron donating group) which induces coordination bonds with lanthanide metal ions is quite reported in literature.<sup>45</sup>

The tert-butyl function is a moderate EDG group, but besides this feature, especially in the coordination chemistry field, a noticeable steric effect should be also considered. Nevertheless, the aforesaid Eu(III) complex was obtained in good yield, purity and it shows a good coordination stability even in protic solvents.

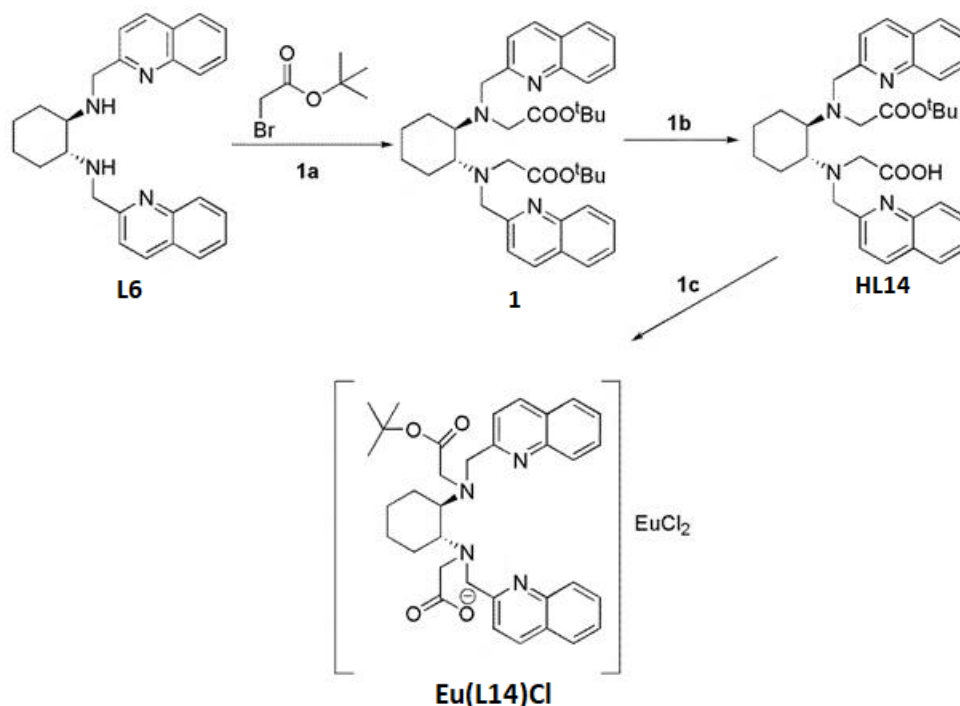
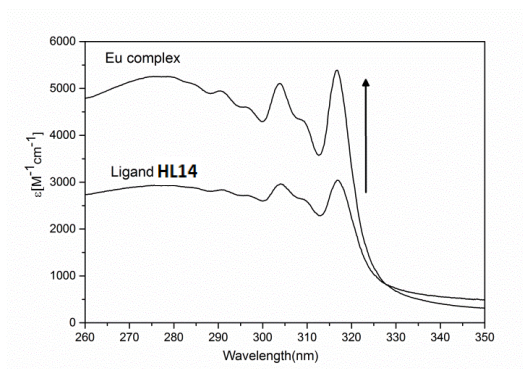


Figure 16. Synthetic protocol discussed in this paper. The configuration of the stereogenic centers is (R,R). Reagents and conditions: (1a) tert-butyl bromoacetate 3 eq, K<sub>2</sub>CO<sub>3</sub> 3.2 eq, acetonitrile, rt, 12 h; (1b) HCOOH 99%, rt, overnight; (1c) EuCl<sub>3</sub>·6H<sub>2</sub>O 1.2 eq, H<sub>2</sub>O:MeOH 9:1, rt, 12h.

### 3.3.2.2. Optical spectroscopy

The UV absorption spectrum of a solution of the ligand L14 in ethanol ( $5 \cdot 10^{-5}$  M) is presented in Figure 17a, together with the one of the Eu(III) complex ( $10^{-4}$  M in ethanol). In both cases, strong absorptions are detected in the 260-320 nm spectral range. In particular, a broad band peaking around 270 nm, and several narrower components around 290, 295, 305, 310 and 320 nm, are clearly visible. All these absorptions can be attributed to the electronic transitions involving the quinoline ring (i.e.  $\pi \rightarrow \pi^*$  and  $n \rightarrow \pi^*$ ).<sup>46</sup> Upon complexation with Eu(III) ions a hyperchromic effect of the absorption bands is observed. This behaviour has been already observed in the case of similar ligands containing the pyridine chromophore instead of the quinoline one.<sup>52</sup>

(a)



(b)

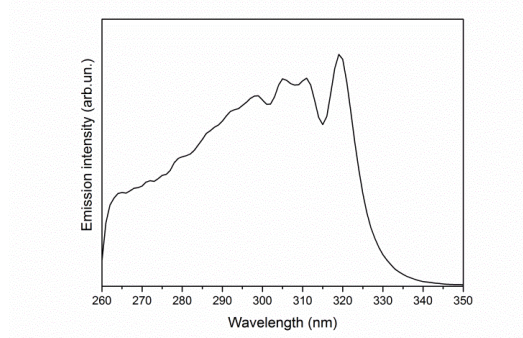


Figure 17. (a) UV Absorption spectra of HL14 and Eu(L14)Cl.  $[HL14] = 5 \cdot 10^{-5}$  M;  $[Eu(L14)Cl] = 10^{-4}$  M. (b) Excitation spectrum of Eu(L14)Cl,  $[Eu(L14)Cl] = 10^{-4}$  M,  $\lambda_{em.} = 618$  nm). All the solutions are in ethanol.

As clearly showed from examination of Figure 30b, the excitation spectrum of the complex monitoring the Eu(III) emission around 620 nm, is similar to its absorption spectrum (Figure 17a), apart from the relative intensity of the peaks. This is a clear evidence of the sensitization of the Eu(III) luminescence by the quinoline ring of the ligand HL14. Consequently, upon excitation at 317 nm, the typical luminescence emission of Eu(III), due to f-f transitions, was detected both in the solid state and in ethanol solution (Figure 18).

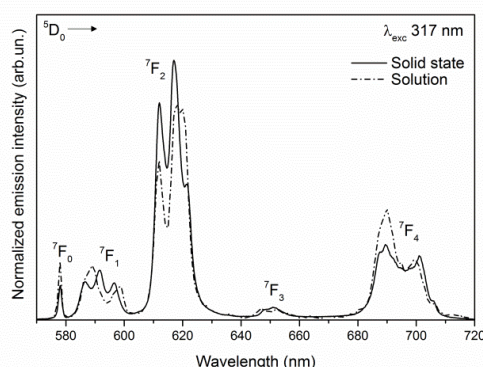


Figure 18. Luminescence emission spectra of  $\text{Eu}(\text{L14})\text{Cl}$  in the solid state and in ethanol solution ( $10^{-4}$  M). The spectra are normalized to the area of the  ${}^5\text{D}_0 \rightarrow {}^7\text{F}_1$  band.

In principle, the examination of the Eu(III) emission spectrum allows to get several conclusions about the geometric environment of the metal ion.<sup>47</sup> In particular, in the complex  $\text{Eu}(\text{L14})\text{Cl}$ , both in the solid state and in solution, the Eu(III) ion is located in a very distorted environment, as the  ${}^5\text{D}_0 \rightarrow {}^7\text{F}_2$  band, whose intensity is hypersensitive to the lack of inversion symmetry, is dominant in the spectrum. In addition, the presence of only one component in the region of  ${}^5\text{D}_0 \rightarrow {}^7\text{F}_0$  transition, calls for the existence of a dominant Eu(III) species. The sizable intensity of this band (in particular for the complex in solution) is in agreement with an axial symmetry of the Eu(III) environment (compatible with  $C_1$ ,  $C_s$ ,  $C_2$  or  $C_{2v}$  point groups).<sup>47</sup> As the ligand around the metal ion is  $C_1$  symmetric, it is reasonable to expect the same point symmetry for Eu(III) in the complex.

Nevertheless, as clearly reported in Figure 18, even though the two emission spectra are similar they are not exactly superimposable. The values of the asymmetry ratio<sup>21,22</sup> are slightly different in the two cases (4.73 for the solid

sample and 4.16 in solution). Most probably two slightly different geometric environments are involved for the two cases.

The luminescence decay curves of the Eu(III)  $^5D_0$  excited state (Figure 19) have also been recorded upon excitation at 317 nm, i.e. in the ligand absorption transitions. In both cases, the decays show an initial fast component, followed by a long exponential tail. The exponential tails are well fitted by a single exponential function and the calculated observed lifetimes are 0.84 ms in the solid state and 0.79 ms in solution. This result suggests, in agreement with the conclusions arising from the inspection of the luminescence emission spectra, the presence of a dominant emitting complex, whose nature is similar in the solid state and in solution. On the other hand, the presence of a faster component with a decay time in the  $\mu\text{s}$  range cannot be neglected. This is probably related to the presence of a diluted emitting impurity.

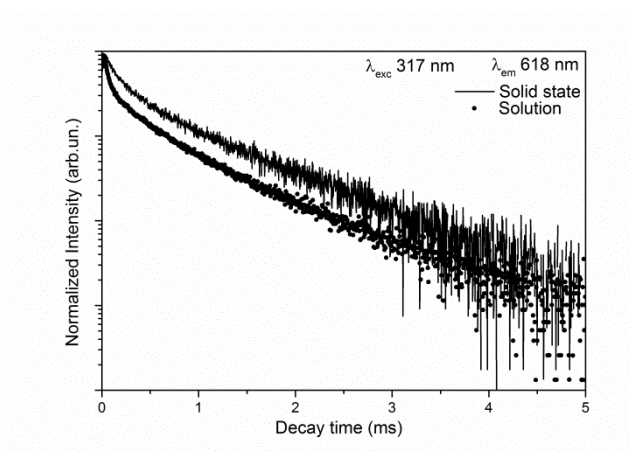


Figure 19. Eu(III)  $^5D_0$  decay curves of Eu(L14)Cl in the solid state and in ethanol solution ( $10^{-4}$  M).

Concluding, we synthesized an uncommon  $C_1$ -symmetric chiral ligand, *N, N'*-bis[(2-quinolylmethyl]-cyclohexanediamine-*N*-*tert*-butylacetate *N'*-acetic acid, which is capable to efficiently sensitizes the red luminescence of Eu(III) ion. Moreover, the Eu(III) ion is located in a strongly distorted geometric environment, both in the solid state and in ethanol solution, as documented by the inspection of the Eu(III) luminescence emission spectra, and the decay time of the  $^5D_0$  Eu(III) luminescence falls in the ms range. All these features promote this complex as good candidate for applications in the biomedical field where stability



and solubility in protic polar solvent is strongly required. In addition, as the complex is chiral, it may display chiroptical phenomena, such as CPL (Circularly Polarized Luminescence).

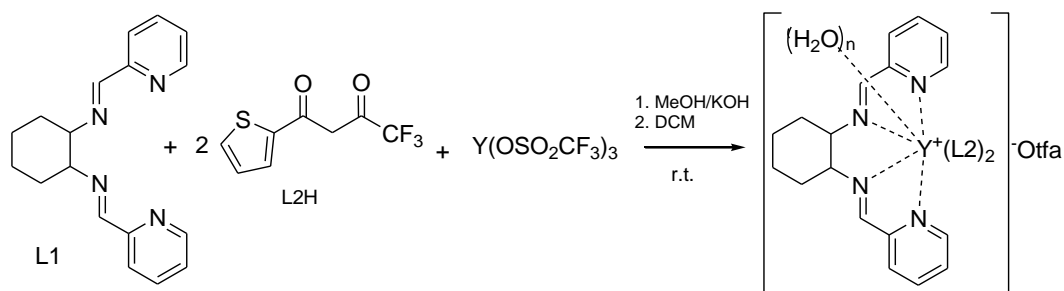
### 3.3.3. *Complexes of rare earth ions embedded in Poly(lactic-co-glycolic acid) (PLGA) nanoparticles: procedures, techniques and characterization*

#### 3.3.3.1. *Materials*

PLGA (poly[D/L-lactide-co-glycolide], 50:50/75:25 lactide-glycolide ratio, CAS 26780-50-7), ethanol ( $\geq 99\%$  purity, CAS 64-17-5), PVA (poly[vinyl alcohol], CAS 9002-89-5), Glycine (CAS 56-40-6), Dichloromethane (CAS 75-09-2) were purchased from Sigma Aldrich. Acetone ( $\geq 99\%$  purity) was purchased from Merck.  $\text{Eu}(\text{CF}_3\text{SO}_3)_3$  and  $\text{Y}(\text{CF}_3\text{SO}_3)_3 \cdot 6\text{H}_2\text{O}$  (Aldrich, 98%) was stored under vacuum for several days at  $80^\circ\text{C}$  and then transferred in a glove box.

#### 3.3.3.2. *Synthesis*

*N,N'*-bis(2-pyridylmethylidene)-1,2-(*R,R+S,S*)-cyclohexanediamine (**L1**) and *rac*- $[\text{Eu}(\text{L1})(\text{L2})_2(\text{H}_2\text{O})]\text{CF}_3\text{SO}_3$  were already described in the experimental part of Chapter 1. As far as the synthesis of the new *Rac*- $[\text{Y}(\text{L1})(\text{L2})_2(\text{H}_2\text{O})] \cdot \text{CF}_3\text{SO}_3$  complex is concerning, it has been obtained by following the same approach used for the analogous Eu(III) derivative, accordingly to Scheme 1.

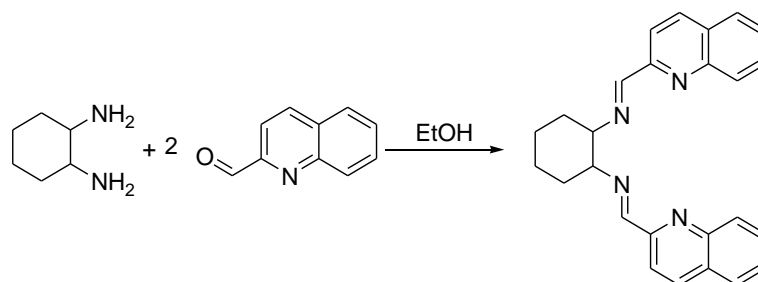


Scheme 1. Synthesis of complex  $[\text{Y}(\text{L1})(\text{L2})_2(\text{H}_2\text{O})_n] \cdot \text{CF}_3\text{SO}_3$

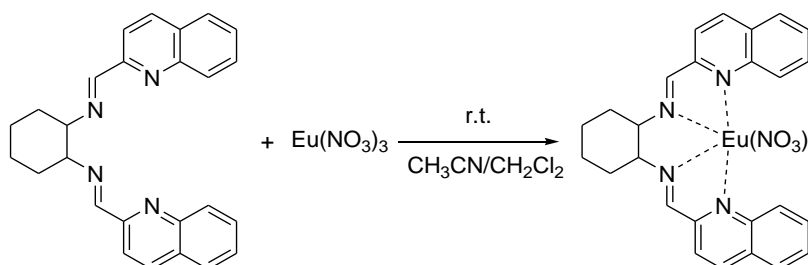
*Rac*- $[\text{Y}(\text{L1})(\text{L2})_2(\text{H}_2\text{O})] \cdot \text{CF}_3\text{SO}_3$ : Yield 65%.  $^1\text{H-NMR}$  ( $\text{CDCl}_3$ )  $\delta$  (ppm): 8.74 (s, 2H HC=N), 8.69 (d,  $J=4.70$  Hz, 2H Py), 8.07 (m, 4H, Py), 7.69 (d,  $J=4.92$  Hz, 2H,

Py), 7.64 (d,  $J=3.13$  Hz, 2H, thiophene), 7.56 (d,  $J=4.25$  Hz, 2H, thiophene), 7.13 (t,  $J=4.25$  Hz, 2H, thiophene), 4.27 (m, 2H, “CH” cyclohexane), 3.51 (m, 1H, cyclohexane), 2.75 (m, 2H, cyclohexane), 2.21 (m, 2H, cyclohexane), 1.89-1.50 (m, 3H; cyclohexane). UV-Vis absorption spectroscopy (ACN):  $\epsilon(280\text{ nm})$ :  $64600\text{ M}^{-1}\text{cm}^{-1}$ ;  $\epsilon(350\text{ nm})$ :  $65600\text{ M}^{-1}\text{cm}^{-1}$ .

Apart the new Eu-complex **Eu(L4)** whose synthesis and characterization have been described in literature<sup>24</sup> as well as herein in the experimental part of Chapter 4. The *N, N'*-bis(2-quinolylmethylidene)- 1,2-(*R,R+S,S*)-cyclohexanediamine (**L3**)<sup>23</sup> (Scheme 2) as well as the **Eu(L3)(NO<sub>3</sub>)<sub>3</sub>**<sup>23</sup> (Scheme 3) were synthesized in the past from our research group and the new ligand *N*-quinolyl-*N,N',N'*-*trans*-1,2-cyclohexylenediaminetriacetic acid (**L4**) was obtained by following the procedures reported in our recent literature<sup>24</sup> (refer to experimental part of Chapter 4 for details).



Scheme 2. Synthesis of ligand L3



Scheme 3. Synthesis of **Eu(L3)(NO<sub>3</sub>)<sub>3</sub>**

**L3** (*bis*(2-quinolylmethylidene)- 1,2-(*R,R+S,S*)-cyclohexanediamine): In a flask containing an ethanol solution (2mL) with 1,2-diamminocyclohexane (1.3 gr, 0.01167 mol), a ethanolic solution (2 mL) of quinoline-2-carbaldehyde) (3.6 gr,

0.023 mol) has been slowly added at 0°C. After the adding, the ice-bath has been removed to establish the room temperature for overnight. The white product precipitating has been filtered and washed three times with cold ethanol (5 mL). To increase the yield the ethanol solution can be concentrated to obtain other precipitate.

**L3**: White solid. Yield 85%.  $^1\text{H NMR}$  (600 MHz,  $\text{CDCl}_3$ )  $\delta$  (ppm): 8.52 (s, 2H), 8.11 – 8.04 (m, 4H), 8.03 (d,  $J = 8.5$  Hz, 2H), 7.74 (d,  $J = 8.0$  Hz, 2H), 7.66 (dd,  $J = 11.2, 3.9$  Hz, 2H), 7.49 (t,  $J = 7.4$  Hz, 2H), 3.78 – 3.56 (m, 2H), 2.00 – 1.77 (m, 6H), 1.64 – 1.46 (m, 2H).  $^{13}\text{C}$  (50 MHz,  $\text{CDCl}_3$ )  $\delta$  (ppm): 24.58, 32.93, 74.06, 118.76, 127.33, 127.82, 128.91, 19.67, 136.55, 147.90, 155.15, 162.07.

$\text{Eu}(\mathbf{L3})(\text{NO}_3)_3$ : a DCM solution (0.5 mL) containing imine ligand ( 50 mg , 0.17 mmol) was added to ACN solution (5 mL) containing lanthanum nitrate salts (77.18 mg , 0.17 mmol). After few minutes of the adding, a white precipitate was formed and the solution has been kept under stirring overnight. Before the work-up, the solution has been cooled at 0°C to increase the recovery of precipitate which has been collected with filtration and washed three times with a cooled ACN/DCM (1:1) solution. White solid. Yield: 72%. Elemental Analysis Calculated:  $\text{C}_{28}\text{H}_{27}\text{EuN}_8\text{O}_9$  (MW: 771.53) C, 43.59; H, 3.53; N, 14.52; O, 18.66. Founded: C, 43.51; H, 3.47; N, 14.46; O, 18.60.

### 3.3.3.3. Preparation of PLGA nanoparticles (PLGA-Nps)

PLGA-Nps were prepared by modified classic single emulsion method (o/w) at 20°C.<sup>56</sup> 10 mg of PLGA were dissolved in 1 mL of organic solution (85% acetone and 15% ethanol), then the obtained solution was added dropwise to 10 mL of aqueous solution (PVA 1%, Glycine 100 mM, pH 9) and emulsified through 3 cycles of sonication (power 8 RMS for 10s with rest 5s/cycle). The emulsion was stirred (2000 RPM) overnight at 20°C to evaporate the organic phase.

Afterwards, samples were centrifuged at 4°C 11000 rpm for 15 minutes (Eppendorf Centrifuge 5804 R): the pellet was suspended in 5mL of Milli-Q water

and centrifuged again. Finally, the purified nanoparticles were suspended in 1 mL of PBS solution pH 7,4 (or Milli-Q water) for the subsequent analysis and the storage at 4°C, otherwise suspended in 1 mL of PBS added with mannitol 4% as cryoprotectant for lyophilisation. Nanoparticles with both polymeric combinations Poly(lactic(50%)-co-glycolic acid(50%)), briefly PLGA 50:50 and Poly(lactic(75%)-co-glycolic acid(25%)), briefly PLGA 75.25, were prepared using the same method.

In the case of PLGA nanoparticles with entrapped complexes,  $10^{-3}$  mmol of each complex were dissolved together with 10 mg of PLGA in the organic solution (85% acetone and 15% ethanol). The following steps were the same of the method above. Only in the case of PLGA nanoparticles with entrapped complexes, a MICROSON™ Ultrasonic Cell Disruptor was used as emulsification system.

#### *3.3.3.4. Elemental analysis*

Elemental analyses were carried out by using a EACE 1110 CHNOS analyzer.

#### *3.3.3.5. Differential Scanning Calorimetry (DSC)*

These analysis were performed in Milli-Q water to evaluate the melting temperature ( $T_m$ ) of the polymeric matrix containing the Eu(III) complexes. In particular, 700 $\mu$ L of each sample were loaded in the sample cell, while the same volume of Milli-Q was loaded in the reference one. A scanning was performed from 10°C to 90°C (2°C/min): finally,  $T_m$  was calculated using the program Lauch NanoAnalyze. Data were fitted with the sum between Gaussian function and General function to calculate the relative melting point with 99% of confidence.

#### *3.3.3.6. Atomic Force Microscopy (AFM)*

20 $\mu$ L of each sample (described in the above section) was loaded on a bracket covered by inert mica surface. After 15 minutes for solvent evaporation, the analysis was performed using semi contact mode with different scanning frequencies (3 to 1 Hz) in order to produce an optimized AFM image; finally, the

images were elaborated by the Gwyddion program for AFM analysis and a statistical study was performed to compare results to DLS data.

### 3.3.3.7. *Dynamic Light Scattering (DLS) and Zeta Potential (ZP)*

A first analysis was performed at room temperature with a Zeta NanoSizer in PBS buffer to measure the size and Z-potential. The samples were diluted 10 times from the stock solutions to perform each analysis.

### 3.3.3.8. *Luminescence and decay kinetics*

Room temperature luminescence was measured with a Fluorolog 3 (Horiba-Jobin Yvon) spectrofluorometer, equipped with a Xe lamp, a double excitation monochromator, a single emission monochromator (mod. HR320) and a photomultiplier in photon counting mode for the detection of the emitted signal. All the spectra were corrected for the spectral distortions of the setup.

In decay kinetics measurements, a Xenon microsecond flashlamp was used and the signal was recorded by means of multichannel scaling method. True decay times were obtained using the convolution of the instrumental response function with an exponential function and the least-square-sum-based fitting program (SpectraSolve software package). The total quantum yields ( $\Phi_{\text{Tot}}$ ) have been obtained by secondary methods described in literature<sup>26</sup> by measuring the visible emission spectrum of quinine bisulfate in 1N H<sub>2</sub>SO<sub>4</sub> solution, a fluorescence quantum yield reference sample ( $\Phi = 54.6\%$ ).  $\Phi_{\text{Tot}}$  for the complexes has been calculated by  $[(A_s \cdot F_u \cdot n^2) / (A_u \cdot F_s \cdot n_0^2)] \cdot \Phi_s$  equation; where: u subscript refers to unknown and s to the standard and other symbols have the following meanings:  $\Phi$  is quantum yield, A is absorbance at the excitation wavelength, F the integrated emission area across the band and n's are respectively index of refraction of the solvent containing the unknown (n) and the standard (n<sub>0</sub>) at the sodium D line and the temperature of the emission measurement.

### 3.3.4. *New Eu(III)-based complex with a C1 symmetric chiral ligand: a spectroscopic study: procedures, techniques and characterization*

#### 3.3.4.1. *Materials*

EuCl<sub>3</sub>·6H<sub>2</sub>O, Dichloromethane (DCM), Methanol (MeOH), Deuterated Chloroform (CDCl<sub>3</sub>), Cyclohexane and Ethyl acetate were purchased from Sigma-Aldrich; Acetonitrile (ACN), Ethanol (EtOH) and Formic acid 99% were purchased from Carlo Erba Reagents; activated neutral alumina (Al<sub>2</sub>O<sub>3</sub>), tert-butyl 2-bromoacetate, (1*R*, 2*R*)-*trans*-cyclohexane-1,2-diamine and quinoline-2-carbaldehyde were purchased from Alfa Aesar. Acetonitrile (ACN) was got from Proligo Reagents and Potassium carbonate anhydrous (K<sub>2</sub>CO<sub>3</sub>) were bought from Baker Reagents.

#### 3.3.4.2. *Synthesis*

*N, N'*-bis[(2-quinolylmethyl)-cyclohexanediamine-*N, N'*-tert-butyl]diacetate (**1**). The diamine **L6** (1.44 g, 3.64 mmol, 1 eq) was dissolved at room temperature in a mixture of anhydrous ACN (60 mL) and anhydrous K<sub>2</sub>CO<sub>3</sub> (11.65 mmol, 1.61 g, 3.2 eq) under Argon atmosphere; then a solution of tert-butyl 2-bromoacetate (11 mmol, 1.6 ml, 3 eq) in anhydrous ACN (10 mL) was added dropwise with a syringe over 5 min. The reaction was stirred at room temperature for 24h, and the formation of the desired product was monitored by TLC (Thin Layer Chromatography) on alumina (R<sub>f</sub>: 0.65, DCM:MeOH 95:5). The reaction mixture was quenched by a Brine solution (30 mL) and the crude product was extracted with DCM, and the solvent was then removed under vacuum to yield brownish oil (~2.87 g). The desired product was purified by chromatography on activated neutral alumina (Al<sub>2</sub>O<sub>3</sub>), in gradient elution (Cyclohexane: Ethyl acetate = 8:2→7:3). The product **1** was obtained as yellowish oil [1.61 g, 2.58 mmol, Yield: 71%, purity ≥ 80% (<sup>1</sup>H-NMR)].

<sup>1</sup>H-NMR (CDCl<sub>3</sub>) δ (ppm) 8.07 (d, J=7.76 Hz, 2H), 8.03 (d, J= 7.90 Hz, 2H), 7.92 (d, J=7.76 Hz, 2H), 7.75 (d, J= 7.10 Hz), 7.70 (m, 2H), 7.50 (m, 2H), 4.16 (m 2H), 3.86 (d, J<sub>GEM</sub>=14 Hz, 2H), 3.49 (d, J<sub>GEM</sub>=17.22 Hz, 2H, H), 3.31 (d, J<sub>GEM</sub>=17.22

Hz, 2H), 2.71 (m, 2H), 2.18 (m, 2H), 1.74 (m, 2H), 1.46 (s, 18H), 1.28 (m, 2H), 1.12 (m, 2H).

*N,N'*-bis[(2-quinolylmethyl)-cyclohexanediamine-*N*-tert-butylacetate *N'*-acetic acid (**HL14**). The diester **1** (248 mg, 0.40 mmol) was dissolved at room temperature in formic acid 99% (4.2 mL), and the obtained dark solution was stirred for 24h. The formation of **HL14** was monitored by TLC on Al<sub>2</sub>O<sub>3</sub> (DCM:MeOH 95:5; R<sub>f</sub>: 0.32). The pH of the reaction mixture was adjusted to ~ 7 by using NaOH 10 M aq, and the product was extracted with DCM. The solvent was removed under vacuum to obtain a yellowish solid, which was purified by chromatography on activated neutral alumina (Al<sub>2</sub>O<sub>3</sub>) in gradient elution (DCM:MeOH = 95:5 → 90:10). The product **HL14** was obtained as a white solid (69.6 mg, 0.123 mmol; Yield: 30%). <sup>1</sup>H-NMR (CDCl<sub>3</sub>) δ (ppm) 8.09 (d, J=8.24 Hz, 2H), 7.97 (m, [doublet overlapped], 1H), 7.94 (m [doublet overlapped], J=8.24 Hz, 1H), 7.82 (d, J=8.24 Hz, 1H), 7.77 (t, [doublet overlapped], 2H), 7.73 (t, J=7.27 Hz, 2H), 7.56 (d, J=7.27 Hz, 2H), 7.17 (d, J=8.24 Hz, 1H), 4.13 (d, J=13.38 Hz, 1H), 4.07 (d, J=15.15 Hz, 1H), 3.94 (d, J=13.38 Hz, 1H), 3.52 (m, 1H), 3.33 (m, 4H), 2.89 (m, 1H), 2.27 (m, 1H), 2.17 (m, 2H), 1.83 (m, 2H), 1.78 (m, 2H), 1.46 (s, 9H), 1.12 (m, 2H). ESI-MS(Scan ES+; *m/z*): 569 [M+H]<sup>+</sup>, (Scan ES-; *m/z*): 567 [M-H]<sup>-</sup>

**Eu(LI4)Cl** : the Eu(III) complex was synthesized at room temperature by addition of a slight excess of lanthanide salts (EuCl<sub>3</sub>·6H<sub>2</sub>O, 1.2 equiv.) to a warm solution (70°C) of the ligand **HL14** in a mixture of H<sub>2</sub>O: MeOH 9:1. After the adjustment of the pH value to ~ 7 by means of KOH aq 2M, a white solid was formed and collected by filtration (22.6 mg, Yield: 32%).

### 3.3.4.3. <sup>1</sup>H and <sup>13</sup>C-NMR spectroscopy

Unless a special NMR instrument is available, the traditional NMR spectroscopy is limited to diamagnetic metals. Since the paramagnetic Eu(III) and Tb(III) ions would give <sup>1</sup>H-NMR spectra characterized by broad resonances, the NMR characterization was limited to the intermediates of the synthetic routes and to the final ligands.

Nuclear magnetic resonance (NMR) experiments were performed at 298.15 K using a 600 MHz Bruker Avance III spectrometer equipped with a triple resonance TCI cryogenic probe. Spectra were usually recorded in CDCl<sub>3</sub> and, unless otherwise noted, chemical shifts are expressed as ppm and referenced to the internal standard tetramethylsilane (TMS). One dimensional NMR spectra were recorded with 8 or 16 scans and a spectral width of 12019 Hz. All spectra were manually phased and baseline corrected using TOPSPIN 3.2 (Bruker, Karlsruhe, Germany). Chemical shift, multiplicity (s, singlet; d, doublet; t, triplet; m, multiplet; b, broad), coupling constants and integration area are reported.

#### *3.3.4.4. ESI-MS measurements*

Electrospray ionisation mass spectrometry (ESI-MS) was performed with a Finnigan LXQ Linear Ion Trap (Thermo Scientific, San Jose, CA, USA) operating in positive ion mode. The data acquisition was under the control of Xcalibur software (Thermo Scientific). A MeOH solution of sample was properly diluted and infused into the ion source at a flow rate of 10  $\mu$ L/min with the aid of a syringe pump. The typical source conditions were transfer line capillary at 275 °C; ion spray voltage at 4.70 kV; sheath, auxiliary and sweep gas (N<sub>2</sub>) flow rates at 10, 5 and 0 arbitrary units, respectively. Helium was used as the collision damping gas in the ion trap set at a pressure of 1 mTorr.

#### *3.3.4.5. Luminescence and decay kinetics*

Room temperature luminescence was measured with a Fluorolog 3 (Horiba-Jobin Yvon) spectrofluorometer, equipped with a Xe lamp, a double excitation monochromator, a single emission monochromator (mod. HR320) and a photomultiplier in photon counting mode for the detection of the emitted signal. All the spectra were corrected for the spectral distortions of the setup.

In decay kinetics measurements, a Xenon microsecond flashlamp was used and the signal was recorded by means of multichannel scaling method. True decay times were obtained using the convolution of the instrumental response function



with an exponential function and the least-square-sum-based fitting program (SpectraSolve software package).

#### 3.3.4.6. *UV Absorption spectroscopy*

Room temperature absorption spectra were measured with a Cary 60 UV-Vis spectrophotometer, equipped with a Xenon lamp single source (80 Hz), Czerny-Turner monochromator and a photomultiplier (dual silicon diode detectors). Employed scan rate: 300 nm/min in the 200-800 nm range.

### 3.4. *References*

1. [S. C. Gaglio, C. De Rosa, A. Romeo, M. Perduca, F. Piccinelli, *Optical Materials* **2019**, 94, 249-256].
2. [V. Saxena, M. Sadoqi, J. Shao *J. of Photochem. and Photobiol. B: Biology*, **2004**, 74, 29–38].
3. [F. Danhier, E. Ansorena, J. M. Silva, R. Coco, A. Le Breton, V. Préat *J. of Controlled Release* **2012**, 161, 505–522].
4. [M.L. Hans, A.M. Lowman *Curr. Opin. Solid State Mater. Sci.* **2002**, 6, 319–327].
5. [A. Reisch, A. Runser, Y. Arntz, Y. Mély, A. S. Klymchenko *Acs Nano* **2015**, 9(5), 5104–5116].
6. [J. Hu, J. Guo, Z. Xie, D. Shan, E. Gerhard, G. Qian, J. Yang *Acta Biomaterialia* **2016**, 29, 307–319].
7. [C. Fornaguera, N. Feiner-Gracia, G. Calderó, M.J. García-Celmac, C. Solans *Colloids and Surfaces B* **2016**, 147, 201–209].
8. [T. Betancourt, K. Shah, L. Brannon-Peppas *J. Mater. Sci: Mater. Med.* **2009**, 20; 387–395].
9. [P. P. Wyss, L. C. Herrera, N. S. Bouteghmes, M. Sarem, W. Reichardt, J. Leupold, J. Hennig, V. P. Shastri *ACS Omega* **2016**, 1, 182–192].
10. [L. J. Cruz, I. Que, M. Aswendt, Alan Chan, M. Hoehn, C. Löwik *Nano Res.* **2016**, 9(5), 1276–1289].
11. [R. Reul, N. Tsapis, H. Hillaireau, L. Sancey, S. Mura, M. Recher, J. Nicolas, J.-L. Coll, E. Fattal *Polym. Chem.* **2012**, 3, 694-702].
12. [A. Reisch, A. S. Klymchenko *Small* **2016**, 12(15), 1968–1992].

13. [F. Meng, J. Wang, Q. Ping, Y. Yeo *ACS Nano* **2018**, 12, 6458–6468].
14. [B. Andreiuk, A. Reisch, V. G. Pivovarenko, A. S. Klymchenko *Mater. Chem. Front.* **2017**, 1, 2309].
15. [A. Wagh, S. Y. Qian, B. Law *Bioconjugate Chem.* **2012**, 23, 981–992].
16. [E. Kemal, T. F. Abelha, L. Urbano, R. Peters, D. M. Owen, P. Howes, M. Green, L. A. Dailey *RSC Adv.* **2017**, 7, 15255-15264].
17. [E. Kemal, R. Peters, S. Bourke, S. Fairclough, P. Bergstrom-Mann, D. M. Owen, L. Sandiford, L. A. Dailey, M. Green *Photochem. Photobiol. Sci.* **2018**, 17, 718-721].
18. [E. S. Khameneh, M. M. Amini, S. Kakaei, A. Khanchi *Radiochimica Acta* **2018**, 106(11), 897-907].
19. [M. Leonzio, M. Bettinelli, L. Arrico, M. Monari, L. Di Bari, F. Piccinelli *Inorg. Chem.* **2018**, 57, 10257–10264].
20. [M. Shakweh, M. Besnard, V. Nicolas, E. Fattal *Eur. J. Pharm Biopharm.* **2005**, 61(1-2), 1-13].
21. [E. W. J. L. Oomen and A. M. A. van Dongen *J. Non. Cryst. Solids* **1989**, 111, 205–213].
22. [R. Reisfeld, E. Zigansky, M. Gaft *Mol. Phys.* **2004**, 102, 1319–1330].
23. [M. Mihorianu, M. Leonzio, M. Monari, L. Ravotto, P. Ceroni, M. Bettinelli, F. Piccinelli *Chem. Sel.* **2016**, 1, 1996–2003].
24. [F. Piccinelli, C. De Rosa, A. Melchior, G. Faura, M. Tolazzi, M. Bettinelli. *Dalt. Trans.* **2019**, 48, 1202-1216].
25. [M. Mihorianu, M. Leonzio, M. Bettinelli, F. Piccinelli *Inorg. Chim. Acta* **2015**, 438, 10–13].
26. [D. F. Eaton, *Pure Appl. Chem.* **1988**, 60, 1107–1114].
27. [D. Parker, P. K. Senanayake, J. A. G. Williams *J. Chem. Soc. Perkin Trans. 2* **1998**, 2129–2140].
28. [C. Li, Y. Liu, Y. Wu, Y. Sun and F. Li, *Biomat.* **2013**, 34, 1223–1234].
29. [A. Brandner, T. Kitahara, N. Beare, C. Lin, M. T. Berry and P. S. May, *Inorg. Chem.* **2011**, 50, 6509–6520].
30. [J. C. G. Bünzli, S. V. Eliseeva, in *Comprehensive Inorganic Chemistry II (Second Edition): From Elements to Applications*, Elsevier **2013**, 8, 339–398].
31. [F. Ramazani, W. Chen, C.F. van Nostrum, G. Storm, F. Kiessling, T. Lammers, W.E. Hennink, R.J. Kok *Int. J. Pharm.* **2016**, 499(1-2), 358-367].

32. [R. Yang, C. da Costa, M. J. Fuchter, A. J. Campbell, *Nat. Photonics* **2013**, 7, 634].
33. [W. Sparks, J. Hough, L. Kolokolova, T. Germer, F. Chen, S. DasSarma, P. Das Sarma, F. Robb, N. Manset, I. Reid, *J. Quant. Spectrosc. Radiat. Transfer* **2009**, 110, 1771].
34. [T. Novikova, A. Pierangelo, A. De Martino, A. Benali, P. Validire, *Opt. Photonics News* (**2012**) 26].
35. [F. Piccinelli, A. Speghini, M. Monari, M. Bettinelli, *Inorg. Chim. Acta* **2012**, 385, 65].
36. [F. Piccinelli, M. Bettinelli, A. Melchior, C. Grazioli, M. Tolazzi, *Dalton Trans.* **2015**, 44, 182].
37. [M. Leonzio, A. Melchior, G. Faura, M. Tolazzi, F. Zinna, L. Di Bari, F. Piccinelli, *Inorg. Chem.* **2017**, 56, 4413–4422].
38. [J. Broder, A. Majumder, E. Porter, G. Srinivasamoorthy, C. Keith, J. Lauderdale, A. Sornborger, *J. Opt. Soc. Am. A Opt. Image* **2007** Sci Vis 24:2921–2931].
39. [A. Sornborger, J. Broder, A. Majumder, G. Srinivasamoorthy, E. Porter, SS. Reagin, C. Keith, JD. Lauderdale *J. Opt. Soc. Am. A Opt. Image* **2008** Sci Vis 25:2185–2194].
40. [F. Piccinelli, C. De Rosa, S. Zanzoni, M. Bettinelli, *J. of Luminescence*, **2018**, 193, 114-118].
41. [J. E. Dengler, M. W. Lehenmeier, S. Klaus, C. E. Anderson, E. Herdtweck, B. Rieger, *Eur. J. Inorg. Chem.* **2011**, 336].
42. [S.-J. Choi, J.-H. Cho, I. Im, S.-D. Lee, J.-Y. Jang, Y.-M. Oh, Y.-K. Jung, E.-S. Jean, Y.-C. Kim, *Eur. J. of Med. Chem.* **2010**, 45].
43. [J. Falbe and M. Regitz, *Römpp-Chemie Lexikon* (9th edn), Thieme, Stuttgart, **1989**, pp. 415].
44. [P. Bisel, L. Al-Momani, M. Müller, *Org. Biomol. Chem.*, **2008**, 6, 2655–2665].
45. [Z. Wu, X. Wang, T. Tao, Y. Zhang, Y. Liu, H. Fong, *J. Appl. Polym. Sci.* **2007**, 103, 3617–3622].
46. [W.-R. Huck, T. Bürgi, T. Mallat, A. Baiker, *J. Catal.* **2003**, 216, 276].
47. [K. Binnemans, *Coord. Chem. Rev.* **2015**, 295, 1].
48. [H.K. Makadia HK, S.J. Siegel *Polymers (Basel)* **2011** Sep 1; 3(3):1377-1397].

## CHAPTER 4- Interaction of new Ln(III) complexes with relevant bioanalytes

### 4.1. *Introduction*

The new library of Eu(III) and Tb(III) (Figure 2, pag.124) designed and developed in this PhD project has been successfully employed for studying the interaction with relevant bioanalytes, in physiological buffer as well as in a simulated extracellular solution, (refer to Chapter 5).

In principle, although several organic fluorophores could be used for the above-mentioned purpose, the well-known properties of the lanthanides such as long excited state lifetimes (usually in the milliseconds range), large energy shift between absorbed and emitted radiations (in the case of ligand sensitization) and very narrow emission bands are more useful in this context.

In the field of the lanthanides complexes, several ways could be employed to signal the presence of a specific analyte. Among the main methods, one particularly exploited is the change in the emission intensity, as well as the variation in the asymmetry ratio  $R$ , indicative of the degree of asymmetry of the coordination polyhedron around the Eu(III) ion. The direct chelation of the biomolecules to the metal center, can decrease the number of quenchers, usually solvent molecules within the coordination sphere of the metal ion, resulting in a decrease of the multiphonon relaxation process. This gives rise to an increase of the observed lifetime of metal ion and a concomitant increase of the luminescence intensity. In this context, the capability of the complex to bind the analytes of interest can be partially predicted by the determination of the *hydration number*  $q$ , indicative of the free sites accessible around the metal center (Chapter 1).

The application of the lanthanide luminescence in the biological field is particularly challenging, since several features should be considered for an efficient and selective probe-analyte interaction.

One of the main drawbacks to overcome is surely the *i) competition* with other biomolecules present in the environment. In a real biological sample, the total enhancement or decrease of the intensity of the luminescence signal could not

only due to the analyte under investigation, since many other interferents could generate an analogous response.

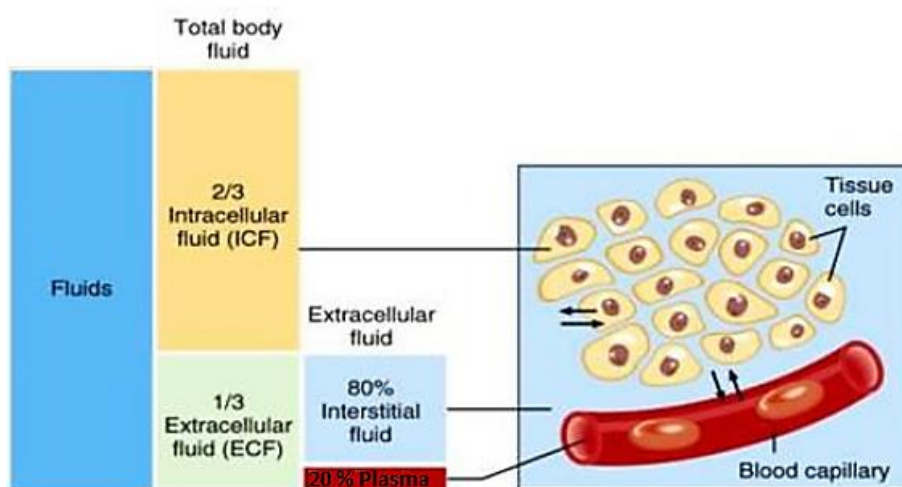
Another important concern is the *ii) biocompatibility* of the complex (i.e. no release of the toxic metal ion). This can be partially predicted by the determination of the stability constants in biological environment. Usually, any decomposition or exchange reaction of the Ln ions would result in a loss of the luminescence intensity and a possible toxic exposure of the cells to the free Ln ions. In the biological field, also the *iii) localization/permeability of the probe* is another fundamental feature to consider and it is difficult to predict precisely in advance.

In the purposes of this PhD project, the main biological targets concern the components of the extracellular fluid (ECF). The current Chapter and the next Chapter 5 are devoted to the study of the interactions between our luminescent probes and the selected bioanalytes.

In this Chapter, a complete structural and spectroscopic characterization of the Ln(III)-complexes under investigation is presented.

The major part of the mass body is made of water; the total body distribution of the water in mammals is classified in *intracellular* and *extracellular* compartment. About two thirds of the total fluids is intracellular fluid within cells, and one third is the extracellular fluid.<sup>1</sup>

The main part of the ECF is the interstitial fluid that surrounds cells, while the remaining parts are blood plasma and, even less the cerebrospinal fluid (Scheme 1).



Scheme 1. Schematic representation of the body fluids composition

In a simplified model where just the main bioanions (Table 1) and the most abundant serum proteins (0.4 mM) are considered, it has been possible to investigate the luminescence response of our Ln(III)-complexes under physiological conditions. These experiments show promising results for *bicarbonate ion*, the *serum protein (BSA)* and the *citrate ion* whose study referred to Chapter 5, it has involved a more sophisticated and productive screening (High throughput screening, HTS) in microplate reader.

Anion	Extracellular fluid	Intracellular fluid	Cerebrospinal fluid
Cl <sup>-</sup>	104-115	3-15	115-130
HCO <sub>3</sub> <sup>-</sup>	24-27	10-12	20-23
SO <sub>4</sub> <sup>2-</sup>	0.4-0.6	0.3-0.4	0.06-0.2
Phosphate	1.2-1.3	0.8-1.2	0.15
Lactate	0.6-2.3	3-22	0.5-2.2
Citrate	0.1-0.3	2-4	0.05-0.25

Table 1. Typical concentration ranges (mM) of selected anions in humans (intracellular values vary considerably with cell type). From <sup>2</sup>

The reversible anion binding at lanthanide centres in aqueous media has emerged as an effective means of signalling and sensing the presence of selected anions by modulating different charge density on the metal, and ligand modification, this latter responsible of the local steric demand around the metal centre. In this context, the selectivity for a target anion can be engineered, and the affinity constant modulated to target the desired concentration range.

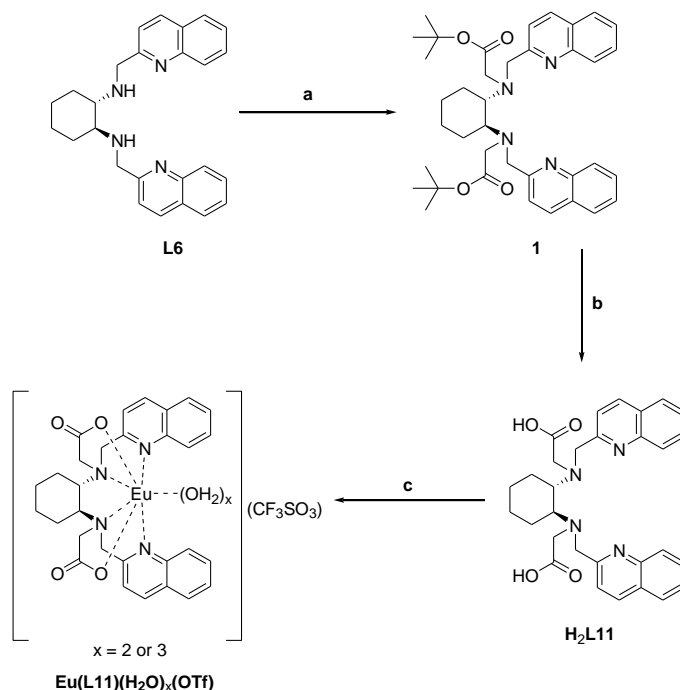
A future application within the living cells should be surely attractive, but up to now, the current biological information concerning permeability, localization, toxicity and excretion of our complexes is not sufficient to allow biosensing in *in cellulo* experiments.

## 4.2. Complexes structure: synthesis and characterization

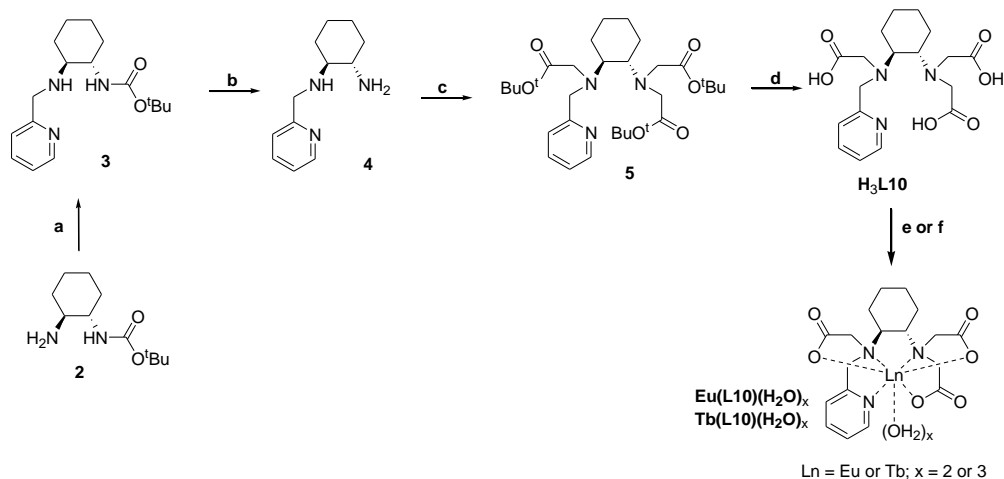
### 4.2.1. Synthesis

The synthesis of the ligands and the relative Ln(III) complexes discussed in this chapter are presented in Schemes 2-6.

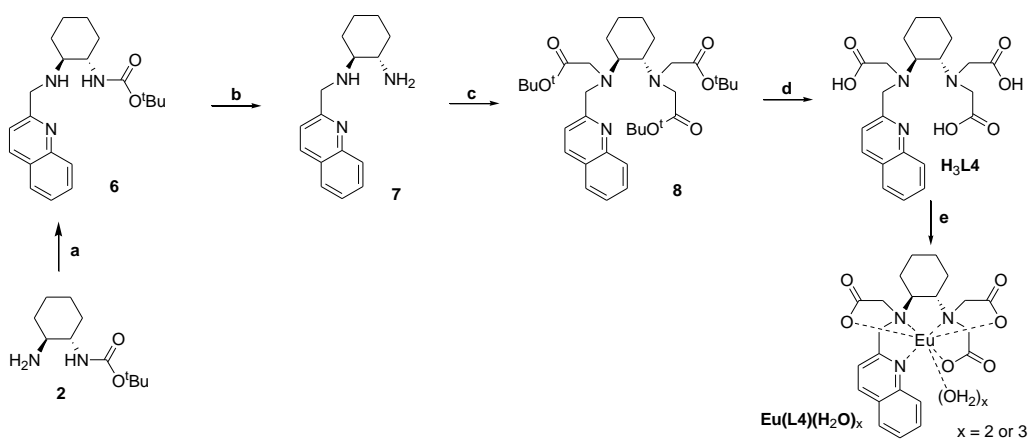
The chemistry of the bis-Pyridine derivatives **Eu(L9)Cl** and **Tb(L9)Cl** (Scheme 3) was already described,<sup>3</sup> as well as that one of the bis-Quinoline derivative **Eu(L11)OTf** which exploits the N-alkylation of the amine **L6** (Scheme 2), whose synthesis has been reported previously,<sup>4</sup> in addition to the synthesis of **2** whose synthesis has been performed as known in literature.<sup>5</sup> The synthesis of tris acidic ligand **H<sub>3</sub>L10** (Scheme 3) and **H<sub>3</sub>L4** (Scheme 4) with *C<sub>1</sub>*-symmetric ligands, involves the straightforward chemistry of the t-Butyloxycarbonyl (BOC) protective group. In this context, the derivative **2** (scheme 3) can be obtained in good yield as previously reported.<sup>5</sup> All the ligands (**H<sub>3</sub>L10** and **H<sub>3</sub>L4**) and the relative Ln complexes (**Eu** and **Tb(L10)** and **Eu(L4)**) have been obtained in good yield and with a high degree of purity (see the experimental section for details).



Scheme 2. Synthetic protocol for the synthesis of **H<sub>2</sub>L11** and **Eu(L11)(CF<sub>3</sub>SO<sub>3</sub>)**. (a) tert-butyl bromoacetate 3 eq, K<sub>2</sub>CO<sub>3</sub> 3.2 eq, CH<sub>3</sub>CN, room temperature, 12 h; (b) HCl 6M aq. 80°C, 12h; (c) Eu(OTf)<sub>3</sub> 1 eq, 2-propanol, room temperature, 12h.



Scheme 3. Synthetic protocol for the synthesis of the ligand **H<sub>3</sub>L10**, and the relative Ln(III) complexes **Eu(L10)** and **Tb(L10)**. (a) Pyridine-2-carbaldehyde 1 eq, absolute ethanol, room temperature, 12h; NaBH<sub>4</sub> 1.2 eq, MeOH, room temperature, 12h; (b) Trifluoroacetic Acid:dichloromethane (1:3), room temperature, 12h; (c) tert-butyl bromoacetate 3.5 eq, N,N-Diisopropylethylamine 3.5 eq, CH<sub>3</sub>CN, room temperature, 12 h; (d) HCl 6M aq. 80°C, 12h; (e) Eu(OTf)<sub>3</sub> 1 eq, 2-propanol:ethanol (1:1), room temperature, 12h or (f) TbCl<sub>3</sub>·6H<sub>2</sub>O 1 eq, water, room temperature, 12h.

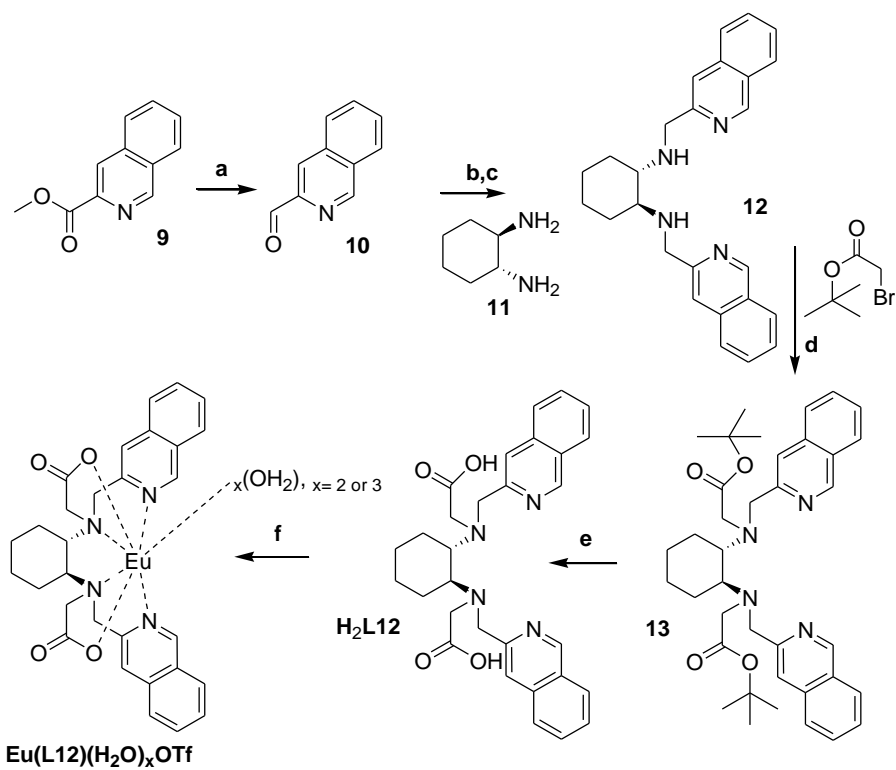


Scheme 4. Synthetic protocol for the synthesis of the ligand **H<sub>3</sub>L4** and the relative Eu(III) complex **Eu(L4)**. (a) Quinoline-2-carbaldehyde 1 eq, absolute ethanol, room temperature, 12h; NaBH<sub>4</sub> 1.2 eq, MeOH, room temperature, 12h (b) Trifluoroacetic Acid:dichloromethane (1:3), room temperature, 12h; (c) tert-butyl bromoacetate 3.5 eq, N,N-Diisopropylethylamine 3.5 eq, CH<sub>3</sub>CN, room temperature, 12 h; (d) HCl 6M aq. 80°C, 12h; (e) Eu(OTf)<sub>3</sub> 1 eq, 2-propanol:ethanol (8:2), room temperature, 12h.

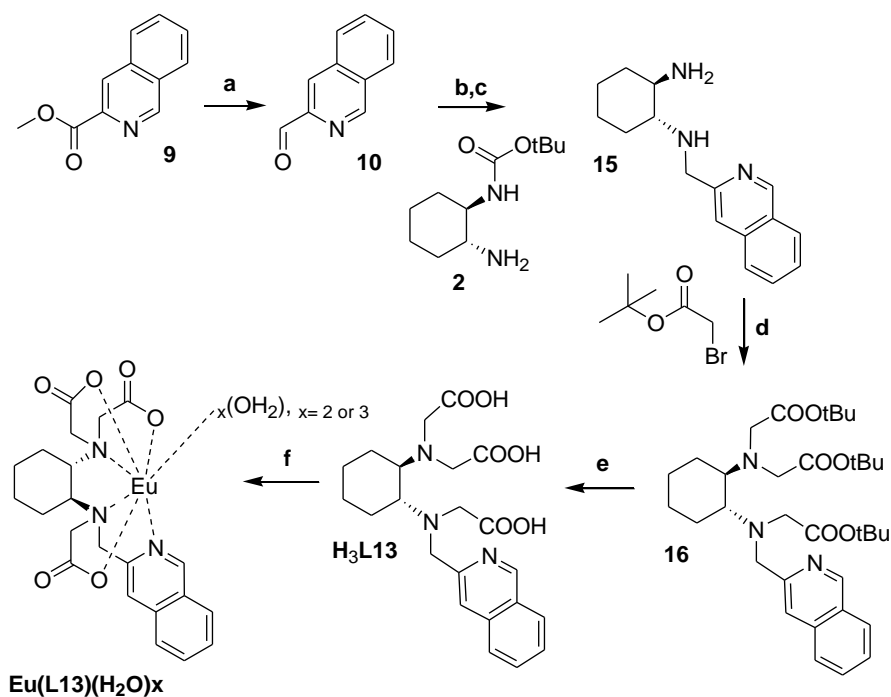
As far as the synthesis of **Eu(L12)OTf** and **Eu(L13)** complexes are concerned (Scheme 5 and 6), we adapted the synthetic route reported in Scheme 2, 3 and 4 to the synthesis of Eu(L12)OTf and Eu(L13). Worth mentioning is the use of the cheaper methyl ester **9** to obtain the initial aldehyde **10** by means of selective



reduction with Diisobutylaluminium hydride (DIBALH) 1M in toluene (Scheme 5 and 6, see experimental part for more details).



Scheme 5. a) Diisobutylaluminium hydride (DIBAL-H) 1M in toluene 1.7 eq, -78°C; b) Isoquinoline-3-carbaldehyde  $\approx 1.1$  eq, absolute ethanol, room temperature, 12h; c) NaBH<sub>4</sub> 1.8 eq, MeOH, room temperature, 5h; d) tert-butyl bromoacetate 2.7 eq, K<sub>2</sub>CO<sub>3</sub> 2.7 eq, CH<sub>3</sub>CN, room temperature, 12 h; e) HCl 6M aq. 80°C, 12h; f) Eu(OTf)<sub>3</sub> 1 eq, 2-propanol, room temperature, 12h; (For more details see experimental part).



Scheme 6. a) Diisobutylaluminium hydride (DIBAL-H) 1M in toluene 1.7 eq,  $-78^\circ\text{C}$ ; b) Isoquinoline-3-carbaldehyde 1 eq, absolute ethanol, room temperature, 12h; c)  $\text{NaBH}_4$  1.2 eq, MeOH, room temperature, 5h; d) *tert*-butyl bromoacetate 3.5 eq, *N,N*-diisopropylethylamine 3.5 eq,  $\text{CH}_3\text{CN}$ , room temperature, 12 h; e) HCl 6M aq.  $80^\circ\text{C}$ , 12h; f)  $\text{Eu}(\text{OTf})_3$  1 eq, water: methanol (9:1), room temperature, 1h. (For more details see experimental part).

#### 4.2.2. Characterization: Stability constant

The intrinsic stability of the metal complex is a fundamental requirement for all kind of application, and in biological field plays a crucial role.

The stability constant (binding constant or formation constant) is an equilibrium constant for the formation of a complex in solution, and it is a measure of the thermodynamic stability of the complex.

In this work, two different notations are used for the equilibrium constant:  $K$  is used to describe the stepwise equilibrium constant, and  $\beta$  for the overall equilibrium constant or formation constant.

*Potentiometric* and *spectrophotometric acid-base titrations* have been performed in order to obtain all the equilibrium constants found in this work. Potentiometric

titration allows an easy determination of the protonation constants of the each ligand.

A progressive number of equilibrium constant ( $K_1$ ,  $K_2$  and  $K_3$ ) could be recovered in a stepwise protonation of the same molecule. The mathematical relation between  $K$  and  $\beta$  values is depicted in Figure 1, where the logarithm  $\log \beta$  of the constants are deduced from the equation below.<sup>6</sup>

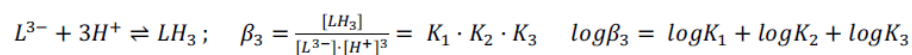
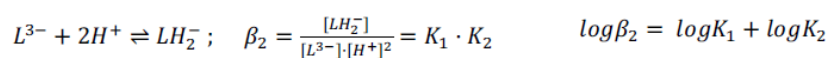
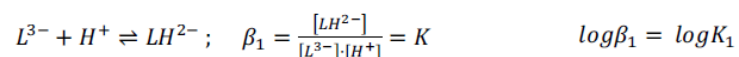


*Figure 1. Stability constant of a triacidic-ligand.*

The ligands and Ln-complexes studied by acid-base potentiometric or spectrophotometric titrations ( $T = 298.2$  K and  $\mu = 0.1$  M NaCl) have been summarized in Figure 2.

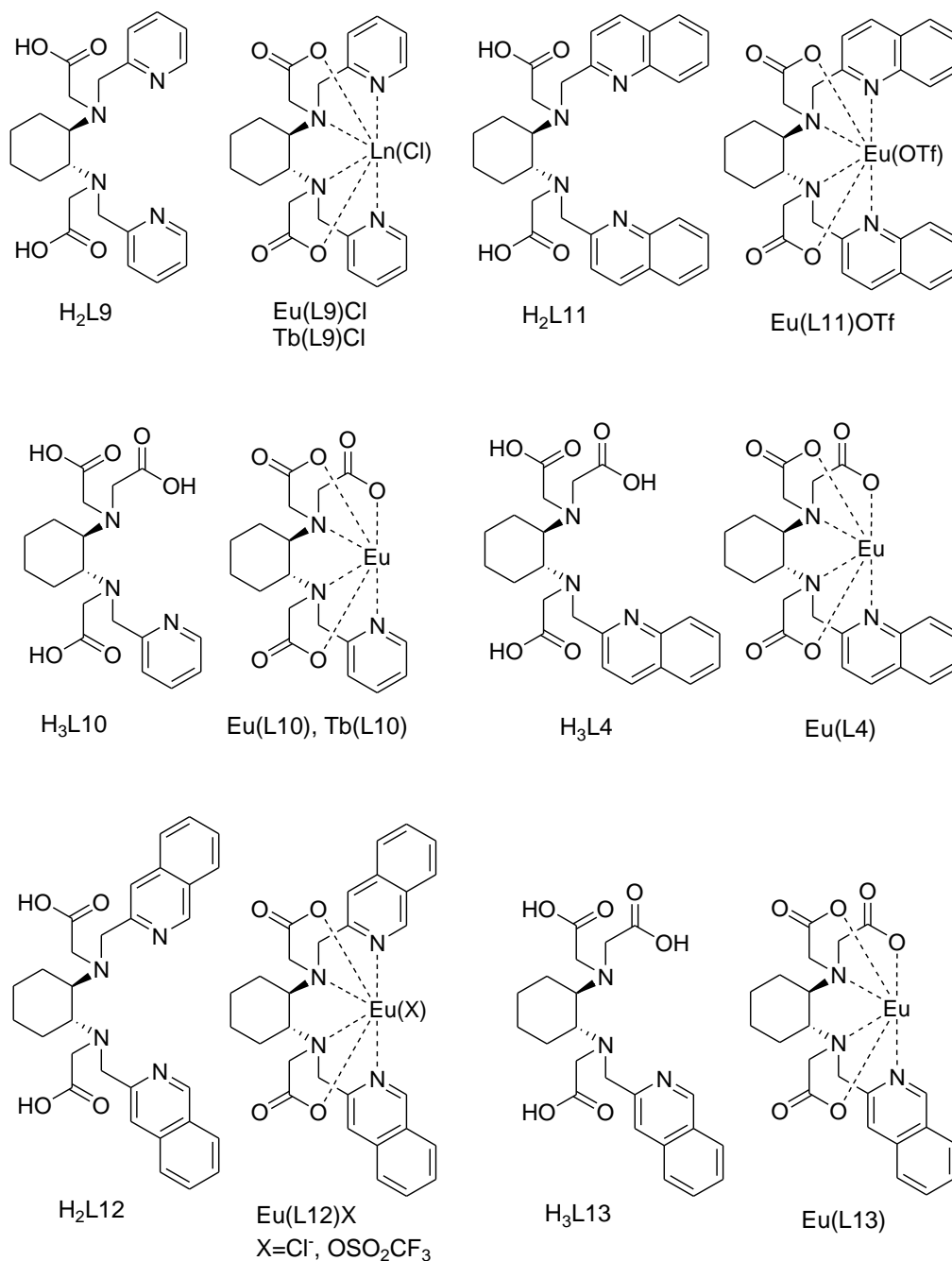


Figure 2. Ligands and Ln-complexes studied by Potentiometric and Spectrophotometric acid-base titrations. Charges and water molecules omitted for clarity.

The best fit of the data is performed by either *Hyperquad* and *Hypspec* program (for potentiometry or spectrophotometry, respectively).

The pH/mV trend of the potentiometry and the UV-Vis absorbance changes in the spectrophotometry both associated to the speciation curves of the protonated

species LH to LH<sub>n-1</sub> are complementarily techniques used for studying the chemical equilibria of the ligands under investigation.

Since the potentiometry technique is more accurate and precise was mostly preferred with respect to the spectrophotometric acid-base titrations. The recommended concentration of ligand is around 1 mM<sup>6</sup> but when it was not possible to reach this value (essentially for solubility issues), the spectrophotometric acid-base titrations have been performed. This technique required a smaller amount of ligand.

The stability constants of the Ln-complexes **Eu(L9)Cl** and **Tb(L9)Cl** (Figure 2) based on *N,N'*-bis(2-pyridylmethyl)-*trans*-1,2-diaminocyclohexane-*N,N'*-diacetic acid (**L9**) ligand have been obtained by acid-base potentiometric titration, whereas the derivatives **Eu(L4)**, **Eu(L10)** and **Tb(L10)**, **Eu(L11)OTf**, **Eu(L12)OTf** and **Eu(L13)** (Figure 2) have been determined by acid-base spectrophotometric titrations.

#### 4.2.2.1. Potentiometric acid-base titrations

In this method, the electromotive force (emf) between two electrodes in contact with a solution is measured by means of *Nernst equation* (eq.1).

$$E = E^{0'} + \frac{RT}{nF} \ln \frac{[S^{z+}]}{[S^{(z-n)+}]}$$

*Equation 1. Nernst equation of a generic species S simplified with concentrations instead of activity a; E is the observed emf, E<sup>0'</sup> is the standard emf for the redox couple oxidized specie/reduced specie, n is the number of electrons involved in the reduction of S, R is the gas constant and F is the Faraday constant.*

This emf is affected by temperature and the species in solution, and is correlated to their activity, for this reason a thermostatic bath (T 298.15 K) and μ (0.1 M) are kept constant in order to use concentrations instead of activities (Figure 3). The principle of method is based on one electrode of reference and a second one used as measuring electrode sensitive towards the analyte of interest. In our case, upon calibration of the electrode, the initial solution inside the cell contains the ligand dissolved in HCl 0.1 M (pH≈2) for the first acid-base titration up to pH≈11,

afterwards the solution was acidified again and the right amount of metal was added in order to prepare the system for the complexation studies.

Moreover, a combined glass electrode has been used as reference and indicator electrode at the same time, for measuring the activity of  $H^+$  ions.

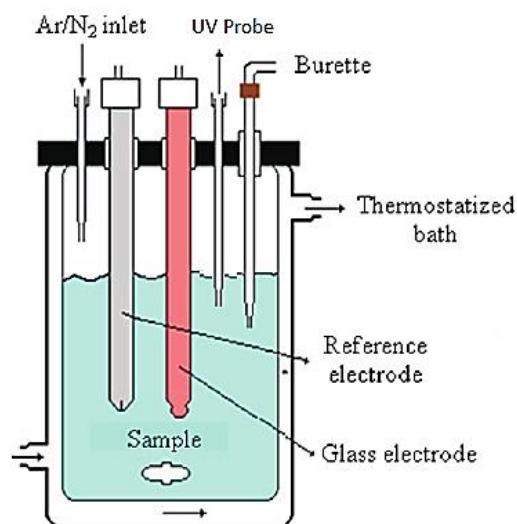


Figure 3. Principle of method for potentiometric (without UV probe) and spectrophotometric acid-base titrations.

Afterwards, the additions and the measurements were controlled by a personal computer. All the titrations were performed on solutions containing the ligand in concentrations range 0.6-1 mM, depending on the experiment, and for the complexation studies in solution, a 1:1 ligand to metal mole ration was employed. All the data collected from the potentiometric titration (the emf, the concentrations of the initial species, the initial volume, the calibration data obtained previously) are processed with *Hyperquad program*<sup>7,8</sup> in order to get the speciation model which better fits the experimental data.

The best fit of the potentiometric data was obtained for all ligands (L4, L9, L10, L11, L12 and L13) when four protonated species were considered (Figure 4).

The obtained protonation data  $\log K_n$  are reported in Table 2 along with the constants for similar ligand containing the chiral DACH backbone: (i.e. CDTA<sup>9</sup> (1,2-cyclohexanediaminetetraacetic acid) (Figure 4).

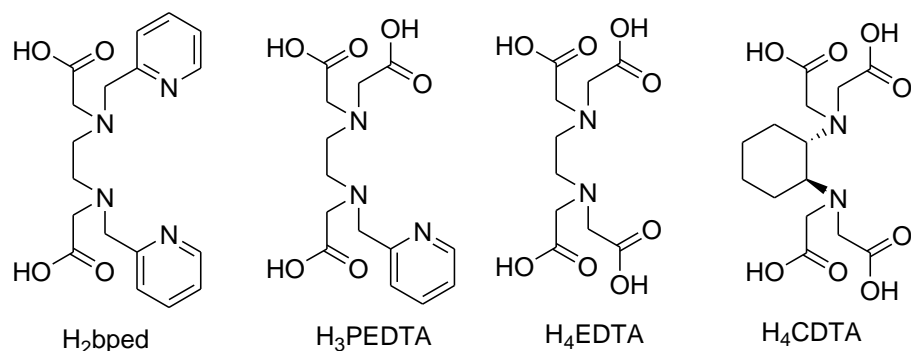


Figure 4. The four species model adopted for simulation in Hyperquad program; bped=*N,N'*-bis(2-pyridylmethyl)ethylenediamine-*N,N'*-diacetate; *N*-(pyrid-2-yl-methyl)-ethylenediamine-*N,N,N'*-triacetic acid=*PEDTA*; ethylene-diaminetetraacetic acid=*EDTA*; *CDTA*=*trans*-1,2-diaminocyclohexane-*N,N,N',N'*-tetraacetic acid

	<b>H<sub>2</sub>L11</b>	<b>H<sub>3</sub>L10</b>	<b>H<sub>3</sub>L4</b>	<b>H<sub>2</sub>L12</b>	<b>H<sub>3</sub>L13*</b>	<b>H<sub>2</sub>L9<sup>a</sup></b>	<b>CDTA<sup>b</sup></b>
<b>logK<sub>1</sub></b>	9.37(3)	10.26(2)	10.53(3)	9.22(2)	10.53(3)	9.72(2)	9.43(2)
<b>logK<sub>2</sub></b>	5.85(7)	6.33(7)	6.29(9)	5.76(6)	6.29(9)	5.87(7)	6.01(2)
<b>logK<sub>3</sub></b>	3.5(1)	3.7(1)	3.6(2)	3.27(7)	3.6(2)	2.9(1)	3.68(2)
<b>logK<sub>4</sub></b>	1.8(3)	2.0(1)	2.8(2)	1.77(7)	2.8(2)	2.2(2)	2.51(5)

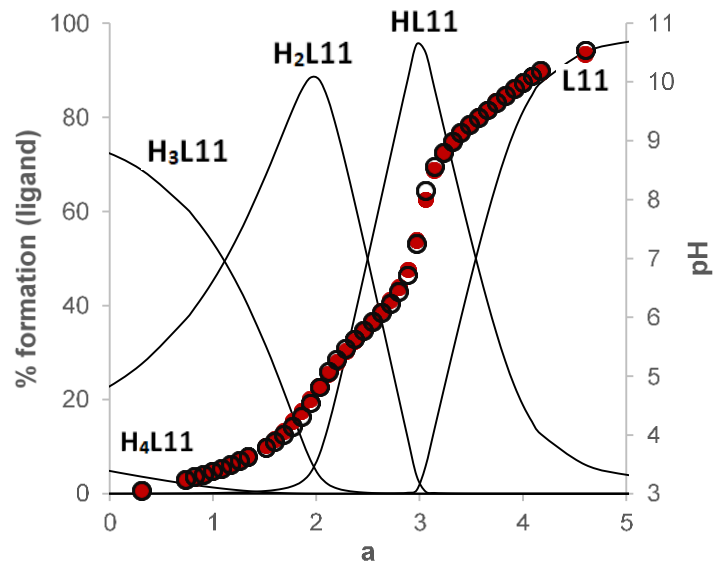
a) ref.<sup>3</sup> ; b) ref.<sup>9</sup>,  $\mu = 0.15$  M NaCl

Table 2. Protonation constants ( $\log K_n$ ,  $K_n = [LH_n]/([H] \cdot [LH_{n-1}])$ ) of the ligands *L4*, *L9*, *L10*, *L11*, *L12* and *L13* with their confidence intervals ( $T = 298.15$  K and  $\mu = 0.1$  M NaCl). Additional protonation data for similar ligands are also reported. \* It was assumed that the tris Isoquinoline *L13* had the same protonation constants of the bis Isoquinoline derivative *L12*. Charges omitted for clarity

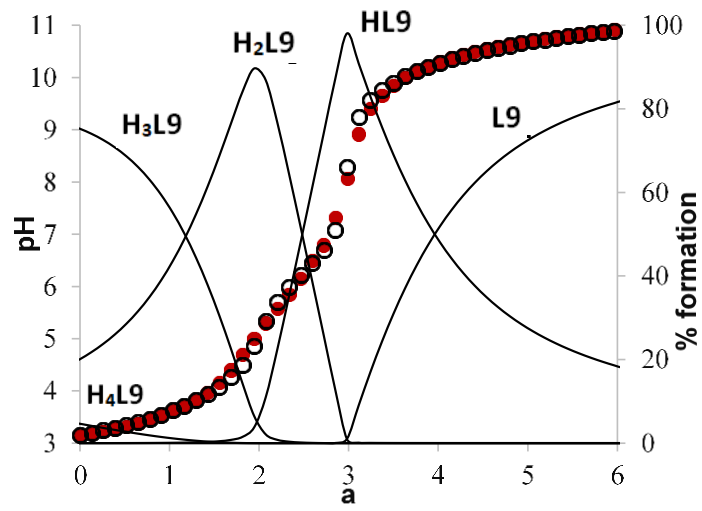
The potentiometric titration curve for all the ligands are displayed in Figure 5 along with the speciation, calculated with the Hyss program<sup>7</sup> by using the experimental conditions and the protonation constants found.

It is worth noting a similar trend in the speciation of all the ligands under investigation. Two clear inflection points at 2 and 3 equivalents of free OH<sup>-</sup> are detected corresponding to the maximum concentration for the generic species LH<sub>2</sub> and LH respectively.

a)

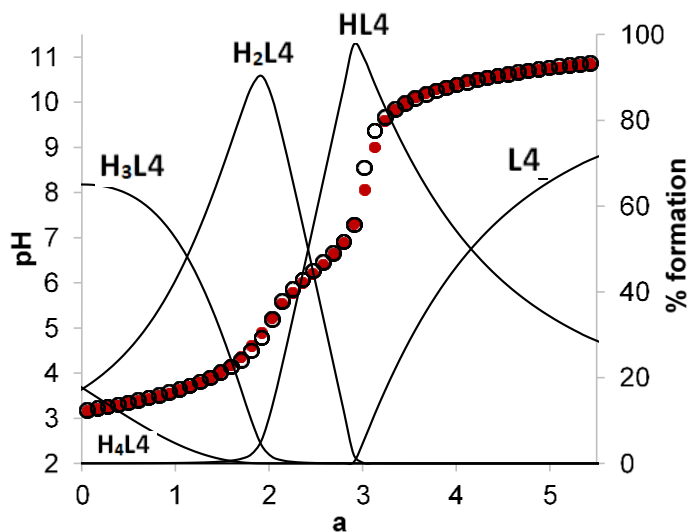


b)





c)



d)

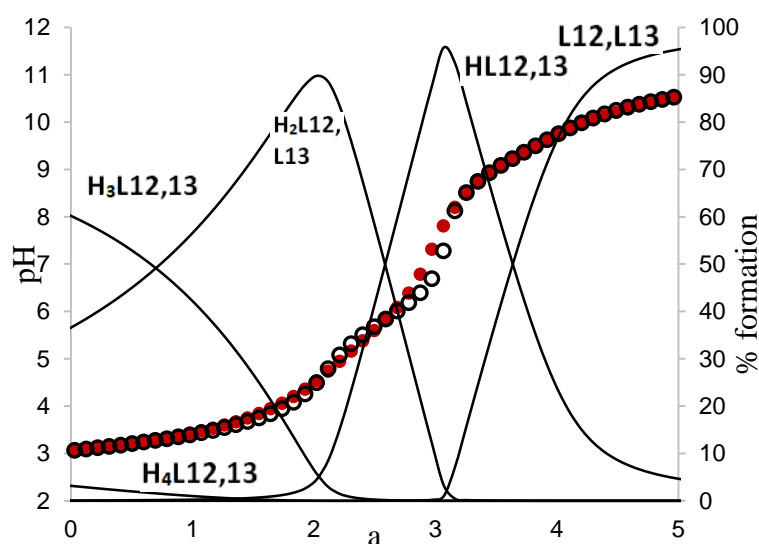


Figure 5 a) Speciation and Titration curve (● observed and ○ calculated pH) for the ligand L11 obtained at  $T = 298.15 \text{ K}$  and  $\mu = 0.1 \text{ M NaCl}$  ( $[L] = 0.9 \text{ mM}$ ),  $a = (\text{moles of free OH}) / (\text{moles of L})$ ; b) Speciation and titration curve (● observed and ○ calculated data) for the ligand L9, ( $[L] = 0.6 \text{ mM}$ ), c) Speciation and titration curve (● observed and ○ calculated data) for the ligand L4, ( $[L] = 0.7 \text{ mM}$ ); d) Speciation and titration curve (● observed and ○ calculated data) for the ligand L12 and L13 ( $[L] = 0.72 \text{ mM}$ ). This latter plot assumed that the tris Isoquinoline L13 had the same protonation constants of the bis Isoquinoline derivative L12. Charges and water molecules omitted for clarity.

As can be clearly seen from the inspection of the  $\log K$  values, the presence of two weakly basic ( $\log K_1$  and  $\log K_2$ ) and two quite strong acidic ( $\log K_3$  and  $\log K_4$ ) sites are present in each ligand. As previously reported for CDTA<sup>10</sup>, the first

protonation constant can be assigned to a tertiary amine ( $\log K_1 \approx 6.9 - 10.7$ , depending on the substituents).<sup>11</sup>

The following order of protonation concerns the heteroaromatic rings ( $\log K_2$  and  $\log K_3$ ) since they are in line with the protonation constants of 2-methylpyridine (picoline) and quinoline ( $\log K = 6.06$  for picoline,  $\log K = 4.97$  for quinoline).<sup>12, 13</sup>

Assuming that the protonation constants of Quinoline ring are the same of Isoquinoline one, the remaining protonation constants ( $\log K_4$  for L11 and L12,  $\log K_3$  and  $\log K_4$  for L10, L4 and L13) could be ascribed to acetate moieties.<sup>14</sup>

This sequence of protonation is in agreement with those suggested for H<sub>2</sub>bped via UV-vis and NMR spectroscopy study.<sup>15</sup>

#### 4.2.2.2. Spectrophotometric acid-base titrations

As already mentioned, the potentiometric acid-base titrations are preferable for the higher accuracy and precision. Nevertheless, even the spectrophotometric acid-base titrations have been performed as a complementary technique for the acquisition of further information.

The formation constants of the Eu(III) and Tb(III) complexes with the ligands L4, L10, L11, L12 and L13 (Figure 2) have been determined by acid-base spectrophotometric titration. The Figure 6 show the absorbance changes of the ligand (L10) upon addition of base to an equimolar solutions of a) **Eu(L10)** or b) **Tb(L10)** (Figure 6).

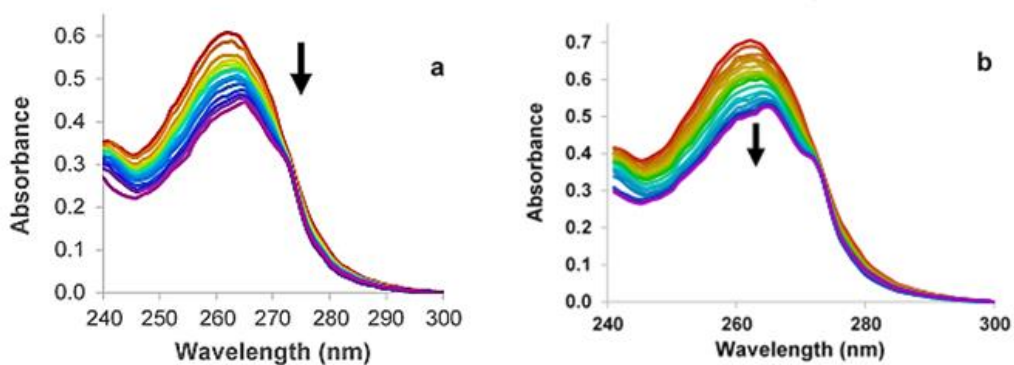


Figure 6. UV-Vis absorption spectra changes during the acid-base titration (in the pH range 2.3-11.5) for the

ligand: a) L10 (0.13 mM), b) L10 (0.15 mmol dm<sup>-3</sup>), in the presence of equimolar Eu(III) and Tb(III) respectively. T = 298.15 K and  $\mu = 0.1$  M NaCl.

The changes of the absorption spectra during the titration of complexes containing the quinoline rings are reported in Figure 7. During the titration a decrease of the absorbance is recorded for all the complexes.

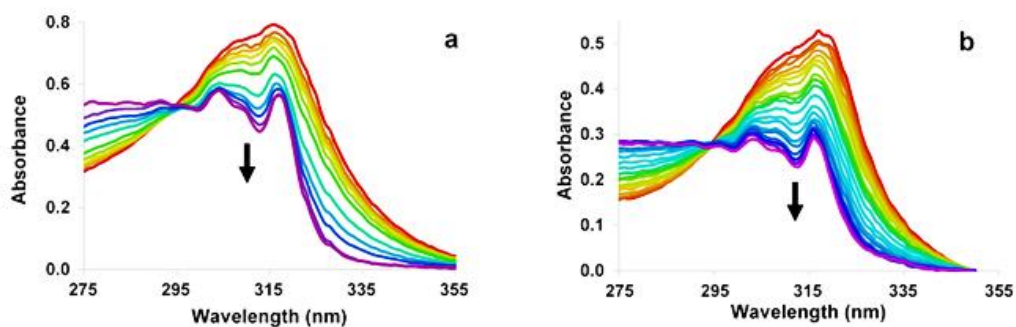
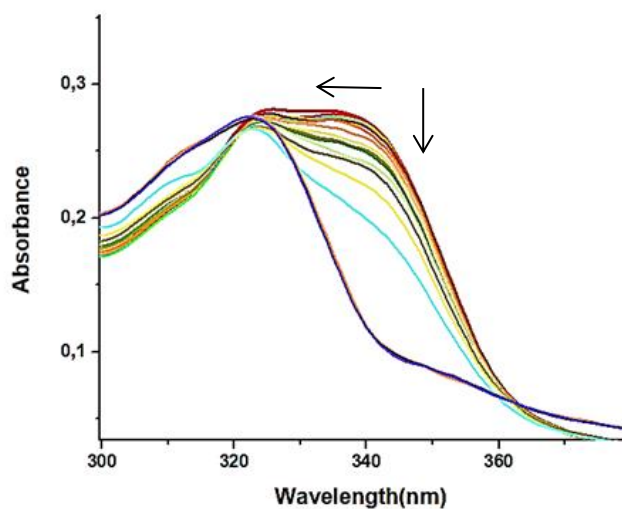


Figure 7. UV-Vis absorption spectra changes during the acid-base titration (pH ~2.3-11.5) in the presence of equimolar Eu(III) for the ligands a) L11 (0.08 mmol dm<sup>-3</sup>), and b) L4 (0.09 mmol dm<sup>-3</sup>). All spectra at T = 298.15 K and  $\mu = 0.1$  mol dm<sup>-3</sup> NaCl.

On the other hand, in the case of the Isoquinoline derivatives **L12** and **L13** a significant shift of the peak around 340 nm is noticed (Figure 8 a-b).

a)



b)

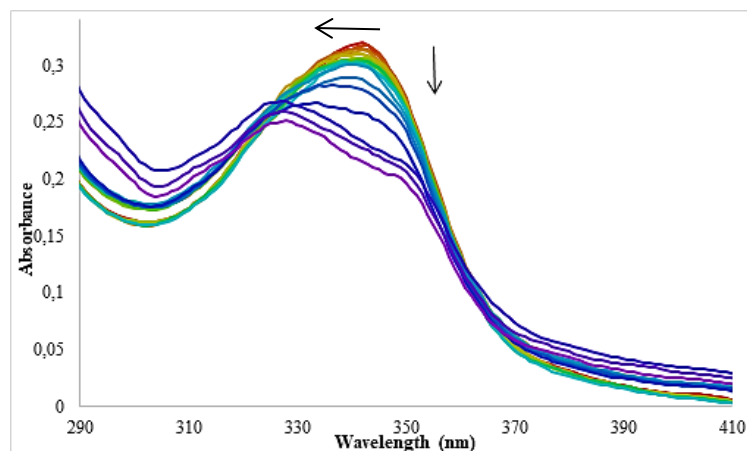
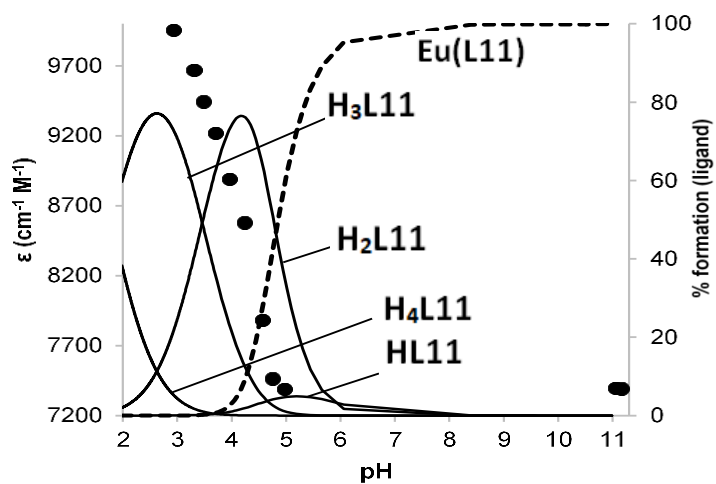


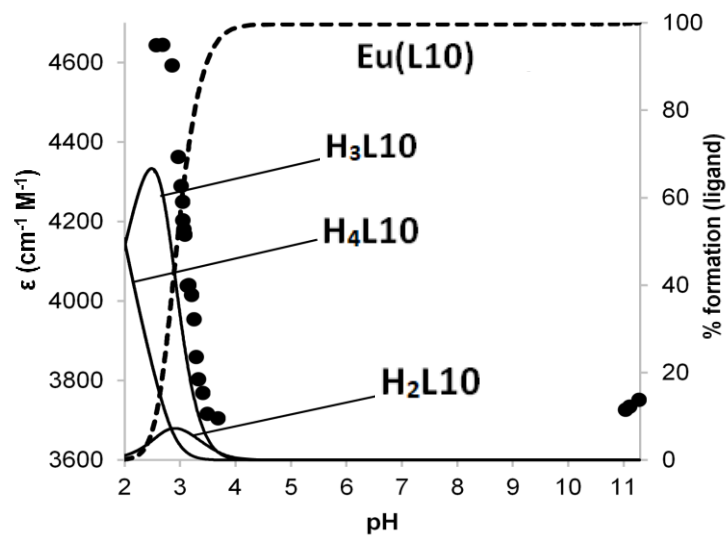
Figure 8. UV-Vis absorption spectra changes during the acid-base titration ( $\text{pH} \sim 2.3\text{-}11.5$ ) in the presence of a) equimolar Eu(III) for the ligand L12 ( $0.045 \text{ mmol dm}^{-3}$ ) and b) equimolar Eu(III) for the ligand L13 ( $0.090 \text{ mmol dm}^{-3}$ ) at  $T = 298.15 \text{ K}$  and  $\mu = 0.1 \text{ mol dm}^{-3} \text{ NaCl}$ .

The evolution of the absorbance data with the pH can be used to determine the speciation in solution in the 2-11 range of pH (Figure 9).

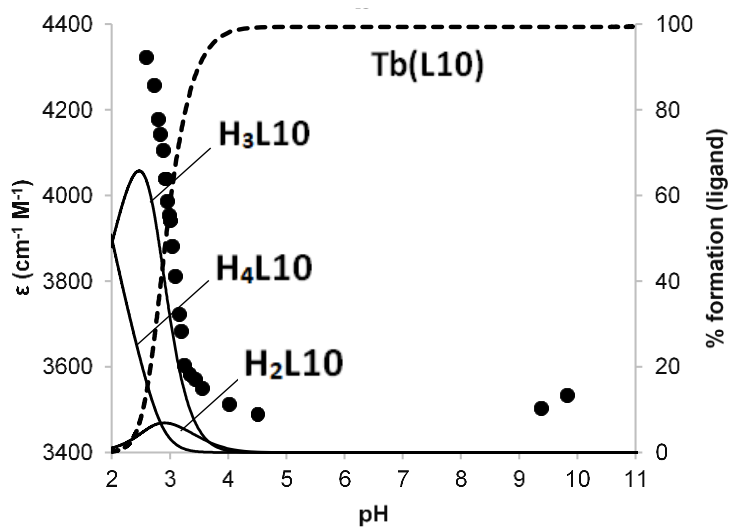
a)



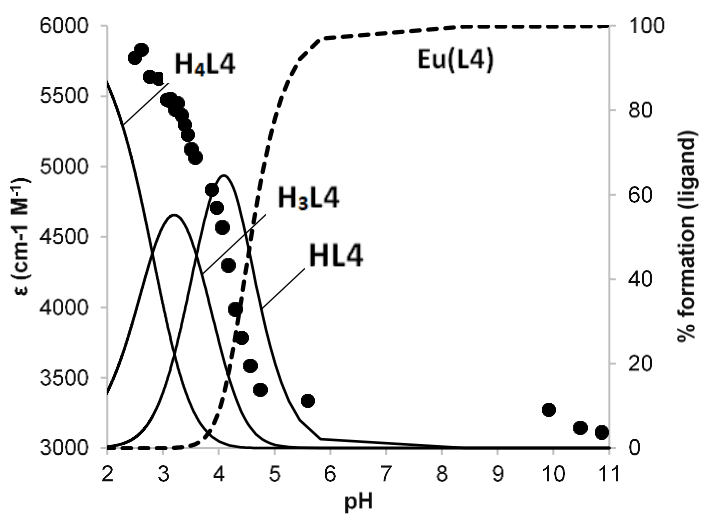
b)



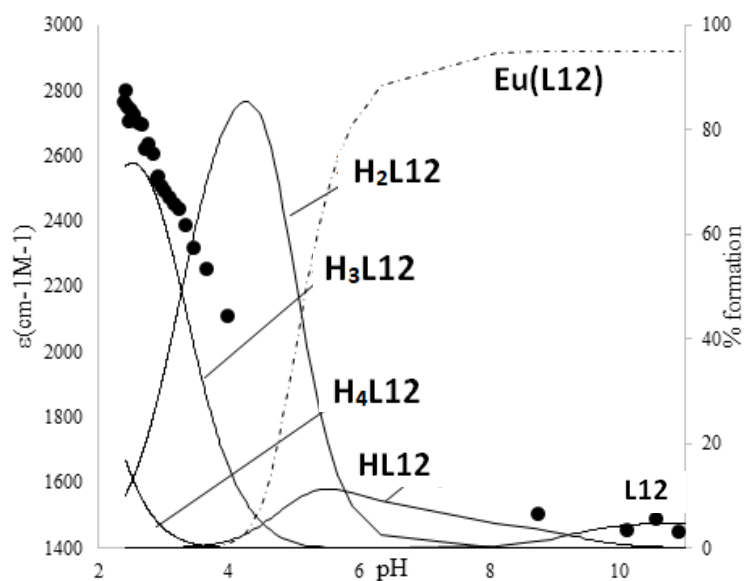
c)



d)



e)



f)

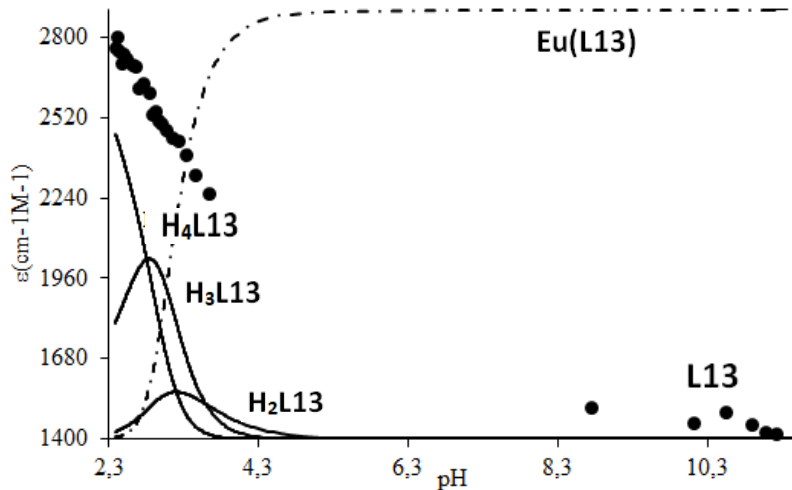


Figure 9. Species distribution of the complexes for the ligands a) L11 (0.08 mM), b) L10 (0.13 mM) c) L10 (0.15 mM), d) L4 (0.09 mM) e) L12 (0.045 mM) and f) L13 (0.09 mM) with Eu(III) (ratio 1:1 M:L, or with Tb(III) in ratio 1:1 M:L, with a little excess of metal), along with the molar absorptance values at  $\lambda=318\text{nm}$  (for the ligands L11 and L4),  $\lambda=265\text{ nm}$  (for ligand L10) and  $\lambda=328\text{nm}$  (for the ligands L12 and L13) obtained by acid-base spectrophotometric titration at  $T = 298.15\text{K}$  and  $\mu = 0.1\text{ M}$ . Charges and negligible species (below 5%) omitted for clarity.

The same plot for the Tb(L10) complexes is very similar to its Eu(III) analogous. (Figure 9 b-c). For all the Eu(III) and Tb(III) complexes reported in Figure 9, the formation of the coordination compound is accompanied by a fast decrease of  $\epsilon_\lambda$ .

The best fit of the data has been obtained when only the ML species was considered; the formation constants obtained for Eu(III) and Tb(III) are reported in Table 3a along with those available for similar ligands (Table 3b, for sake of comparison). According to this model, at pH = 7.4 the ML species is largely predominant in all cases (>99%).

**a)**

Complex	L11	L10	L4	L9 (a)	L12	L13
Eu(III)L	9.97(8)	15.68(1)	12.6(2)	11.2(3)	10.62(2)	15.1(3)
Eu(III)L(OH)	-	-	-	2.2(6)	-	-
Tb(III)L	-	15.70(2)	-	11.4(2)	-	-
Tb(III)L(OH)	-	-	-	2.0(3)	-	-
Gd(III)L	-	-	-	-	-	-
Gd(III)L(OH)	-	-	-	-	-	-

**b)**

Complex	bped <sup>b</sup>	PEDTA <sup>d</sup>	CDTA <sup>d</sup>	HEDTA <sup>c</sup>
Eu(III)L	-	-	19.6	15.4
Eu(III)L(OH)	-	-	-	-
Tb(III)L	-	-	20.0	-
Tb(III)L(OH)	-	-	-	-
Gd(III)L	12.37	15.56	19.6	-
Gd(III)L(OH)	2.1	-	-	-

a) ref.3; b) ref.16,  $\mu = 0.16$  M NaCl; c) HEDTA: *N*-Carboxymethyl-*N'*-(2-hydroxyethyl)-*N,N'* ethylenediglycine, ref. 17; d) ref.18

Table 3. a) Formation constants ( $\log\beta$ ) complexes of the ligands L11, L10, L4, L12 and L13 (with Eu(III) and Tb(III) at  $T = 298.15$  K and  $\mu = 0.1$  M NaCl); b) other similar complexes have been added for comparison. Charges omitted for clarity.

As expected on the basis of the strong oxophilicity of Ln(III) ions<sup>19</sup> the stability constants for the triacetate ligands (L4, L10 and L13) are higher than their diacetate analogues (L11, L9 and L12, respectively). Moreover, the stability constants of the Ln(III) complexes with the quinoline-substituted ligands (L4,

L11) and isoquinoline substituted ligands (L12, L13) are lower than for their pyridine analogues (L10 and L9 respectively). This result could be due to a weaker interaction with the metal ion, in particular in the case of the quinoline complex **Eu(L11)OTf**. This can be related to an increased steric hindrance, due to the size of the heteroaromatic fragment. In the perspective of *in vitro* application experiments, the values of these formation constants appear promising, in particular for triacetate-based ligands (**L10** and **L4**) whose stability is close to that of macrocyclic ligands possessing similar coordination ability and already employed in molecular imaging applications (*i.e.* DO3A derivatives with  $\log\beta$  values in the 18-21 range).<sup>20</sup>

#### 4.2.2.3. *Characterization: UV-visible Absorption and Luminescence*

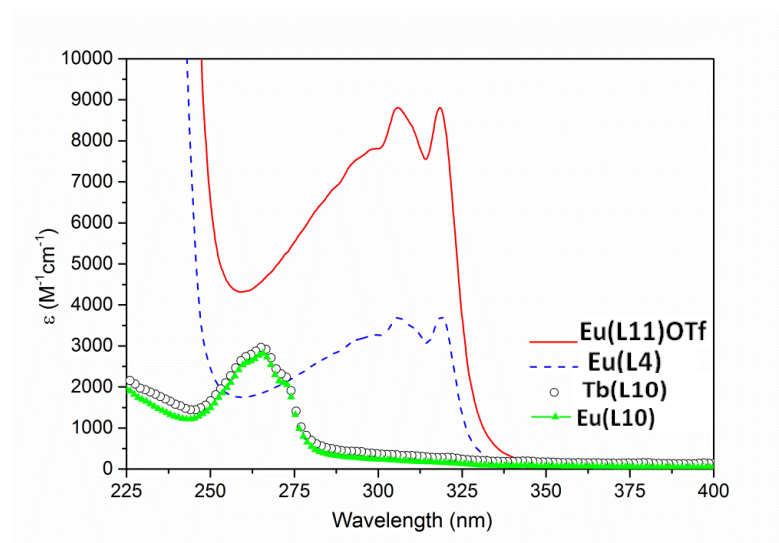
Upon complexation of the ligand with the metal center two main effects could be observed: i) a *hyperchromic effect*, which involves evident enhancements of the molar extinction coefficient ( $\epsilon$ ), and/or ii) a *bathochromic or red shift* towards upper values of maximum absorption wavelength.

In our case, the major part of the Ln-complexes showed both effects, with a higher molar extinction coefficient and red shifted peaks of 3-4 nm respect to the ligand.

The UV-Vis electronic absorption spectra in aqueous solution for complexes **Eu(L11)OTf**, **Eu(L10)**, **Tb(L10)**, and **Eu(L4)** are depicted in Figure 10a, whereas the complexes **Eu(L12)OTf** and **Eu(L13)** are presented in Figure 10b.



a)



b)

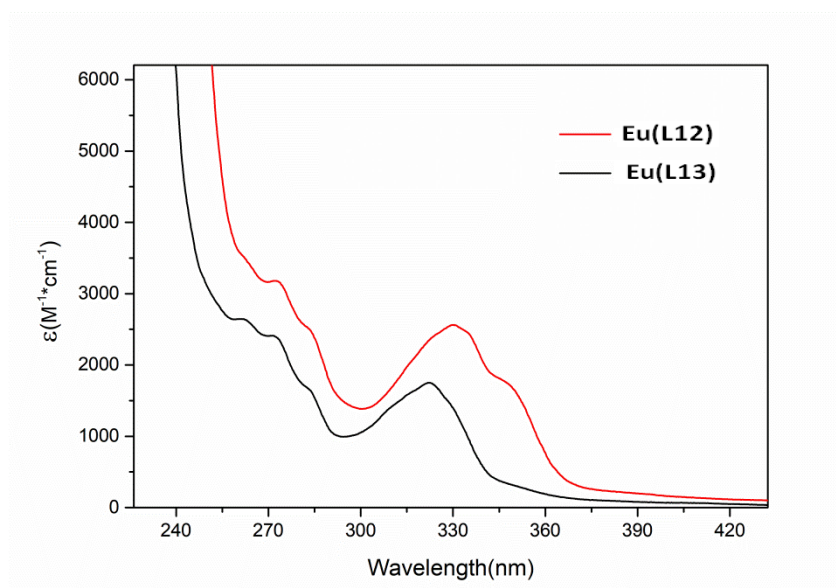


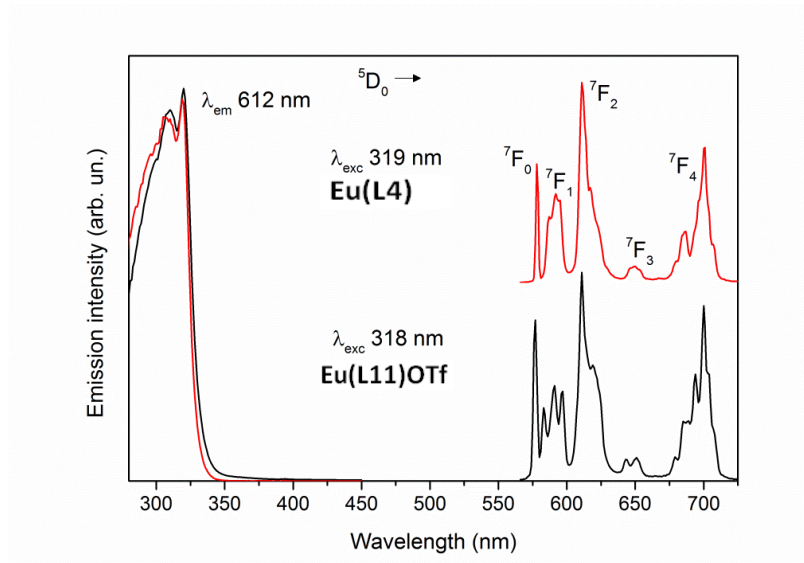
Figure 10. UV-Vis absorption spectra for complexes a) *Eu(L11)OTf*, *Eu(L10)*, *Tb(L10)*, *Eu(L4)* and b) *Eu(L12)OTf*, *Eu(L13)* in water. Charges and water molecules omitted for clarity.

The spectra of the complexes containing the same heteroaromatic antenna [complexes with **L11** or **L4** (quinoline fragment), complexes with **L10** (pyridine fragment)] are superimposable, whereas the complex with **L12** is rather red shifted respect to the complex with **L13**.

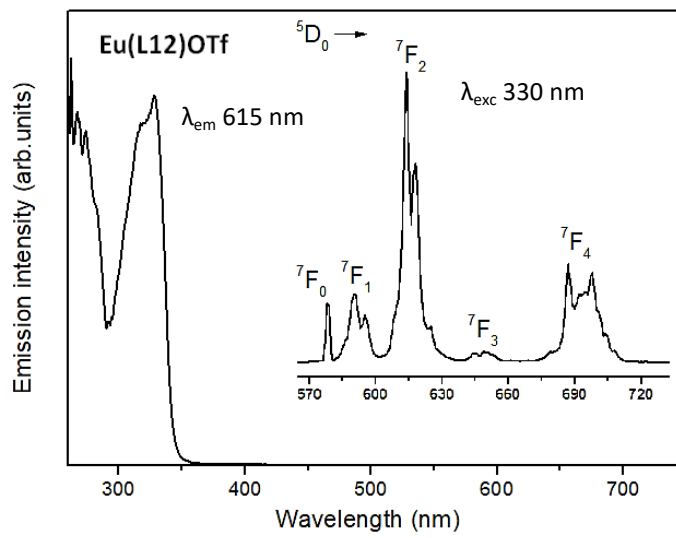
When the number of chromophoric units is different, the main differences concern the values of the molar extinction coefficient ( $\epsilon$ ), as well as observed for complex **Eu(L11)OTf** and **Eu(L4)**, and a red shifted maximum absorption wavelength, such as the case of complex **Eu(L12)OTf** and **Eu(L13)** (Figure 10). For example, the  $\epsilon_{\lambda}$  value of the complex **Eu(L11)OTf** [ $\epsilon_{(318\text{ nm})} = 8800\text{ M}^{-1}\text{cm}^{-1}$ ] is about twice as much as the one of complex **Eu(L4)** [ $\epsilon_{(318\text{ nm})} = 3800\text{ M}^{-1}\text{cm}^{-1}$ ]. Comparing the absorption spectra of the pyridine ones derivatives with the other complexes (Figure 10), it is worth noting that the more extended  $\pi$  electronic cloud gives rise to a red-shift of the main absorption band of the two quinoline complexes **Eu(L11)OTf** and **Eu(L4)**. This phenomenon is even more evident for the isoquinoline derivatives **Eu(L12)OTf** and **Eu(L13)** (Figure 10b).

Excitation spectra of the complexes **Eu(L11)OTf**, **Eu(L10)**, **Eu(L4)** and **Eu(L9)Cl** dissolved in water upon monitoring the  $^5\text{D}_0 \rightarrow ^7\text{F}_2$  transition of Eu(III) ( $\lambda_{\text{em}} = 612\text{-}615\text{ nm}$ ) are shown in the Figures 11 and 12 (left). In the case of Tb(III) complex **Tb(L10)**, the excitation spectrum has been recorded monitoring the  $^5\text{D}_4 \rightarrow ^7\text{F}_5$  transition of Tb(III) ( $\lambda_{\text{em}} = 545\text{ nm}$ , Figure 12). As all the spectra are superimposable with the corresponding absorption ones, an efficient ligand to metal energy transfer mechanism works in all the complexes under investigation. Whereas the pyridine ring is capable to sensitize both Eu(III) and Tb(III) luminescence<sup>3</sup> the quinoline and isoquinoline rings effectively sensitize only Eu(III) ion.

a)



b)



c)

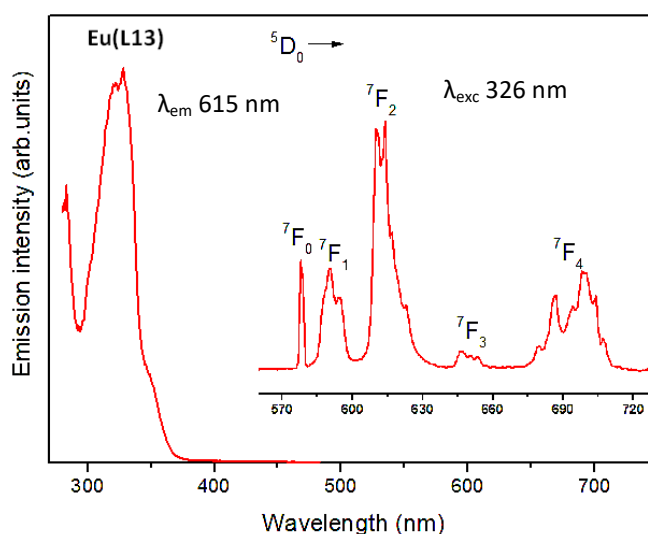


Figure 11. Luminescence excitation spectra (left) and emission spectra (right) of a) Eu(III) complex Eu(L4) and Eu(L11)OTf b) complex Eu(L12)OTf, c) complex Eu(L13), in water solution ( $10^{-4}$  M) at 298 K. Charges and water molecules omitted for clarity.

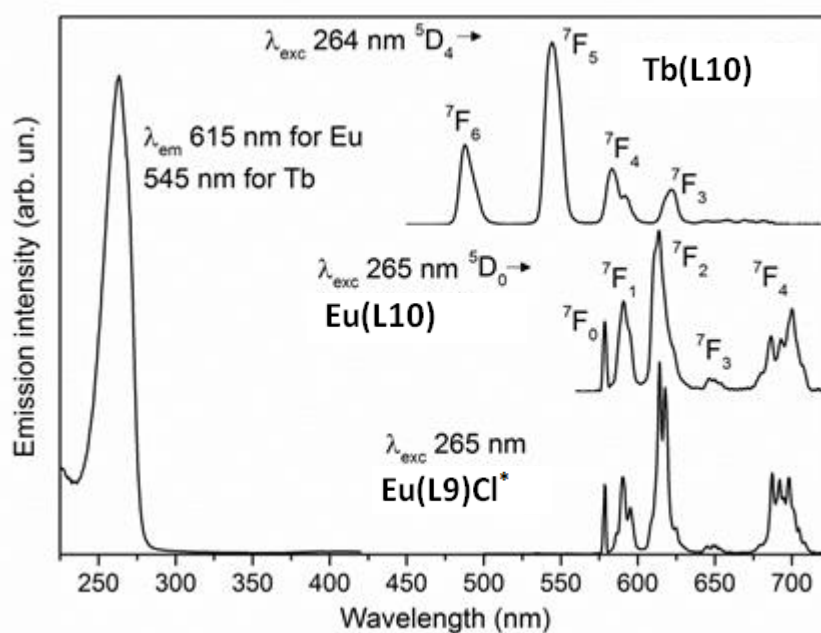


Figure 12. Luminescence excitation spectra (left) and emission spectra (right) of Eu(III) complex Eu(L10) and Eu(L9)Cl and Tb(III) complex Tb(L10) in water solution ( $10^{-4}$  M) at 298 K. \*data from ref.3. Charges and water molecules omitted for clarity.

The luminescence emission spectra depicted on the right of Figures 11 and 12 show the presence of the typical  $f-f$  transitions of the Eu(III) or Tb(III).

Upon excitation of the pyridine ring ( $\lambda_{exc} = 265$  nm) the complexes **Eu(L10)** and **Eu(L9)Cl** showed a visual red luminescence while the complex **Tb(L10)** a green

one. Upon excitation of the quinoline ring ( $\lambda_{exc} = 319$  nm) a red luminescence is detected for the complexes **Eu(L11)OTf** and **Eu(L4)**. Besides the hypersensitive  $^5D_0 \rightarrow ^7F_2$  transition which dominates the spectrum in all the Eu(III) emission spectra, one strong  $^5D_0 \rightarrow ^7F_0$  band is also detected (in particular in the case of quinoline-based complexes). All this is compatible with the presence of emitting species where the point symmetry of Eu(III) deviates from the inversion symmetry and is characterized by an axial character.<sup>21</sup>

The  $C_n$  ( $C_n$  is a  $360^\circ/n$ -fold rotation axis),  $C_{nv}$  (when a plane of symmetry contains the rotational axis) or  $C_s$  (plane of symmetry) are the only possible point symmetry in the presence of sizeable intensity of the  $^5D_0 \rightarrow ^7F_0$  transition.<sup>21</sup>

In our case, the  $C_s$  symmetry can be ruled out due to the presence of the chiral ligand. As far as the luminescence decay curves of the  $^5D_0$  and  $^5D_4$  excited states of Eu(III) and Tb(III) are concerning, all measurements of the complexes under investigation were recorded in aqueous solution. As clearly observed in one of the representative examples reported in Figure 13, all the curves are well fitted by a single exponential function by confirming the existence of a main emitting species in solution.

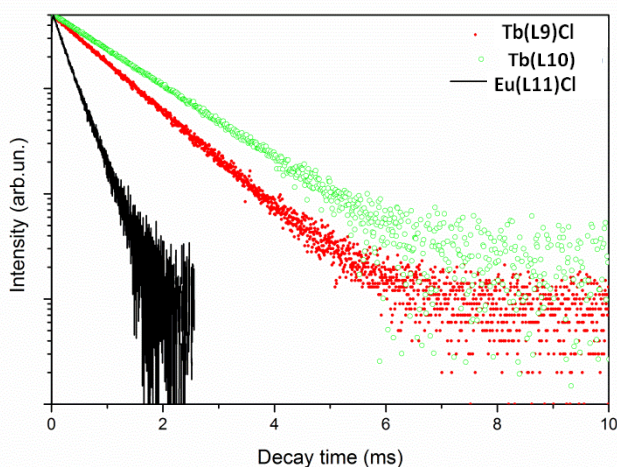


Figure 13. Luminescence decay curves from  $^5D_0$  excited state of Eu(III) in **Eu(L11)Cl** complex ( $\lambda_{exc} = 318$  nm;  $\lambda_{em} = 612$  nm) and from  $^5D_4$  excited state of Tb(III) in **Tb(L9)Cl** and **Tb(L10)** complexes ( $\lambda_{exc} = 265$  nm;  $\lambda_{em} = 543$  nm) in  $H_2O$ . Charges and water molecules omitted for clarity.

The observed lifetimes, in water and deuterium oxide, are summarized in Table 4, together with the values of the hydration number ( $q$ ), the radiative lifetime, the intrinsic and the total quantum yields (already defined in Chapter 1).

Complex	$\tau_{\text{obs}}$		$\tau_{\text{rad}}$	$q$	$\Phi_{\text{Ln}}(\%)$	$\Phi_{\text{Tot}}(\%)$	$\eta_{\text{sens}}(\%)$
	H <sub>2</sub> O	D <sub>2</sub> O					
Eu(L9)Cl	0.30(1)	1.70(1)	3.00 <sup>a</sup>	2.7(1)	10.0 <sup>c</sup>	6.1	61
Eu(L11)Cl	0.29(1)	1.68(1)	3.22 <sup>a</sup>	2.8(1)	9.0 <sup>c</sup>	2.6	29
Eu(L10)	0.33(1)	3.56(1)	3.66 <sup>a</sup>	2.7(1)	9.0 <sup>c</sup>	5.67	63
Eu(L4)	0.33(1)	2.15(1)	3.34 <sup>a</sup>	2.5(1)	9.9 <sup>c</sup>	4.0	40
Tb(L9)Cl	0.94(1)	2.15(1)	5.98 <sup>b</sup>	2.6(5)	15.7 <sup>d</sup>	10.0	64
Tb(L10)	1.16(1)	3.53(1)	6.86 <sup>b</sup>	2.4(5)	16.9 <sup>d</sup>	11.2	66
Eu(L12)OTf	0.28(1)	1.30(1)	3.74	2.7(1)	--	--	--
Eu(L13)	0.29(1)	1.87(1)	4.59	2.8(1)	--	--	--

Table 4. Observed and radiative excited state lifetimes (ms) for Eu(III) and Tb(III) complexes along with the number of water molecules ( $q$ ) obtained from data fitting. Intrinsic ( $\Phi_{\text{Ln}}$ ), total ( $\Phi_{\text{Tot}}$ ) quantum yields and  $\eta_{\text{sens}}$  ( $=\Phi_{\text{Tot}}/\Phi_{\text{Ln}}$ ) are also reported. a) estimated from the analysis of the Eu(III) emission spectra by using the formula reported by Werts et al.<sup>22</sup> b) calculated by  $\tau_{\text{rad}} = \tau_{\text{obs}}/\Phi_{\text{Ln}}$ ;  $\tau_{\text{obs}}$  and  $\Phi_{\text{Ln}}$  have been determined in H<sub>2</sub>O. c) estimated in aqueous solution thanks to the formula  $\tau_{\text{obs}}/\tau_{\text{rad}}$ . d) determined by using the reference standard.

The number of water molecules in the inner coordination sphere of the metal ion in each complex is, in practice, the same (around 2.5).

The intrinsic quantum yield of the lanthanide ion ( $\Phi_{\text{Ln}}$ ), defined by number of emitted/absorbed photons, when lanthanide ions is directly excited, is around 10% and 16% for the Eu(III) and Tb(III) complexes, respectively (Table 4). The higher values of the intrinsic quantum yield for the Tb(III)-based complexes is due to the energy gap between the emitting level and the lower lying ones, that is bigger in the case of Tb(III) so as to limit the multiphonon relaxation process. As already mentioned in chapter 1, for the estimation of  $\eta_{\text{sens}}$  we need to know the total quantum yield ( $\Phi_{\text{Tot}}$ ) is defined by the number of photons emitted by the lanthanide ion/number of photons absorbed by the ligand. Since,  $\Phi_{\text{Tot}} = \eta_{\text{sens}} \cdot \Phi_{\text{Ln}}$ ,  $\eta_{\text{sens}} = \Phi_{\text{Tot}}/\Phi_{\text{Ln}}$ .  $\Phi_{\text{Tot}}$  for all the complexes has been determined by using a reference standard of known quantum yield (quinine bisulfate;  $\Phi = 54.6\%$ ; see experimental section for details).  $\eta_{\text{sens}}$  is in the 60-70% range for Eu(III) and Tb(III) complexes containing the pyridine chromophore, whilst the Eu(III)

complexes containing the quinoline fragment show a significantly lower sensitization efficiency (in particular for Eu(L11)OTf,  $\eta_{\text{sens}} = 29\%$ ). This seems to be related to the longer Y-N<sub>heterocycle</sub> bond distances found by DFT calculations (see below), in the case of quinoline-based complexes. In this context, it is useful to remember that the probability of the energy transfer from an antenna ligand (S = sensitizer) to a metal ion (A = acceptor) is strongly dependent on the S-A distance, for both the most common energy transfer processes taking place in lanthanide-based complexes (dipole-dipole and exchange mechanisms).<sup>23</sup>

In particular, the longer is the distance, the lower is the energy transfer probability and the sensitization efficiency. The seemingly low total quantum yields ( $\Phi_{\text{Tot}}$  in the 3-11% range) must be reassessed in the light of the following statements: *i*) the quantum yield of many lanthanide and d-block compounds used for cellular imaging is in the 4-10% range;<sup>24, 25</sup> *ii*) the total quantum yield of our complexes, is expected to grow upon interaction of the complex with a target analyte thanks to the concomitant displacement of water molecules from the metal ion. For these reasons, we believe that the class of complexes under investigation can be considered a promising family of optical probes for sensing application.

### **4.2.3. Data elaboration and computational models**

#### **4.2.3.1. DFT calculations**

As single crystals suitable for X-ray diffraction experiments was not obtained, all the complexes under investigation (Figure 2) have been studied by means of the density functional theory (DFT) calculations, in order to get the most probable structures in solution. Since the paramagnetic Eu(III) and Tb(III) complexes are rather difficult to model computationally, the analogues of the diamagnetic Y(III) ion have been studied. It has been shown that Y(III) complexes may serve as suitable models for the Eu(III) analogues,<sup>3,26,27,28</sup> in agreement with the fact that for the lanthanide contraction<sup>29</sup> its ionic radius differs from the one of Eu(III) ion by only about 0.05 Å [and less for Tb(III)].

Solvent effects were considered by using the *polarizable continuum model* (PCM). Calculations have been carried out by using either Gaussian 09 or Gaussian 16.<sup>30</sup>

All final geometries were checked in order to get the conformation with the minimal vibrational energy.

The complexes studied were the ones based on the **L11** and **L12** bisacetate ligands. Among the possible coordination geometries, the *cis*-O,O; *cis*-N,N one has been demonstrated to be much less stable, in the case of bpcd, than the other *trans* -O,O and *trans* -N<sub>Py</sub>,N<sub>Py</sub> geometries (Figure 14).<sup>3</sup> For this reason, we have taken into account only these more stable coordination modes, also in the case of **L11** and **L12** ligands.

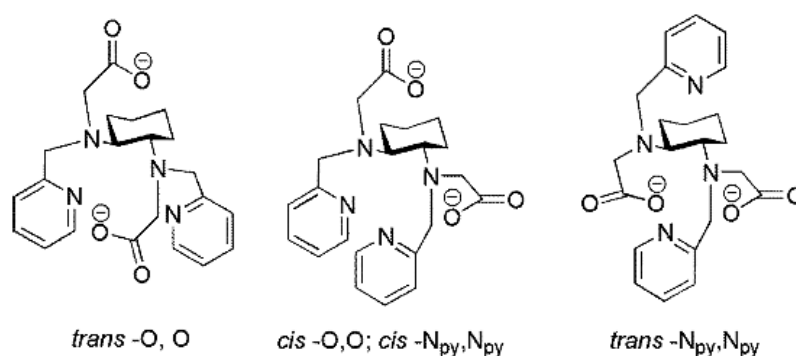


Figure 14. Hypothetical Coordination Geometries of  $L9^{2-}$

When five water molecules have been considered at the beginning of the calculation, only *two* of them were retained in the first coordination sphere of the metal ion at the end.

Also in the case of the complexes with the triacetate ligands:  $[Y(L10)(H_2O)_2]$ ,  $[Y(L4)(H_2O)_2]$  and  $[Y(L13)(H_2O)_2]$ , only *two water molecules* are bound to the metal ion at the end of the calculation. Therefore, the more stable coordination geometries are reported in Figure 15.



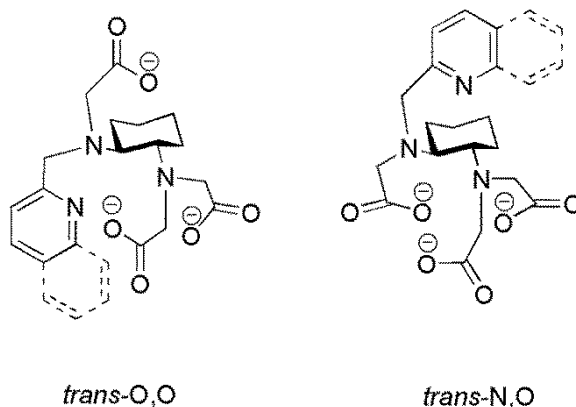
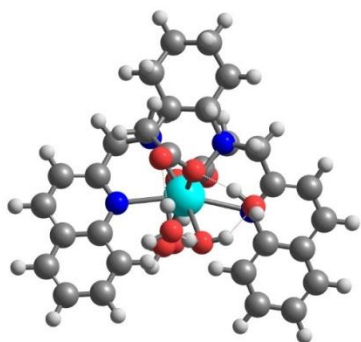


Figure 15. The more stable coordination geometries of  $L10^{3-}$  and  $L4^{3-}$  ligands (same conclusion apply also for the ligand  $L13^{3-}$ ).

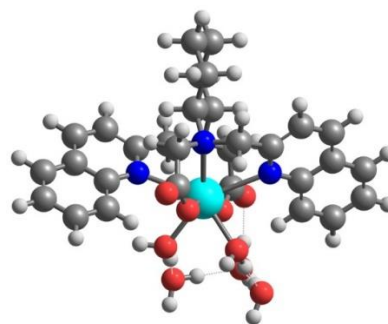
As well as observed for the Ln-complexes based on bpcd as ligand,<sup>3</sup> the number of water molecules (2) revealed by the DFT calculation are in partial agreement with the ones calculated by luminescence spectroscopy (around 2.5, see above). In this context, this discrepancy is not so dramatic, although the Horrock's equation, used for the calculation of the hydration number  $q$ , is also a little bit sensitive to water molecules in the second coordination sphere.<sup>31</sup>

Finally, in Figure 16, we report the minimum energy structures of **L11**, **L10** and **L4** based Y(III) complexes. Each complex structure shows a 8-fold coordination at the metal center due to the presence of a 6-fold coordinating ligand and two water molecules.

a)



b)



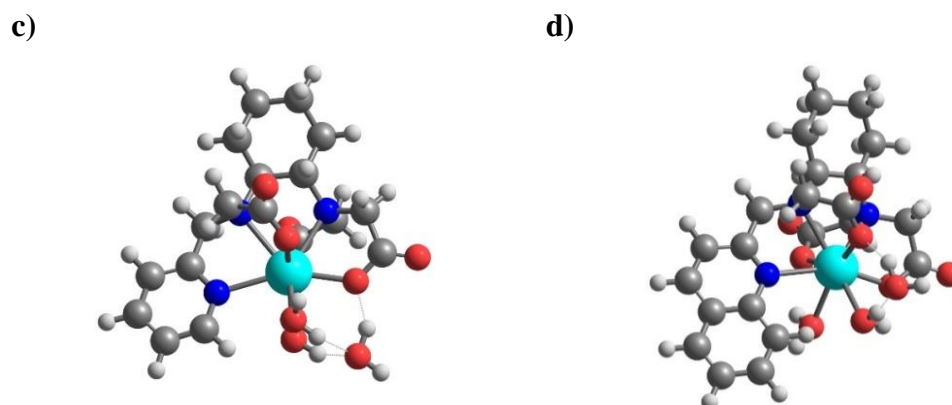
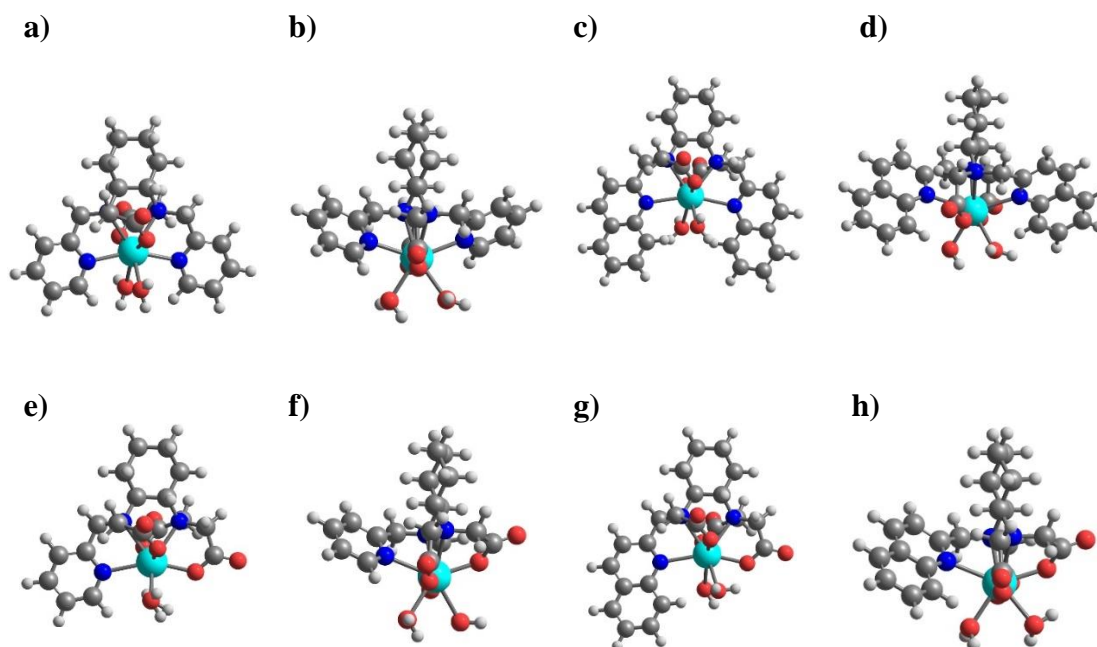


Figure 16. Minimum energy structures of (a)  $[Y(\text{trans-O,O-L11})(\text{H}_2\text{O})_5]^+$ ; (b)  $[Y(\text{trans-N,N-L11})(\text{H}_2\text{O})_5]^+$ ; (c)  $[Y(\text{trans-O,O-L10})(\text{H}_2\text{O})_3]$ ; (d)  $[Y(\text{trans-O,O-L4})(\text{H}_2\text{O})_3]$ . Labels: blue= nitrogen atom; red=oxigen atom; light blue= yttrium atom; white=hydrogen atom; grey=carbon atom.

The increase of steric crowding when passing from pyridine - substituted ligands can be clearly seen in Figure 17 (c-d and g-h respectively for the **L11** and **L4** derivatives) where the C-H bond(s) in position 8 of the quinoline ring point(s) towards the metal center cavity.



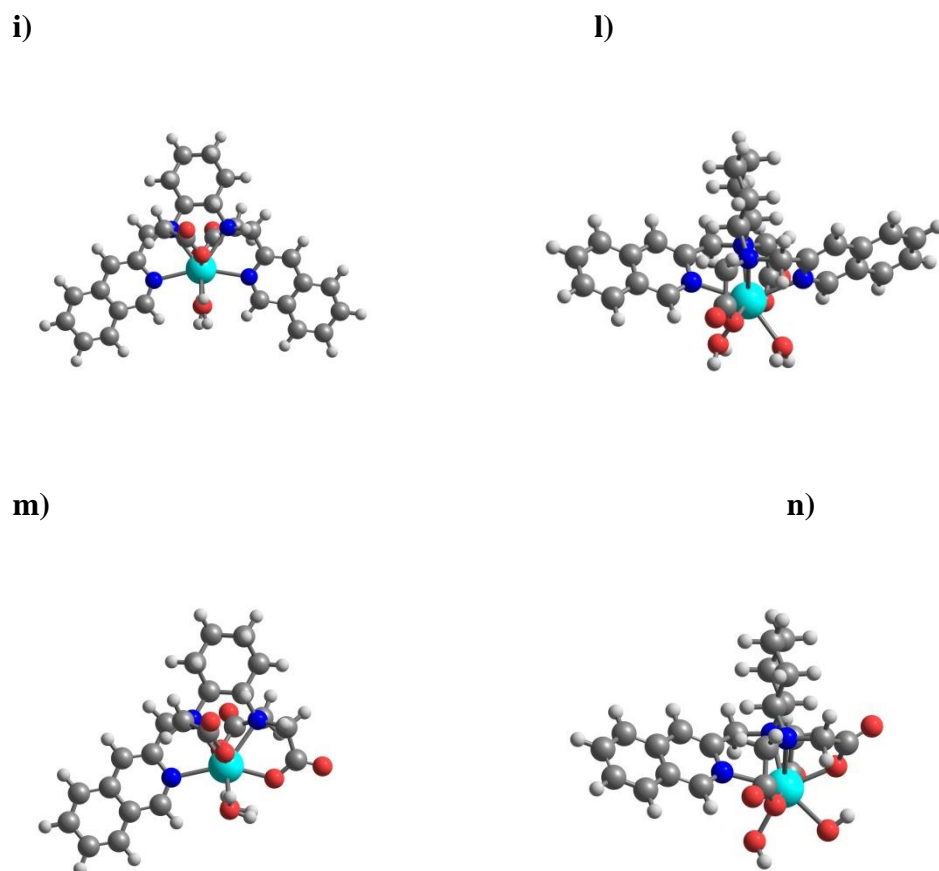


Figure 17. Minimum energy structures of (a)  $[Y(\text{trans-O,O-L9})(\text{H}_2\text{O})_2]^+$ ; (b)  $[Y(\text{trans-N,N-L9})(\text{H}_2\text{O})_2]^+$ ; (c)  $[Y(\text{trans-O,O-L11})(\text{H}_2\text{O})_2]^+$ ; (d)  $[Y(\text{trans-N,N-L11})(\text{H}_2\text{O})_2]^+$ ; (e)  $[Y(\text{trans-O,O-L10})(\text{H}_2\text{O})_2]$ ; (f)  $[Y(\text{trans-N,O-L10})(\text{H}_2\text{O})_2]$ ; (g)  $[Y(\text{trans-O,O-L4})(\text{H}_2\text{O})_2]$ ; (h)  $[Y(\text{trans-N,O-L4})(\text{H}_2\text{O})_2]$ ; (i)  $[Y(\text{trans-O,O-L12})(\text{H}_2\text{O})_2]^+$ ; (l)  $[Y(\text{trans-N,N-L12})(\text{H}_2\text{O})_2]^+$ ; (m)  $[Y(\text{trans-O,O-L13})(\text{H}_2\text{O})_2]$ ; (n)  $[Y(\text{trans-N,O-L13})(\text{H}_2\text{O})_2]$ . Labels: blue= nitrogen atom; red=oxigen atom; light blue= yttrium atom; white=hydrogen atom; grey=carbon atom.

From the inspection of the obtained bond distances (Table 5) it is clearly evident that the substitution of pyridine by quinoline or isoquinoline has nearly no effect on the Y(III)-O<sub>acetate</sub> bonds and Y(III)-N<sub>amine</sub> distances.

The Y(III)-O<sub>water</sub> bonds are slightly longer in the pyridine triacids (2.539 Å) as it could be justified by the lower charge on the metal ion, while in the quinoline and isoquinoline complexes they are only slightly affected.

On the other hand, the aforementioned steric hindrance at the metal ion in the case of bulky quinoline ring could be responsible for the lengthening of the Y(III)-N<sub>heterocycle</sub> bond, which increases significantly when Py is replaced by

quinoline ( $\Delta\text{Py}\rightarrow\text{Q} \sim +0.11 \text{ \AA}$ ). This indicates the weaker interaction of the quinoline with respect to pyridine ligands with the metal ion.

This evidence should contribute to the loss of stability of the quinoline complexes respect to the pyridine analogues (an average difference of  $\sim 1.4$  and  $3.4$  log units for the di and tri-acetate ligands). The isoquinoline complexes possess a stability which is in the middle between the one of Py and quinoline complexes. It is expected that quinoline has also a notable impact on the solvation properties of the complex which often have a strong influence on the stability.

Complex	Y-O <sub>acetate</sub>	Y-N <sub>amine</sub>	Y-N <sub>heterocycle</sub>	Y-O <sub>water</sub>
[Y( <i>trans</i> -O,O L9)(H <sub>2</sub> O) <sub>2</sub> ] <sup>+</sup>	2.262	2.550	2.525	2.448
[Y( <i>trans</i> -N,N L9)(H <sub>2</sub> O) <sub>2</sub> ] <sup>+</sup>	2.292	2.610	2.503	2.492
[Y( <i>trans</i> -O,O L11)(H <sub>2</sub> O) <sub>2</sub> ] <sup>+</sup>	2.268	2.557	2.661	2.464
[Y( <i>trans</i> -N,N L11)(H <sub>2</sub> O) <sub>2</sub> ] <sup>+</sup>	2.284	2.567	2.594	2.482
[Y( <i>trans</i> -O,O L10)(H <sub>2</sub> O) <sub>2</sub> ]	2.286	2.568	2.550	2.474
[Y( <i>trans</i> -N,O L10)(H <sub>2</sub> O) <sub>2</sub> ]	2.300	2.595	2.546	2.539
[Y( <i>trans</i> -O,O L4)(H <sub>2</sub> O) <sub>2</sub> ]	2.286	2.574	2.654	2.458
[Y( <i>trans</i> -N,O L4)(H <sub>2</sub> O) <sub>2</sub> ]	2.290	2.576	2.642	2.478
[Y( <i>trans</i> -O,O L12)(H <sub>2</sub> O) <sub>2</sub> ] <sup>+</sup>	2.262	2.577	2.526	2.451
[Y( <i>trans</i> -N,N L12)(H <sub>2</sub> O) <sub>2</sub> ] <sup>+</sup>	2.283	2.565	2.614	2.463
[Y( <i>trans</i> -O,O L13)(H <sub>2</sub> O) <sub>2</sub> ]	2.259	2.554	2.525	2.505
[Y( <i>trans</i> -N,O L13)(H <sub>2</sub> O) <sub>2</sub> ]	2.262	2.578	2.548	2.508

**Table 5** Selected bond distances ( $\text{\AA}$ ) of the complexes in Figure 17.

#### 4.2.3.2. *cEST and Solverstat*

Equilibrium speciation tool (cEST)<sup>32</sup> is an Excel add-in for the simulation of chemical equilibria in solution. This statistical software calculates the concentrations in equilibrium of species in non-aqueous and aqueous systems. It is exploited for complexation, acid-base, redox and solubility equilibria. The computational models obtained with cEST are effectively used for homogeneous or heterogeneous equilibrium systems.<sup>33, 34</sup>

Also, SolverStat<sup>35</sup> is an Excel add-in that performs advanced statistical tests on least squares regression data, and in the present PhD thesis it was employed for

the fitting of the formation constants of some Ln(III) complexes with the bioanalytes under investigation.

The optimization of the data has been performed by minimizing the sum of the squares differences between the experimental and the calculated data. In order to decide the most reliable model, some statistic parameters have been taken into account; the best model for each system should present the lowest confidence interval (obtained from the standard deviation of the refined constants, 95% confidence) and Akaike Information Criteria Corrected (AICc).<sup>36</sup>

The AICc parameter is a correction of the AIC parameter for populations  $<10$ , and is based on the least-squares approach.

### 4.3. *Sensing of $\text{HCO}_3^-$ : the screening in cuvette with Ln-complexes based on Pyridine and Quinoline rings*

#### 4.3.1. *Introduction*

The bicarbonate ion plays a crucial role in several cellular processes, including pH homeostasis, kidney function and sperm maturation. In this context, an abnormal decrease of the  $\text{HCO}_3^-$  anion is the cause of the metabolic acidosis. Patients with chronic kidney disease due to metabolic acidosis show low serum bicarbonate concentrations.<sup>37,38</sup>

Moreover, the knowledge of the concentration and distribution of  $\text{HCO}_3^-$  is fundamental for understanding the control of many biological processes such as cyclic-AMP regulation, through reversible binding to a soluble adenylyl cyclase enzyme.

Moreover, the mis-expression (def. Incorrect expression of a gene) of carbonic anhydrase (CA) is associated with a variety of tumour types. CA-II deficiency syndrome in humans can give rise to renal tubular acidosis, osteoporosis and mental retardation.<sup>2</sup>

The necessity of a new method to detect the bicarbonate ion is due to the limitations of the current methods mostly relying on gross measurement of  $\text{H}^{14}\text{CO}_3^-$  uptake or the intracellular pH, which can be subject to systematic error.

### 4.3.2. *Ln(III)-complexes-HCO<sub>3</sub><sup>-</sup> adducts: luminescence and affinity constants*

The increasing addition of the analyte to one of the Ln-complex under investigation **Eu(L10)** (Figure 2) gives rise to a consistent enhance of the luminescence intensity, in particular the intensity band of the transition  ${}^5D_0 \rightarrow {}^7F_2$  (Figure 18).

It is reasonable to assume that  $\text{HCO}_3^-$  anion coordinates the Eu(III) ion, displacing the quenchers water molecules from the inner coordination sphere. Besides to this effect, a concomitant decrease of the transition  ${}^5D_0 \rightarrow {}^7F_0$  has been detected, resulting in a minor axial geometry of the Eu(III) environment. Upon coordination to Eu(III), the  $\text{HCO}_3^-$  anion is capable to increase the degree of the asymmetry around the metal ion, as ruled by the increase of the *asymmetry ratio R* (Chapter 3).

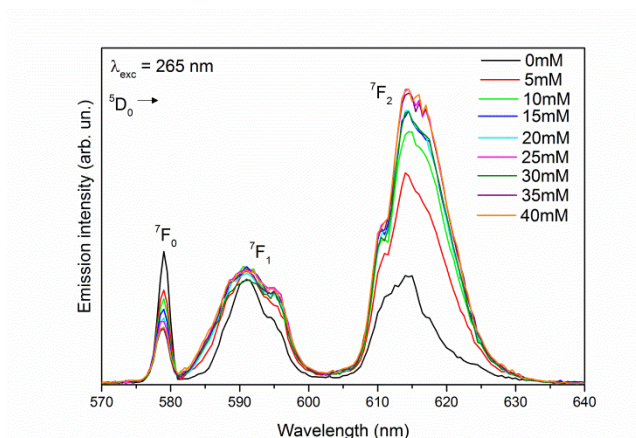


Figure 18. *Eu(III) luminescence emission spectra of the complex Eu(L10) (limited to 570-640 nm range) upon addition of bicarbonate ion. The concentration of the anion is reported. MOPS-buffered solution (pH 7.4)*

Actually, all the Eu(III) complexes under investigation (Figure 19) showed increasing value of *R*, during the titration with bicarbonate ion.<sup>39</sup>

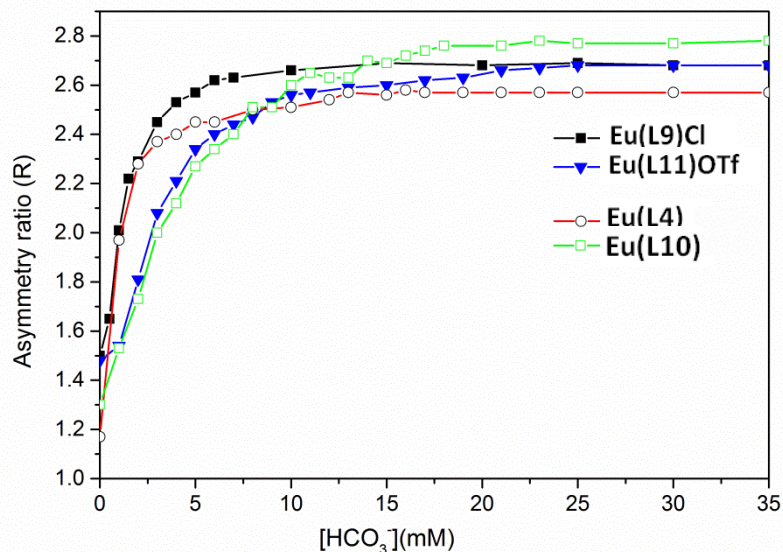


Figure 19. Asymmetry ratio ( $R$ ) for the Eu(III) complexes vs.  $[\text{HCO}_3^-]$  concentration plots. MOPS-buffered solution (pH 7.4).

In all cases, a logarithmic-like trend is observed, and an asymptote is reached after the addition of 10 mM of anion for Eu(III) complex with **L9** ligand (Figure 19). On the other hand, the asymptotic value is reached only after the addition of hydrogen carbonate at 15-20 mM, in the case of all the other complexes [Eu(L11)OTf, Eu(L10) and Eu(L4)]. The sensitivity of the optical response to the  $\text{HCO}_3^-$  concentration can be qualitatively evaluated by analyzing the slope of the graph in the range of biological interest where the hydrogen carbonate concentration is related to serious metabolic acidosis (0-10 mM). As can be seen in Figure 19, **Eu(L9)Cl** and **Eu(L4)** complexes show the best sensitivity. The binding interactions between hydrogen carbonate and the Eu(III) complexes were studied using the Benesi-Hildebrand equation adapted to the values of the asymmetry ratio, as described in the experimental section. Since, there is linearity in the plot of  $R_0/(R - R_0)$  vs.  $[\text{HCO}_3^-]^{-2}$  for Eu(L9)Cl and Eu(L11)OTf (Figure 20 and 21) and in the plot of  $R_0/(R - R_0)$  vs.  $[\text{HCO}_3^-]^{-1}$  for Eu(L10) and Eu(L4) (Figure 22), the stoichiometry of the hydrogen carbonate adducts is 1:1 for Eu(L10) and Eu(L4) complexes and 1:2 for Eu(L9)Cl and Eu(L11)OTf ones.

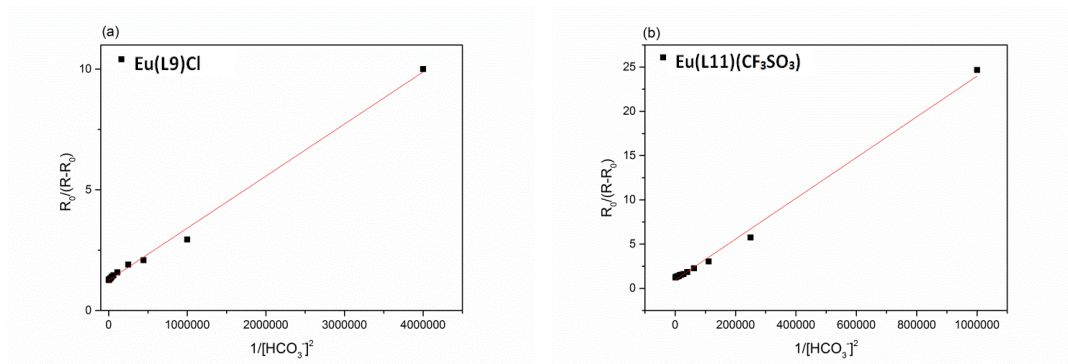


Figure 20. Benesi–Hildebrand plot vs  $[\text{HCO}_3^-]^2$  ( $M^{-2}$ ) for (a)  $[\text{Eu}(\text{L9})]^+$  and (b)  $[\text{Eu}(\text{L11})]^+$  complexes.  $R_0$  is the asymmetry ratio of the starting complex;  $R$  is the asymmetry ratio after each addition of the analyte.  $R$  and  $R_0$  have been calculated from the relative Eu(III) luminescence emission spectrum.

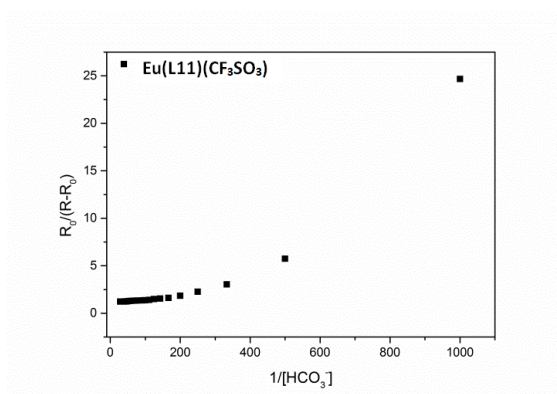


Figure 21. Benesi–Hildebrand plot of  $R_0/(R-R_0)$  vs  $[\text{HCO}_3^-]$  in the case of  $[\text{Eu}(\text{L11})]^+$  complex: the non-linear trend points out that the stoichiometry of the probe/ $\text{HCO}_3^-$  adduct is different from 1:1.

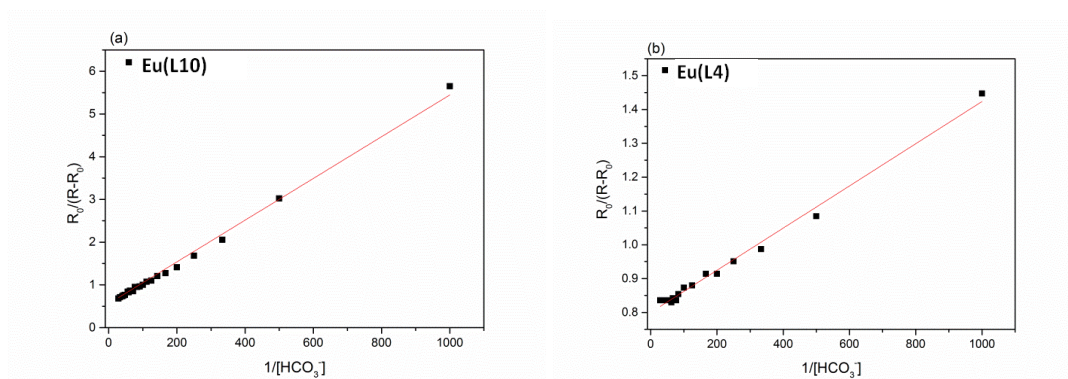


Figure 22. Benesi–Hildebrand plot vs  $[\text{HCO}_3^-]^{-1}$  ( $M^1$ ) for (a)  $\text{Eu}(\text{L10})$  and (b)  $\text{Eu}(\text{L4})$  complexes.  $R_0$  is the asymmetry ratio of the starting complex;  $R$  is the asymmetry ratio after each addition of the analyte.  $R$  and  $R_0$  have been calculated from the relative Eu(III) luminescence emission spectrum.



The *apparent* (*def.* conditions dependent) affinity constants  $\log(K)$  calculated by the intercept/slope ratio of the Benesi-Hildebrand equations are summarized in Table 6.

<b>Complex</b>	<b><i>n</i></b>	<b>log<i>K</i></b>
Eu(L9)Cl/Tb(L9)Cl	2	5.76(8)/5.94(8)
Eu(L11)(CF <sub>3</sub> SO <sub>3</sub> )	2	4.62(8)
Eu(L10)	1	2.06(8)
Eu(L4)	1	3.11(8)

Table 6. Apparent affinity constants ( $\log K$ ) constant for the formation of the adducts with bicarbonate ( $\text{HCO}_3^-$ ),  $[\text{complex}] + n\text{-bicarbonate} \rightleftharpoons [\text{complex}(\text{bicarbonate})_n]$  ( $T = 298 \text{ K}$ ,  $\text{pH } 7.40 (\pm 0.05)$ ,  $I = 0.1 \text{ M NaCl}$ ,  $40 \mu\text{M complex}$ ), determined through fluorimetric titration. Charges omitted for clarity

Since the affinity of the anion for the Ln(III) centre is mainly determined by coulombic attraction it is not surprising that the cationic complexes Eu(L9)Cl and Eu(L11)OTf can coordinate the hydrogen carbonate anion with high affinity constants. To the best of our knowledge, a value of  $\log K$  higher than 4, in the case of hydrogen carbonate ion, is unprecedented in the literature and this is probably related to the unusual number of target anions bound to the metal center. The Eu(III) in these complexes can bind up to 2 hydrogen carbonate units. This could be mainly due, as discussed in the introduction, to the lower number of donating atoms in the ligand (6-fold coordination) than in the case of ligands commonly employed for Ln(III)-based luminescence anion sensing (NOTA and DOTA-like possessing 7-fold coordination). Two possible structures of the 1:2 hydrogen carbonate adducts, differing by the bicarbonate coordination, have been investigated (Figure 23). The *bis*-monodentate hydrogen carbonate seems to be the only possible isomer being  $10.3 \text{ kcal mole}^{-1}$  more stable than the *bis*-bidentate one (also the latter presents an imaginary vibrational mode corresponding to the opening of two Y-O bonds). The optimization of the 1:2 adduct with both hydrogen carbonate coordination modes (one bi- and one mono-dentate) led always to a *bis*-monodentate structure.

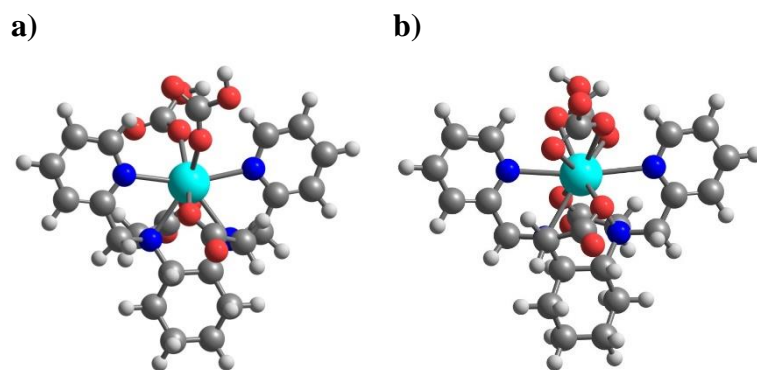


Figure 23. Minimum energy structures of the  $[Y(\text{trans-O,O-L9})(\text{HCO}_3)_2]^-$  complexes obtained in PCM water with a) bis-monodentate and b) bis-bidentate hydrogen carbonate coordination modes. Labels: blue= nitrogen atom; red=oxygen atom; light blue= yttrium atom; white=hydrogen atom; grey=carbon atom.

Due to the neutral charge of Eu(L10) and Eu(L4) complexes, it is not surprising to find in their adducts with hydrogen carbonate a lower binding constants and a 1:1 stoichiometry. It is also reasonable to assume that the negative charge of the 1:1 adduct hampers the formation of the bis-anionic 1:2 species. Furthermore, it is worth to be underlined that the presence of the quinoline ring affects the stability of the adduct with hydrogen carbonate. In the case of cationic complexes, the adduct with quinoline is less stable than the one with pyridine. On the contrary, an opposite trend is observed for the neutral complexes. The reasons of such behavior in the case of the diacid ligand could be found in the high steric hindrance of the heteroaromatic ring which, at least for the *trans*-O,O-L11 isomer (Figure 17c), presents two hydrogen atoms pointing towards the inner coordination sphere, thus likely to hinder the coordination of hydrogen carbonate and maybe giving rise to an affinity constant one order of magnitude lower than for the pyridine-based analog. Here, we demonstrate how, thanks to a modulation of the steric hindrance at the metal ion using Ln(III)-complexes (Ln=Eu,Tb) based on Pyridine and Quinoline rings, it is possible to tune the affinity (and the selectivity) of the complexes towards  $\text{HCO}_3^-$ .

As far as the affinity of the analogous Tb(III) complexes towards bicarbonate is concerned, we expect a behavior similar to the one observed for Eu(III) derivatives, since Eu(III) and Tb(III) complexes are often isostructural due to the similarity of their ionic radii.<sup>19</sup> As expected, the calculated affinity constant for

Tb(L9)Cl complex, chosen as representative example, is similar to the one of Eu(L9)Cl (Table 6 and Figure 24).

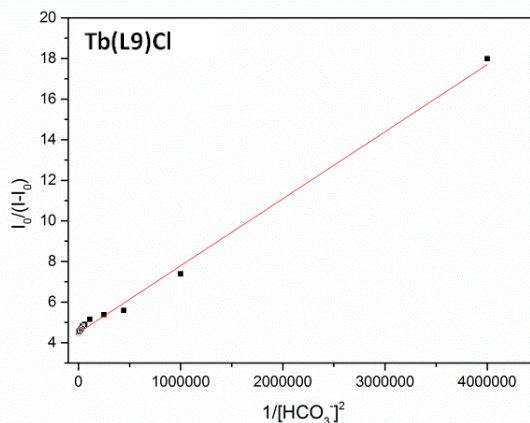


Figure 24. Benesi–Hildebrand plot vs  $[\text{HCO}_3^-]^{-2}$  ( $\text{M}^{-2}$ ) for the  $[\text{Tb}(\text{L9})]^+$  complex.  $I_0$  is the emission intensity at 546 nm of the starting complex;  $I$  is the emission intensity at 546 nm after each addition of the analyte.

#### 4.3.3. Conclusions: general remarks on Bicarbonate ion

The most efficient and selective optical probes for hydrogen carbonate, capable to detect this anion in *cellulo* or in extracellular fluid, are based on charged and neutral Eu(III) and Tb(III) complexes of heptadentate ligands.<sup>40–43</sup>

The cationic  $\text{Ln}(\text{L9})^+$  and  $\text{Ln}(\text{L11})^+$  complexes, and the neutral  $\text{Ln}(\text{L10})$  and  $\text{Ln}(\text{L4})$  ones are highly stable in aqueous solution ( $9.97 < \log \beta < 15.68$ ) and they exist as a couple of isomeric compounds differing by the ligand stereochemistry (*trans*-N,N and *trans*-O,O for  $\text{L9}^{2-}$  and  $\text{L11}^{2-}$ ; *trans*-O,O and *trans*-N,O for  $\text{L10}^{3-}$  and  $\text{L4}^{3-}$ ).

The efficient antenna effect observed for both derivatives of Quinoline [ $\text{Eu}(\text{L11})\text{OTf}$ ,  $\text{Eu}(\text{L4})$ ] and Pyridine rings [ $\text{Ln}(\text{L9})\text{Cl}$ ,  $\text{Ln}(\text{L10})$ ,  $\text{Ln}=\text{Eu}^{3+}$ ,  $\text{Tb}^{3+}$ ] could be exploited for promising application in the detection of bicarbonate concentration in physiologic solution.

The unprecedented affinity towards this anion, found for  $\text{Eu}(\text{L9})^+$  and  $\text{Eu}(\text{L11})^+$  ( $\log K$  5.76 and 4.62, respectively) candidates these molecules for the detection of the bicarbonate ion also in the presence of competitive species, typical of a real biological sample, where the measurement of the  $\text{HCO}_3^-$  concentration is critical in assessing metabolic acidosis. In this context, since both the enantiomers of the

analog Tb(L9)Cl weakly interact with L-lactate ( $\log K = 1.3 - 1.45$ ),<sup>26</sup> a strong selectivity for hydrogen carbonate is expected in a solution containing both analytes.

As far as the Isoquinoline derivatives are concerned, their application for signaling the target ion will be widely discussed in Chapter 5.

#### 4.4. ***Sensing of Serum albumin (BSA): the screening in cuvette with Ln-complexes based on Pyridine and Isoquinoline rings (1R, 2R)***

##### 4.4.1. ***Introduction***

One of the most important proteins type in biological fluids belong to the family of serum albumins, which represent 52% of the protein composition in the circulatory system. They play many physiological and pharmacological functions.<sup>44</sup> Moreover, these proteins have the peculiar properties to bind a wide variety of hydrophobic ligands such as fatty acids, bilirubin, drugs, steroids, anaesthetics and several dyes.<sup>45-47</sup>

They possess a limited number of binding sites with high specificity<sup>48</sup> which confers a crucial role in the transport and deposition of a variety of endogenous and exogenous substances in the blood.<sup>49</sup>

Human serum albumin (HSA) and Bovine serum albumin (BSA) are the most extensively studied serum albumins, and they are classified as homologous proteins.<sup>50</sup> Human serum albumin (HSA) is the most important and wide constituent of the human blood plasma and works as a protein storage component. Changes of the albumin levels in blood could be induced by several disorders, including liver disease, neoplasia, nephrotic syndrome, severe dehydration and more.

It is therefore important in clinical diagnosis to design an analytical method for the quantification of these proteins. Serum albumin has previously been shown to bind to lanthanide complexes<sup>50-52</sup> and often, as a consequence of the interaction, significant changes of the Eu(III) and Tb(III) luminescence emission features<sup>43, 53-56</sup> as well as of the protein fluorescence<sup>57-61</sup> have been observed. Such evidences

offer the possibility to detect these proteins by means of optical spectroscopy techniques.

In the present PhD thesis, the interaction of two water soluble Eu(III) luminescent complexes towards BSA has been deeply investigated by means of optical spectroscopy, and the binding constants of the adducts in aqueous solution have been obtained. In addition, the docking calculations have been also performed to get structural details on the complex-protein species.

As far as the coordination chemistry of the complexes under investigation is concerned, the two probes are quite similar but differ in the nature of the heteroaromatic antenna (pyridine vs isoquinoline; Figure 25).

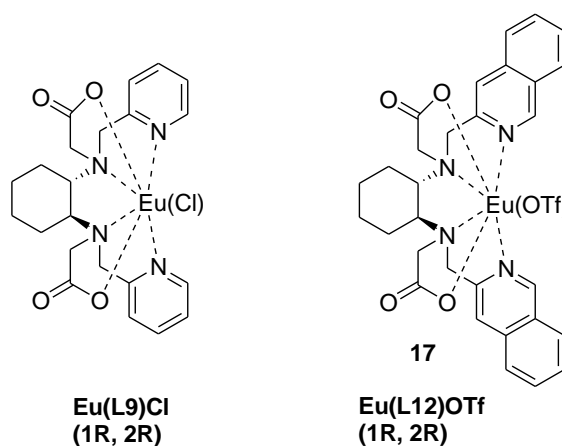
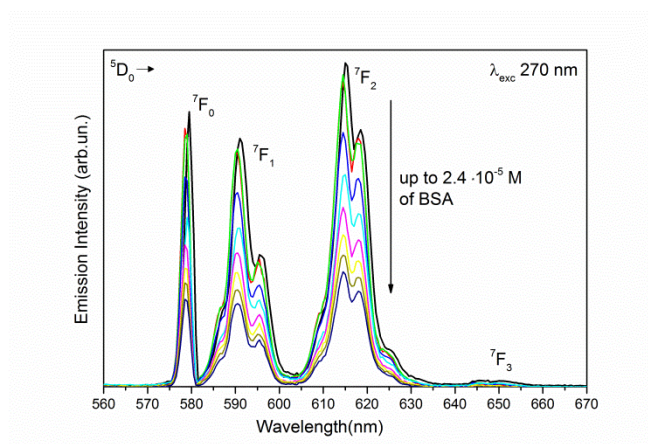


Figure 25. Molecular structure of the Eu(III) complexes for BSA detection

#### 4.4.2. Luminescence: evolution of the emission spectra during the titration

Upon titration of the Eu(III) complexes with BSA, two opposite trends have been obtained: in the case of Eu(L9)Cl a gradual decrease of the Eu(III) luminescence intensity is observed; on the other hand, a noticeable enhancement of the lanthanide emission has been observed for Eu(L12)OTf (Figure 26).

(a)



(b)

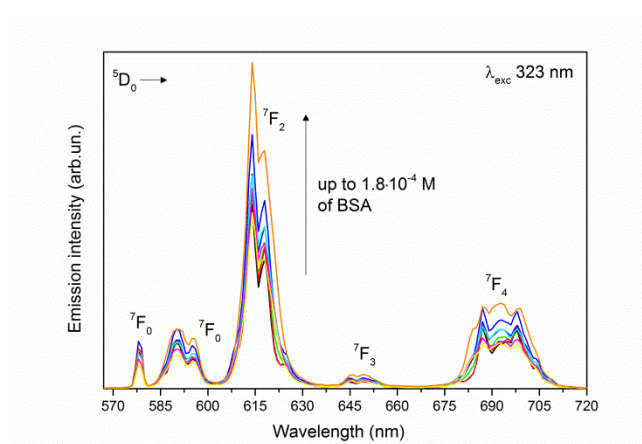


Figure 26. Evolution of the Eu(III) luminescence emission of (a) Eu(L9)Cl complex (80  $\mu\text{M}$ ) in MOPS-buffered solution (pH 7.4) upon addition of BSA in the  $0\text{-}2.4 \cdot 10^{-5}$  M concentration range and (b) Eu(L12)OTf complex (80  $\mu\text{M}$ ) upon addition of BSA in the  $0\text{-}1.8 \cdot 10^{-4}$  M concentration range, at 298 K.

The relative binding constants Eu(III) complexes-protein have been determined through cEST/Solverstat program reported in Table 7.

Complex-BSA	$n$	Log( $K$ )
Eu(L12)OTf	1	$4.03 \pm 0.74$ (0.07%)
Eu(L9)Cl	1	$2.88 \pm 0.58$ (5.08%)

Table 7. Apparent affinity constants ( $\log K$ ) constant for the formation of the adducts with BSA:  $[\text{complex}] + n \cdot \text{BSA} \rightleftharpoons [\text{complex}(\text{BSA})_n]$  ( $T = 298$  K, pH 7.40 ( $\pm 0.05$ ),  $I = 0.15$  M NaCl, 0.1 mM complex), determined through cEST/Solverstat fitting. Charges omitted for clarity.

In the case of Eu(L9)Cl, the overlap in the UV spectral region between the BSA (280 nm) and the complex (270 nm) has limited the addition of the protein up to  $2.4 \cdot 10^{-5}$  M, concentration whose absorbance value is within the Lambert-Beer law. On the contrary, the concentration limit of BSA can be extended to  $1.8 \cdot 10^{-4}$  M in the case of Eu(L12)OTf complex, whose excitation wavelength is quite red-shifted (328 nm). It is worth evidencing that for the absorption measurements with microplate reader has been possible to raise to concentration of the protein up to typical extracellular range (0.4 mM), essentially for the lower optical path of the instrumentation.

#### 4.4.2.1. Luminescence: excitation spectra and $^5D_0$ lifetimes measurements

In order to study in detail the BSA-Ln(III)complexes interaction, the luminescence decay of the  $^5D_0$  excited state have been also collected. The Eu(L9)Cl complex has not showed any significant change in the observed lifetime (fixed around 0.30 ms) during the titration with the protein, whilst for the Eu(L12)OTf complex the lifetime increases considerable (Figure 27).

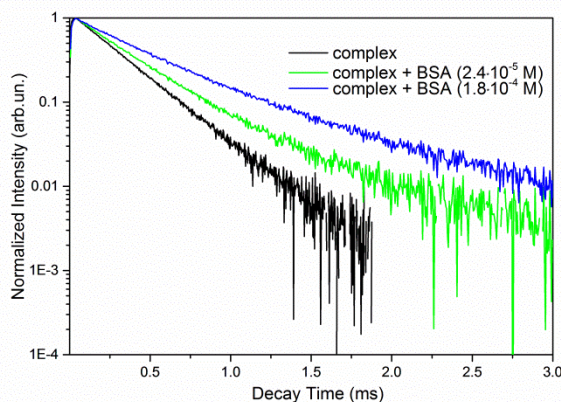


Figure 27. Luminescence decay curves of the  $^5D_0$  excited state of Eu(III) for Eu(L12)OTf complex ( $80 \mu\text{M}$ ) upon addition of BSA.

When BSA and the complex are both present in solution, the decay curves cannot be easily fitted by a single exponential function since more than one emitting species (complex/protein adducts) is present in solution. Upon addition of the protein, the increase of the  $^5D_0$  excited state lifetime [0.28 ms for the complex alone, 0.34 ms and 0.50 ms after the addition of BSA ( $2.4 \cdot 10^{-5}$  M and  $1.8 \cdot 10^{-4}$  M,

respectively)] is possibly due to the displacement of the water molecules around the metal ion by the coordinating groups of the protein, which gives rise to weaker multiphonon relaxation process.<sup>62,63</sup>

This phenomenon is also accompanied by an increase of the luminescence quantum yield which gives rise to an increase of the Eu(III) luminescence intensity. In the literature, it has been found that Ln(III) complexes in which the metal ion is bound to two water molecules (such as in our case) are susceptible to displacement of these molecules by competitive binding of endogenous serum anions *such as carbonate or protein carboxylic acid residues*.<sup>64</sup> On the contrary, in the case of Eu(L9)Cl complex, the protein-complex interaction does not affect the number of water molecules bound to the metal ion and the decrease of the Eu(III) emission intensity could be due to aspects related to *the efficiency of the ligand to metal energy transfer*. In literature, the decrease in sensitization of Eu(III) in complexes upon interaction with BSA, due to a *less efficient energy transfer mechanism*, where the tryptophan residues in the protein found in domain I and II (Trp-134 and Trp-213) are involved<sup>45</sup> (Figure 28).

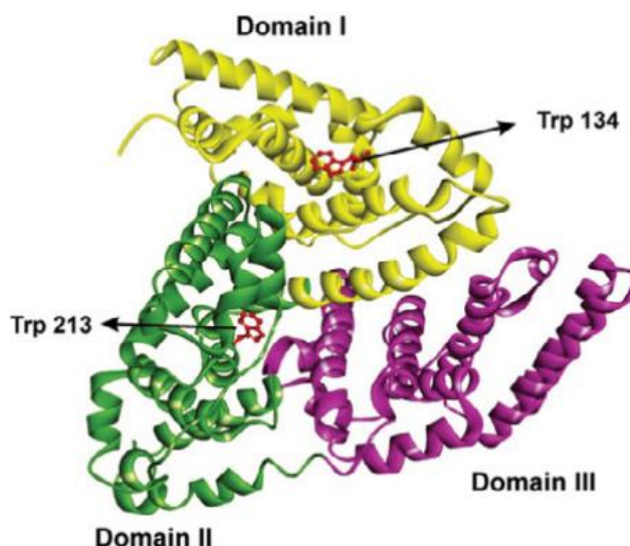


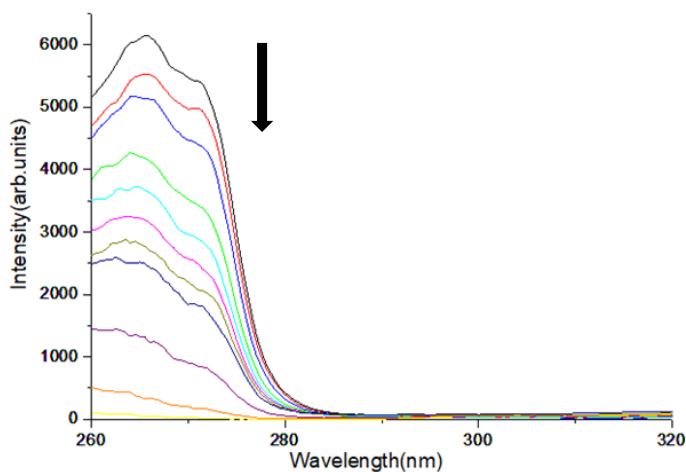
Figure 28. Secondary structure of BSA. From ref.65

Upon addition of the protein, the excitation spectrum of Eu(L9)Cl showed a progressive decrease of the peak around 265 nm, indicative of a decreased sensitization of Eu(III) luminescence by pyridine rings. However, the absence of



peaks around 280 nm ruled out the involvement of the tryptophan rings in the sensitization mechanism (Figure 29 a).

a)



b)

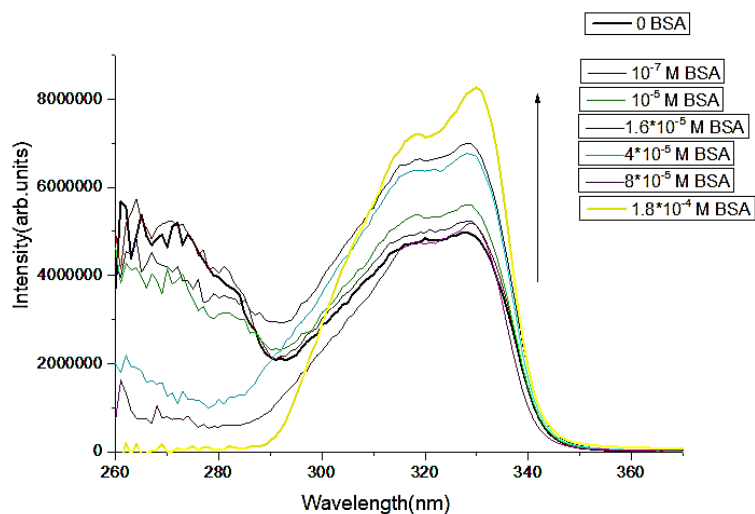


Figure 29. Excitation spectra of Eu(III) for: (a) Eu(L9)Cl complex ( $80 \mu\text{M}$ ) in MOPS-buffered solution (pH 7.4) upon addition of BSA in the  $0\text{-}2.4 \cdot 10^{-5} \text{ M}$  concentration range ( $\lambda_{em} = 614 \text{ nm}$ ); and (b) Eu(L12)OTf complex ( $80 \mu\text{M}$ ) upon addition of BSA in the  $0\text{-}1.8 \cdot 10^{-4} \text{ M}$  concentration range at 298 K ( $\lambda_{em} = 611 \text{ nm}$ ).

The unusual behavior of the Eu(L9)Cl complex pointed out a different nature of the protein-complex interaction, where the Trp-134 and 213 are not significantly involved in the bond with Eu(III) and the coordination sphere of the metal ion is preserved. On the contrary the excitation spectra of the Eu(L12)OTf complex

showed an opposite trend with an increase of the emission intensity for the peak around 330 nm (Figure 29 b).

In addition, the increase of the asymmetry ratio  $R$  upon addition of the protein (from 3.80 at the begin of the titration to 4.20 at the end, data not shown) in the case of Eu(L12)OTf complex, is indicative of the direct involvement of the coordination sphere of the metal center in the interaction with the protein. On the contrary, the  $R$  values (around 1.55) do not changed during the titration with the Eu(L9)Cl complex.

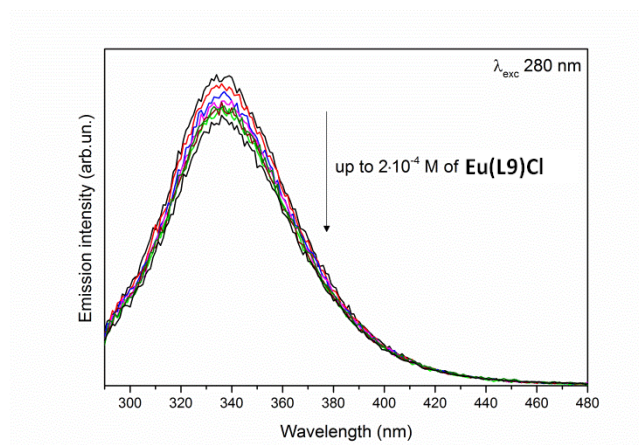
#### 4.4.2.2. *Luminescence: fluorescence of the protein*

The intrinsic fluorescence of BSA is mainly due to tryptophan residues, Trp-134 and Trp-213, and to a much lesser extent to tyrosine and phenylalanine residues. Trp-134 is located at the surface of the protein, in domain I, while Trp-213 is located inside the protein structure in domain II.

In order to get more insights for the protein-complex interaction mechanism, the evolution of the protein fluorescence upon addition of the Eu(III) complex has been also investigated.

The Lambert-Beer law applies in a wide concentration range of the Eu(III) complexes (up to 0.2 mM), in a fixed background solution of the protein (5  $\mu$ M). The titrations with the two Eu-complexes evidenced a decrease of the fluorescence intensity, which was particularly marked in the case of Eu(L12)OTf complex and almost negligible for Eu(L9)Cl (Figure 30 a-b).

(a)



(b)

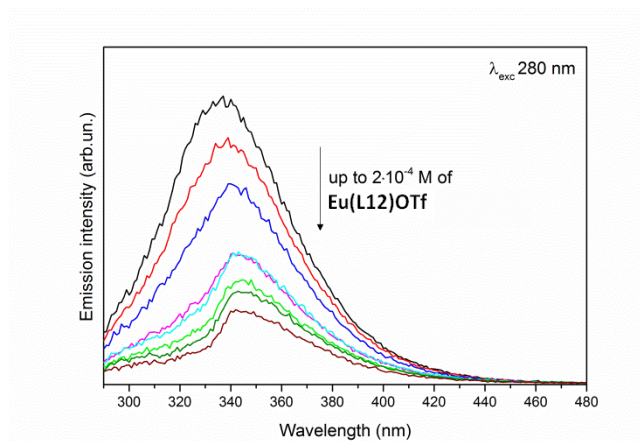


Figure 30. Evolution of the fluorescence spectrum of BSA ( $5\mu\text{M}$  solution) upon addition of increasing amount of (a)  $\text{Eu}(\text{L9})\text{Cl}$  and (b)  $\text{Eu}(\text{L12})\text{OTf}$  complexes. MOPS buffer (pH 7.4).

The maximum emission peak of the protein remained mostly unchanged for the  $\text{Eu}(\text{L9})\text{Cl}$  complex, whereas a red shift of  $\approx 10$  nm has been detected for the  $\text{Eu}(\text{L12})\text{OTf}$  complex (up to 340 nm).

In accordance to the literature, the red shift of the emission wavelength is probably due to *conformational changes in protein structure upon binding with the  $\text{Eu}(\text{L12})\text{OTf}$  complex*, with concomitant increase of the polarity and hydrophilicity around the tryptophan residues.<sup>66</sup> This finding is in agreement with a direct interaction between Trp fragments and the complex.

The protein fluorescence quenching by the complexes can result from a variety of phenomena including molecular interactions such as collisional (or dynamic) quenching and static quenching.<sup>67</sup>

As a consequence of collisional quenching, the excited-state fluorophore is deactivated upon contact with some other molecules in solution (the  $\text{Eu}(\text{III})$  complex, in our case). Alternatively, fluorophore can form non-fluorescent adducts with the complex, at the ground-state. This process is referred to a static quenching. In order to discriminate between static or dynamic quenching, we should measure the lifetime of the protein excited state. The fluorescence decay of BSA was best fitted to a biexponential function, and the corresponding averaged lifetimes,  $\langle\tau_{\text{av}}\rangle$  remained unaltered upon addition of both complexes (around 7.5

ns). This indicated that the quenching of the fluorescence follows a *static mechanism* and a ground-state complex between BSA and each Eu(III) complex should be present in solution.<sup>67</sup>

Concerning docking calculations, since the paramagnetic Eu(III) complexes are rather difficult to model computationally, the analogues of the diamagnetic Y(III) ion have been studied.

We can conclude that the Y(III) complex with *L9 ligand* does not remain in the binding sites where Trp 213 and 134 are located (very high  $\Delta G$  for this interaction). On the other hand, the complex finds different available cavities on the surface protein (Figure 31).

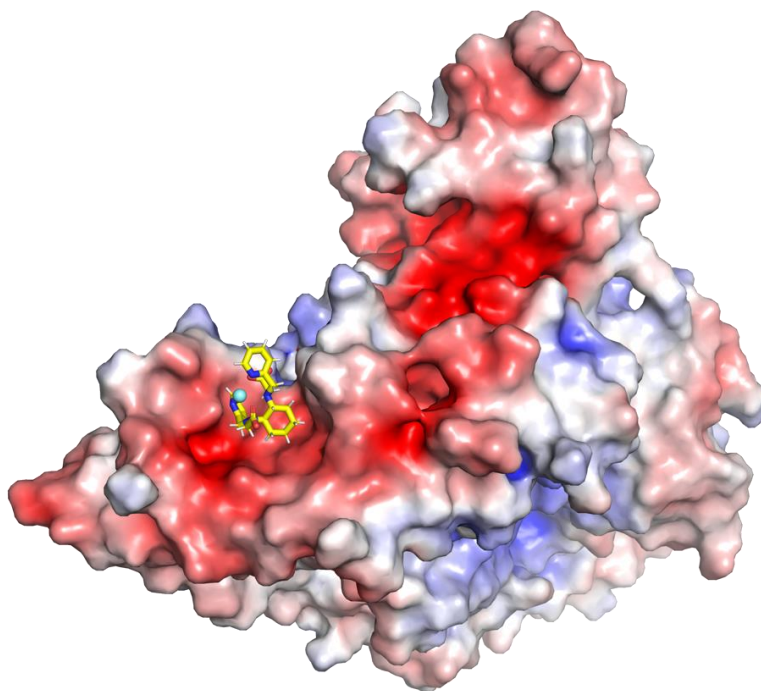


Figure 31. Structural cavities on the BSA surface (in red), explored by the  $Y(L9)^{3+}$  complex.

It remains in these cavities for the last 50 ns of the simulation (half of the total simulation time). Finally, the metal ion is capable to exchange water molecules of the inner coordination sphere with other water molecules located at the surface of the protein without changing the “hydration state” of the complex. This in agreement with data reported in Figure 32, which shows that the number of inner sphere water molecules in bulk water and in the adduct with BSA remained unchanged.

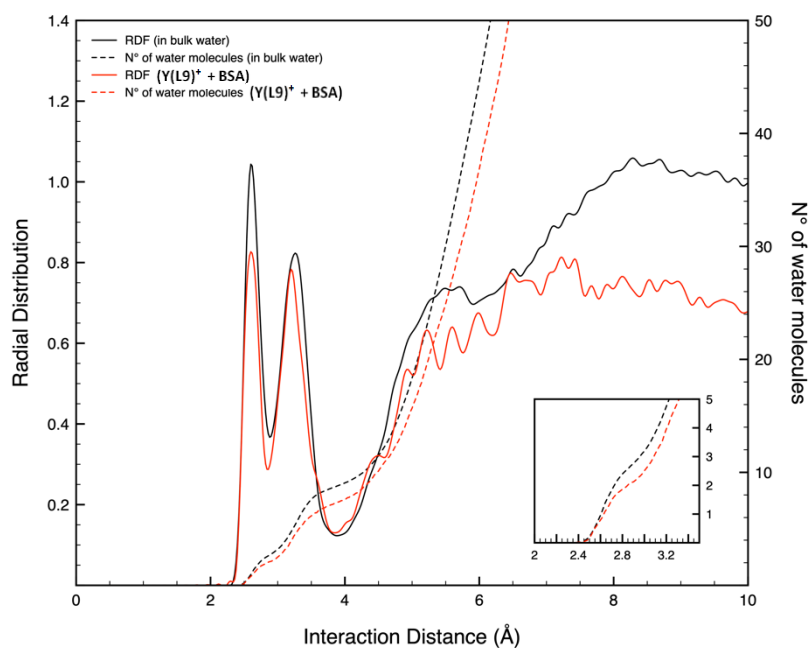


Figure 32. Graphical representation of the radial distribution function and the number of water molecules in function of the interaction distance between the  $YL9^+$  and water, during a simulation in bulk water and in the simulation with BSA, black and red respectively.

Regarding the  $Eu(L12)^+$  (=YL12) docked to the binding sites of TRP-134 and 213, we observed that the complex remains only in the TRP-134 binding site, through all the simulation time. As it can be seen on Figure 33, the distance between YL12 and the side chain of TRP-134 remains constant around 6.8 Å over the simulated 100 ns.

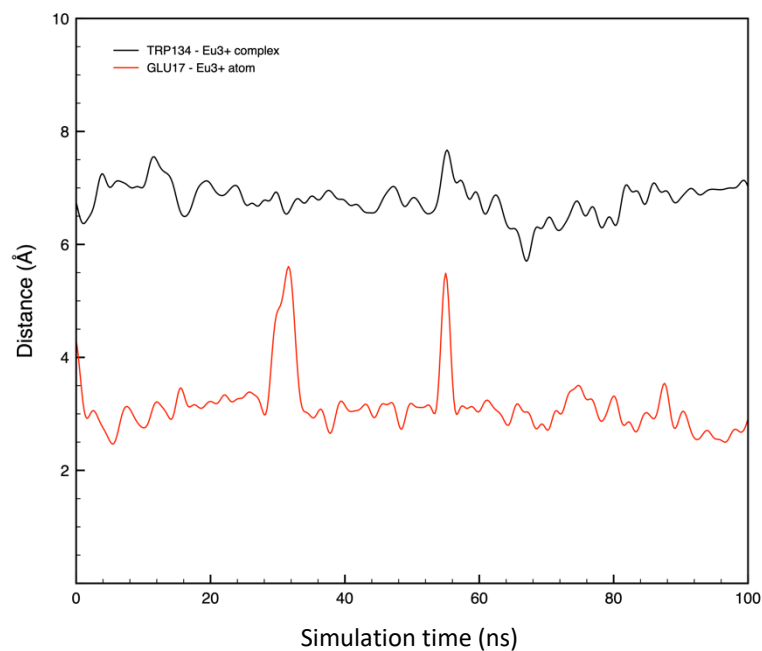


Figure 33. Graphical representation of the distance between the side chain of TRP-134 and the YL12 (black) and GLU-17 and  $Y^{3+}$  atom (red).

This result is in agreement with the experimental results with respect to the interaction that was observed between the complex and one of the tryptophan's. Additionally, it was also experimentally observed that the complex loses one of coordinated waters, which is possibly substituted by a closed amino acidic residue. The radial distribution analysis in Figure 34, revealed that while in bulk water the complex has two molecules of water in its first solvation sphere ( $\approx 2.45$  Å), when it is docked to the binding site of TRP-134 the complex has just one molecule of water in the first solvation sphere.

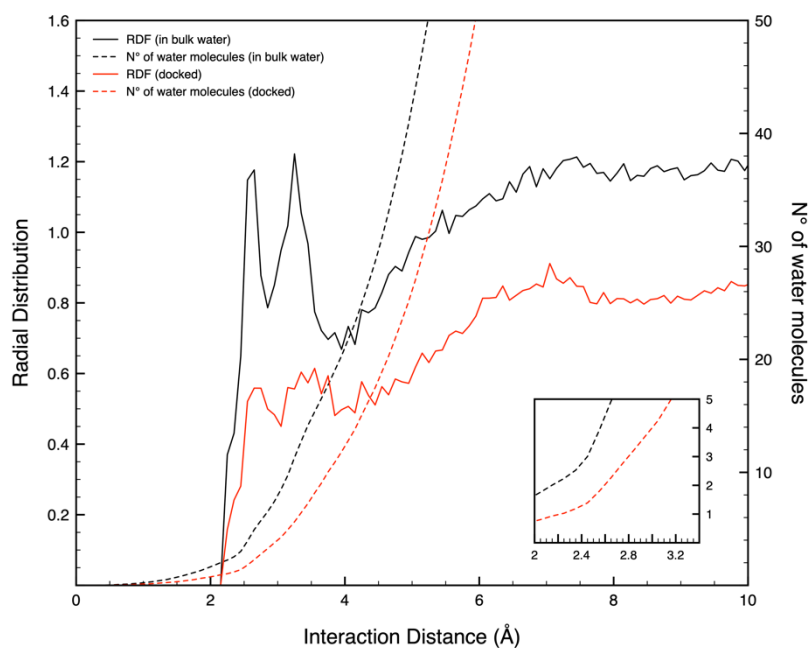


Figure 34. Graphical representation of the radial distribution function (RDF) and the number of water molecules in function of the interaction distance between the  $Y(L12)^+$  and water, in bulk water and docked in the binding site of TRP-134, black and red respectively

At this point, a closer look on which amino acid residues are closer to the complex revealed that the side chain of a glutamic acid (GLU17, in the fragment E17) distances on average  $3.1 \text{ \AA}$  from the  $Y^{3+}$  ion and it is bound to the metal ion through the carboxylic group (Figure 35).

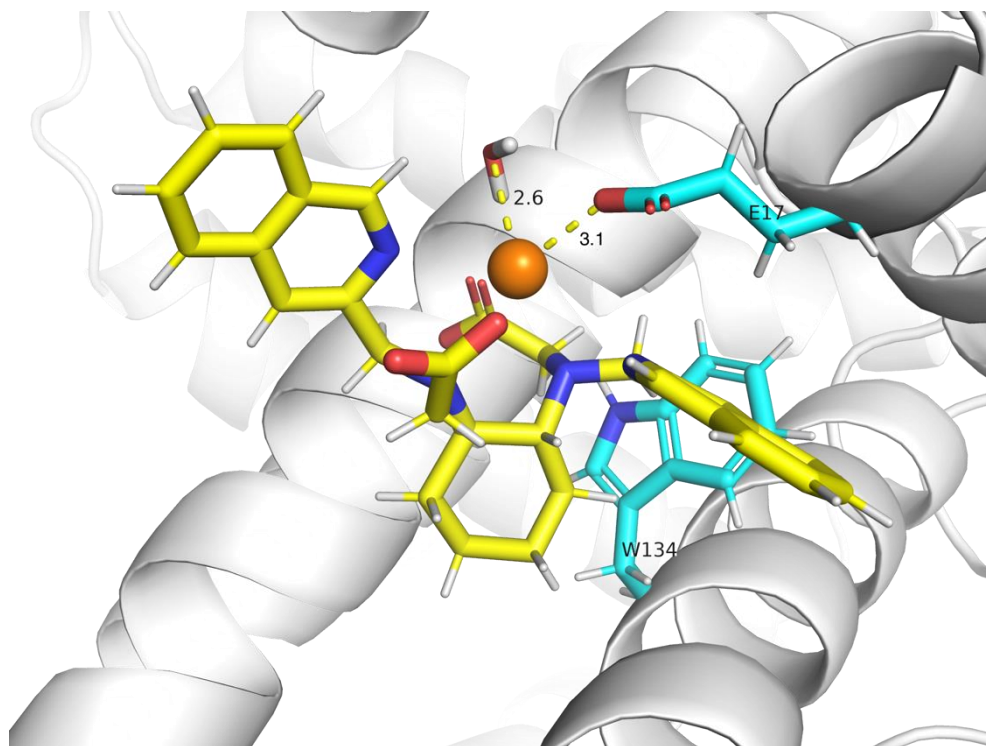


Figure 35. Close-up on the  $\text{Eu}(\text{L12})^+$  bound to BSA

#### 4.4.3. Conclusions

Concluding, the luminescence changes observed upon the **Eu(L12)OTf complex-BSA** interaction foresee the displacement of one water molecules from the metal center by the coordinating groups of the protein (the carboxylic group of the GLU17 residue), by enhancing emission intensity and lifetimes of the Eu(III) in the complex. The interaction occurs close to the indole ring of the TRP-134 unit (distance Y-TRP134  $\sim 6.8$  Å). Upon interaction, the structural changes of the protein get worse the efficiency of the fluorescence emission, as clearly reported in Figure 30b.

On the other hand, the luminescence changes in the case of the **Eu(L9)Cl** complex have been explained by a protein/complex interaction which takes place on the surface of the protein, far from the Tryptophan units, without a direct involvement of the Eu(III) inner coordination sphere. These remarks have been also confirmed in the quite low evolution of the protein fluorescence during titration with the Eu(L9)Cl complex (Figure 30 a).



The overall hydration state remained constant, by resulting in unchanged emission lifetime of the Eu(L9)Cl. As far as the decrease of the lanthanide luminescence is concerned, two main effects could occur: *i*) the interaction of the Pyridine fragments with the external residue of the protein cavities that influences the antenna-metal center distance, and *ii*) a change in the excited state energy of the ligand by resulting in a lower efficiency of the energy transfer to the metal center.

#### 4.5. ***Experimental part: procedures, techniques and characterization***

##### 4.5.1. ***Materials***

EuCl<sub>3</sub>·6H<sub>2</sub>O, Dichloromethane (DCM), Methanol (MeOH), Deuterated Chloroform (CDCl<sub>3</sub>), Cyclohexane and Ethyl acetate were purchased from Sigma-Aldrich; Acetonitrile (ACN), Ethanol (EtOH) and Formic acid 99% were purchased from Carlo Erba Reagents; tert-butyl 2-bromoacetate, (1*R*, 2*R*)-*trans*-cyclohexane-1,2-diamine and quinoline-2-carbaldehyde were purchased from Alfa Aesar. Acetonitrile (ACN) were get from Proligo Reagents and Potassium carbonate anhydrous (K<sub>2</sub>CO<sub>3</sub>) were bought from Baker Reagents.

Solvents were dried when required using an appropriate drying agent. As far as the reactions in anhydrous conditions are concerned, the Schlenk-line technique was carried out using an atmosphere of dry Argon.

The water used was obtained in high purity from the 'Millipore Elix 10' purification system. Eu(CF<sub>3</sub>SO<sub>3</sub>)<sub>3</sub> and (Aldrich, 98%) were stored under vacuum for several days at 80°C and then transferred to the glove box. All other chemicals were purchased from Alfa Aesar and Acros Organics.

4-Morpholinepropanesulfonic acid (MOPS) buffer 15 mM was dissolved in purified bi-distillate water, followed by addition of NaCl 0.9% m/v for obtaining the ionic strength of physiological conditions. The pH value was corrected to physiological range by dropwise addition of freshly prepared NaOH 10 M until pH≈7.4. Stock solution of Bovine Serum Albumin (BSA) (purity ≥ 99%, purchased from Roth) was freshly prepared by dissolving the protein in MOPS buffer (pH≈7.4). The complete dissolution of BSA was reached without mechanical shaking, but just after 20-25 min with spontaneously diffusion in

buffer. Upon dissolution, the protein solution was kept in the dark at 4 °C before use.

All other anionic solutions were freshly prepared by dissolving in buffer with using the sonication so far as was required.

Thin-layer chromatography was carried out on neutral alumina plates (Fluka Analytical) or silica plates (Sigma-Aldrich) and visualized under UV lamp (254 nm). The cationic exchange chromatography was performed on SCX cartridges (1g or 2g) purchased from “Agilent Technologies-sample Prep solutions”.

#### 4.5.2. *Synthesis*

The synthesis of the ligands and the relative Ln(III) complexes discussed in this chapter are presented in Schemes 2-6.

The synthesis of **L9** ligand and the relative Eu(III) and Tb(III) complexes have been widely presented in the past from our research group.<sup>3</sup> For more simplicity, the synthesis of the corresponding **Eu(L9)Cl** and **Tb(L9)Cl** is recalled herein.

**Eu/Tb(L9)Cl**: The chloride lanthanum salts (45 mg, 0.121 mmol) has been added to aqueous solution (2 mL) of diacetic acid (50 mg, 0.121 mmol). Under vigorously stirring, the initial acid pH has been raised to neutral pH (almost 6.5) using aqueous solution (4 mL) of KOH (27 mg, 0.484 mmol). After 8 hours all the water has been removed under reduce pressure and the resulting residue has been suspended in Ethanol (10 mL). The solution has been cooled to -18 °C and kept to this temperature overnight to increase the precipitation of inorganic salts. The suspending solid has been removed by filtration and the clear ethanol solution has been concentrated to obtain the desiderated complexes. **Europium Chloride complex.** Yield: 51%. MS(ESI) m/z: 563.18 [M-Cl], 580 [M-Cl+H<sub>2</sub>O], 594.85 [M-Cl+MeOH]; **Terbium Chloride complex.** Yield: 53%. MS(ESI) m/z: 596.25[M-Cl], 600.92 [M-Cl+MeOH].

*N,N'*-bis(2-quinolinmethyl)-*trans*-1,2-diaminocyclohexane *N,N'*-*tert*-butyl diacetate (1*R*, 2*R*)(**1**): Ligand **L6** (1.8 g, 4.54 mmol) already described in literature,<sup>4</sup> was dissolved in a mixture of anhydrous acetonitrile (80 mL) and anhydrous potassium carbonate under inert condition (Argon). Then, a solution of *tert*-Butyl 2-bromoacetate (1.68 ml, 11.4 mmol), in anhydrous acetonitrile (15

mL) was added dropwise over ten minutes. After stirring 12 h at room temperature dichloromethane was added and the reaction mixture was washed with brine solution. The organic phase was evaporated under reduced pressure to give 3.3 g of yellowish oil. The crude product was purified by chromatography on activated neutral alumina (Al<sub>2</sub>O<sub>3</sub>, Cy:AcOEt from 9:1 to 1:9) giving 2.50 g of a yellowish oil (yield: 88%). <sup>1</sup>H-NMR (CDCl<sub>3</sub>) δ (ppm) 8.07-8.04 (m, 4H, quinoline), 7.92 (d, J=7.76 Hz, 2H, quinoline), 7.75 (d, J= 7.10 Hz, 2H, quinoline), 7.69 (7, J=7.68 Hz, 2H, quinoline), 7.50 (t, J=7.40 Hz, 2H, quinoline), 4.16 (m, 2H, methylene-ester), 3.86 (d, J<sub>GEM</sub>=13.75 Hz, 2H, methylene-ester), 3.49 (d, J<sub>GEM</sub>=17.22 Hz, 2H, methylene-quinoline), 3.31 (d, J<sub>GEM</sub>=17.22 Hz, 2H, methylene-quinoline), 2.71 (m, 2H, methylene-cyclohexane), 2.18-1.12 (m, 8H, cyclohexane), 1.46 (s, 18H). Elemental Anal. Calc. for C<sub>38</sub>H<sub>48</sub>N<sub>4</sub>O<sub>4</sub> (MW 624,8): C, 73,05; H, 7,74; N, 8,97; O, 10,24 Found: C, 72.89 ; H, 7.51; N, 9.03; O, 10.36

*N,N'*-bis(2-quinolinmethyl)-*trans*-1,2-diaminocyclohexane *N,N'*-diacetic acid (1*R*, 2*R*) (**H<sub>2</sub>L11**, as ammonium salt): **1** (1.20 g, 1.92 mmol) was dissolved in HCl aq (6 M, 30 ml); the obtained reaction mixture was stirred for 12 h at 80°C. The reaction mixture was washed with ethyl acetate and the aqueous phase was evaporated under reduced pressure. The obtained brownish oil (2.47 g) was suspended in 10 ml of methanol, aqueous ammonia solution was added until pH 8-9 was reached and 1.05 g of a yellowish solid were obtained after chromatography [(C18 column; eluent H<sub>2</sub>O:Acetonitrile 4:6 +0.1% NH<sub>4</sub>OH aq 30% w/w (50 ml)]. This solid was further purified by trituration in DCM:AcOEt:EtOH 1:2:2 at 80 °C for 30 minutes, obtaining 548 mg of a yellowish solid (ligand **3**, yield: 52%). UV-Vis absorption spectroscopy (water:methanol 9:1): ε(316 nm): 6728 M<sup>-1</sup>cm<sup>-1</sup>. <sup>1</sup>H-NMR (CD<sub>3</sub>OD) δ (ppm) 8.05-7.48 (m, 12H, quinoline), 3.74-3.55 (m, 8H, methylene-ester/quinoline), 2.39 (m, 2H, cyclohexane), 1.98 (m, 2H, cyclohexane), 1.67-1.28 (m, 6H, cyclohexane). UV-Vis spectroscopy: ε(316 nm)= 6248 M<sup>-1</sup>cm<sup>-1</sup> (methanol). Elemental Anal. Calc. for C<sub>30</sub>H<sub>38</sub>N<sub>6</sub>O<sub>4</sub> (MW 546.7): C, 65,91; H, 7,01; N, 15,37; O, 11,71 Found: C, 65.79 ; H, 7.09; N, 15.27; O, 11.59.

The cationic complex **Eu(L11)OTf** has been synthesized as follows: the ammonium salt of Ligand **H<sub>2</sub>L11** (100 mg, 0.182 mmol) was dissolved in hot

(60°C) 2-propanol (7 ml). Upon cooling, Europium(III) trifluoromethanesulfonate 98% (109 mg, 0.182 mmol) was added portion-wise, and a yellowish suspension was formed. After neutralization with KOH 2M aq (pH  $\approx$ 7), the reaction mixture was stirred at room temperature for 2h. The suspension was centrifuged, and the solid collected was suspended in methanol (5 ml). The resulting solid was removed by centrifugation, and the filtrate was concentrated under reduced pressure to give 44 mg of the desired product as a beigeish solid (yield: 30%). UV-Vis spectroscopy:  $\epsilon$ (319 nm): 8808 M<sup>-1</sup>cm<sup>-1</sup> (water). Elemental Anal. Calc. for C<sub>31</sub>H<sub>30</sub>EuF<sub>3</sub>N<sub>4</sub>O<sub>7</sub>S·(H<sub>2</sub>O)<sub>2</sub> (MW 847.6): C, 43,93; H, 4,04; N, 6,61; O, 16,99; S, 3,78 Found: C, 43,87; H, 4,00; N, 6,48; O, 17,04; S, 3,89.

*{2-[(Pyridyl-2-ylmethyl)-amino]-cyclohexyl}-carbamic acid tert-butyl ester (3)*: Compound **2** (0.670 g, 3.13 mmol) was added to a solution of 2-pyridinecarboxyaldehyde (3.13 mmol) in ethanol (35 ml) and stirred at room temperature for 12h. Sodium borohydride was slowly added to the mixture. The reaction was monitored by TLC (SiO<sub>2</sub>, Cyclohexane:Ethyl acetate 7:3+ NH<sub>4</sub>OH 30% w/w) and after 4h the mixture was extracted twice with dichloromethane and the solvent removed under reduced pressure to give the compound **3** as yellowish oil, in quantitative yield, which were used in next step without further purification.

*N-Pyridyl-2-ylmethyl-cyclohexane-1,2-diamine (4)*: Compound **3** (3.13 mmol) was added to a trifluoroacetic acid 98% w/w (13 ml) and dichloromethane (40 ml) solution and stirred at room temperature for 12h. The solvent was removed under reduced pressure, and the obtained trifluoroacetate salt ( $\approx$ 3 g) was purified by cationic exchange chromatography (eluent: NH<sub>3</sub> 3M in MeOH) to give the free amine **4**. Yield 38%. <sup>1</sup>H-NMR (CDCl<sub>3</sub>)  $\delta$  (ppm) 8.52 (m, 1H), 7.62 (t, J= 7.54 Hz, 1H), 7.34 (d, J= 7.70 Hz, 1H), 7.13 (t, J= 5.90 Hz, 1H), 4.03 (dd, J<sub>GEM</sub>= 14.09 Hz, 1H), 3.83 (dd, J<sub>GEM</sub>= 14.09 Hz, 1H), 3.64 (m, 1H), 2.43 (m, 1H), 2.18 (m, 2H), 1.88 (m, 1H), 1.75 (m, 1H), 1.70 (m, 1H), 1.35-1.04 (m, 5H). Elemental Anal. Calc. for C<sub>12</sub>H<sub>19</sub>N<sub>3</sub> (MW 205.3): C, 70,20; H, 9,33; N, 20,47 Found: C, 70.15 ; H, 9.19; N, 20.44.

*N-picolyl-N,N',N'-trans-1,2-cyclohexylenediamine-tert-butyl triacetate (5)*. Under inert atmosphere, compound **4** (1.94 mmol) was dissolved in an anhydrous acetonitrile (40 ml) solution of N,N-Diisopropylethylamine (6.8 mmol). Then, tert-Butyl 2-bromoacetate (6.8 mmol) in anhydrous Acetonitrile (10 mL) was added dropwise. The reaction was monitored using TLC (SiO<sub>2</sub>, Rf: 0.47, DCM:MeOH 95:5+ 0.5% NEt<sub>3</sub>) and after 12 h, water (approx. 25 mL) was added and the reaction mixture was extracted twice with dichloromethane. The combined organic phases were dried on anhydrous Na<sub>2</sub>SO<sub>4</sub> and the solvent was evaporated under reduced pressure to give 0.580 g of crude product which was purified by chromatography (on Silica gel, DCM/MeOH 95:5 + 0.5% Triethylamine, Rf: 0.47) giving rise to compounds **5** (yield 58%). Compound **5**: <sup>1</sup>H-NMR (CDCl<sub>3</sub>) δ (ppm) 9.97 (d, J=6.56, 1H), 8.79 (d, J=7.91, 1H), 8.34 (t, J=7.91, 1H), 7.94 (t, J=6.56, 1H), 6.30 (dd, J<sub>GEM</sub>= 17.64 Hz, 1H), 5.94 (dd, J<sub>GEM</sub>= 17.64 Hz, 1H), 4.55 (dd, J<sub>GEM</sub>= 16.93 Hz, 2H), 3.53 (m, 2H), 3.44 (dd, J<sub>GEM</sub>= 16.93 Hz, 2H), 2.66 (m, 3H), 2.08 (m, 2H), 1.78 (m, 2H), 1.45 (s, 27H), 1.12 (m, 3H). Elemental Anal. Calc. for C<sub>30</sub>H<sub>49</sub>N<sub>3</sub>O<sub>6</sub> (MW 547): C, 65,78; H, 9,02; N, 7,67; O, 17,53 Found: C, 65,70; H, 8,95; N, 7,73; O, 17,41

*N-picolyl-N,N',N'-trans-1,2-cyclohexylenediaminetriacetic acid (H<sub>3</sub>L10 as ammonium salt)*. Compound **5** (1.12 mmol) was added to an aqueous HCl (6M, 22 ml) solution and stirred at ≈80°C for 12h. After neutralization with NaOH, extraction with DCM was performed and the resulting aqueous solution was evaporated under reduced pressure. The solid was washed with ethanol for 1h at 80°C. Upon cooling, the suspension was filtered to remove all the insoluble inorganic salts and the resulting solution was evaporated under reduced pressure and the crude product was purified by ionic exchange chromatography to give the corresponding product **H<sub>3</sub>L10** (yield = 24%). Compound **H<sub>3</sub>L10** : UV-Vis spectroscopy: ε(262 nm): 4830 M<sup>-1</sup>cm<sup>-1</sup> (water). ESI-MS(Scan ES+; m/z): 468 (100%); 469 (20%) ([Na<sub>4</sub>(L10)]<sup>+</sup>). Elemental Anal. Calc. for C<sub>18</sub>H<sub>34</sub>N<sub>6</sub>O<sub>6</sub> (MW 430.5): C, 50,22; H, 7,96; N, 19,52; O, 22,30 Found: C, 50.18 ; H, 7.90; N, 19.47; O, 22.18.

**Eu(L10)** has been synthesized as follows: Ligand **H<sub>3</sub>L10** (60 mg, 0.140 mmol) was partially dissolved in a mixture of 2-propanol:ethanol 1:1 (4 ml) by heating at  $\approx 60^\circ\text{C}$ . Then, europium(III) trifluoromethanesulfonate 98% (83.6 mg, 0.140 mmol) was added portion-wise and the pH of the solution was carefully adjusted to 7 by addition of KOH 2M aq. The obtained suspension was stirred at room temperature for 12h. The collected solid ( $\approx 94$  mg) was re-crystallized in methanol ( $\approx 10$  ml) and Et<sub>2</sub>O ( $\approx 30$  ml) solution to yield 70 mg (yield 95%) of a whitenish solid **Eu(L10)**. UV-Vis spectroscopy:  $\epsilon(265 \text{ nm}): 3390 \text{ M}^{-1}\text{cm}^{-1}$  (water). ESI-MS(Scan ES+;  $m/z$ ): 552 (100%); 550 (90%) ([NaEu(L10)]<sup>+</sup>). Elemental Anal. Calc. for C<sub>18</sub>H<sub>22</sub>EuN<sub>3</sub>O<sub>6</sub>·(H<sub>2</sub>O)<sub>2</sub> (MW 564.4): C, 38,31; H, 4,64; N, 7,45; O, 22,68 Found: C, 38.28; H, 4,54; N, 7.40; O, 22.51.

**Tb(L10)**: Ligand **H<sub>3</sub>L10** (27 mg, 0.063 mmol) was dissolved in water (3 ml), then Terbium(III) chloride hexahydrate (23.5 mg, 0.063 mmol) was added portion-wise and the pH of the solution was carefully adjusted to 7 by addition of KOH 2M aq. The obtained solution was stirred at room temperature for 12h. The solvent was removed under reduced pressure and the residue was re-crystallized in methanol ( $\approx 2$  ml) and Et<sub>2</sub>O ( $\approx 15$  ml) solution yielding a white solid after centrifugation (34 mg of **Tb(L10)**, quantitative yield). UV-Vis spectroscopy:  $\epsilon(266 \text{ nm}): 4008 \text{ M}^{-1}\text{cm}^{-1}$  (water). ESI-MS(Scan ES+;  $m/z$ ): 558 (100%) ([NaTb(L10)]<sup>+</sup>). Elemental Anal. Calc. for C<sub>18</sub>H<sub>22</sub>TbN<sub>3</sub>O<sub>6</sub>·(H<sub>2</sub>O)<sub>2</sub> (MW 571.3): C, 37,84; H, 4,59; N, 7,35; O, 22,40 Found: C, 37.78; H, 4,50; N, 7.30; O, 22.37.

*{2-[(Quinolyl-2-ylmethyl)-amino]-cyclohexyl}-carbamic acid tert-butyl ester (6)*: Compound **2** (0.670 g, 3.13 mmol) was added to a solution of 2-quinolinecarboxyaldehyde (3.13 mmol) in ethanol (35 ml) and stirred at room temperature for 12h. Sodium borohydride was slowly added to the mixture. The reaction was monitored by TLC (SiO<sub>2</sub>, Cyclohexane:Ethyl acetate 7:3+ NH<sub>4</sub>OH 30% w/w) and after 4h the mixture was extracted twice with dichloromethane and the solvent removed under reduced pressure to give the corresponding compound **6** as yellowish oil, in quantitative yield, which were used in next step without further purification.

*N*-Quinolyl-2-ylmethyl-cyclohexane-1,2-diamine (**7**): Compound **6** (3.13 mmol) was added to a trifluoroacetic acid 98% w/w (13 ml) and dichloromethane (40 ml) solution and stirred at room temperature for 12h. The solvent was removed under reduced pressure, and the obtained trifluoroacetate salt ( $\approx 3$  g) was purified by cationic exchange chromatography (eluent: NH<sub>3</sub> 3M in MeOH) to give the desired product **7**. (Yield 61%) <sup>1</sup>H-NMR (CDCl<sub>3</sub>)  $\delta$  (ppm) 8.13 (d, J= 8.33 Hz, 1H), 8.08 (d, J= 8.56 Hz, 1H), 7.81 (d, J= 8.33 Hz, 1H), 7.71 (t, J= 7.74 Hz, 1H), 7.55-7.48 (m, 2H), 4.25 (dd, J<sub>GEM</sub>= 14.55 Hz, 1H), 4.07 (dd, J<sub>GEM</sub>= 14.55 Hz, 1H), 3.71 (m, 1H), 2.50 (m, 1H), 2.18 (m, 2H), 1.92 (m, 1H), 1.75 (m, 1H), 1.70 (m, 1H), 1.35-1.04 (m, 5H). Elemental Anal. Calc. for C<sub>16</sub>H<sub>21</sub>N<sub>3</sub> (MW 255.4): C, 75,26; H, 8,29; N, 16,46 Found: C, 75.21 ; H, 8.22; N, 16.39.

*N*-quinolyl-*N,N',N'*-*trans*-1,2-cyclohexylenediamine-*tert*-butyl triacetate (**8**). Under inert atmosphere, compound **7** (1.20 mmol) was dissolved in an anhydrous acetonitrile (25 mL) solution of *N,N*-Diisopropylethylamine (4.19 mmol.). Then, *tert*-Butyl 2-bromoacetate (4.19 mmol) in anhydrous Acetonitrile (5 mL) was added dropwise. The reaction was monitored using TLC (SiO<sub>2</sub>, R<sub>f</sub>: 0.47, DCM:MeOH 95:5+ 0.5% NEt<sub>3</sub>) and after 12 h, water (approx. 25 mL) was added and the reaction mixture was extracted twice with dichloromethane. The combined organic phases were dried on anhydrous Na<sub>2</sub>SO<sub>4</sub> and the solvent was evaporated under reduced pressure to give 0.580 g of crude product which was purified by chromatography (on Silica gel, DCM/MeOH 95:5 + 0.5% Triethylamine, R<sub>f</sub>: 0.47) giving rise to compounds **8** (yield = 55%). <sup>1</sup>H-NMR (CDCl<sub>3</sub>)  $\delta$  (ppm) 8.12 (m, 2H), 8.07 (d, 1H), 7.81 (d, J=7.92, 1H), 7.67 (t, J=7.71, 1H), 7.51 (t, J=7.29, 1H), 4.32 (dd, J<sub>GEM</sub>= 13.79 Hz, 1H), 3.94 (dd, J<sub>GEM</sub>= 13.79 Hz, 1H), 3.60 (m, 2H), 3.52 (m, 4H), 2.81 (m, 1H), 2.67 (m, 1H), 2.15 (m, 1H), 2.09 (m, 1H), 1.74 (m, 2H), 1.45 (s, 27H), 1.14 (m, 4H). Elemental Anal. Calc. for C<sub>34</sub>H<sub>51</sub>N<sub>3</sub>O<sub>6</sub> (MW 597.8): C, 68,31; H, 8,60; N, 7,03; O, 16,06 Found: C, 68,27; H, 8,51; N, 7,00; O, 15.97.

*N*-quinolyl-*N,N',N'*-*trans*-1,2-cyclohexylenediaminetriacetic acid (**H<sub>3</sub>L4** as ammonium salt). Compound **8** (0.652 mmol) was added to an aqueous HCl (6M,

13 ml) solution and stirred at  $\approx 80^\circ\text{C}$  for 12h. After neutralization with NaOH, extraction with DCM was performed and the resulting aqueous solution was evaporated under reduced pressure. The solid was washed with ethanol for 1h at  $80^\circ\text{C}$ . Upon cooling, the suspension was filtered to remove all the insoluble inorganic salts and the resulting solution was evaporated under reduced pressure and the crude product was purified by ionic exchange chromatography to give the corresponding product **H<sub>3</sub>L4**, (yield = 40%). UV-Vis spectroscopy:  $\epsilon$  (316 nm) =  $2908\text{ M}^{-1}\text{cm}^{-1}$ (water). ESI-MS (Scan ES+;  $m/z$ ): 513 (100%); 514(25%) ( $[(\text{NH}_4)\text{Na}_3(\text{L4})]^+$ ). Elemental Anal.  $\text{C}_{22}\text{H}_{36}\text{N}_6\text{O}_6$  (MW 480.6): C, 54,99; H, 7,55; N, 17,49; O, 19,98 Found: C, 54.90 ; H, 7.46; N, 17.42; O, 20.01.

**Eu(L4)** has been synthesized as follows: ligand **H<sub>3</sub>L4** (60 mg, 0.125 mmol) was partially dissolved in a mixture of 2-propanol:ethanol 8:2 (6 ml) at  $\approx 60^\circ\text{C}$ . Then,  $\text{Eu}(\text{CF}_3\text{SO}_3)_3$  98% (75 mg, 0.125 mmol) was added portion-wise followed by KOH 2M aq until  $\text{pH} \approx 7$ . The obtained suspension was stirred at room temperature for 12h. The solid was removed under centrifugation, and the solution were dried under reduced pressure to give  $\approx 112$  mg of a white solid, which was re-crystallized in ethanol ( $\approx 10$  ml) and  $\text{Et}_2\text{O}$  ( $\approx 40$  ml) solution, yielding a white solid after centrifugation (55 mg; yield 76%). UV-Vis spectroscopy:  $\epsilon$  (319 nm) =  $3725\text{ M}^{-1}\text{cm}^{-1}$ (water). ESI-MS(Scan ES+;  $m/z$ ): 602 (100%); 600 (92%) ( $[\text{NaEu}(\text{L4})]^+$ ). Elemental Anal. Calc. for  $\text{C}_{22}\text{H}_{24}\text{EuN}_3\text{O}_6 \cdot (\text{H}_2\text{O})_2$  (MW 614.4): C, 43,00; H, 4,59; N, 6,84; O, 20,83 Found: C, 42.97; H, 4.54; N, 6.74; O, 20.76.

*Isoquinoline-3-carbaldehyde (10)*: Under inert conditions, Diisobutylaluminium hydride (DIBAL-H) 1M in toluene (54.5 mL, 55 mmol) was added dropwise to a stirred solution of the methyl ester **9** (6 g, 32 mmol) in anhydrous toluene (200 mL) at  $-78^\circ\text{C}$ . The mixture was stirred at this temperature for 50 minutes and then allowed to reach  $0^\circ\text{C}$ . Under an Argon flow, 1 M HCl (48 mL) was added by slowly dropwise addition and the resulting suspension was filtered through celite pad. The filtrate was diluted with water (350 mL) and extracted with Ethyl Acetate ( $3 \cdot 350$  mL). The combined organic phases were washed with saturated aqueous NaCl, dried over  $\text{Na}_2\text{SO}_4$  and the solvents were evaporated in vacuo to



give 3.44 g of a reddish solid, which was used in the next step without further purification. Yield: 68%, purity: 80% mol. <sup>1</sup>H-NMR (CDCl<sub>3</sub>) δ (ppm) 7.78 [2H, t, J=7.74 Hz]; 7.99 [1H, d, J=7.74 Hz]; 8.05 [1H, d, J=7.74 Hz]; 8.36 [1H, s]; 9.35 [1H, s]; 10.25 [1H, -CHO]. <sup>13</sup>C-NMR (CDCl<sub>3</sub>): 121.78 (CH-Ar), 127.79 (CH-Ar), 128.62 (CH-Ar), 130.21 (CH-Ar), 130.52 (-C-Ar), 131.44 (CH-Ar), 135.24 (-C-Ar), 146.81 (-C-CHO), 153.25 (CH-N-CHO), 193.35 (CHO).

*N,N'*-Bis-isoquinolin-3-ylmethyl-cyclohexane-1,2-diamine (**12**): Trans-Cyclohexane 1,2-diamine (**11**) (1.55 g, 13.56 mmol) was added at RT to a stirred solution of Isoquinoline-3-carbaldehyde (2.34 g, 14.9 mmol) in EtOH absolute anhydrous (145 ml). The yellowish reaction mixture was stirred to room temperature for 12h; then, upon cooling at ≈0°C sodium borohydride (0.923 g, 24.4 mmol) was directly added one pot to the mixture to get a clear reddish solution, and was left under stirring at room temperature for 5h.

The reaction mixture was quenched with water, followed by liquid extraction of the product with dichloromethane. The collected organics were washed with brine in order to clarify the phases, and dried over sodium sulfate; upon removal of the solvent under reduced pressure, 3.47 g of yellowish oil was obtained, which was used as such in the following reaction. Yield: 65%, purity: 80% mol.

<sup>1</sup>H-NMR (CDCl<sub>3</sub>) δ (ppm) 9.17 (s, 2H, isoquinoline), 7.88 (m, 2H, isoquinoline), 7.74 (d, J= 8.27 Hz, 2H, isoquinoline), 7.64 (s, 2H, isoquinoline), 7.61 (m, 2H, isoquinoline), 7.51 (m, 2H, isoquinoline), 4.16 (d, J<sub>GEM</sub>=13.70 Hz, 2H, methylene), 4.06 (d, J<sub>GEM</sub>=13.70 Hz, 2H, methylene), 2.51 (d, 2H, "CH" cyclohexane), 2.22 (m, 2H, cyclohexane), 1.77 (m, 3H, cyclohexane), 1.14-1.41 (m, 2H, cyclohexane), 1.00 (m, 1H, cyclohexane). <sup>13</sup>C-NMR (CDCl<sub>3</sub>) δ (ppm) 25.21 (2 CH<sub>2</sub>), 25.39 (CH<sub>2</sub>), 31.38 (CH<sub>2</sub>), 52.42 (CH), 55.35 (CH), 57.60 (2 CH<sub>2</sub>), 118.02 (-2CH Ar), 126.42 (-2CH), 126.78 (-2CH), 127.54 (-C), 127.62 (-C-), 130.45 (-2CH), 136.40 (-2C-), 152.22 (-2CH), 153.59 (-2CH), 153.85 (-C-N), 154.35 (-C-N).

*{[2-(tert-Butoxycarbonylmethyl-isoquinolin-3-ylmethyl-amino)-cyclohexyl]-isoquinolin-3-ylmethyl-amino}-acetic acid tert-butyl ester (**13**):* Amine **12** (0.844 mmol) was dissolved in a mixture of anhydrous acetonitrile (13 mL) and

anhydrous potassium carbonate (0.315 g, 2.28 mmol) under inert condition (Argon). Then, a solution of tert-Butyl 2-bromoacetate (0.312 ml, 2.11 mmol), in anhydrous acetonitrile (5 mL) was added dropwise over 5 minutes. After stirring 12 h at room temperature dichloromethane was added and the reaction mixture was washed with brine solution. The organic phase was evaporated under reduced pressure to give 0.588 g of yellowish oil. The product was purified by chromatographic column on activated neutral alumina (Al<sub>2</sub>O<sub>3</sub>). Conditioning with Cy:AcOEt 7:3, elution with Cy:AcOEt 6:4 to 1:9 (Rf: 0.35), for removing the more apolar impurities, followed by complete collection of the product with AcOEt:MeOH 9:1, giving 380 mg of a yellowish solid. Yield:72% Purity: ≈70% mol. <sup>1</sup>H-NMR (CDCl<sub>3</sub>) δ (ppm) 9.04 (s, 1H), 8.10 (s, 1H), 7.98 (m, 1H), 7.88 (d, J= 7.39 Hz, 2H), 7.74 (m, 3H), 7.56 (m, 4H), 4.26 (m, 6H), 4.04 (m, 1H), 3.62 (m, 1H), 2.79 (m, 1H), 2.31 (m, 2H), 1.83 (m, 3H), 1.46 (s, 18H), 1.28-1.02 (m, 4H).

*[[2-(Carboxymethyl-isoquinolin-3-ylmethyl-amino)-cyclohexyl]-isoquinolin-3-ylmethyl-amino}-acetic acid (H<sub>2</sub>L12, ligand as ammonium salt):* the previous tert-butyl ester **13** (crude, ≈5.15 mmol) was dissolved in HCl aq (6 M, 80 ml); the obtained reaction mixture was stirred for 12 h at 80°C. The reaction mixture was reduced under reduced pressure until around half volume; the remaining residue containing the trifluoroacetate salt was purified by cationic exchange chromatography SCX (eluent: NH<sub>3</sub> 3M in MeOH, 2g X 14) giving 1.55 g of the desired product as a brownish solid. Yield: 55%, purity: ≈70% mol. <sup>1</sup>H-NMR spectrum (DMSO) δ ppm: 9.31-9.21 (m, 2H), 8.15-8.05 (m, 2H), 8.01-7.89 (m, 2H), 7.80-7.71 (m, 2H), 7.69-7.58 (m, 2H), 4.96-4.71 (m, 1H, CH<sub>2</sub>), 4.30-3.63 (m, 4H, CH<sub>2</sub>), 3.56-3.21 (m, 3H, CH<sub>2</sub>), 2.30-1.82 (m, 3H, Cy), 1.76-1.50 (m, 3H, Cy), 1.37-0.96 (m, 4H, Cy). UV-Vis absorption spectroscopy (methanol): ε(322 nm): 5174 M<sup>-1</sup>cm<sup>-1</sup>. ESI-MS (Scan ES+; m/z): 573 (100%)=510 (deprotonated ligand) + K<sup>+</sup> + Na<sup>+</sup>.

The cationic complex **Eu(L12)OTf** has been synthesized as follows: Ligand **H<sub>2</sub>L12** (60 mg, 0.110 mmol) was dissolved in hot (55°C) 2-propanol (4 ml). Upon cooling, europium(III) trifluoromethanesulfonate 98% (66 mg, 0.110 mmol) was added portion-wise, and a yellowish suspension was formed. After neutralization

with KOH 2M aq (pH  $\approx$ 7), the reaction mixture was stirred at room temperature for 12h. The suspension was centrifuged, the filtrate was concentrated under reduced pressure, and the resulting solid (105 mg) was purified by dissolution in methanol, followed by precipitation in diethyl ether. Upon centrifugation, 28.6 mg of the desired complex as a beigeish solid was collected. Yield: 32%. UV-Vis spectroscopy:  $\epsilon(323 \text{ nm})$ :  $4510 \text{ M}^{-1}\text{cm}^{-1}$  (water);  $\epsilon(323 \text{ nm})$ :  $7251 \text{ M}^{-1}\text{cm}^{-1}$  (methanol). ESI-MS(Scan ES+;  $m/z$ ): 663 (100%); 661 (90%); (MW deprotonated ligand [510]+Eu [151]= 661, ESI+:661/663).

*N-Isoquinolin-3-ylmethyl-cyclohexane-1,2-diamine* (**15**): *trans*-1,2-(2-Aminocyclohexyl)-carbamic acid tert-butyl ester (**2**) (1.45 g, 6.75 mmol) was added at RT to a stirred solution of isoquinoline-3-carbaldehyde **10** (1.06 g, 6.75 mmol) in anhydrous EtOH (80 ml). The orangish reaction mixture was stirred to room temperature for 12h; then, upon cooling at  $\approx 0^\circ\text{C}$  sodium borohydride (0.306 g, 8.10 mmol) was directly added one pot to the mixture to get a clear yellowish solution. After 4h, the reaction mixture was quenched with water and the product was extracted with dichloromethane. The collected organics were washed with brine solution and dried over sodium sulfate; upon removal of the solvent under reduced pressure, 2.40 g of a brownish oil was used as well as without further purification (quantitative yield, purity  $\approx$  75% mol). *{2-[(Isoquinolin-3-ylmethyl)-amino]-cyclohexyl}-carbamic acid tert-butyl ester*:  $^1\text{H-NMR}$  ( $\text{CDCl}_3$ )  $\delta$  (ppm) 9.18 (s, 1H), 7.92 (d,  $J=7.85 \text{ Hz}$ , 1H), 7.76 (d,  $J=8.26 \text{ Hz}$ , 1H), 7.64 (m, 2H), 7.53 (t,  $J=7.45 \text{ Hz}$ , 1H), 4.15 (d,  $J=14.30 \text{ Hz}$ , 1H), 3.96 (d,  $J=14.30 \text{ Hz}$ , 1H), 3.36 (m, 1H, Cy), 3.11 (m, 1H, Cy), 2.31 (m, 2H, Cy), 2.10 (m, 2H, Cy), 1.94 (m, 2H, Cy), 1.74-1.58 (m, 2H, Cy), 1.43 (s, 9H).  $^{13}\text{C-NMR}$  ( $\text{CDCl}_3$ )  $\delta$  (ppm) 24.81 (CH<sub>2</sub>), 25.011 (CH<sub>2</sub>), 25.18 (CH<sub>2</sub>), 28.403 (3-CH<sub>3</sub>), 32.84 (CH<sub>2</sub>), 51.72 (-2CH), 57.87 (CH<sub>2</sub>), 79.17 (C -CH<sub>3</sub>), 118.16 (CH-Ar), 126.38 (CH-Ar), 126.81 (CH-Ar), 127.53 (-C-Ar), 127.63 (-C-Ar), 130.53 (CH-Ar), 136.41 (CH-Ar), 152.13 (-CH-Ar), 153.38 (N-C-Ar), 156.22 (C=O). *{2-[(Isoquinolin-3-ylmethyl)-amino]-cyclohexyl}-carbamic acid tert-butyl ester* (6.75 mmol) was added to a trifluoroacetic acid 98% w/w (26 ml) and dichloromethane (52 ml) solution and stirred at room temperature for 12h. The solvent was removed under reduced

pressure, and the obtained residue was purified by cationic exchange chromatography (eluent:  $\text{NH}_3$  3M in MeOH) to give 880 mg of the free amine NH-BOC deprotected **15**. Yield=51%, Purity=93% mol.  $^1\text{H-NMR}$  ( $\text{CDCl}_3$ )  $\delta$  (ppm) 9.18 (s, 1H), 7.91 (d,  $J=8.3$  Hz, 1H), 7.76 (d,  $J=8.3$  Hz, 1H), 7.66-7.61 (m, 2H), 7.53 (t,  $J=7.4$  Hz, 1H), 4.17 (dd,  $J_{\text{GEM}}=13.69$  Hz, 1H), 3.95 (dd,  $J_{\text{GEM}}=13.69$  Hz, 1H), 2.49-2.40 (m, 1H), 2.26-2.20 (m, 1H), 2.20-2.09 (m, 2H), 1.91-1.77 (m, 2H), 1.74-1.59 (m, 2H), 1.31-1.15 (m, 1H), 1.15-1.02 (m, 1H).  $^{13}\text{C-NMR}$  ( $\text{CDCl}_3$ )  $\delta$  (ppm) 25.30 (CH<sub>2</sub>), 31.36 (CH<sub>2</sub>), 35.38 (CH<sub>2</sub>), 35.87 (CH<sub>2</sub>), 52.35 (-CH), 55.29 (-CH), 63.49 (-CH<sub>2</sub>), 118.10 (CH-Ar), 126.41 (CH-Ar), 126.77 (-C-Ar), 127.53 (-C-Ar), 127.60 (CH-Ar), 130.50 (CH-Ar), 136.42 (CH-Ar), 152.25 (-CH-Ar), 153.46 (N-C-Ar).

*{tert-Butoxycarbonylmethyl-[2-(tert-butoxycarbonylmethyl-isoquinolin-3-ylmethyl-amino)-cyclohexyl]-amino}-acetic acid tert-butyl ester (16)*: the previous deprotected amine **15** (3.45 mmol) was completely dissolved in anhydrous acetonitrile (50 mL). Afterwards, N,N-Diisopropylethylamine (2.10 ml, 12.08 mmol) was added dropwise over 10 minutes under inert condition (Argon). Then, a solution of tert-butyl 2-bromoacetate (1.78 ml, 12.08 mmol), in anhydrous acetonitrile (10 mL) was added dropwise over 10 minutes. After stirring 12 h at room temperature dichloromethane was added and the reaction mixture was washed with brine solution. The organic phase was evaporated under reduced pressure to give 2.2 g of brownish oil. The product was used as well as without further purification. Crude, purity:  $\approx 55\%$  mol.  $^1\text{H-NMR}$  ( $\text{CDCl}_3$ )  $\delta$  (ppm) 9.16 (broad, 1H), 8.79 (d, 1H;  $J=7.77$  Hz); 8.63 (s; 1H); 8.12 (d, 1H;  $J=8.40$  Hz); 8.07 (t, 1H;  $J=7.14$  Hz); 8-7.83 (broad, 1H); 6.42 (d, 1H;  $J=17.22$  Hz, CH<sub>2</sub>); 6.21 (d, 1H;  $J=17.22$  Hz, CH<sub>2</sub>); 4.48 (d, 2H;  $J=15.96$  Hz, CH<sub>2</sub>); 4.30 (d, 2H;  $J=15.96$  Hz, CH<sub>2</sub>); 4.08-3.94 (broad, 2H, Cy); 3.71 (m, 2H, Cy); 3.63-3.37 (broad, 2H, CH<sub>2</sub>); 3.35-3.31 (m, 1H, Cy); 3.15 (m, 1H, Cy); 2.66-2.57 (broad, 1H, Cy); 2.04 (m, 1H, Cy); 1.43 (s; 27H, tBu); 1.15-1.04 (broad, 2H, Cy).

*{Carboxymethyl-[2-(carboxymethyl-isoquinolin-3-ylmethyl-amino)-cyclohexyl]-amino}-acetic acid (H<sub>3</sub>L13, ligand as ammonium salt)*: the previous tert-butyl

ester **16** (crude,  $\approx 1.90$  mmol) was dissolved in HCl aq (6 M, 80 ml) and stirred for 15 h at 80°C. The volume of the reaction mixture was halved under reduced pressure and the product was purified by cationic exchange chromatography SCX (eluent: NH<sub>3</sub> 3M in MeOH, 2g cartridges x 7) giving 313 mg of the desired product as a brownish solid. Yield: 34%, purity:  $\approx 65\%$ . <sup>1</sup>H-NMR (DMSO)  $\delta$  ppm: 9.88 (s, 1H), 8.17-8.04 (m, 2H), 7.97-7.87 (m, 2H), 7.68-7.54 (m, 1H), 5.21-5.10 (d broad, 1H, CH<sub>2</sub>), 4.44-4.32 (d broad, 1H, CH<sub>2</sub>), 4.30-4.22 (d broad, 1H, CH<sub>2</sub>), 4.15-4.03 (m, 2H, CH<sub>2</sub>), 4.00-3.91 (m, 1H, CH<sub>2</sub>), 3.56-3.19 (m, 2H, CH<sub>2</sub>), 2.28-2.13 (m, 1H, Cy), 2.04-1.86 (m, 2H, Cy), 1.76-1.54 (m, 3H, Cy), 1.35-1.06 (m, 4H, Cy). UV-Vis absorption spectroscopy (methanol):  $\epsilon(332 \text{ nm})$ : 3420 M<sup>-1</sup>cm<sup>-1</sup>. ESI-MS (Scan ES+;  $m/z$ ): 512 (100%) = [Na<sub>2</sub>KHL]<sup>+</sup>; L = L13<sup>3-</sup>.

The complex **Eu(L13)** has been synthesized as follows: ligand **H<sub>3</sub>L13** (300 mg, 0.625 mmol) was dissolved at room temperature in a mixture of water: methanol 9:1 (10 ml). Then, europium(III) trifluoromethanesulfonate 98% (374 mg, 0.625 mmol) was added portion-wise, and a yellowish suspension was formed. After neutralization with KOH 2M aq (pH  $\approx 7$ ), the reaction mixture was stirred at room temperature for 1h. The suspension was centrifuged to furnish 187 mg of the desired complex **7** as a yellowish solid. Yield: 52%. UV-Vis spectroscopy:  $\epsilon(328 \text{ nm})$ : 2851 M<sup>-1</sup>cm<sup>-1</sup> (methanol).

As far as <sup>1</sup>H and <sup>13</sup>C-NMR spectroscopy; ESI-MS measurements; Luminescence and decay kinetics and UV Absorption spectroscopy are concerning: see the experimental part of Chapter 3 for technical information.

### 4.5.3. *Elemental analysis*

The analyses were carried out by using a EACE 1110 CHNOS analyzer.

### 4.5.4. *Potentiometric titrations*

The protonation constants of the all ligands (**L4**, **L10**, **L11**, **L12** and **L13**) and the formation constants of the **L9** derivatives have been determined by acid-base potentiometric titrations.

The titration cell was maintained at constant temperature ( $298.15 \pm 0.1$  K) using a circulatory bath. A computer-controlled potentiometer (Amel Instruments, 338 pH Meter) collected the electromotive force (emf) values measured by means of a combined glass electrode (Metrohm Unitrode 6.0259.100). Before each titration the electrode was calibrated by an acid-base titration with standard HCl and NaOH solutions and the carbon dioxide contamination in solution was checked by Gran method.<sup>68</sup> Titrations were performed in duplicate on solutions containing the ligand (typical concentration around 0.6-0.9 mM) and an excess of standard HCl by adding standard NaOH solution. The pH range was varied from an initial approximate value of 2.3 to about pH 11.5. All the solutions were prepared with ultrapure water ( $>18$  M $\Omega$  cm) from a Milli-Q system (ELGA Purelab Option-Q) and the ionic strength ( $\mu$ ) was adjusted to 0.1 M by using appropriate amounts of NaCl (Sigma-Aldrich). Among 50-70 points were collected in each titration and processed with Hyperquad.<sup>8</sup>

#### **4.5.5. Spectrophotometric titrations**

The formation constants of the remaining Ln(III) complexes (Eu(L4), Eu(L10), Tb(L10), Eu(L11)OTf, Eu(L12)OTf and Eu(L13), Figure 2) were determined by UV-Vis spectrophotometric acid-base titrations.<sup>69</sup> A Varian Cary 50 instrument equipped with a fibre optic (optical path of 10mm) was used. The wavelength range investigated was 240-300 nm for **L10** and 275-355 nm for **L4** and **L11** in the same pH range and  $\mu$  as in the potentiometry. The titration cell was maintained at  $T = 298.15 \pm 0.15$  K by means of a circulatory bath, and contained both the ligand (ligand **L11**, 0.08 mM with Eu(III); ligand **L10**, 0.13 mM with Eu(III), 0.15 mM with Tb(III); ligand **L4**, 0.09 mM with Eu(III)) and Ln(III) (1:1 L:Ln(III) ratio, with a slight metal excess). The NaOH and HCl stock solutions were the same used during the potentiometric titrations. The stock solutions of Eu(III) and Tb(III) were prepared by dissolving their chloride hexahydrate salts (Sigma-Aldrich). The lanthanide content in the stock solutions was determined by EDTA titration, using xylenol orange as indicator.<sup>70</sup> Free acid concentrations in lanthanide solutions were checked by Gran's method.<sup>68</sup> Formation constants were

calculated by simultaneous fit of the absorbance values at several wavelengths using HypSpec.<sup>8</sup>

#### **4.5.6. Luminescence and decay kinetics**

Room temperature luminescence was measured with a Fluorolog 3 (Horiba-Jobin Yvon) spectrofluorometer, equipped with a Xe lamp, a double excitation monochromator, a single emission monochromator (mod. HR320) and a photomultiplier in photon counting mode for the detection of the emitted signal. All the spectra were corrected for the spectral distortions of the setup.

In decay kinetics measurements, a Xenon microsecond flashlamp was used and the signal was recorded by means of multichannel scaling method. True decay times were obtained using the convolution of the instrumental response function with an exponential function and the least-square-sum-based fitting program (SpectraSolve software package). The total quantum yields ( $\Phi_{\text{Tot}}$ ) have been obtained by secondary methods described in the literature<sup>71</sup> by measuring the Visible emission spectrum of quinine bisulfate in 1N H<sub>2</sub>SO<sub>4</sub> solution, a fluorescence quantum yield reference sample ( $\Phi = 54.6\%$ ).  $\Phi_{\text{Tot}}$  for the complexes has been calculated by  $[(A_s \cdot F_u \cdot n^2)/(A_u \cdot F_s \cdot n_0^2)] \cdot \Phi_s$  equation; where: u subscript refers to unknown and s to the standard and other symbols have the following meanings:  $\Phi$  is quantum yield, A is absorbance at the excitation wavelength, F the integrated emission area across the band and n's are respectively index of refraction of the solvent containing the unknown (n) and the standard (n<sub>0</sub>) at the sodium D line and the temperature of the emission measurement (Figures 36-41).

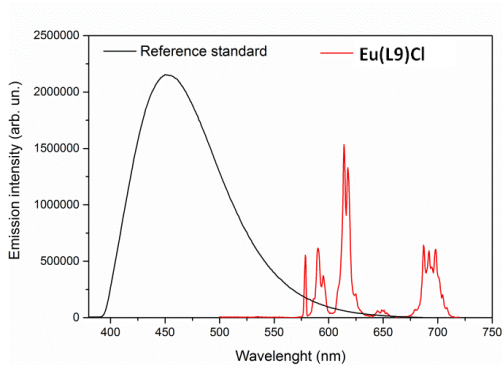


Figure 36. Overlap of the emission spectra of the reference standard and  $\text{Eu(L9)Cl}$  for the Quantum Yield measurement. Slits width was adjusted as 3/3 nm for excitation and 1.5/1.5 nm for emission.  $A_s = 0.06$ ;  $A_u = 0.073$ .  $\lambda_{exc} = 347$  nm and 270 nm, for the standard and the complex, respectively.

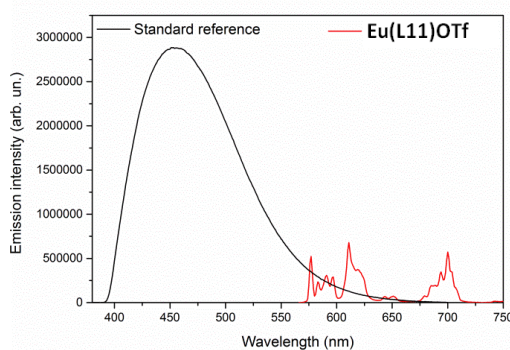


Figure 37. Overlap of the emission spectra of the reference standard and  $\text{Eu(L11)OTf}$  for the Quantum Yield measurement. Slits width was adjusted as 4/4 nm for excitation and 2/2 nm for emission.  $A_s = 0.06$ ;  $A_u = 0.09$ .  $\lambda_{exc} = 347$  nm and 319 nm, for the standard and the complex, respectively.

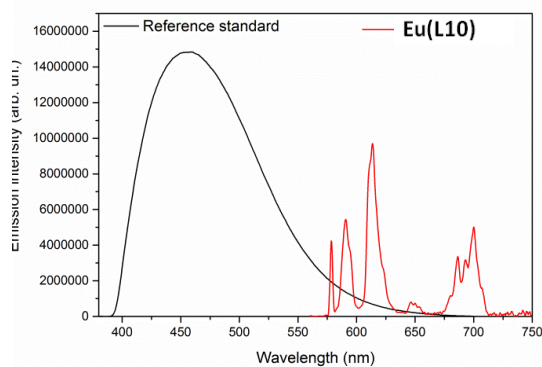


Figure 38. Overlap of the emission spectra of the reference standard and  $\text{Eu(L10)}$  for the Quantum Yield measurement. Slits width was adjusted as 3/3 nm for excitation and 3/3 nm for emission.  $A_s = 0.06$ ;  $A_u = 0.088$ .  $\lambda_{exc} = 347$  nm and 266 nm, for the standard and the complex, respectively.



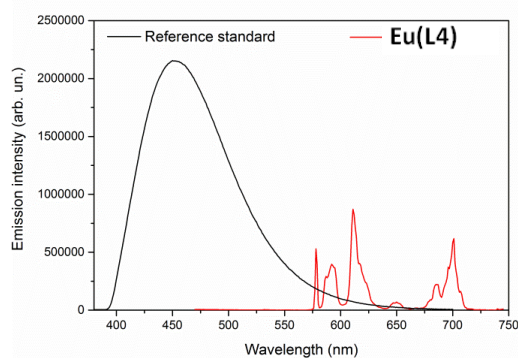


Figure 39. Overlap of the emission spectra of the reference standard and Eu(L4) for the Quantum Yield measurement. Slits width was adjusted as 3/3 nm for excitation and 1.5/1.5 nm for emission.  $A_s = 0.06$ ;  $A_u = 0.0875$ .  $\lambda_{exc} = 347$  nm and 319 nm, for the standard and the complex, respectively.

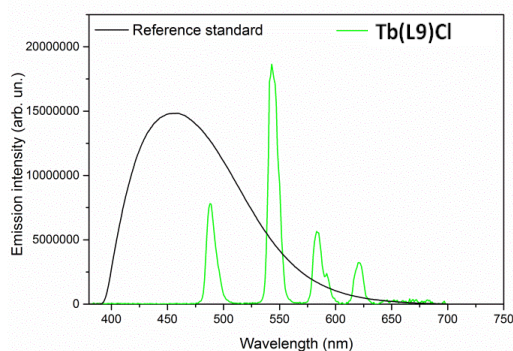


Figure 40. Overlap of the emission spectra of the reference standard and Tb(L9)Cl for the Quantum Yield measurement. Slits width was adjusted as 3/3 nm for excitation and 3/3 nm for emission.  $A_s = 0.06$ ;  $A_u = 0.072$ .  $\lambda_{exc} = 347$  nm and 270 nm, for the standard and the complex, respectively. **For the measurement of the intrinsic quantum yield ( $\phi_{Ln}$ ), direct excitation of Tb(III) was performed ( $\lambda_{exc} = 377$  nm) on a solution of the complex with  $A_u = 0.03$ .**

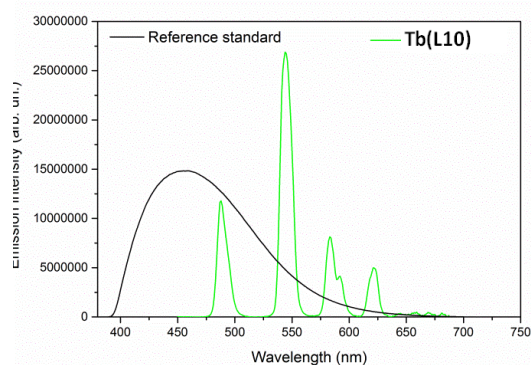


Figure 41. Overlap of the emission spectra of the reference standard and Tb(L10) for the Quantum Yield measurement. Slits width was adjusted as 3/3 nm for excitation and 3/3 nm for emission.  $A_s = 0.06$ ;  $A_u = 0.068$ .  $\lambda_{exc} = 347$  nm and 270 nm, for the standard and the complex, respectively. **For the measurement of the intrinsic quantum yield ( $\phi_{Ln}$ ), direct excitation of Tb(III) was performed ( $\lambda_{exc} = 377$  nm) on a solution of the complex with  $A_u = 0.011$ .**

#### 4.5.7. Luminescence sensing of $\text{HCO}_3^-$

The binding interactions between hydrogen carbonate and the Eu(III) complexes were studied using the double reciprocal plot following the Benesi-Hildebrand equation<sup>72</sup> adapted to the values of the asymmetry ratio ( $R$ ) of the Eu(III) emission spectra:

$$\frac{R_0}{R - R_0} = \frac{R_0}{R_\infty - R_0} + \frac{R_0}{\{K(R_\infty - R_0)[\text{HCO}_3^-]^n\}}$$

where  $R_0$ ,  $R$ , and  $R_\infty$  are the asymmetry ratio of Eu(III) in the complexes considered in the absence of hydrogen carbonate, at an intermediate hydrogen carbonate concentration and at a concentration of complete interaction, respectively. In the above equation,  $K$  is the binding constant and  $n$  the number of hydrogen carbonate anion bound to the metal center and  $[\text{HCO}_3^-]$  is the hydrogen carbonate concentration.

#### 4.5.8. Molecular Docking (MD)

##### 4.5.8.1. Methods

$\text{Eu}^{+3}$  complexes, *Figure 1*, were docked against the bovine serum albumin crystal structure (PDB code: 4F5S) using the Autodock suite version 4.2.6.<sup>73</sup> Two flexible docking experiments for each complex against two binding sites were performed. These were chosen in order to include the two tryptophan residues of the structure. The flexible residues were selected according a cut-off of 6Å of the each tryptophan residue: R194, L197, R198, S201, W213, N217, A341, V342, S343, D450, L454 and E16, E17, F126, K127, A128, D129, E130, K132, F133, W134, N158, N161, Q165 around W213 and W134, respectively. Since, Autodock suite doesn't include by default the  $\text{Eu}^{+3}$  parameters in its force-field, those were manually added to the parameter's library. For each Autodock run a cluster analysis over 100 binding poses were performed.

#### 4.5.8.2. MD Simulations

From each docking cluster analysis, a docked structure from the better cluster was chosen for perform small molecular dynamics simulations. All MD simulations were carried out using the GROMACS program, version 2016.5.<sup>74</sup>

Since the  $\text{Eu}^{+3}$  parameters are not included by default in the most commonly used force-fields, they had to be included manually into the force-field. Also, because  $\text{Eu}^{+3}$  interacts in a non-covalent way with the remaining molecular structure, it was treated as an ion. Therefore, the parameters of each component of the docked structured was prepared differently. The molecule without  $\text{Eu}^{3+}$  was parametrized with the ANTECHAMER suite,<sup>75</sup> the protein was parametrized using the pdb3gmx form GROMACS with the AMBER99SB force-field, and the  $\text{Eu}^{+3}$ , as was mentioned above, was treated as an ion.  $\text{Eu}^{+3}$  parameters were included manually in the force-field.<sup>76</sup> Water and ion molecules (0.154 M of  $\text{Na}^+/\text{Cl}^-$  to mimic physiological conditions) were added to complete the system. The system was then equilibrated through a complete workflow: steepest descents minimization of 5000 steps, NVT equilibration of 100 ps, NPT equilibration of 100 ps, and MD production under the NPT ensemble for 100 ns at room temperature. A pull code with  $5000 \text{ kJ mol}^{-1} \text{ nm}^{-2}$  of force between the nitrogen, oxygen, and  $\text{Eu}^{3+}$  atoms was included in the MD production to keep the integrity of the complexes. All calculations were performed within a GPU node available by the computational platform from the “*Centro Piattaforme Tecnologiche*” of the University of Verona.

#### 4.6. References

1. [Tortora G. *Principles of anatomy and physiology* (5th ed.). **1987** New York, NY: Harper and Row. p. 693, ISBN 978-0-06-350729-6].
2. [S. J. Butler, D. Parker, *Chem. Soc. Rev.* **2013**, 42, 1652–1666].
3. [M. Leonzio, A. Melchior, G. Faura, M. Tolazzi, F. Zinna, L. Di Bari and F. Piccinelli, *Inorg. Chem.*, **2017**, 56, 4413–4422].
4. [M. Mihorianu, M. Leonzio, M. Monari, L. Ravotto, P. Ceroni, M. Bettinelli and F. Piccinelli, *Chem. Sel.* **2016**, 1, 1996–2003].

5. [D. W. Lee, H. J. Ha and W. K. Lee, *Synth. Commun.*, **2007**, 37, 737–742].
6. [A. E. Martell, *Determ. and Use of Stab. Constants*, **1992**, VCH].
7. [L. Alderighi, P. Gans, A. Ienco, D. Peters, A. Sabatini, A. Vacca, *Coord. Chem. Rev.* **1999**, 184, 311–318].
8. [P. Gans, A. Sabatini, A. Vacca, *Talanta* **1996**, 43, 1739–1753].
9. [E. M. Gale, S. Mukherjee, C. Liu, G. S. Loving and P. Caravan, *Inorg. Chem.*, **2014**, 53, 10748–10761].
10. [R. Ferreirós-Martínez, D. Esteban-Gómez, C. Platas-Iglesias, A. de Blas, T. Rodríguez-Blas, *Dalton Trans.* **2008**, 5754–65].
11. [A. V. Rayer, K. Z. Sumon, L. Jaffari, A. Henni, *J. Chem. Eng. Data* **2014**, 59, 3805–3813].
12. [G. Anderegg, *Helv. Chim. Acta*, **1974**, 57, 1340–1346].
13. [K. Kahmann, H. Sigel and H. Erlenmeyer, *Helv. Chim. Acta*, **1964**, 47, 1754–1763].
14. [H. Kitano, Y. Onishi, A. Kirishima, N. Sato and O. Tochiyama, *Radiochim. Acta*, **2006**, 94, 541–547].
15. [P. Caravan, S. J. Rettig, and C. Orvig, *Inorg. Chem.* **1997**, 36, 1306–1315].
16. [P. Caravan, P. Mehrkhodavandi and C. Orvig, *Inorg. Chem.*, 1997, **36**, 1316–1321].
17. [S. L. Wu, and W. D. Horrocks, *Anal. Chem.* **1996**, 68, 394–401].
18. [R. M. Smith and A. E. Martell, *Sci. Total Environ.*, **1987**, 64, 125–147].
19. [P. Di Bernardo, A. Melchior, M. Tolazzi, P. L. Zanonato, *Coord. Chem. Rev.* **2012**, 256 (1–2), 328–351].
20. [L. Tei, Z. Baranyai, L. Gaino, A. Forgács, A. Vágner and M. Botta, *Dalt. Trans.*, **2015**, 44, 5467–5478].
21. [K. Binnemans, *Coord. Chem. Rev.*, **2015**, 295, 1–45].
22. [M. H. V. Werts, R. T. F. Jukes and J. W. Verhoeven, *Phys. Chem. Chem. Phys.*, **2002**, 4, 1542–1548].
23. [D. L. Dexter *The J. Chem. Phys.* **1953**, 21, 836].
24. [D. Parker, P. K. Senanayake and J. A. G. Williams, *J. Chem. Soc. Perkin Trans.* **1998**, 2, 0, 2129–2140].
25. [C. Li, Y. Liu, Y. Wu, Y. Sun and F. Li, *Biomat.* **2013**, 34, 1223–1234].
26. [M. Leonzio, A. Melchior, G. Faura, M. Tolazzi, M. Bettinelli, F. Zinna, L. Arrico, L. Di Bari and F. Piccinelli, *New J. Chem.*, **2018**, 42, 7931–7939].
27. [P. Di Bernardo, P. L. L. Zanonato, A. Bismondo, A. Melchior and M. Tolazzi,

- Dalton Trans.*, **2009**, 4236–4244].
28. [A. C. Mendonça, A. F. Martins, A. Melchior, S. M. Marques, S. Chaves, S. Villette, S. Petoud, P. L. Zanonato, M. Tolazzi, C. S. Bonnet, É. Tóth, P. Di Bernardo, C. F. G. C. Geraldés and M. A. Santos, *Dalton Trans.*, **2013**, 42, 6046–57].
  29. [S. Cotton, *Lanth. and Act. Chem.*, John Wiley & Sons, Ltd, **2006**].
  30. [M. J. Frisch, G. W. Trucks, H. B. Schlegel, G. E. Scuseria, M. A. Robb, J. R. Cheeseman, G. Scalmani, V. Barone, G. A. Petersson, H. Nakatsuji, et al., *Gaussian 16 Revis.* **2016**, A 03].
  31. [R. M. Supkowski, W. D. W. Horrocks, *Inorg. Chim. Acta* **2002**, 340, 44–48].
  32. [P. Polese, M. Tolazzi, A. Melchior, *J. Therm. Anal. Calorim.* **2018**, 2].
  33. [H. Brandenburg, J. Krahmer, K. Fischer, B. Schwager, B. Flöser, C. Näther, F. Tuzek, *Eur. J. Inorg. Chem.* **2018**, 2018, 576–585].
  34. [S. G. Lanas, M. Valiente, M. Tolazzi, A. Melchior, *RSC Adv.* **2016**, 6, 42288–42296].
  35. [C. Comuzzi, P. Polese, A. Melchior, R. Portanova, M. Tolazzi, *Talanta* **2003**, 59, 67–80].
  36. [D. Posada, T. R. Buckley, *Syst. Biol.* **2004**, 53, 793–808].
  37. [C. A. Wagner, J. Kovacicova, P. A. Stehberger, C. Winter, C. Benabbas and N. Mohebbi, *Nephron - Physiol.*, **2006**, 103, p1-6].
  38. [J. D. Kopple, K. Kalantar-Zadeh and R. Mehrotra, *Kidney Int. Suppl.*, **2005**, 67, S21–S27].
  39. [F. Piccinelli, C. De Rosa, A. Melchior, G. Faura, M. Tolazzi, M. Bettinelli. *Dalton Trans.* **2019**, 48, 1202-1216].
  40. [S. J. Butler, B. K. McMahon, R. Pal, D. Parker and J. W. Walton, *Chem. - A Eur. J.*, **2013**, 19, 9511–9517].
  41. [D. Imperio, G. B. Giovenzana, G. L. Law, D. Parker and J. W. Walton, *Dalt. Trans.*, **2010**, 39, 9897–9903].
  42. [Y. Bretonniere, M. J. Cann, D. Parker and R. Slater, *Org. Biomol. Chem.*, **2004**, 2, 1624–1632].
  43. [D. G. Smith, R. Pal and D. Parker, *Chem. - A Eur. J.*, **2012**, 18, 11604–11613].
  44. [K. D. Volkova, V.B. Kovalska, M.Yu. Losytskyy, A. Bento, L. V. Reis, P. F. Santos, P. Almeida, S. M. Yarmoluk, *J Fluoresc.* **2008**, 18, 877–882].
  45. [D. Carter, J.X. Ho, *Advances in Protein Chemistry.* **1994**, Vol. 45, Academic Press, New York, pp. 153-203].

46. [S. Curry, H. Mandelkow, P. Brick, N. Franks, *Nat. Struct. Biol.* **1998**, 5, 827-835].
47. [J.A. Reynolds, S. Herbert, H. Polet, J. Steinhardt, *Biochemistry* **1967**, 6, 937-947].
48. [F. Moreno, M. Cortijo, J.G. Jimenez, *Photochem. Photobiol.* **1999**, 69, 8-15].
49. [T. Kosa, T. Maruyama, M. Otagiri, *Pharm. Res.* **1997**, 14 (11) 1607-1612].
50. [X.-L. Han, F.-F. Tian, Y.-S. Ge, F.-L. Jiang, L. Lai, D.-W. Li, Q.-L. Yu, J. Wang, C. Lin, Y. Liu, *Journal of Photochemistry and Photobiology B: Biology* **2012**, 109, 1–11].
51. [P. Caravan, *Acc. Chem. Res.* **2009**, 42, 851–862].
52. [M. K. Thompson, D. M. J. Doble, L. S. Tso, S. Barra, M. Botta, S. Aime, K. N. Raymond, *Inorg. Chem.* **2004**, 43, 8577–8586].
53. [Kr G. Shyamal, S. Swarna Kamal, M. Manini, P. S. Sardar, and G.Sanjib *Inorg. Chem.* **2013**, 52, 1476–1487].
54. [Y. O. Fung, W. Wu, C.-T. Yeung, H.-K. Kong, K. K.-Cheng Wong, W.-S. Lo, G.-L. Law, K.-L. Wong, C.-K. Lau, C.-S. Lee, and W.-T. Wong . *Inorg. Chem.* **2011**, 50, 5517–5525].
55. [SK Ghorai, SK Samanta, M. Mukherjee and G.Sanjib *J. Phys. Chem. A* **2012**, 116, 8303–8312].
56. [S. Comby and T. Gunlaugsson, *Acs Nano*, 2011, 5(9), 7184–7197].
57. [G. Sumit, A. Zafar, D. Srikanth, P. Ashis, *J. Luminescence* **2017**, 187, 46–52].
58. [J. Bao, Z. Zhang, R. Tang, H. Han, Z. Yang, *J. Luminescence* **2013**, 136 68–74].
59. [Z. Yang, R. Tang, Z. Zhang, *J. Mol. Struct.* **2012**, 1030 19–25].
60. [L. Shen, Z. Yang, R. Tang, *Spectr. Act. Part A: Mol. and Biomol. Spectr.* **2012**, 98, 170–177].
61. [Z. Zhang, R. Tang, *J. Mol. Struct.* **2012**, 1010, 116–122].
62. [A. Brandner, T. Kitahara, N. Beare, C. Lin, M. T. Berry and P. S. May, *Inorg. Chem.*, **2011**, 50, 6509–6520].
63. [J. C. G. Bünzli and S. V. Eliseeva, *Elsevier*, **2013**, vol. 8, pp. 339–398].
64. [S. Aime, E. Gianolio, E. Terreno, G.B. Giovenzana, R. Pagliarin, M. Sisti, G. Palmisano, M. Botta, M.P. Lowe, D. Parker, *J. Biol. Inorg. Chem.* **2000**, 5, 488–497].
65. [H. Alsamamra, M. Abuteir, S. Darwish *J. Biomed.Sci.* **2019**, vol 8, NO 1:2].

66. [J. Li, J. Li, Y. Jiao, C. Dong, *Spectrochim. Acta A Mol. Biomol. Spectrosc.* **2014**, 118, 48–54].
67. [J.R. Lakowicz, *Principles of Fluorescence Spectroscopy*, **2006**, 3rd ed., Springer, New York].
68. [G. Gran, *Analyst*, **1952**, 77, 661].
69. [L. Toso, G. Crisponi, V. M. Nurchi, M. Crespo-Alonso, J. I. Lachowicz, D. Mansoori, M. Arca, M. A. Santos, S. M. Marques, L. Gano, J. Niclós-Gutiérrez, J. M. González-Pérez, A. Domínguez-Martín, D. Choquesillo-Lazarte and Z. Szewczuk, *J. Inorg. Biochem.*, **2014**, 130, 112–121].
70. [G. H. Jeffrey, J. Bassett, J. Mendham and R. C. Denney, *Vogel's textbook of quantitative chemical analysis*, John Wiley & Sons, **1990**, 5th edn., vol. 14].
71. [D.F. Eaton *Pure & Appl. Chem.*, **1988**, 60, 7, 1107-1114].
72. [H. A. Benesi and J. H. Hildebrand, *J. Am. Chem. Soc.*, **1949**, 71, 2703–2707].
73. [Morris G.M, Huey R, Lindstrom W, et al (**2009**) AutoDock4 and AutoDockTools4: Automated docking with selective receptor flexibility. *J. Com. Chem.* 30: 2785–2791].
74. [(**2005**) GROMACS: fast, flexible, and free. 26:1701–1718].
75. [(**2005**) Antechamber: an accessory software package for molecular mechanical calculations. 25:1157–1174].
76. [van Veggel FCJM, Reinhoudt DN (**1999**) *New, Accurate Lennard-Jones Parameters for Trivalent Lanthanide Ions*, Tested on [18]Crown–6. *Chemistry – A European Journal* 5:90–95].

## CHAPTER 5- High Throughput Screening (HTS) for detection of bioanalytes by means of Eu(III)-complexes based on Isoquinoline.

### 5.1. Introduction

As already discussed, one of the main drawbacks concerning the biosensing is the overlap between the absorption wavelengths of the probe and the biomolecules in the biological fluid under investigation.

An efficient luminescent bioprobe should be excited at least above 300 nm. Below this excitation wavelength, the majority of the biochromophores absorbs light by hampering the use of optical probes with an excitation wavelength below 300 nm. Furthermore, the irradiation in the far UV spectral region is rather phototoxic for cells, an additional reason to prefer bioprobes with longer excitation wavelength.

Among the several Ln(III)-complexes described in Chapter 4, the most promising bioprobes are surely the *Isoquinoline* di- and tri-acidic derivatives (Figure 1), whose excitation wavelength around 325 nm is quite red-shifted with respect to the analogous *Quinoline* (318 nm), and even more to the *Pyridine* derivatives (265 nm).

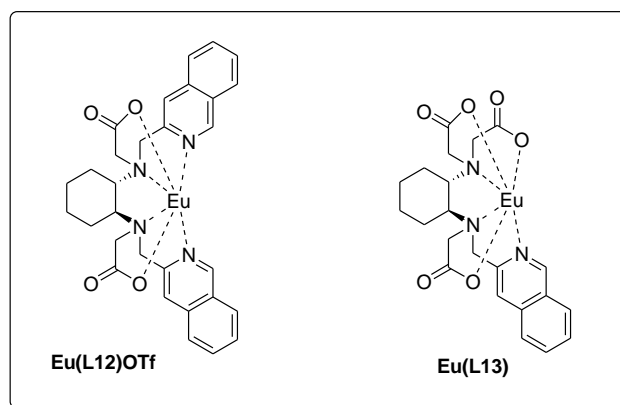


Figure 1. Eu(III)-complexes employed for sensing with HTS techniques, in accordance with similar physiological conditions (pH 7.4, ionic strength 0.9% NaCl w/v, T:25°C). Reference label from Chapter 4.

In order to find out a promising target capable to detect important analytes in the medical field, the possibility to explore simultaneously the interaction of a promising compound towards several biological targets is fundamental for reducing waste and time of analysis. In that context, the HTS is a method for



evaluating new target candidates by exploiting the microplates containing different biomolecules for a rapid and efficient screening. With this mind, whereas in the Chapter 4, all the luminescence measurements have been performed in a quartz cuvette with a traditional fluorometer, in this chapter the HTS has been used as alternative method to evaluate the luminescence response of the complexes **Eu(L12)OTf** and **Eu(L13)**, in the presence of bioanalytes contained in the extracellular fluid (ECF).

The main advantages to use a microplate reader instead of a traditional fluorometer concern the major *i) efficiency* and the *ii) reproducibility* of the data, since the addition have been quickly performed with an Eppendorf Multipette, with at least 6 measurement replicas. Moreover, the overall well volume of the microplate is around 250  $\mu\text{l}$ , by requiring *iii) a minor quantity* of sample to analyze. This is convenient when expensive molecules are used.

## 5.2. *Sensing of the main components of ECF*

### 5.2.1. *The oxophilic anions*

The main components of the ECF have been already listed in Table 1 of Chapter 4, but for sake of clarity are summarized again. Their typical extracellular concentration ranges are also reported:

- Bicarbonate ion (24-27 mM)
- Citrate ion (0.1-0.3 mM)
- Serum albumins ( $\approx$ 0.4 mM)
- L-lactate ion (0.6-2.3 mM)
- Sulphate ion (0.4-0.6 mM)
- Phosphate ion (1.2-1.3 mM)

It is worth evidencing that the extracellular matrix denotes all body fluid outside of cells, and consists of plasma, interstitial, and transcellular fluid.

The above biological composition is referred to the more simplified composition of the interstitial and transcellular fluids, which it is mainly composed by cations and anions, whereas the plasma contains mostly water but also, hormones, clotting

factors, glucose and different proteins.<sup>1</sup> As far as the protein contribution is concerned, only the major albumins have been considered, in their typical extracellular concentration range of 0.4 mM. Some other electrolytes, like NaCl are in a typical ECF (concentration ~ 100 mM). We take into account its contribution, since NaCl is present in the working buffer solution.

As already discussed in Chapter 3, all the trivalent lanthanide ions are classified as Hard acids and according to the "hard and soft (Lewis) acids and bases" (HSAB) theory they should preferentially interact with oxophilic ions like bicarbonate, citrate, lactate.

### ***5.2.2. The Bicarbonate ions: luminescence and binding constants***

The sensing experiments towards bicarbonate ion have been already discussed in Chapter 4, for Pyridine and Quinoline-based complexes. Some interesting results have been also observed in the case of Isoquinoline derivatives.

The increasing addition of the analyte to the complex **Eu(L12)OTf**, is capable to modify considerably the geometric environment around the metal center (change of R value from the initial value of 2.88 to 5.05 in the presence of 28 mM of NaHCO<sub>3</sub>). This is related to a consistent enhancement of the <sup>5</sup>D<sub>0</sub>→<sup>7</sup>F<sub>2</sub> luminescence intensity (Figure 2). The HCO<sub>3</sub><sup>-</sup> anion coordinates the Eu(III) ion, possibly displacing the water molecules from the inner coordination sphere, by reducing the undesirable multiphonon relaxation process. A decrease of the emission intensity of the <sup>5</sup>D<sub>0</sub>→<sup>7</sup>F<sub>0</sub> transition has been also detected, resulting in a minor axial geometry of the Eu(III) environment.

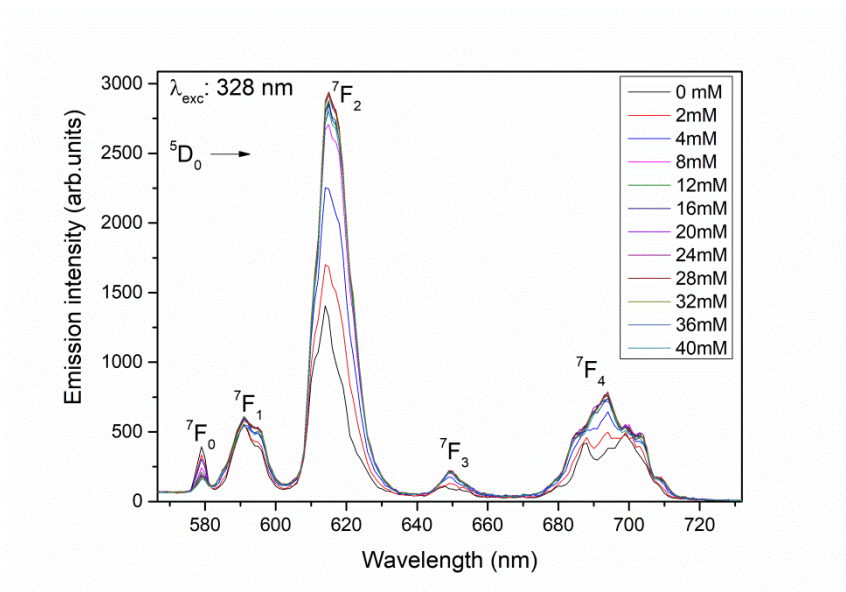
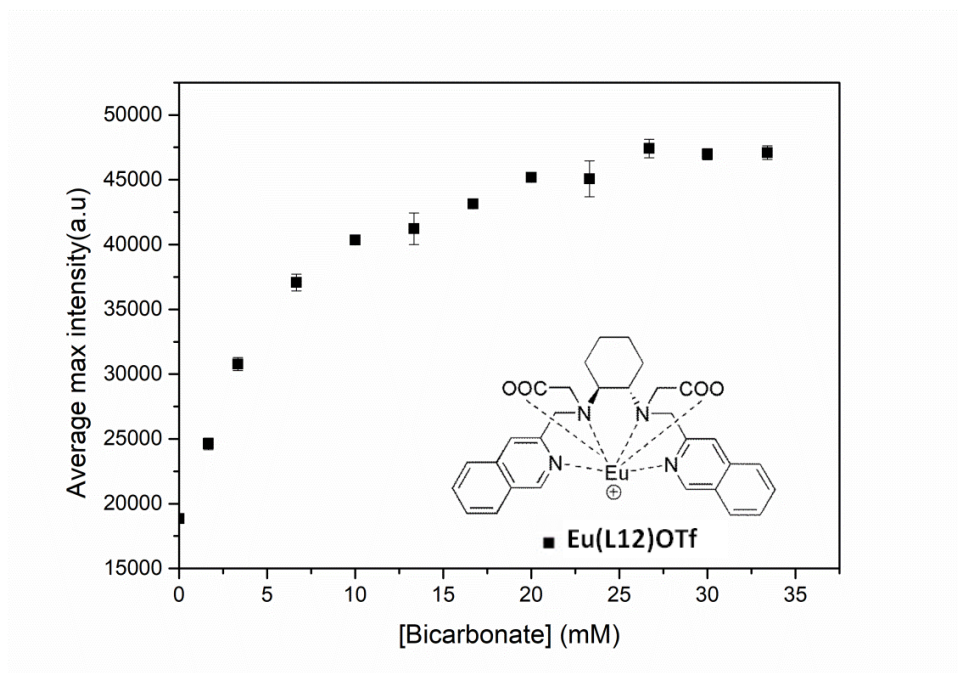


Figure 2. Eu(III) luminescence emission spectra of the complex Eu(L12)OTf [0.1 mM] in MOPS buffer 15 mM pH≈7.4, NaCl 0.15 mM; Excitation wavelength: 328 nm; Bandwidth Emission wavelength: 3 nm, Bandwidth Excitation wavelength: 10 nm, Gain: 109. The concentration of the anion is reported.

It is worth evidencing the trend of the average maximum intensity as a function of the target anion concentration. For both complexes **Eu(L12)OTf** and **Eu(L13)**, we observe an increase of this intensity, even if some discrepancies should be analyzed (Figure 3). In particular, *i*) the different relationship between intensities values and concentration of the target ion. A rapid parabolic enhancement has been obtained for the complex Eu(L12)OTf, whereas a linear increase has been observed for the complex Eu(L13). *ii*) the differences in the absolute emission intensity due to the number of chromophoric units in the complex. In fact, upon the same experimental conditions, complex Eu(L12)OTf shows higher maximum luminescence intensity than complex Eu(L13). Another important feature concerns *iii*) the different sensitivity of the complexes Eu(L12)OTf and Eu(L13) in the working concentration range of the ion. The bis-Isoquinoline complex Eu(L12)OTf showed the best sensitivity in the concentration range of  $\text{HCO}_3^-$  connected with the metabolic acidosis disease (2-10 mM, ref. Chapter 4). In fact, in complex Eu(L12)OTf, we detect an intensity increase of the luminescence around 120% ( $\approx 10$  mM  $\text{HCO}_3^-$ ), whilst for complex Eu(L13) only around 30% ( $\approx 10$  mM  $\text{HCO}_3^-$ ).

a)



b)

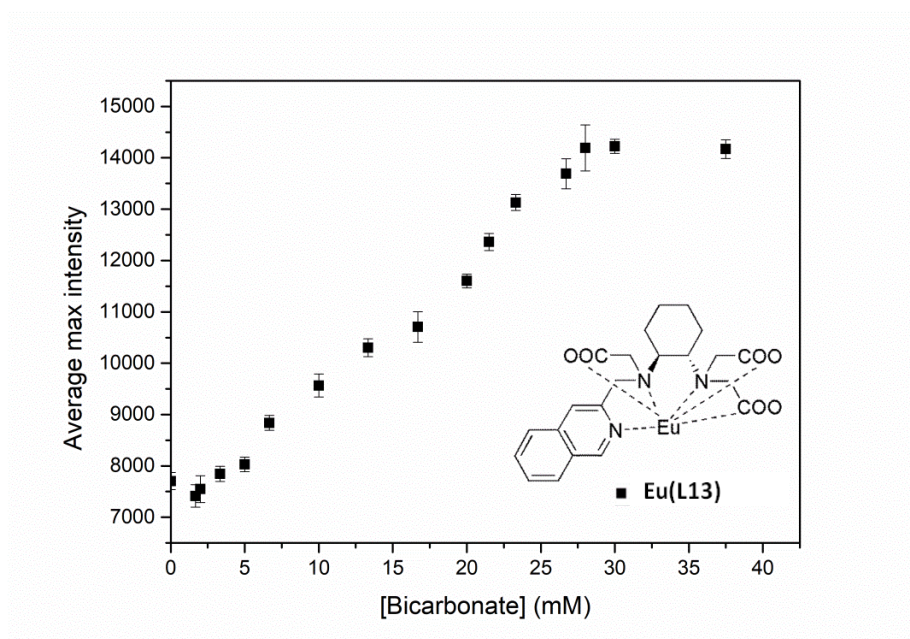


Figure 3. Average \* maximum intensity vs.  $[HCO_3^-]$  concentration plots for the complexes a)Eu(L12)OTf,  $I_{max} \approx 1.47$  fold increase,  $LOD = 0.123$  mM and b)Eu(L13),  $I_{max} \approx 0.85$  fold increase,  $LOD = 2.32$  mM . \* It is referred to an average of luminescence intensity upon 6 replicas. Emission wavelength: 615 nm, bandwidth: 20 nm, Excitation wavelength: 328 nm, bandwidth: 20 nm, Gain: 109.

The affinity constants have been calculated by means of cEST/Solverstat<sup>2,3</sup> software (Table 1, see Chapter 4, for details).

<b>Complex-HCO<sub>3</sub><sup>-</sup></b>	<b><i>n</i></b>	<b>Log(<i>K</i>)</b>
Eu(L12)OTf	2	4.60 ± 0.15 (1.58%)
Eu(L13)	1	3.38 ± 0.05 (0.78%)

Table 1. Apparent affinity constants (*logK*) constant for the formation of the adducts with bicarbonate (HCO<sub>3</sub><sup>-</sup>), [complex]<sup>+</sup>+*n*-bicarbonate ⇌ [complex(bicarbonate)<sub>*n*</sub>]<sup>+</sup> (*T* = 298 K, *pH* 7.40 (±0.05), *I* = 0.15 M NaCl, 0.1 mM complex), determined through cEST/Solverstat fitting. Charges omitted for clarity

As observed for the cationic complexes described in Chapter 4, two bicarbonate anions can bind the metal center also in the case of cationic complex Eu(L12)OTf. This results in a higher affinity constant (Table 1).

### 5.2.3. *The promising Citrate ion: luminescence and binding constants*

#### 5.2.3.1. *Introduction*

Citrate is a water soluble tricarboxylic acid and is characterized by an important roles in many biological processes.

In fact, it is well known that low levels of citrate in urine (usually around 10 - 12 μmol/g) may involve several kidney dysfunctions and even prostate cancer (1 - 3 μmol/g).<sup>4</sup>

Moreover, Citrate serum levels were abnormally high in patients with primary hyperparathyroidism (pHPT) which is characterized by skeletal involvement and/or renal lithiasis (RL) as main complications, essentially for the ability to subtract calcium salts.<sup>5</sup>

The most important roles involve the glycolysis and the Krebs cycle, where the Citric acid is produced in the mitochondria by the donation of a 2-carbon residue from acetyl-CoA to oxaloacetic acid. The excess of citric acid formed in the mitochondria during the Krebs cycle can also be transported to the cytoplasm where is converted into oxaloacetate and acetyl-CoA. The resulting acetyl-CoA is used in fatty acids and isoprenoid synthesis.<sup>4,6</sup>

Many examples in literature reports studies on citrate as a mere interfering agent<sup>7-</sup><sup>15</sup> or as analytes to be quantified.<sup>16-18</sup>

Some affinity constants found in literature for luminescent adducts between lanthanide complexes and citrate are listed in Table 2, where the positively-charged Ln(III) complexes interact stronger with the target anion.

Ref.	[19]	[20]	[17]	[18]	[21]	[16]
Log(K)	3.65	3.95**	4.80*	5.21	5.26*	6.02

Table 2. Apparent affinity constants of some Ln(III) complexes towards citrate,  $T = 298.15$  K,  $\mu = 0.1$  M NaCl,  $pH = 7.4$ . \*  $T = 295$  K, \*  $0.1$  M NaCl,  $4$  mM KCl,  $0.1$  M HEPES and  $0.9$  mM  $\text{NaH}_2\text{PO}_4$ , \*\*  $10$  mM ZnCl<sub>2</sub>.

### 5.2.3.2. Ln(III)-complexes-Citrate adducts: effects of the interferences

The simple calculation of the ratio  $[A^-]/[HA]$  by means of the Henderson-Hasselbach equation (1a) furnishes the predominant species under investigation, at the physiological  $pH=7.4$ .

$$\text{Log} \frac{[A^-]}{[HA]} = pH - pka \quad (\text{eq. 1a})$$

The already discussed bicarbonate possesses the following protonation constants  $pK_{a1} = 6.11$  and  $pK_{a2} = 9.87$  at  $298.15$  K, whereas the Citrate has three  $pK_a$  values:  $3.13$ ,  $4.76$  and  $6.40$  at  $T = 298.15$  K.<sup>6</sup>

Thus, under physiological conditions, the citrate is fully deprotonated.

On the other hand, according to the equation 1b, the predominant form of the C-based oxoanion is  $\text{HCO}_3^-$ .

$$\frac{[A^-]}{[HA]} = 10^{(pH-pka)} \quad (\text{eq. 1b})$$

Where  $[A^-]$  and  $[HA]$  are respectively the concentration of the conjugate base and the acid of the species under investigation.

As far as the carbonate ion is concerning the equations are:

$$\frac{[CO_3^{2-}]}{[HCO_3^-]} = 10^{(7.4-9.87)} = \frac{1}{10^{2.47}} \approx 1:295 \text{ (eq. 2)}$$

$$\frac{[HCO_3^-]}{[H_2CO_3]} = 10^{(7.4-6.11)} = \frac{10^{1.29}}{1} \approx 20:1 \text{ (eq. 3)}$$

In first analysis, just considering the electronic density of the target analyte, citrate shows a higher value. Since the probe-analyte interaction is mainly ruled by electrostatic interactions, we expect a higher affinity constant in the case of citrate adduct. This conclusion applies in the case of Eu(L13), where a 1:1 complex to analyte molar ratio is noticed for both citrate and  $HCO_3^-$  anions (compare Table 1 and 3).

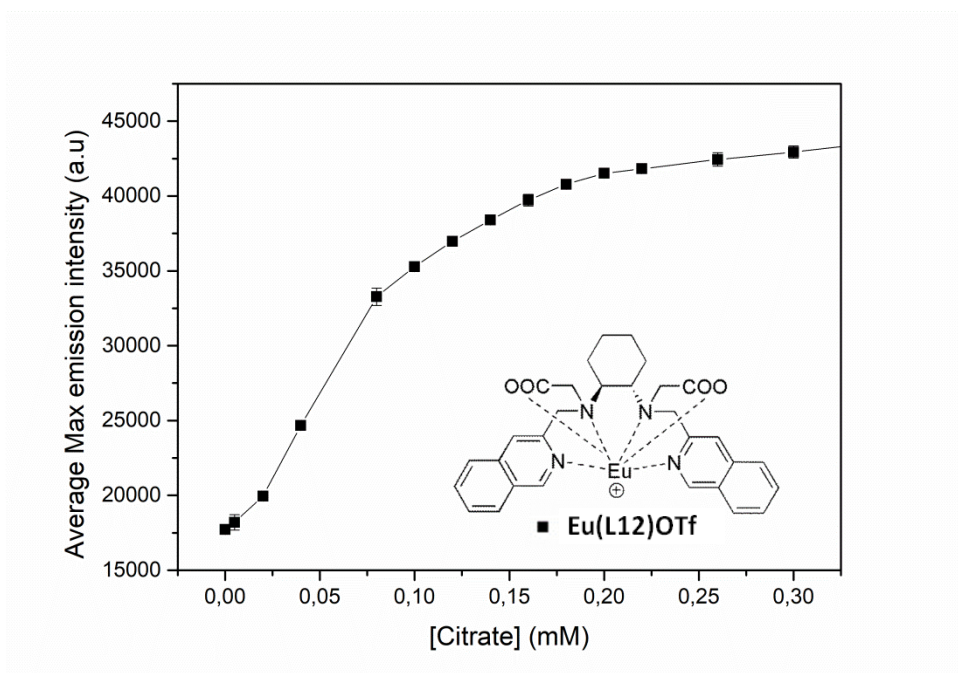
<b>Complex-Citrate</b>	<b>n</b>	<b>Log(K)</b>
Eu(L12)OTf	1	4.11 ± 0.26 (2.92%)
Eu(L13)	1	4.06 ± 0.15 (1.79%)

Table 3. Apparent affinity constants ( $\log K$ ) constant for the formation of the adducts with Citrate:  $[complex] + n\text{-citrate} \rightleftharpoons [complex(citrate)_n]$  ( $T = 298 \text{ K}$ ,  $pH 7.40 (\pm 0.05)$ ,  $I = 0.15 \text{ M NaCl}$ ,  $0.1 \text{ mM complex}$ ), determined through cEST/Solverstat fitting. Charges omitted for clarity

Regarding the different stoichiometry in the adducts with  $HCO_3^-$  and citrate involving Eu(L12)OTf, several remarks should be pointed out. In particular, upon interaction between the charged complex Eu(L12)OTf and the bicarbonate ion, the neutral resulting adduct could bind another bicarbonate molecules, whereas the adduct of the same complex Eu(L12)OTf with citrate ion would assume a double negative charge. This hampers the coordination of additional citrate molecules, according to columbic repulsions.

As far as the luminescence trends are concerned, both complexes Eu(L12)OTf and Eu(L13) showed a considerable enhancement of the average maximum intensity, due to the already discussed displacement of the water molecules bound to the metal center (Figure 4). The increase of the luminescence emission intensity for Eu(L12)OTf complex upon titration with citrate is around 1.44 fold; almost the same increase observed in for the bicarbonate ion.

a)



b)

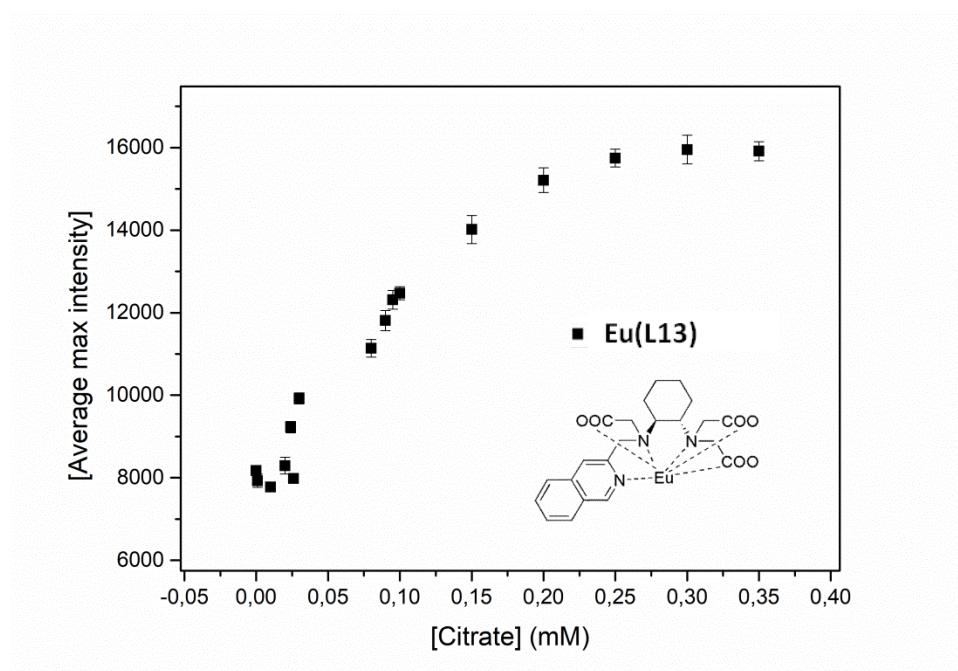


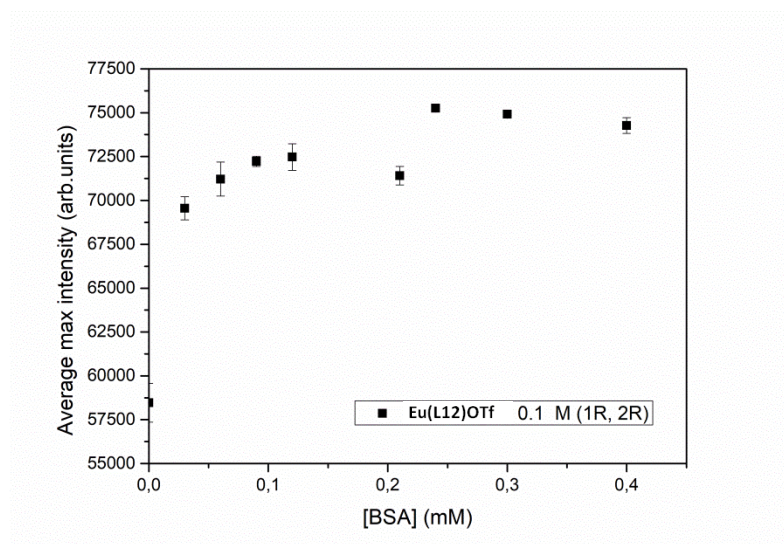
Figure 4. Average \* maximum intensity vs. [Citrate] concentration plots for the complexes a)Eu(L12)OTf 0.1 mM,  $I_{max} \approx 1.44$  fold increase,  $LOD=0.028$  mM and b)Eu(L13) 0.1 mM,  $I_{max} \approx 0.95$  fold increase,  $LOD=0.011$  mM.\* It is referred to an average of luminescence intensity upon 6 replicas. Emission wavelength: 615 nm, bandwidth: 20 nm, Excitation wavelength: 328 nm, bandwidth: 20 nm, Gain: 109.



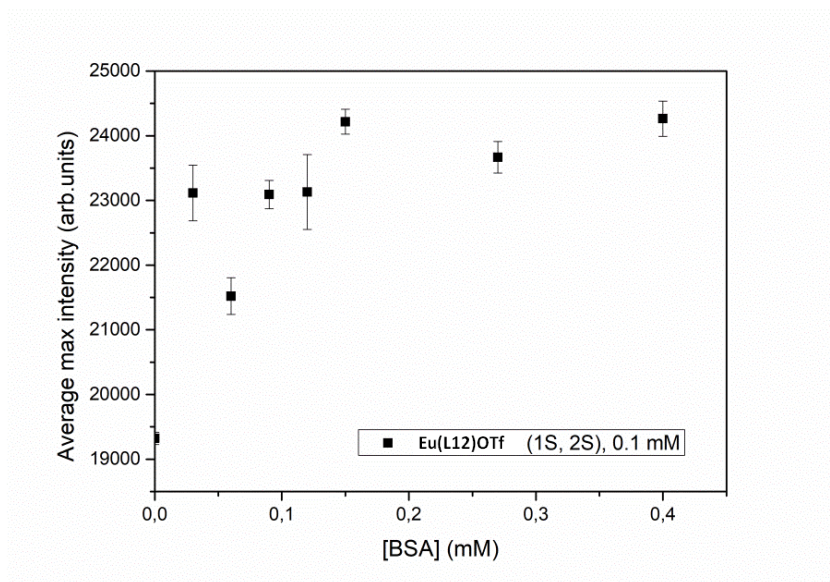
The study of the interaction on the *Serum albumins*, in our case represented by the more accessible and cheaper BSA, has been described in Chapter 4. In that contest, the complexes Eu(L9)Cl and Eu(L12)OTf were analysed in traditional quartz cuvettes in a lower concentration range for the protein (around 0.2 mM), due to the major optical path respect to the microplate one.

Since the protein is chiral, the interaction of the enantiopure complexes Eu(L12)OTf and Eu(L13) would generate two different diastereoisomeric adducts. With this in mind, both enantiomer forms (1R, 2R/ 1S, 2S) of the complexes have been investigated but similar increases of the luminescence response are detected. Upon the progressive addition of the protein up to its extracellular concentration range (0.4 mM,  $Abs_{328\text{ nm}}[Eu(L12)OTf, Eu(L13)] < 1$ ), upon excitation at 328 nm, an overall enhancement of the signal around 25-30% (Figure 5 a-d) has been detected for both enantiomers of the complexes Eu(L12)OTf and Eu(L13).

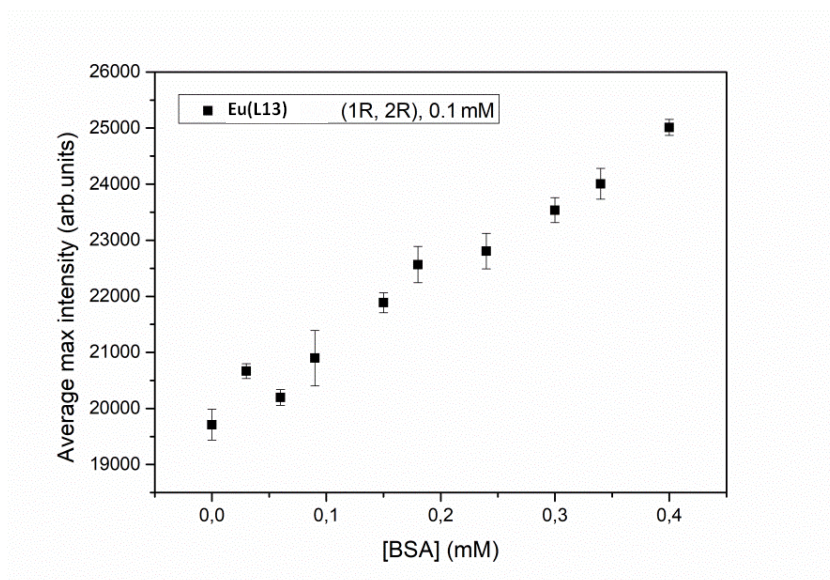
a)



b)



c)



d)

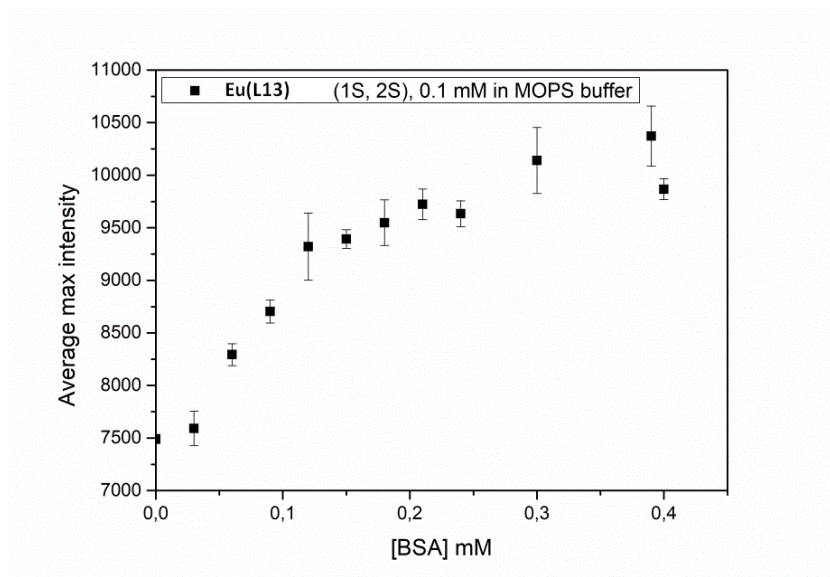


Figure 5. Average \* maximum intensity vs. [BSA] concentration plots for the complexes a)Eu(L12)OTf (1R, 2R), Luminescence increase  $\approx 27\%$ ; b) Eu(L12)OTf (1S, 2S), Luminescence increase  $\approx 25\%$ ; c)Eu(L13) (1R, 2R), Luminescence increase  $\approx 27\%$ ; d) Eu(L13) (1S, 2S), Luminescence increase  $\approx 31\%$ . \* It is referred to an average of luminescence intensity upon 6 replicas. Emission wavelength: 615 nm, bandwidth: 20 nm, Excitation wavelength: 328 nm, bandwidth: 20 nm, Gain: 109.

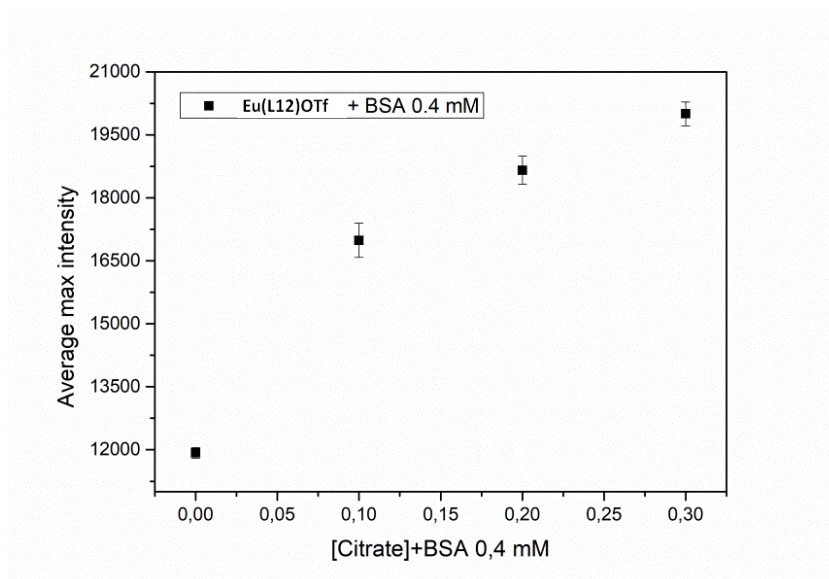
As well as observed for the two adducts of the complex Eu(L12)OTf with the bicarbonate or citrate ion, it is not possible to correlate the major affinity constant for the analyte with the most selective and sensitive probe. In fact, even if the affinity constants of the Isoquinoline complexes (Eu(L12)OTf and Eu(L13)-protein adducts (Table 4) are similar to the corresponding adducts with the citrate ion (Table 3) the higher sensitivity is still maintained for the citrate. These remarks are clearly showed in Figure 10, where the luminescence enhancements in the present of the protein were just 25-30%, respect to the  $\approx 150\%$ -100% emission increases obtained upon the interaction of the complexes Eu(L12)OTf and Eu(L13) with the citrate ion. Another crucial experiment has been reported in (Figure 6 a-b), where the final emission intensity of the complex Eu(L12)OTf in a background solution of the protein (0.4 mM) and increasing citrate (up to 0.3 mM) is 0.68 fold increased. On the other hand, when the protein concentration is

increasing in a background solution of citrate (0.3 mM), the final emission intensity is just 0.28 fold increased, by evidencing the major affinity for the anion.

<b>Complex-BSA</b>	<b><i>n</i></b>	<b>Log(<i>K</i>)</b>
Eu(L12)OTf	1	4.03 ± 0.74 (0.07%)
Eu(L13)	1	4.15 ± 0.35 (3.82%)

Table 4. Apparent affinity constants ( $\log K$ ) constant for the formation of the adducts with BSA:  $[\text{complex}] + n \cdot \text{BSA} \rightleftharpoons [\text{complex}(\text{BSA})_n]$  ( $T = 298 \text{ K}$ ,  $\text{pH } 7.40 (\pm 0.05)$ ,  $I = 0.15 \text{ M NaCl}$ ,  $0.1 \text{ mM complex}$ ), determined through cEST/Solverstat fitting. Charges omitted for clarity.

a)



b)

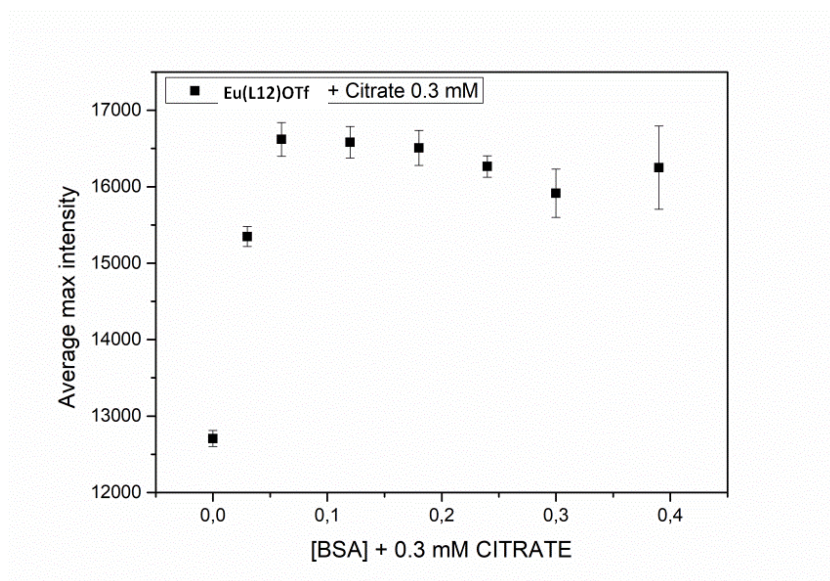


Figure 6. Average \* maximum intensity vs. [BSA] or [Citrate] concentration plots for the complexes a)Eu(L12)OTf (1S, 2S) 0.1 mM, Luminescence increase  $\approx 68\%$ , in a fixed background of BSA:0.4 mM ; b) Eu(L12)OTf (1S, 2S) 0.1 mM, Luminescence increase  $\approx 28\%$ , in a fixed background of Citrate:0.3 mM;\* It is referred to an average of luminescence intensity upon 6 replicas. Emission wavelength: 615 nm, bandwidth: 20 nm, Excitation wavelength: 328 nm, bandwidth 20 nm, Gain: 100.

It is worth noting that the bicarbonate and citrate adducts with complex Eu(L12)OTf show similar emission intensity (close to 40000 arb.un.) (Figure 7).

What is different is the slope of the curves: in particular, in the same range of concentration (i.e. 0-2 mM) the optical response towards citrate is much more sensitive. In fact, the final emission intensities are the same, but with very different slopes in the working range of the target analytes, where the citrate concentration is almost ten times lower than the one of bicarbonate ion. On the other hand, also the complex Eu(L12)OTf in the presence of BSA gave unexpected results, by revealing the lowest sensitivity, even if its affinity constant around 4, is close to citrate one (Figure 7, orange line). In fact, the sensitivity of the optical response towards a particular analyte is related not only to the probe-analyte affinity but also to the overall luminosity of the adduct. The adducts with citrate and bicarbonate show higher overall luminosity than the BSA adduct.

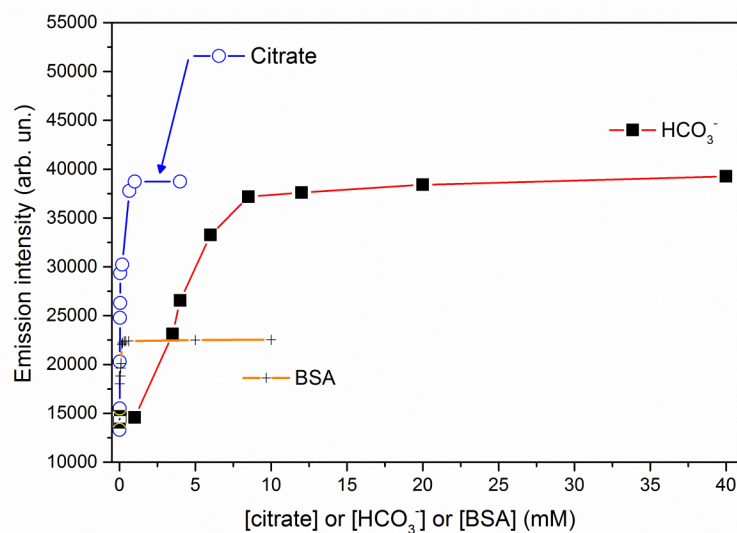


Figure 7. Emission intensity vs. [Citrate] (blue curve), or [Bicarbonate] (red curve) or [BSA] (orange curve) for the complex Eu(L12)OTf 0.1 mM, pH=7.4 in MOPS, T=25°C, NaCl: 0.15 M, [Complex]:0.1 mM. Emission wavelength: 615 nm, bandwidth: 20 nm; Excitation wavelength: 328 nm, bandwidth: 20 nm, Gain: 109.

### 5.2.3.3. Minor interferences: luminescence studies

As for the other main components of the ECF, the decrease in sensitivity for both complexes Eu(L12)OTf and Eu(L13) is represented by the following order:  $\text{HPO}_4^{2-} > \text{SO}_4^{2-} \approx \text{L-lactate}$ . This can be evinced by the inspection of the changes of the overall luminescence intensity upon titration with these analytes (Table 5).

Complex-analyte	Luminescence Changes	%
Eu(L12)OTf- $\text{HPO}_4^{2-}$	+	9
Eu(L13)- $\text{HPO}_4^{2-}$	-	7.5
Eu(L12)OTf (1R,2R; 1S, 2S)-lactate	+	≈6
Eu(L13) (1R,2R; 1S, 2S)-lactate	-	<1
Eu(L12)OTf- $\text{SO}_4^{2-}$	-	4
Eu(L13)- $\text{SO}_4^{2-}$	-	2

Table 5. Luminescence changes recorded for the isoquinoline-based complexes upon titration with  $\text{HPO}_4^{2-}$ , lactate and  $\text{SO}_4^{2-}$ . Changes + or – indicates respectively an increase or decrease of the signal.

Despite the negligible effect of the L-lactate on the luminescence spectra of the Eu(III)-complexes based on the Isoquinoline ring (Table 5), it is worth evidencing that the sensitivity of the Ln-complexes (actually the one based on L9 ligand) towards the L-lactate has been already investigated in the past from our research group.<sup>22</sup> In this case, the progressive addition of the L-lactate produced a consistent increase of the total luminescence. Moreover, a different CPL (Circularly Polarized Luminescence) activity in the presence of the metabolite has been observed for the two enantiomers, by revealing the highest CPL sensitivity for the enantiomer 1R, 2R.

#### 5.2.3.4. Citrate: the detection in extracellular fluid

In order to simulate the real extracellular conditions, the sensing experiments of all the relevant analytes of ECF have been performed in complex matrix. All the following sensing experiments presupposed that the *Total luminescence intensity* ( $I_{tot}$ ) is due to the sum of the individual intensities ( $I_i$ ) referred to the adducts of each species ( $i$ ) present in solution, weighed for their relative percentage molar composition ( $mol \% i$ ). (Eq. 4)

$$I_{tot} = \sum_i (mol\%)_i * I_i \quad (eq. 4)$$

In order to get reliable measurements, and thus a real comparison among the components of the ECF, all the sensing experiments have been performed with the same instrumental conditions and concentration of the starting complex, with an average luminescence response obtained upon at least six replicas of measurements.

With this in mind, several sensing experiments have been planned, in particular, 1) citrate has been added to a matrix containing bicarbonate and BSA at their typical extracellular concentration (Figure 8).

In this context, it is worth evidencing that for each point of the titration plot, where the citrate is added in a fixed background of bicarbonate (25 mM) and protein (0.4 mM), the luminescence should be considered as the overall contribution of all luminescent adducts (EuLbic<sub>2</sub>, EuLBSA, EuL and progressive

EuLcit) each weighed for their relative amount (Figure 9). This speciation plot has been obtained by using Hyss program.<sup>23</sup>

The obtained luminescence increase around 30% (Figure 8) is explained with the evident increase of the EuL-citrate adduct concentration (blue line, Figure 9), whose final formation (around 10%, blue line in Figure 9) foresaw a slight decrease of the EuL-BSA adduct ( $\approx 3\%$ ) and EuLbic<sub>2</sub> adduct ( $\approx 4\%$ ).

Moreover, since the final emission intensities of citrate (0.3 mM) and bicarbonate (25 mM) adducts are quite comparable (Figure 7) the effective luminescence change is mainly attributed the displacement of the BSA by citrate from the complex that produces a luminescence increase around 30%.

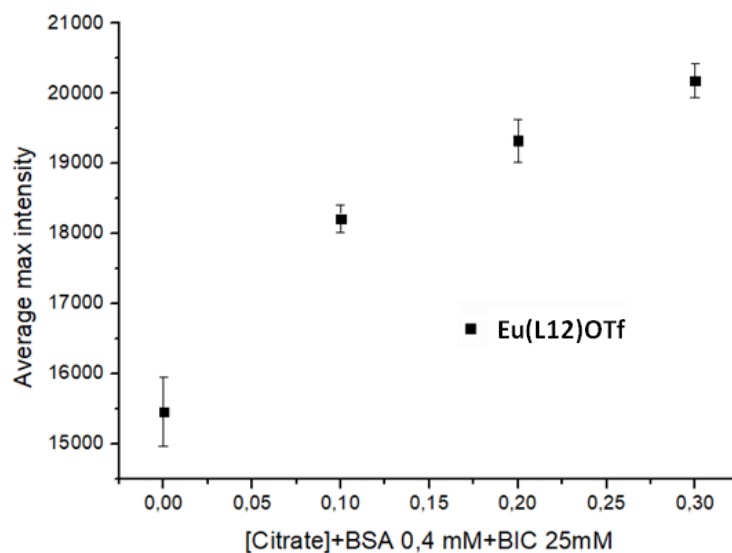


Figure 8. Plot of average \* maximum intensity vs. [Citrate] in a fixed background of BSA 0.4 mM and Bicarbonate 25 mM for the complex Eu(L12)OTf (1S, 2S), where **the appreciated luminescence increase has been around 30%**. \* It is referred to an average of luminescence intensity upon 6 replicas. Emission wavelength: 615 nm, bandwidth: 20 nm, Excitation wavelength: 328 nm, bandwidth: 20 nm, Gain: 100.



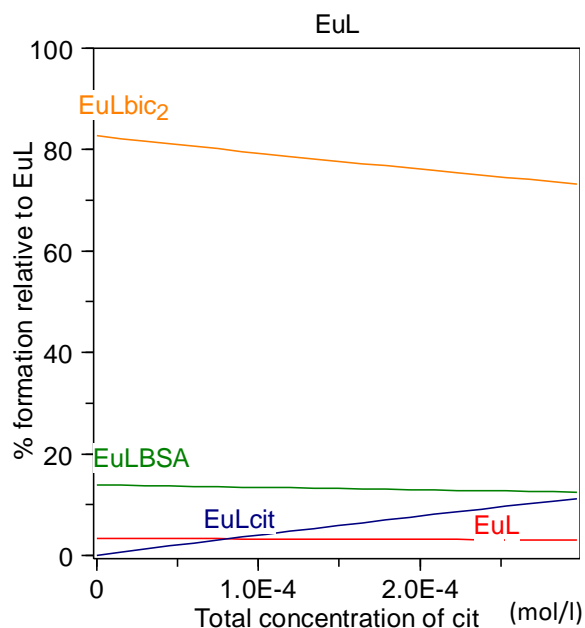


Figure 9. Estimated\* speciation of the adducts between the Eu(III)-complex **Eu(L12)OTf** (red line) with Bicarbonate (orange line) BSA (green line) and Citrate (Blue curve) during citrate addition. \* By using the Hyss program.

This result could be compared with the theoretical plot (Figure 10) of the total luminescence calculated by using equation 4 at three different citrate concentration (0, 0.15 and 0.3 mM). As mentioned before the percentage of each species has been estimated by Hyss program,<sup>23</sup> whilst the luminescence intensity for each adducts has been evinced from the plot reported in Figure 7.

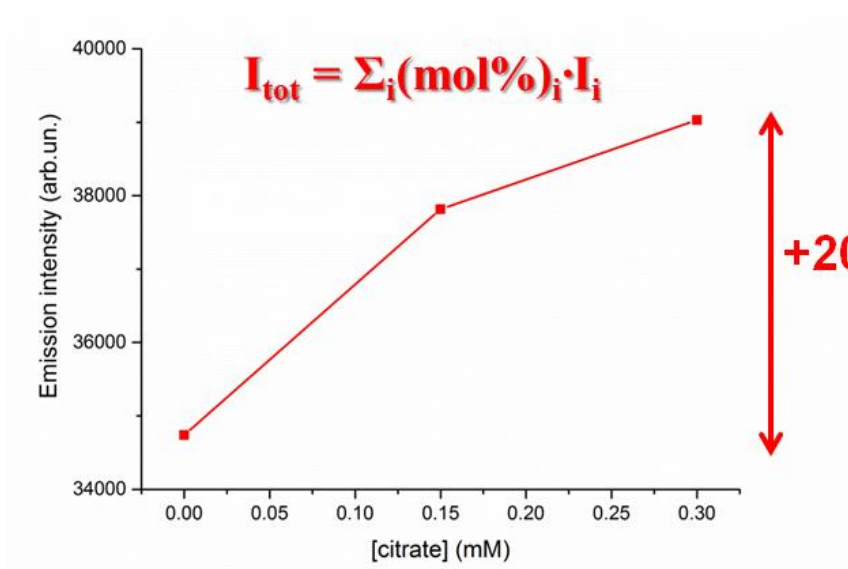


Figure 10. Theoretical plot obtained by equation 4.

It is worth noting that the theoretical luminescence enhancement around 20% is quite comparable with the experimental luminescence variation depicted in Figure 8; the slight discordance with the observed value could be attributed to matrix effects.

In a second experiment, 2) the bicarbonate was added up to the physiological range (25 mM), in a matrix with fixed concentration of BSA (0.4 mM) and citrate (0.3 mM) (Figure 11).

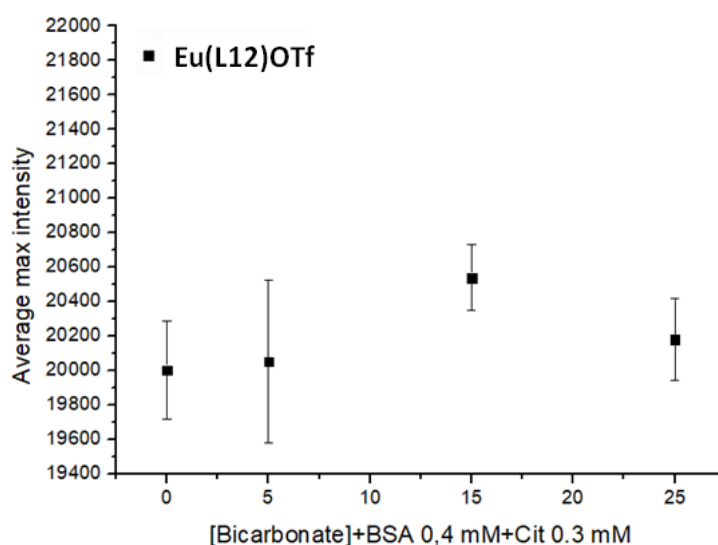


Figure 11. Plot of average \* maximum intensity vs. [Bicarbonate] in a fixed background of BSA 0.4 mM and Citrate 0.3 mM for the complex Eu(L12)OTf (1S, 2S), where the luminescence response has been mostly unchanged. \* It is referred to an average of luminescence intensity upon 6 replicas. Emission wavelength: 615 nm, bandwidth: 20 nm, Excitation wavelength: 328 nm, bandwidth: 20 nm, Gain: 100.

In this case, during the progressive addition of bicarbonate, the increase of the EuLbic<sub>2</sub> adduct concentration (orange line, Figure 12) is related to a concomitant decreasing amount of the EuL-BSA, EuL-citrate adducts and EuL (Figure 12) so as to give rise to a compensation in the total emission intensity. In conclusion, the overall luminescence intensity does not change during the titration, since the main initial contribution to the luminescence is due to the EuL-citrate, whose decrease during the titration (blue curve, Figure 12) is compensated by the EuL-bicarbonate adduct formed. The formation of this adduct compensates also the loss of luminescence intensity due to the decreasing amount of EuLBSA adduct (Figure

12). This is also in agreement with the theoretical plot obtained by equation 4 (Figure 13).

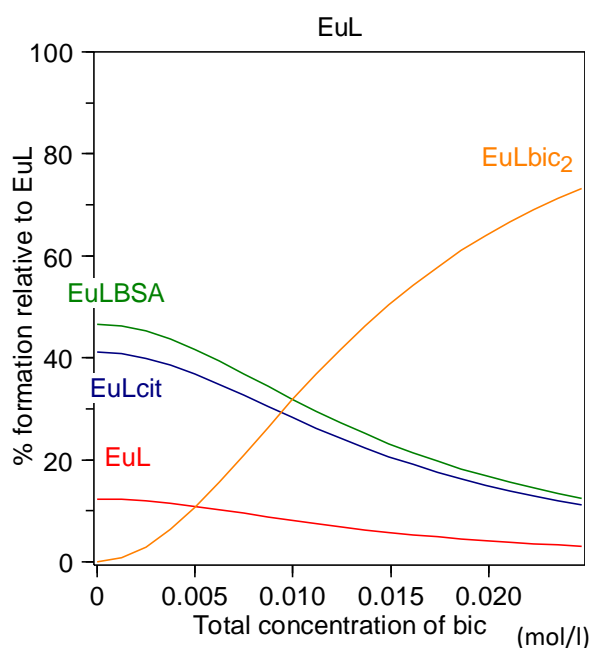


Figure 12. Estimated\* speciation of the adducts between the Eu(III)-complex Eu(L12)OTf (red line) with Bicarbonate (orange line) BSA (green line) and Citrate (Blue curve) during bicarbonate addition. \* By using the Hyss program.

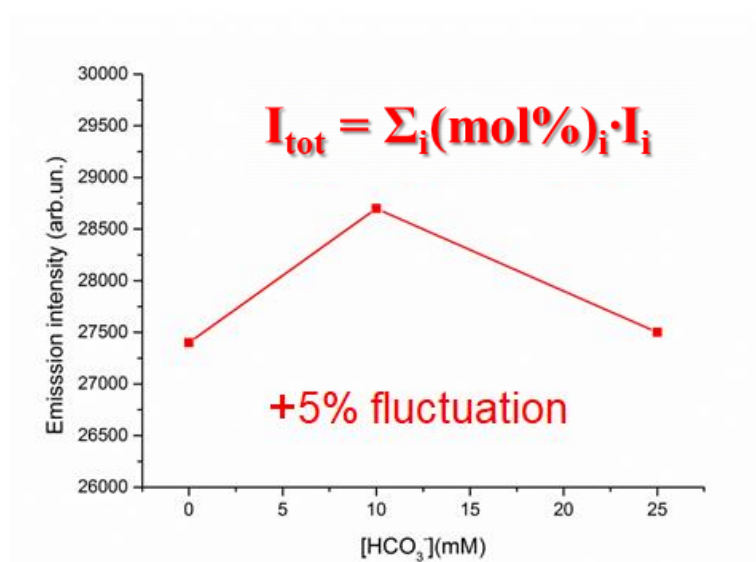


Figure 13. Theoretical plot obtained by equation 4.

Another experiment has been performed by 3) adding the BSA (up to 0.5 mM) in a fixed background of citrate (0.3 mM) and bicarbonate (25 mM). In this case a

slight decrease ( $\approx 10\%$  at 0.4 mM BSA) of the luminescence intensity has been appreciated (Figure 14).

This can be explained by an increase of the EuL-BSA adduct concentration ( $\approx 13\%$ ) accompanied by a concomitant decrease of the EuL-bicarbonate ( $\approx 7\%$ ) and EuL-citrate ( $\approx 3\%$ ) adducts (Figure 15).

Since the overall luminosity of the EuL-BSA adduct is the lowest one compared to the adducts with citrate and bicarbonate in extracellular range, a slight loss in luminescence intensity is noticed. This is also in partial agreement with the theoretical plot obtained by equation 4 (Figure 16).

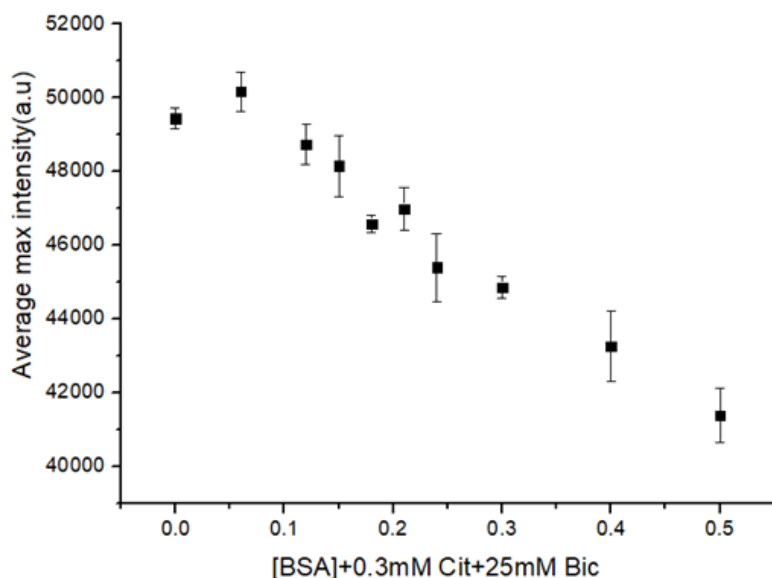


Figure 14. Plot of average \* maximum intensity vs. [BSA]mM in a fixed background of Bicarbonate 25 mM and Citrate 0.3 mM for the complex **Eu(L12)OTf** (1S, 2S), where a decrease of the luminescence response around 12% has been appreciated. \* It is referred to an average of luminescence intensity upon 6 replicas. Emission wavelength: 615 nm, bandwidth: 20 nm, Excitation wavelength: 328 nm, bandwidth: 20 nm, Gain: 109.

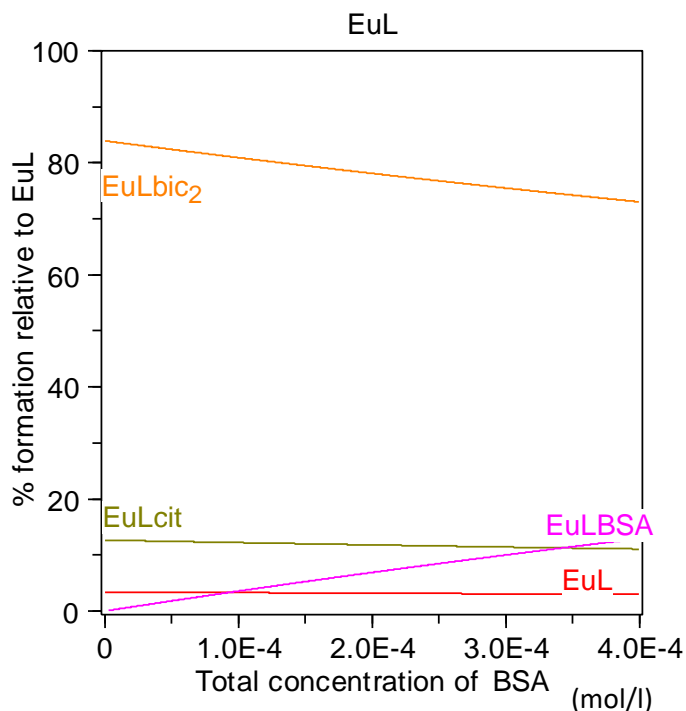


Figure 15. Estimated\* speciation of the adducts between the Eu(III)-complex Eu(L12)OTf (red line) with Bicarbonate (orange line), Citrate (green curve) and BSA (pink curve) during BSA addition. \* By using the Hyss program.

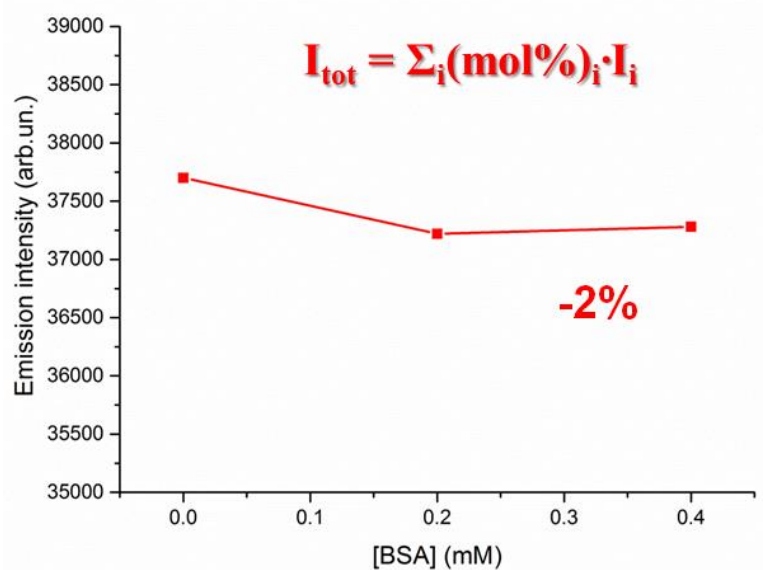


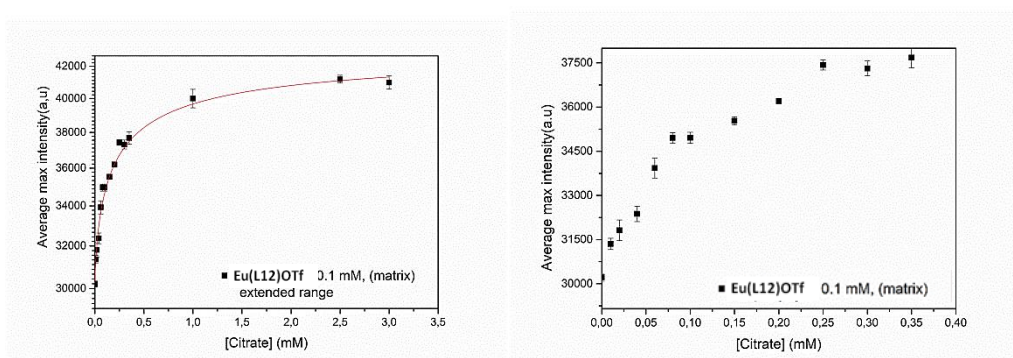
Figure 16. Theoretical plot obtained by equation 4.

A last experiment was performed by 4) adding citrate (0-3.5 mM) to a simulated serum fluid containing BSA (0.4 mM), Sodium hydrogen carbonate (28 mM), di-

Sodium hydrogen phosphate (1.3 mM), L-lactate (2.3 mM) and Sodium Sulfate (0.6 mM). After each addition of a solution containing the Eu(III)-complex, immediate HTS analysis with the microplate reader has been performed. (Refer to experimental part for more details).

As far as the luminescence emission spectra are concerned, upon progressive addition of the citrate, the final emission reached a moderate increase around 23% and 16% respectively for complex Eu(L12)OTf and Eu(L13) (Figure 17).

a)



b)

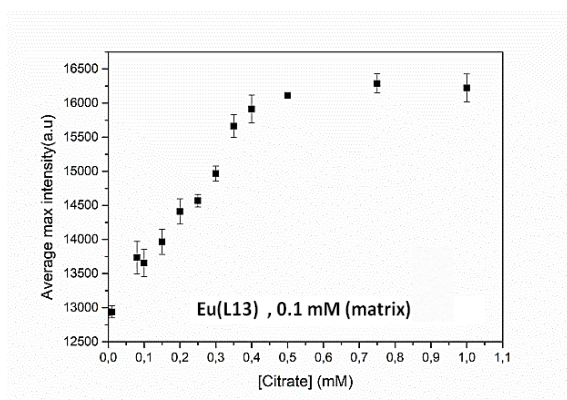


Figure 17. Average \* maximum intensity vs. [Citrate] concentration plots for the complexes a) [Eu(L12)]OTf 0.1 mM, right: extended range of Citrate up to asymptote, left: citrate up to 0.3 mM (Increase $\approx$ 23%) and b) Eu(L13) 0.1 mM, citrate up to 0.3 mM (Increase $\approx$ 16%). Emission wavelength: 615 nm, bandwidth: 20 nm; Excitation wavelength: 328 nm, bandwidth: 20 nm, Gain: 109. Fixed background: BSA (0.4 mM), Sodium hydrogen carbonate (28 mM), di-Sodium hydrogen phosphate (1.3 mM), L-lactate (2.3 mM) and Sodium Sulfate (0.6 mM). \* It is referred to an average of luminescence intensity upon 6 replicas.

## 5.2.4. *Sensor membrane for citrate in biosamples*

### 5.2.4.1. *Principle of method*

The last part of my PhD thesis was carried out in the research group of the Dr. A. Duerkop (University of Regensburg, Germany) in order to design a sensor membrane containing the lanthanide complexes for *continuous detection of citrate over the time* in a *flow cell*. A preliminary study by means of the high throughput screening (HTS) on microplate has been performed to select the most promising polymers and Ln-complexes.

The requirements to select the best couple Ln-complex/polymer must ensure several requirements, such as: 1) co-miscibility of the complex (MeOH, DCM typically) and the polymer (N,N-DMF, Acetone, MeOH, EtOH, e.g) into the solvent to form homogenous mixtures. 2) The suitable polymer strongly protect the Ln-complex from the intrusion of the water molecules by reducing the quenching and the leakage, over the time. As far as the interaction with the target analytes are concerned, since the final purpose is the application in flow cell, 3) a *short time luminescence response* and *reversibility* of the binding Ln-complex-analyte are necessarily required.

The analysis in flow cell involves a suitable spectrofluorimeter equipped with a flow cell device. The final application of the analytes in continuous mode by flow cell is usually the crucial step for the fabrication of a *sensor membrane* (def. Ln-complex on polymeric support). The membranes are cut with a hole puncher mounted and protected by a quartz glass inside the flow cell, where the buffer and the target solution are alternately introduced by a pump with a speed of 1.5 mL/min. The response time of the sensor membrane can be reduced, by using thinner membranes (up to 30  $\mu\text{m}$ ). An indicative example of the response obtained with flow cell is depicted in Figure 18.

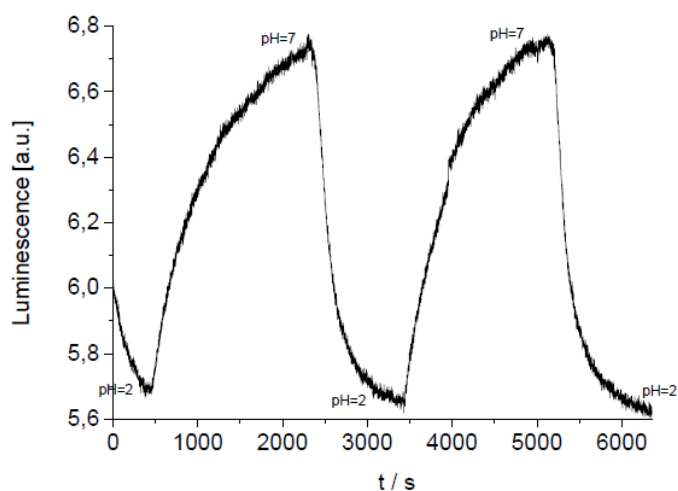


Figure 18. Reversibility of pH sensor membrane from [24]

#### 5.2.4.2. Fabrication of sensor membrane

In order to produce a sensor membrane, the first requirement is the *encapsulation of the europium complex* in a suitable polymer capable to retain the luminescence properties over the time under the physiological conditions (pH, interferents, aqueous solution, e.g). The embedding of the probe in polymers should improve the overall emission intensity as consequence of lower fluorescence background and reduced quenching by the water molecules. In fact, the Ln-complex is “protected” towards the effects of the environment. If the analyte of interest is the only one molecule capable to diffuse through the polymer, a specific diagnostic method is defined, by overcoming the drawback of poor specificity when the probe is in solution.

The procedure for the shallow absorption of the complex on the polymeric support involves the so-called “Knife Coating”. The *sensor cocktail* ( $\approx 300 \mu\text{l}$ ; Ln-complex 0.1-0.2% w/w dissolved in polymer) is homogeneously spread on a transparent polyester film by means of a metal slat (*Knife*), in order to get the sensor foil (thickness around 30-90  $\mu\text{m}$ ) for the measurements.

The typical polymers should be water-permeable like e.g. hydrogels, Eudragits (copolymer of ethyl acrylate, methyl methacrylate and a low content of methacrylic acid ester with quaternary ammonium groups), cellulose-based polymers or various copolymers of polyurethane (PU), poly ethyleneglycol (PEG) and poly acrylonitrile (PAN).



Upon the complete evaporation of the solvent at room temperature (for 12 h) or in stove (max 40 °C), the sensor film is treated with the sample solution, in our case the citrate solution.

Another feature to consider is *the percentage of leaking* of the complex from the *sensor membrane*, which is normally accepted below <10% over a period of 2-3h in continuous analysis.

In order to estimate the leakage, it is possible to simulate the condition of the diffusive exchange in flow cell, by means of a microplate whose diameter wells is the same of the membrane disc. Several discs are cut from the sensor foil for improving the reproducibility, and they are fixed to the bottom of each wells with previous leaching of the plate with 10 µl of acetone (Figure 19).

Upon complete fixing of the membrane discs, the MOPS buffer solution (pH 7.4) is added and a fresh measurement of the microplate is performed as initial “zero point” of the luminescence. After 2h of hydration, the final leakage is evaluated by measuring the overlying buffer solution in a new microplate, and the luminescence response is compared with the initial luminescence for calculating the percentage of leakage.

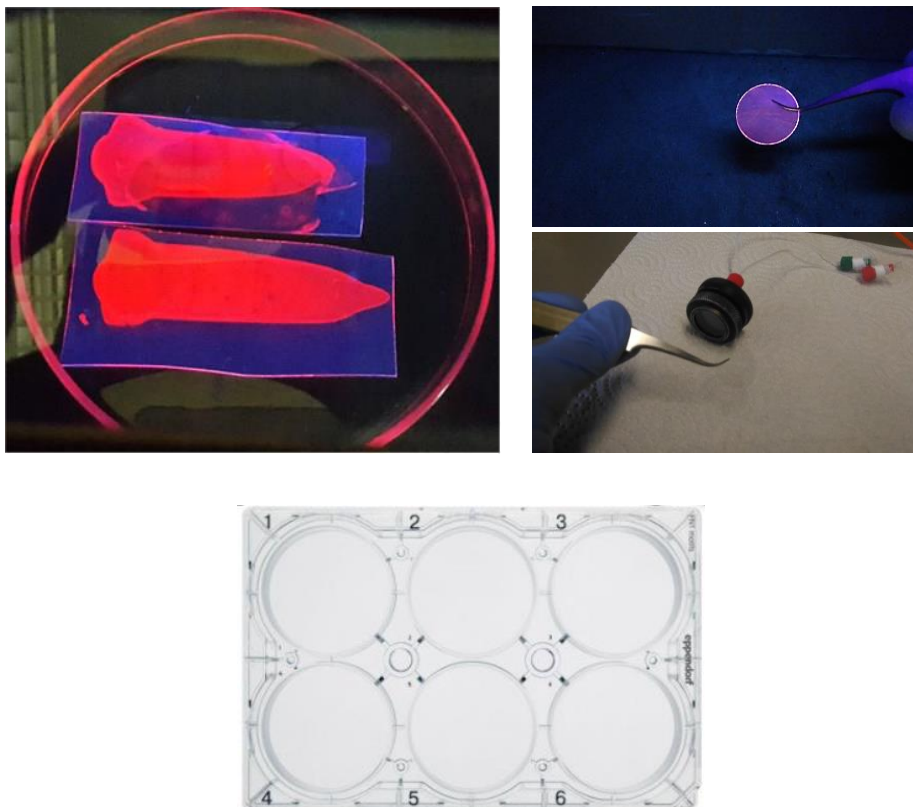


Figure 19. Left (above): Sensor foil containing a Eu(III)-complex upon illumination with a UV lamp [24], right: (above) membrane disc ( $d:20$  mm) for analysis in microplate reader, and (right below) sampler for flow cell. Center below: bottom microplate.

The last requirement for a good sensor membrane is *the permeability of the target analyte* through the sensor membrane, allowing the interaction with the Ln-complex and thus the luminescence response. With this in mind, a preliminary test by using microplate reader could be exploited with the same philosophy of the leakage study. The excess of water used for evaluating the leakage is accurately removed from the membrane discs and a fresh solution of the target ion (in our case a citrate solution) is added for each wells. The plate is *immediately* analyzed to the microplate reader. The new luminescence responses are compared with the initial values of the membrane discs without the analyte (after hydration) in order to calculate the percentage of emission changes.

#### 5.2.4.3. Results and discussions

The polymers containing electron- rich acetate groups showed the lower leakage over the time (2h) of the Ln-complexes, as already reported in the literature.<sup>25</sup> Polymers like polymethyl meta acrylate (PMMA), polyvinyl acetate (PVA) or Eudragit (copolymer of ethyl acrylate, methyl methacrylate and a low content of

methacrylic acid ester with quaternary ammonium groups)<sup>26</sup> furnished an efficient embedding of the Eu(III) complexes with negligible percentage of leakage ( $\approx 5\%$ ). The most homogeneous distribution of the sensor cocktail on the polyester support was obtained by employing a sensor foil thickness of 60  $\mu\text{m}$ . The entrapment of the Ln-complex and the interaction with the analyte are supposed to involve a diffusive mechanism through the membrane. With this in mind, a sufficient swelling of the polymer is crucial: this is hampered when the sensor foil thickness is too small (30  $\mu\text{m}$ ) or too big (90  $\mu\text{m}$ ), since an inhomogeneous distribution of the sensor cocktail mostly occurred. Moreover, bigger the thickness is, higher is the amount of solvents residue, especially of high boiling solvents, by requiring higher temperature in stove or longer evaporation times, not always compatible with the stability of the Ln-complex. With this in mind, the intermediate thickness value of 60  $\mu\text{m}$  is a good compromise. The experimental remarks summarized in Table 6 revealed that the crucial step concerning the diffusion of the citrate ion through the sensor membrane, in order to ensure the interaction with the embedded Eu-complex.

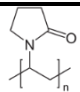
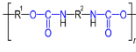
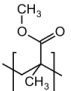
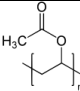
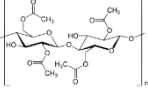
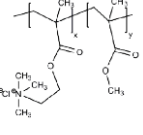
Polymers (P)	Solvents (P)	Structure (P)	Sensor cocktail: [Ln-complex]; Thickness foils	% Leakage	$\Delta$ Lum-Citrate
Polyvinyl- Pyrrolidone (PVP)	10% w/w H <sub>2</sub> O		<b>Eu(L12)OTf</b> : 0.1 % w/w; 60 $\mu$ m, 90 $\mu$ m	>85%	Unchanged
Polyurethane (hydrogels): <b>D4</b> , <b>D7</b> , <b>D640</b>	<b>D4</b> : 10% w/w EtOH:H <sub>2</sub> O (9:1); <b>D7</b> : 20% w/w CHCl <sub>3</sub> ; <b>D640</b> : 10% w/w CHCl <sub>3</sub>		<b>Eu(L12)OTf</b> : 0.1 % w/w; 60 $\mu$ m, 90 $\mu$ m	D4: >80% ; D7: >70%; D640: >65%;	Unchanged
Polymethyl- Methacrylate (PMMA)	10 % w/w CHCl <sub>3</sub>		<b>Eu(L12)OTf</b> : 0.1 % w/w; <b>Eu(L13)</b> : 0.2 % w/w; 60 $\mu$ m, 90 $\mu$ m	$\approx$ 2%	Unchanged
Polyvinylacetate (PVA)	10 % w/w CHCl <sub>3</sub>		<b>Eu(L12)OTf</b> : 0.1 % w/w; <b>Eu(L13)</b> : 0.2 % w/w; 60 $\mu$ m, 90 $\mu$ m	<2%	Unchanged
Cellulosa Acetate (CA)	5 % w/w N,N-DMF		<b>Eu(L12)OTf</b> : 0.1 and 0.2 % w/w; <b>Eu(L13)</b> : 0.2 % w/w; 60 $\mu$ m, 90 $\mu$ m	$\approx$ 2%	Unchanged
PVA/ CA (1:99)	10 % w/w N,N- DMF:H <sub>2</sub> O (9:1)		<b>Eu(L12)OTf</b> : 0.18, 0.5, 0.9, 1.25 % w/w; 60 $\mu$ m, 90 $\mu$ m	0.18 w/w: <2%; 0.5 w/w: <5%; 0.9 and 1.25 w/w: 25%;	Unchanged
D4/ CA (20:80)	10 % w/w Acetone		<b>Eu(L12)OTf</b> : 0.25 % w/w; 60 $\mu$ m.	25%	Unchanged
D640/ CA (10:90); D640/ CA (2:98);	10 % w/w CHCl <sub>3</sub>		<b>Eu(L12)OTf</b> : 0.20 % w/w; 60 $\mu$ m.	20%; 10%	Unchanged
Eudragit RL 100	10 % w/w Acetone		<b>Eu(L12)OTf</b> : 0.10 % w/w; 60 $\mu$ m.	70%	Unchanged
Eudragit RS 100	10 % w/w Acetone		<b>Eu(L12)OTf</b> : 0.10, 0.2 % w/w; <b>Eu(L12)Cl</b> : 0.10% w/w; <b>Eu(L12)OTf</b> : 0.10% w/w; <b>Eu(L9)Cl</b> : 0.10% w/w. 60 $\mu$ m.	<3%	<b>Eu(L12)OTf</b> : (0.2% w/w ) fresh sample in buffer: 5%; after <b>20h in buffer: 30%</b> ; after <b>20h in matrix:</b> <b>23%</b> ;
Eudragit RS:RL 100 (90:10)	10 % w/w Acetone		<b>Eu(L12)OTf</b> : 0.10, 0.2, 0.3 % w/w. 60, 90 $\mu$ m.	5%	Unchanged

Table 6. Sensor membrane in polymers. Ln-complex.: dissolved in MeOH 2% v/v; % Leakage respect to the Luminescence of polymeric residue after 2h in MOPS buffer (pH: 7.4, NaCl: 0.9% w/v); [Citrate]: [Complex]  $\approx$ (1:3).

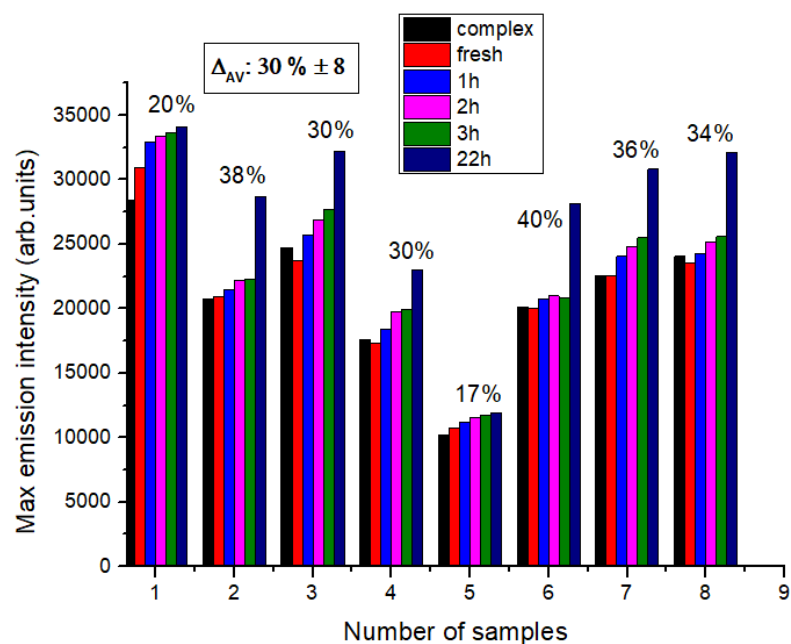
Upon several attempts, the major part of the obtained results ruled out an instantaneous luminescence response upon the interaction of the Eu-complex with the Citrate ion. Nevertheless, as long as the more water-permeable Eudragit RS-

100 is used as polymeric support, the prolonged time reaction allowed the diffusion, by furnishing a moderate luminescence increase around 30% (Figure 20).

This promising results obtained for the **Eu(L12)OTf** complex, unfortunately, must be re-evaluated in the light of the required short time of response and reversibility of the probe-analyte interaction. In fact, prolonged and vigorous washings with buffered solution are not sufficient to displace citrate molecule from the inner coordination sphere of the metal ion.

In each disk of sensor foil settled in the bottom of the microplate, just a part of the initial starting solution of the complex (0.2 % w/w) dissolved in polymer is capable to stay in the polyester support. The fraction of embedded Eu-complex is estimated by comparing its luminescence response in polyester support (upon addition of fresh buffer above the sensor foil disk) with the emission intensities of a solution of the same Ln-complex at known concentration, rigorously upon the same instrumental conditions. Afterwards, upon the estimation of the real concentration of the embedded Eu-complex, both citrate solution and components of extracellular fluid have been proportionally added according to their physiological concentration in complex matrix.

a)



b)

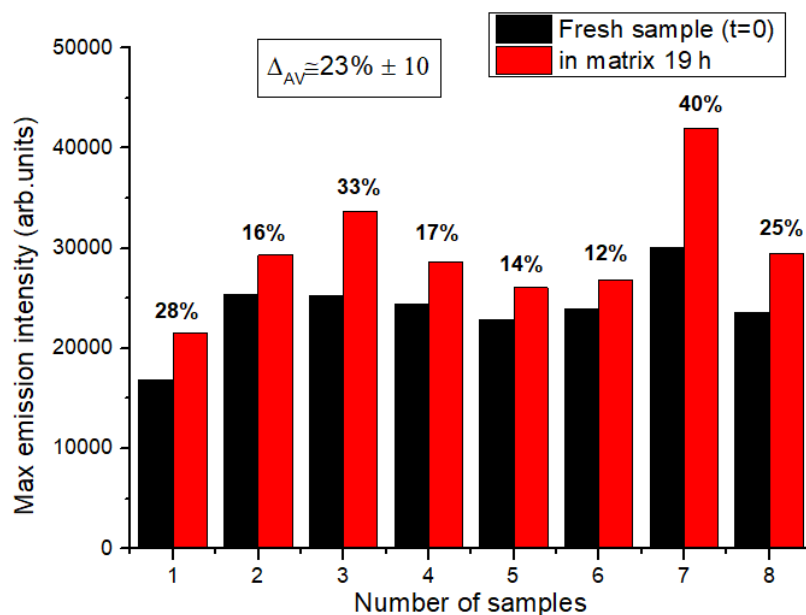


Figure 20. Response of the sensor cocktail containing the  $\text{Eu}(\text{L12})\text{OTf}$  upon 19 h of interaction with Citrate solution. Ratio Ln-complex:citrate (1:3). a) Background solution: MOPS buffer pH 7.4, NaCl 0.9% w/v; b) Background solution: buffered mixture of the ECF containing BSA,  $\text{NaHCO}_3$ , L-lactate,  $\text{Na}_2\text{HPO}_4$ ,  $\text{Na}_2\text{SO}_4$ . Thickness sensor foil: 60  $\mu\text{M}$ , d: 20 mm. The concentration of each components has been added at the same ratio used for the sensing experiment in solution without embedding the complex in polymer Eudragit RS-100.

#### 5.2.4.4. Conclusions

The experimental remarks have revealed the Eu(III)-complexes based on isoquinoline rings are the most promising optical probes for detection of citrate ion both in buffer and in extracellular fluid.

The luminescence responses of the two probes have been proved in the presence of the main interferents of the ECF. The effect of the citrate on the luminescence changes has been studied in the simultaneous presence of other interferents by revealing that the overall luminescence intensity is the sum of the individual intensities of the adducts present in solution, and the changes in the luminescence response should take into account the change of the concentration of the adducts during the titration.

As far as the sensing experiment with the complex Eu(L12)OTf embedded in Eudragit RS-100 (0.2 % w/w of Eu(L12)OTf in polymer), upon addition of citrate, a moderate luminescence increase around 25% has been detected both in buffer and in ECF. Probably the encapsulation in polymer decreases the overall change of the emission intensity as observed when the probe was a complex solution for the detection of citrate. In addition to the low data reproducibility of the technique, even the long time response to citrate (at least 20 h) and the non-reversibility of the probe-analyte interaction also after prolonged and vigorous washings in buffered solution are other important drawbacks to overcome.

Concluding, an innovative optical probe for citrate, based on the advantageous lanthanide luminescence has been discovered by revealing a good response both in simple buffered solution (pH 7.4; NaCl 0.15 M) that in a simulated human extracellular fluid, with an average binding constant comparable with the values reported in literature. Nevertheless, a reliable sensor membrane for continuous detection of citrate is quite far to be obtained. Further studies should improve features such as: *i*) the permeability of the membrane towards the analytes, *ii*) the rate of diffusion through the membrane and *iii*) the homogeneity of the sensor foils often suffering of a low data reproducibility. With this in mind, some improvements could be obtained by using robotic equipment to get higher quality sensor film.

### **5.3. *Experimental part: procedures, techniques and characterization***

#### **5.3.1. *Materials***

The main suppliers were Roth, Merck and Sigma-Aldrich; the purity of reagents and solvents was predominantly above 99%.

The water was obtained in high purity from the 'Millipore Elix 10' purification system.

*4-Morpholinepropanesulfonic acid (MOPS) buffer* 15 mM was dissolved in purified bi-distillate water, by adding 0.9% m/v NaCl for obtaining the ionic strength in physiological conditions. The pH value was corrected to physiological range by dropwise addition of freshly prepared NaOH 10 M until  $\text{pH} \approx 7.4$ . Stock solution of Bovine Serum Albumin (BSA) (purity  $\geq 99\%$ , purchased from Roth) was freshly prepared by dissolving the protein in MOPS buffer ( $\text{pH} \approx 7.4$ ). The complete dissolution of BSA was reached without mechanical shaking, but just after 20-25 min with spontaneously diffusion in buffer. Upon dissolution, the protein solution was kept in the dark at 4°C before use.

All other anionic solutions were freshly prepared by dissolution in MOPS buffer by means of sonication so far as was required.

#### **5.3.2. *Luminescence and decay kinetics measurements***

*In Regensburg Biosensor Department:* a Synergy Neo 2 Hybrid Multi-Mode (Biotek company) plate reader was used for all the luminescent measurements. The main read methods used were mostly endpoint and spectra scanning. The first one to collect the maximum luminescence intensity in a specific wavelength emission (612-615 nm), upon excitation in the antenna wavelength of the Eu-complexes employed (328 nm). The spectra scanning were exploited to get the complete emission spectra between 550-730 nm.

All measurements were collected with temperature control between 23-25 °C.

The instrument is equipped with a light source based on a Xenon flash lamp, and the detector is constituted by a top/bottom monochromator system, for this reason no filters were used to avoid the second orders of the light. The monochromator



bandwidths used are variable, from 3 to 50 nm with 1 nm of increment. The emission and excitation bandwidth were respectively 20/20 nm.

The plates were purchased from Greiner Bio-One GmbH (code 655809) and were made of COC (Cyclic Olefin Copolymer). The 96 wells (d:0.6 mm) black plates with transparent bottom were mostly employed for acquiring also the absorbance measurements, since they were suitable to avoid interference excitation in our antenna wavelengths excitation ( $\lambda$ : 325-328 nm, Abs $\approx$ 0.06). Furthermore, in order to increase the efficiency and the reproducibility of the measurements, an Eppendorf Multipette 20-200  $\mu$ l equipped with 8 channels volume was adopted for all the luminescence experiments. The TPP (Tissue Culture Test Plates, polystyrene) 24 wells (d: 20 mm) transparent plates were used for measuring the sensor foils luminescence.

### ***5.3.3. Sensing experiments***

All the luminescence measurements employed a fresh solution 0.4 mM of the Eu(III) complex previously dissolved in 1.5% v/v of MeOH and diluted in MOPS buffer (pH:7.4, 0.9% m/v NaCl) up to 0.1 mM. All titrations were performed with the addition of the metal complex as last component of the sample, and readily measured with Biotek microplate reader.

Bicarbonate sensing in MOPS buffer 15 mM, pH=7.4, 0.9% p/v NaCl: a starting solution 50 mM of Sodium hydrogen carbonate (Merck) was opportunely diluted as well as was required. Since the typical concentration of the analyte in extracellular fluid is between 24-27 mM<sup>27</sup> an extended range between 1.7-35 mM was examined until the complete saturation of the complex for the calculations of the binding constants.

Citrate sensing in MOPS buffer 15 mM, pH=7.4, 0.9% p/v NaCl: a mother solution of the tri-Sodium citrate dihydrate (Merck) 10 mM was opportunely diluted as well as was required. A wide range for the addition of the citrate between 0.001-5 mM including the extracellular concentration 0.3 mM<sup>27</sup> was narrowly explored to reach the complete saturation of the complex for the calculations of the binding constants.

Citrate sensing in artificial extracellular fluid (inorganic components mostly) in MOPS buffer 15 mM, pH=7.4, 0.9% p/v NaCl: the affinity of the most promising bioanalyte for the Eu(III) complexes was pushed in a multicomponent environment. A background containing a mixture of anions and serum albumin (BSA) was fixed in all the experiment.

The investigated anions were in their typical extracellular concentrations, and the serum albumin was present at its normal concentration of 0.4 mM. Incremental additions of Sodium Citrate were made up to a limit of 2 mM, in the emission intensity of the bands at 550-730 nm (red-emission of trivalent Europium). Thus, an 0.1 mM total concentration of the Eu(III) complex was added to a background solution containing BSA (0.4 mM), Sodium hydrogen carbonate (28 mM), di-Sodium hydrogen phosphate (1.3 mM), L-lactate (2.3 mM) and Sodium Sulfate (0.6 mM) and immediately analyzed on microplate reader.

## 5.4. *References*

1. [Lumen, *Boundless Anatomy and Physiology- Body fluids*-<https://courses.lumenlearning.com/boundless-ap/chapter/body-fluids/>].
2. [P. Polese, M. Tolazzi, A. Melchior, *J. Therm. Anal. Calorim.* **2018**, *2*, DOI 10.1007/s10973-018-7409-2].
3. [C. Comuzzi, P. Polese, A. Melchior, R. Portanova, M. Tolazzi, *Talanta* **2003**, *59*, 67–80].
4. [J. C. G. Bünzli, *Chem. Rev.* **2010**, *110*, 2729–2755].
5. [M.V. Alvarez-Arroyo, M.L. Traba, A. Rapdado, C. de la Piedra, *Urol. Res* **1992**, Vol.20, p.88-90].
6. [S. J. Butler, D. Parker, *Chem. Soc. Rev.* **2013**, *42*, 1652–1666].
7. [R. Carr, R. Puckrin, B. K. McMahon, R. Pal, D. Parker, L. O. Pålsson, *Methods Appl. Fluoresc.* **2014**, *2*, DOI 10.1088/2050-6120/2/2/024007].
8. [Y. Bretonniere, M. J. Cann, D. Parker, R. Slater, *Org. Biomol. Chem.* **2004**, *2*, 1624–1632].
9. [Y. Bretonnière, M. J. Cann, D. Parker, R. Slater, *Chem. Commun.* **2002**, *8*, 1930–1931].
10. [D. Imperio, G. B. Giovenzana, G. L. Law, D. Parker, J. W. Walton, *Dalt. Trans.* **2010**, *39*, 9897–9903].
11. [G. Tircsó, Z. Garda, F. K. Kálmán, Z. Baranyai, I. Pócsi, G. Balla, I. Tóth, *J. Inorg. Biochem.* **2013**, *127*, 53–61].
12. [S. Comby, S. A. Tuck, L. K. Truman, O. Kotova, T. Gunnlaugsson, *Inorg. Chem.* **2012**, *51*, 10158–10168].
13. [X. L. Du, T. L. Zhang, L. Yuan, Y. Y. Zhao, R. C. Li, K. Wang, S. C. Yan, L. Zhang, H. Sun, Z. M. Qian, *Eur. J. Biochem.* **2002**, *269*, 6082–6090].
14. [R. S. Dickins, T. Gunnlaugsson, D. Parker, R. D. Peacock, *Chem. Commun.* **1998**, 1643–1644].
15. [D. G. Smith, B. K. McMahon, R. Pal, D. Parker, *Chem. Commun.* **2012**, *48*, 8520–8522].
16. [B. S. Murray, E. J. New, R. Pal, D. Parker, *Org. Biomol. Chem.* **2008**, *6*, 2085–2094].
17. [D. G. Smith, R. Pal, D. Parker, *Chem. - A Eur. J.* **2012**, *18*, 11604–11613].
18. [D. G. Smith, G. L. Law, B. S. Murray, R. Pal, D. Parker, K. L. Wong, *Chem. Commun.* **2011**, *47*, 7347–7349].

19. [S. J. Butler, B. K. McMahon, R. Pal, D. Parker, J. W. Walton, *Chem. - A Eur. J.* **2013**, *19*, 9511–9517].
20. [B. K. McMahon, D. Parker, *RSC Adv.* **2014**, *4*, 37649–37654].
21. [R. Pal, D. Parker, L. C. Costello, *Org. Biomol. Chem.* **2009**, *7*, 1525–1528].
22. [M. Leonzio, A. Melchior, G. Faura, M. Tolazzi, M. Bettinelli, F. Zinna, L. Arrico, L. Di Bari, F. Piccinelli, *New J. Chem.* **2018**, *42*, 7931–7939].
23. [L. Alderighi, P. Gans, A. Ienco, D. Peters, A. Sabatini, A. Vacca, *Coord. Chem. Rev.* **1999**, *184*, 311–318].
24. [Wafaa Waleed Nafea Al-Qaysi, PhD thesis, **2018**].
25. [Zhichuan Wu, Xueqian Wang, Tingxian Tao, Yudong Zhang, Yi Liu, Hao Fong, *J. Appl. Pol. Sci.* **2007**, Vol 3, p.6,].
26. [A. Sonie, A. Chandra, *Int. Res. J. Pharm.* **2013**, *4* (5)].
27. [S. J. Butler, B. K. McMahon, R. Pal, D. Parker, J. W. Walton, *Chem. - A Eur. J.* **2013**, *19*, 9511–9517].
28. [P. Atkinson, K. S. Findlay, F. Kielar, R. Pal, D. Parker, R. A. Poole, H. Puschmann, S. L. Richardson, P. A. Stenson, A. L. Thompson and J. Yu, *Org. Biomol. Chem.*, **2006**, *4*, 1707–1722].

## Final Conclusions

The new library of luminescent Ln(III)-complexes (Ln=Eu, Tb) synthesized and characterized in this PhD project revealed interesting properties for biosensing applications. All the complexes are water soluble and stable at physiological ionic strength and pH. The overall stability constants found are quite high and in accordance with values found in literature for similar complexes and conditions. On the other hand, when the Ln-complexes were not water soluble, the encapsulation in biocompatible PLGA nanoparticles (Chapter 3) were used as a useful study for imaging purposes.

The combined thermodynamic and DFT studies show that the tri-acetate ligands form more stable lanthanide complexes than the di-acetate ones. This is essentially due to the oxophilic character of Ln(III) ions, which prefer to bind ligands containing more oxygen donating atoms. The steric hindrance at the metal ion is also important and it reduces the stability of the di-acetate complex with quinoline rings. On the other hand, the Isoquinoline complexes possess a stability which is in the middle between the one of Pyridine and Quinoline complexes.

All complexes in aqueous solution are 8-fold coordinated, showing two water molecules in the first coordination sphere and one 6-fold coordinating chiral ligand. These water molecules are usually displaced by the target biomarkers, by modulating the luminescent intensity stemming from the optical probe.

As far as the *sensitization mechanism* is concerned, while the pyridine ring is capable to sensitize both Eu(III) and Tb(III) luminescence, the quinoline and isoquinoline rings effectively sensitize only Eu(III) ion. With this in mind, a crucial feature to consider during the design of the luminescent probes concerns the *choice of the metal center and of the heteroaromatic antenna*.

The number of components of the Eu(III)  $^5D_0 \rightarrow ^7F_0$  transition (only one) and the luminescence decay curves, properly fitted by a single exponential function confirm the existence of one main emitting species in solution.

Moreover, as far as *the total quantum yields* of our optical probes are concerned, their values are in agreement with the values found in literature for cell imaging with either lanthanide or d-block complexes (around 10%). Even the sensitization efficiency ( $\eta_{sens}$ ) are higher for pyridine- (61-66%) than for quinoline-based (29-40%) complexes, which may be attributed to the longer Ln(III)-N<sub>heterocyclic</sub> bonds in the latter ones, which get worse the probability of the ligand to metal energy transfer. In fact, the significant increase of the Y(III)-N<sub>heterocycle</sub> bond distance, when Py is replaced by quinoline ( $\Delta Py \rightarrow Q \sim +0.11 \text{ \AA}$ ), indicates the weaker interaction of the quinoline with respect to pyridine ligands with the metal ion. (DFT calculations, Chapter 4).

As far as the *potential application in biosensing field*, all the Ln-complexes have been designed with 6-fold coordinating ligands with displaceable solvent molecules by target molecules present in the biological fluids. It is worth noting that except the Isoquinoline and quinoline derivatives, the other pyridine-based Ln-complexes gave a luminescence response upon excitation around 270 nm. This excitation wavelength is not suitable for sensing experiments in biological fluid, since the majority of the bio-chromophore absorbs light around 300 nm.

Moreover, the chiral DACH backbone allowed a further characterization by means of CPL spectroscopy, as shown in the chapter 3 where the results of a study on tta-based complex of Eu(III) and Sm(III) are presented.

The bioanalytes under investigation have been the components of the extracellular fluid at their typical concentration range. Among the main components of the ECF, the first encouraging response has been obtained for the sensing of the bicarbonate ion. The diacetate Eu/Tb(L9)Cl and Eu(L11)OTf complexes show a  $\log K$  values higher than 4, an unprecedented value in the literature. In addition, the luminescence response towards  $\text{HCO}_3^-$  is particularly selective in the 2-10 mM concentration range of the analyte. This range of concentration is related to serious kidney disease (metabolic acidosis).

Another investigated component of the ECF has been the serum albumin, for simplicity the homologous Bovine Serum Albumin (BSA) was used. In this study,

the Eu(L9)Cl (1R, 2R) and Eu(L11)OTf (1R, 2R) complexes revealed an opposite trend of the Eu(III) luminescence response despite the same experimental conditions. The Eu(L9)Cl complex showed a drastic decrease of the luminescence intensity during the progressive addition of the protein, whereas the Eu(L12)OTf complex revealed a considerable luminescence increase ( $\approx 80\%$ ) with the increasing addition of the BSA. *Docking studies* revealed that the luminescence changes observed for Eu(L12)OTf complex interacting with BSA foresee the displacement of one water molecules from the metal center by the coordinating groups of the protein (the carboxylic group of the GLU17 residue). On the other hand, the luminescence changes in the case of the Eu(L9)Cl complex have been explained by a protein/complex interaction which takes place on the surface of the protein, that influences the efficiency of the energy transfer from Py to lanthanide ion.

The diacetate and triacetate complexes based on Isoquinoline rings have been particularly promising for signalling the citrate ion at its typical extracellular concentration. A considerable enhance of the emission intensity  $\approx 1.5$  fold the initial luminescence emission has been detected for both Eu(L12)OTf and Eu(L13) complexes, with higher probe-citrate binding constant for the diacetate complex. Although the drastic decrease of the luminescence signal respect to the trials in simple buffer, a moderate increase of the intensity of the  ${}^5D_0 \rightarrow {}^7F_2$  transition ( $\approx 20\%$ ) is still appreciated for both Eu(L12)OTf and Eu(L13) complexes when citrate is added to a background matrix simulating a real serum fluid.

The embedding and the diffusion of the citrate through the most permeable Eudragit RS-100 polymer could be the key points for prolonging the stability of the Eu(L12)OTf over the time in view of the design of a reusable *sensor membrane* for citrate ion. Nevertheless, the low data reproducibility of the sensor membrane and an average low luminescence increase (around 25%) for both experiments in buffer and in extracellular matrix are strong drawbacks to overcome for obtaining a competitive method to detect the citrate ion in biological samples.

As far as the detection of the other main components of the ECF, a negligible contribution has been evidenced for phosphate, sulphate and L-lactate.

In the future, it is worth developing new optical probes containing antennae capable to absorb around 350-400 nm, such as Ln-complexes based on coumarin or azaxanthone rings. With this in mind, a reliable inspiration for Tb(III)-complexes based on azaxanthone as antenna is widely discussed in the work of Atkinson and co-workers.<sup>28</sup>



## **Acknowledgements**

I would like to thank my research group Prof. Fabio Piccinelli, my supervisor, and Prof. Marco Bettinelli for all the scientific and moral support during these three years of hard and satisfactory work. It has been a really productive PhD where I had the possibility to collaborate with them and with other experts in order to acquire new knowledge in the field of coordination chemistry and luminescence spectroscopy.

I recommend this PhD in Nanoscience and Advanced Technologies even to other students for the kind of challenging research and for the nice people that I met during this experience.

Special thanks to all the research group of Analytical chemistry and Biosensors of the University of Regensburg (Germany), in particular to my supervisor Dr. Axel Duerkop, for giving me the possibility to learn new skills and experience on their analytical devices. In this period of six months I met also a lot of people that they welcomed me very nicely in their group.

I would like to thank also the Thermodynamics and Modelling Research Group of the University of Udine, for the intense work of collaboration and for inviting me inside their laboratories for testing by myself all the hard work behind the thermodynamic characterization of my Lanthanide complexes.

I also would like to thank all the several co-authors which contributed to the publications and communications related to this thesis.

Thanks to all the PhD students, post docs and other students that I met during this PhD cycle. In particular, all the guys of the previous years including: Irene, Giacomo, Paolo, for the “advices” with Origin program and for all the “Informatic support”. Moreover, all the other guys of the nice lunch break including: Veronica, Elisa, Stefano, Davide, Lorenzo(i), Chiara, Marco, Claudia, Andrea and so on.

Another sincere thank to all the group of NMR group including: Serena, for her patience and availability for the large number of NMR spectra, Carlo, Francesca and so on for their nice companionship.

A special thank also to my family, and in particular to my father that he lost another one of my important events. I am sure that he would be very proud of me.

I would finish this long list of acknowledgments with a great and sincere thank you to my reliable boyfriend EMANUELE for being always present in each moment of my life. I hope that we could soon begin a new chapter of our life.

I hope that I did not forget anybody.